

https://dspace.org/

Application of innovative starch-based platforms in controlled drug delivery.

Dawood, Yusuf

2014-04-25
http://hdl.handle.net10539/14588

Downloaded from a DSpace repository. https://dspace.org/

APPLICATION OF INNOVATIVE STARCH-BASED PLATFORMS IN CONTROLLED DRUG DELIVERY

YUSUF DAWOOD

A dissertation submitted to the Faculty of Health Sciences, University of the Witwatersrand, in fulfillment of the requirements for the degree of Master of Pharmacy

Supervisor:

Professor Viness Pillay

Department of Pharmacy and Pharmacology, University of the Witwatersrand, South Africa

Co-Supervisors:

Professor Yahya E. Choonara and Ms Lisa C. du Toit

Department of Pharmacy and Pharmacology, University of the Witwatersrand, South Africa

Johannesburg, 2013

DECLARATION

I, Yusuf Dawood, declare that this dissertation is my own work. It has being submitted for the degree of Master of Pharmacy in the Faculty of Health Sciences in the University of the Witwatersrand, Johannesburg. It has not been submitted before for any degree or examination at this or any other University.



……

This 19th day of August 2013

RESEARCH OUTPUTS

Conference Proceedings

Poster Presentations

Yusuf Dawood, Asma Seedat, Viness Pillay, Yahya E. Choonara and Lisa C. du Toit. *Influence of Hydration on the Drug-Loading Capacity, Mechanical Strength and Resilience of Cellulosic Multiparticulates.* Poster presented at the 29th Annual Conference of the Academy of Pharmaceutical Sciences, September 2008, Rustenburg (Abstract in Appendix A1).

Yusuf Dawood, Viness Pillay, Yahya E. Choonara and Lisa C. du Toit. *Determination of the Entrapment Efficiency, Friability and Release Profile of Diphenhydramine from Cellulosic Multiparticulates.* Poster presented at the 5th ICPPS conference, September 2009, Potchefstroom (Abstract in Appendix A2).

Yusuf Dawood, Viness Pillay, Yahya E. Choonara and Lisa C. du Toit. *Elucidation of the Potential of Starch-Based Multiparticulates for use as a Platform in Novel Drug Delivery Systems.* Poster presented at the APS UKPHARMSCI conference, September 2010, Nottingham, UK (Abstract in Appendix A3).

Podium Presentations

Yusuf Dawood, Pradeep Kumar, Viness Pillay, Yahya E. Choonara and Lisa C. du Toit. *Elucidation of the Effect of Oxidation and Crosslinking on the Drug Entrapment Efficiency and In vitro Drug Release Behavior of a Starch-Based Multiparticulate Drug Delivery System.* Podium Presentation for the Young Scientist Competition: 6th International Conference on Pharmaceutical and Pharmacological Sciences, September 2011, Durban (Abstract in Appendix A4).

Research Publications

Research Papers

Y. Dawood, V. Pillay, Y.E. Choonara, L.C. du Toit. P. Kumar*. Characterization of Sago and Tapioca Multiparticulates and Elucidation of their Potential Application as the Platform for a Multiparticulate Oral Drug Delivery System.**

* Drafted and submitted for review

Y. Dawood, V. Pillay, Y.E. Choonara, L.C. du Toit. P. Kumar. *Effects of Modifications and Subsequent Optimization of a Multiparticulate Starch-Based Oral Drug Delivery System Employing Sulfasalazine as the Model Drug.** (Abstract in Appendix B1).

* Drafted and submitted for review

Y. Dawood, V. Pillay, Y.E. Choonara, L.C. du Toit. P. Kumar. *In vivo Assessment of Sulfsalazine-Loaded Sago Starch-Based Multiparticulates in the the Large White Pig Model.**

***** Drafted and submitted for review

PATENT

Application of innovative starch-based platforms in controlled drug delivery, University of the Witwatersrand, Yusuf Dawood, Viness Pillay, Yahya Essop Choonara and Lisa Claire du Toit*

* Drafted and submitted for review, 2011

ANIMAL ETHICS DECLARATION

I hereby confirm that the following study entitled "An *in vivo* assessment of novel biocompatible polymeric drug delivery systems in pigs" had received the approval from the Animal Ethics Committee of the University of the Witwatersrand with ethics clearance number 2009/01/05 (Appendix C1).

SYNOPSIS OF DISSERTATION

The oral route presents the most convenient, least invasive and thus the most widely used route for the administration of drugs but displays inherent impediments, related to both the drugs used and the gastrointestinal tract itself, resulting in diminished bioavailability of drugs. Additionally, development of new drug molecules is difficult, expensive, time-consuming and their approval and success is not guaranteed. Development of novel controlled Multiparticulate Oral Drug Delivery Systems (MODDS) aims to address these issues by employing existing drugs and enhancing their oral bioavailibility and safety, thus improving clinical efficacy in many disease states. Multiparticulate drug delivery systems are specialized controlled drug delivery systems that comprise of many discrete units, each loaded with a fraction of the total dose and each possessing the ability to release entrapped drug independently, thus preventing dose dumping and allowing diverse applications within a single dosage form. However, novel drug delivery systems possess disadvantages in that they may be expensive, difficult to reproduce on a large-scale and frequently use synthetic polymers that may not be disintegrated nor excreted to a sufficient extent in vivo. Starch, a natural polymer, is widely available, inexpensive, and biocompatible and can be modified in various ways. Starch is thus available in several forms and compositions, including commercial multiparticulates, allowing it to be used for the development of an effective controlled MODDS.

The essential aim of the study was to functionalize the inert, inexpensive, commercially available, food-grade multiparticulates derived from sago or tapioca starch and employ the multiparticulates as a Starch-Based Platform (SBP) in a MODDS. Following characterization of both starch-based multiparticulates, the sago multiparticulates were selected as the SBP and preliminary optimization of drug entrapment employing diphenhydramine (DPH) as the model drug was conducted using a Box-Behnken experimental design. The pre-optimized formulation displayed superior Drug Entrapment Efficiency (DEE= 59.354%, R^2=0.9257 when compared to the predicted DEE), but demonstrated poor control of drug release. Thus, alternate drugs displaying varying physicochemical characteristics were evaluated and sulfasalazine (SSZ) was ultimately selected as the model drug for the study.

Various modifications of the SBP were attempted with epichlorohydrin-facilitated crosslinking followed by SSZ loading and finally secondary epichlorohydrin crosslinking conferring the best control of drug release coupled with satisfactory drug entrapment and excellent SBP structural stability. The formulation procedure was optimized using a Face Centered Central Composite Design by evaluating the effects of varying the drug loading time (DLT) and secondary crosslinking time (CLT) on the responses of DEE and Mean Dissolution Time (MDT). The optimum formulation conditions was established as DLT=8 hours and CLT=8 hours with predicted DEE and MDT of 40.78% and 171.696 minutes, respectively. Formulation, scaling up and analysis of the optimized SBP revealed that gelatinization and crosslinking had occurred throughout the SBP resulting in incorporation of SSZ into the structure of the SBP, both at the surface and at the core of the SBP. Experimental DEE values for the optimized and scaled-up formulations demonstrated close correlation to the predicted DEE with R^2 values of 0.9813 and 0.9893, respectively. The modifications imparted during optimization caused coalescence of the surface starch granules and resulted in a decrease in surface area and porosity of the SBP. This in turn affected the drug release resulting in MDT values of 163.972 and 166.011 minutes, which translated into R^2 values of 0.9550 and 0.9669 for the optimized and scaled-up formulations, respectively. Drug release from the optimized SBP formulation was found to fit the Higuchi model best with Quasi-fickian diffusion occurring in simulated gastric fluid and anomalous drug transport in simulated intestinal fluid resulting in an overall anomalous drug transport mechanism of drug release.

In vivo SSZ release throughout the gastrointestinal tract was determined directly by measuring plasma SSZ concentrations and indirectly by measuring the plasma concentrations of 5-Acetyl Salicylic Acid (5-ASA) and N-Acetyl-5-ASA and displayed general correlation to the in vitro SSZ behavior determined previously. Furthermore, the in vivo SSZ release of the optimized SBP formulation was compared to a conventional commercially available SSZ formulation, Salazopyrin® with the optimized SBP formulation displaying superior SSZ release characteristics and a vast improvement in the bioavailability of SSZ compared to Salazopyrin®.

ACKNOWLEDGEMENTS

At the time of completion of this research I have worked with a great number of people whose contribution in various ways to this research and the making of this dissertation deserve special mention. It is a pleasure to convey my gratitude to them all in my humble acknowledgement.

First and foremost, I would like to thank the Creator of all things, Most Beneficial and Most Merciful for allowing me this opportunity to pursue this degree and granting me the ability to acquire knowledge, withstand the endevours and gain experience that will guide me through life. You are due all praises.

To my Supervisor and Professor, Viness Pillay, who from the start has required nothing less than excellence, hard work, and commitment, thank you for instilling these qualities in me and I hope this dissertation is a reflection of your support, guidance and dedication to the field of pharmaceutics

To my co-supervisors, Professor, Yahya Choonara, and Ms Lisa du Toit, you were always willing to provide the necessary direction and assistance when needed. The time and effort you invested has only made the completion of this dissertation so much easier. Your valuable feedback and suggestions helped me improve both my lab techniques and my dissertation in many ways. I wish you both all the success in your future endeavours.

To Pradeep Kumar, a special thank you for your assisstance and for all the effort and time you have put into my work. Thank you for your advice and guidance as it was that which ultimately put me on course to accomplish this monumental task.

To Maymoonah Bibi Dawood, my Mother and pillar of strength, thank you for giving me the numerous academic opportunities I know I am extremely privileged to have. It is through your unconditional love, support, guidance, encouragement and, not forgetting, your unfaltering confidence in me that I have (finally) completed my masters successfully. You always believed in me. I am honoured and blessed to have you as my mother and I only hope that I make you proud. You have taught me that with hard work and dedication nothing is impossible. I thank you for always believing in me and my dreams and sacrificing so much just so that my dreams can become a reality.

To my late father, Ayob Dawood, thank you for all the effort that you have have made not only for me but for our entire family. Thank you for taking that leap of faith and placing so much emphasis on educating all of us. I do hope that my effort would make you proud and you are always in my duas.

To my beloved wife and best friend, Nadia, I cannot express my gratitude for always believing in me and with your unwavering support, encouragement, patience and understanding, you provided with the strength to perform better than I expected. You always went out of your way to ensure that I was successful in this endeavour. You have experienced the worst of my moods, with the anxiety attacks at all hours of the day and night, the threats to quit and the numerous tantrum but you never gave up on me. Your unconditional love for me and your belief in my capabilities has allowed me to achieve my goal. Thank you for all your sacrifices for me and for pushing me to complete this dissertation when I had lost the will to do it. I could never have done this without you. I love you more than can be expressed and am eternally grateful to have you in my life.

To my bhai, thank you for always being the voice of reason and encouragement. For your constant motivation and advice, it made all the difference. You have given me courage and showed me that if you want and believe in something hard enough you can make it become a reality.

To my bhabijaan, thank you for always being there for me and for always lending a caring ear when I had to complain and needed support. You have been a sister to me in difficult times and words cannot tell you how grateful I am and will always be for your support and encouragement during those bleak days.

To my sister, Farzanah, thank you for always putting in that extra effort to be sympathetic towards me and succeeding at it. Although out of character but I am very grateful for it as it definitely did help when I needed it the most. Your advice and sacrifices with regard many issues has helped me overcome obstacles which I have faced. It is much appreciated. And finally you get to know what “SECRET RESEARCH” I was conducting.

To Zainul, for being my other brother and getting me through those dim and dark days. Your insight and support eased my mind and provided me with clarity and encouraged me to continue when I felt I could not. I truly appreciate all you have done for me.

Thank you to the “elders” of my family, Rayhana khala, Iazal khalu (my wife’s “father in law”), Chota maam, Habiba mamie and Pappa, for your encouragement and moral and financial support. Your love, affection and discipline toward me have instilled values and character in me that have brought me far in life and I am eternally grateful.

To my new family, the in laws, parents (Ilyas and Mehroon) and siblings (Nas and nunu and muhammed azhar). I would like to sincerely thank you for all your support and for always believing in me. I will always be grateful to you for making the completion of this dissertation so much easier.

To Naseeha, Nabeela, Zainub, Mateenudeen and ALL my nieces, nephews and cousins, there are just too many too names to mention, and extended Springs family (bhabijaan’s imediate family), thank you for the fun times and support that I required to get throught this journey. The support and duas definitely helped me achieve this.

In this time of pursuing my masters degree, I have been fortunate to come in to contact with many people and forged friendships that will last forever and memories that will always stay with me. Many of you I have never known before this yet you play such an integral part in my life and brought me to this point, you have my deepest gratitude. I am truly honoured to have got to spend this time and experience with you. Thank you for the good times, bad times and the world cup times, Ameena Wadee, Kovanya Moodley, Tasneem Rajan, Derusha Frank, Tong-sheng Tsai, Ahmed Seedat, Zaheeda Khan, Caragh Murphy, Clare Dott, Deshika Reddy, Valence Ndesendo, Saffiya laher, Phelix, Oluwatoyin Kolawale, Pius Fasinu, Ndidi Ngulukwa, Steven Mufamadi, Bongani Sibeko.

To Thiresan Govender, thank you for giving me a place to crash after those late nights in the labs and wondering if we were ever going to finish this. Thank you for the valuable friendship and advice you provided me and for truly being there for me when I needed. In you I have found a true friend who I know will always be there for me and I cannot express my gratitude adequately.

To Priya bawa, thank you for your friendship and assistance. Your input into my research and confidence in my abilities have motivated me to complete this work. And thank you for that special sarcasm which provided for entertaining times especially when we got to read the newspaper.

To Yasien Docrat, thank you for your desperate attempts at trying to solve the computer related problems. Sometimes it worked, other times it backfired and thank you for being such a good office mate, co-worker and friend to me and always being there to lend a helping hand.

To Rubina Shaikh, thank you for all the kindness throughout our studies from undergrad years to the torturous nights of animal studies. Thank you for always being there for me.

To my officemates, Latavia and Deshnee, who went from being terrified of the prospect of sharing an office with me to being great friends, thank you for all the good times and laughs and long chats in and out of the office, as for all the other office ongoings, I guess it will just be like that last piece of inside story which is still unaccounted for.

To the staff at Eastern Medicine Depot, thank you all for the encouragement and support throughout this endeavour. It will always be remembered.

To the technical staff, who ensured the labs were always neat and tidy, the late Elizabeth, Mama Florence, Kleinbooi (KB), Bafana, Sello and Tebogo, thank you for your willingness to assist me whenever necessary, even when you did not have to. You always went out of your way to ensure that I got what I needed and I will always be grateful to you.

To Dr Leith Meyer and the staff of the CAS: To Dr. Leith Meyer and Sister Mary-Ann Costello and their team at the Central Animal Services (CAS) at the University of the Witwatersrand, I thank you for all your advice and assistance when undertaking animal studies.

To the staff of the Department of Pharmacy and Pharmacology, Professor Michael Danckwerts, Professor Sandy Van Vuuren, Mr. David Bayever, Ms. Shirona Naidoo, Ms. Neelaveni Padayachee, Ms. Sibongile Sibambo, Ms. Neha Singh and Ms. Busi Damane for their support, assistance and insight.

And finally, to my funders, without whom this research would not have been possible, I would like to extend my heartfelt gratitude to the National Research Foundation of South Africa and The Department of Education.

"Look at a day when you are extremely satisfied at the end. It's not a day when you lounge around doing nothing, it's when you've had everything to do, and you've done it." Margeret Thatcher.

DEDICATION

This work is dedicated to the two most important women in my life, my mother, Maymoonah Bibi Dawood, for all that I am today; and to my beloved Wife, Nadia Dawood, for loving me and making this possible.

TABLE OF CONTENTS

CHAPTER 1

RATIONALE FOR THE DESIGN AND DEVELOPMENT OF A STARCH-BASED MULTIPARTICULATE ORAL DRUG DELIVERY SYSTEM

1.1. Background into the Anatomy and Physiology of the GIT and Bioavailability of Orally Administered Drugs 1

1.2. Effects of Foods and Specific Macronutrients on the Physiology of the GIT 4

1.2.1. Effect of lipids on the physiology of the GIT 7

1.2.2. Effect of proteins on the physiology of the GIT 7

1.2.3. Effect of carbohydrates on the physiology of the GIT 8

1.3. Effects of Concurrent Administration of Food and Drug Formulations 8

1.4. Employment of Macronutrients in Drug Delivery 10

1.4.1. Employment of lipids in drug delivery 10

1.4.2. Employment of proteins and peptides in drug delivery 11

1.4.3. Employment of carbohydrates in drug delivery 12

1.4.3.1. Employment of cellulose in drug delivery 13

1.4.3.2. Employment of chitosan in drug delivery 14

1.4.3.3. Employment of various starches in drug delivery 15

1.4.3.3.1. Pea starch 16

1.4.3.3.2. Maize/ corn starch 16

1.4.3.3.3. Potato starch 17

1.4.3.3.4. Tapioca starch 17

1.4.3.3.5. Sago starch 18

1.5. Rationale and Motivation for the Study 20

1.6. Aim and Objectives 20

1.7. Overview of the Dissertation 21

CHAPTER 2

CHARACTERIZATION OF SAGO AND TAPIOCA MULTIPARTICULATES AND ELUCIDATION OF THEIR POTENTIAL APPLICATION AS A PLATFORM FOR MULTIPARTICULATE ORAL DRUG DELIVERY

2.1. Introduction 24

2.2. Materials and Methods 28

2.2.1. Materials 28

2.2.2. Determination of the size and morphology of the SBPs 28

2.2.2.1. Gravimetric analysis of the SBPs 28

2.2.2.2. Macroscopic analysis of to determine the relative size of the SBPs 28

2.2.2.3. Light microscopic analysis to determine the morphology of the SBPs 29

2.2.2.4. Scanning Electron Microscopy to determine the intrinsic structure of the SBPs 29

2.2.3. Fourier Transform Infrared Analysis to determine structure of the SBPs 29

2.2.4. Colorimetric determination of intrinsic polymer ratio of the SBPs 30

2.2.4.1. Preparation of solutions for colorimetric analysis of SBPs 30

2.2.4.2. Preparation of a standard amylose curve and determination of amylose content in the SBPs 31

2.2.5. Gravimetric analysis to determine the hydration capacity and erosion behavior of the SBPs in water and simulated biological fluids 32

2.2.5.1. Preparation of hydration and erosion media 32

2.2.5.1.1. Deionized water 32

2.2.5.1.2. Simulated gastric fluid 32

2.2.5.1.3. Simulated intestinal fluid 32

2.2.5.2. Determination of the effect of drug-loading and drug release media on the hydration and erosion of the SBPs 32

2.2.6. Buoyancy studies to elucidate the potential of the SBPs to act as a gastro-floatable MODDS 33

2.2.7. Textural analysis to elucidate the effect of hydration on the mechanical behavior of the SBPs 34

2.2.7.1. Determination of the effect of hydration on the resilience of both SBPs 34

2.2.7.2. Determination of the effect of hydration on the hardness and deformation energy of both SBPs 35

2.2.8. Determination of the functional characteristics of SMP and TMP for employment as the platform in the MODDS 36

2.2.8.1. Construction of calibration curves for DPH in SGF and SIF 36

2.2.8.2. Drug entrapment employing the highly water-soluble model drug, DPH..... 36

2.2.8.2.1. Drug entrapment into the SBPs 36

2.2.8.2.2. Elucidation of extent of drug entrapment 36

2.2.8.3. *In vitro* drug release study to determine the ability of SMP and TMP to control the release of DPH in simulated biological fluids..... 37

2.3. Results and discussion 38

2.3.1. Comparison of the size and morphology of SMP and TMP 38

2.3.1.1. General and microscopic morphology of the SBPs 38

2.3.1.2. SEM imaging of intrinsic structure of the SBPs 39

2.3.2. Comparative FTIR representation of structure of SMP, TMP and soluble starch ... 41

2.3.3. Colorimetric ratio of amylose and amylopectin within SBPs 42

2.3.4. Effect of drug-loading and dissolution media on the hydration and erosion of the SBPs 43

2.3.5. Potential of the SBP to be employed as a buoyant MODDS 45

2.3.6. Effect of hydration on the mechanical behavior of the SBPs 45

2.3.7. Functional characteristics of the SBPs 48

2.3.7.1. Calibration curves of DPH in SGF and SIF 48

2.3.7.2. Comparative DPH entrapment of the SBPs 49

2.3.7.3. *In vitro* DPH release characteristics of SBPs 49

2.4. Concluding Remarks 50

CHAPTER 3

OPTIMIZATION OF ENTRAPMENT OF DIPHENHYDRAMINE EMPLOYING THE BOX-BEHNKEN RESPONSE SURFACE METHODOLOGY

3.1. Introduction 51

3.2. Materials and Methods 54

3.2.1. Materials 54

3.2.2. Pre-formulation studies to determine variable parameters which influence drug entrapment of the SBP 54

3.2.2.1. Swelling time 54

3.2.2.2. Drying temperature 54

3.2.2.3. Volume of drug solution 55

3.2.2.4. Concentration of drug solution 55

3.2.2.5. Temperature of drug solution 55

3.2.3. Optimization of the drug entrapment conditions utilizing a Box-Behnken design of experiments 56

3.2.3.1. Generation of a design of experiments through a BBD and subsequent testing 56

3.2.3.2. Determination of drug content and entrapment efficiency 57

3.2.3.3. Optimization of the formulation parameters 57

3.2.3.4. Determination of the *in vitro* drug release behavior of optimized DPH-loaded SBP 58

3.3. Results and Discussion 58

3.3.1. Effect of variable parameters on the drug entrapment of the SBP 58

3.3.2. Measured responses for the experimentally synthesized SBP formulations 61

3.3.3. Comparative analysis between experimental and predicted values for the design generated SBP formulations 63

3.3.4. Effect of independent variables on the mass gain of the SBPs..... 64

3.3.5. Analysis of the Box-Behnken Design 65

3.3.5.1. Analysis of residuals generated by experimental design formulations... 65

3.3.5.2. Determination of the main effects on QDE of SBPs 67

3.3.5.3. Determination of the interactions between independent variable on the QDE of the SBP..... 68

3.3.5.4. Response Analysis of QDE of the DPH-loaded SBP 69

3.3.6. Response optimization..... 71

3.3.7. *In vitro* drug release behavior of optimized DPH-loaded SBP..... 72

3.4. Concluding Remarks..... 73

CHAPTER 4

ELUCIDATION OF THE ABILITY OF THE STARCH-BASED PLATFORM TO ENTRAP AND CONTROL THE RELEASE OF VARIOUS DRUGS

4.1. Introduction 75

4.2. Materials and Methods 80

4.2.1. Materials 80

4.2.2. Determination of the maximum absorbance wavelengths (λmax) of drugs employed in this phase of the study 80

4.2.2.1. Determination of the maximum absorbance wavelength (λmax) of propranolol 80

4.2.2.2. Determination of the maximum absorbance wavelengths (λmax) of captopril 80

4.2.2.3. Determination of the maximum absorbance wavelength (λmax) of furosemide 81

4.2.3. Construction of calibration curves in SIF and SGF for each drug 81

4.2.3.1. Construction of calibration curves for propranolol 81

4.2.3.2. Construction of calibration curves for captopril 81

4.2.3.3. Construction of calibration curves for furosemide 82

4.2.4. Determination of the potential of the SBP to entrap drugs displaying varying physicochemical properties 82

4.2.4.1. Description of experimental apparatus 82

4.2.4.2. Drug entrapment within the SBP 83

4.2.4.3. Elucidation of extent of drug entrapment 84

4.2.5. Determination of the *in vitro* drug release behavior from the SBP 84

4.3. Results and Discussion 85

4.3.1. Maximum absorbance wavelength (λmax) of various drugs employed in this phase of the study 85

4.3.2. Calibration curves of the various drugs in simulated fluids 88

4.3.3. Entrapment and drug content of SBP 90

4.3.4. *In vitro* drug release characteristics of the SBP loaded with model drugs 92

4.4. Concluding Remarks 93

CHAPTER 5

IMPROVEMENT OF THE FUNCTIONAL CHARACTERISTICS BY WAY OF MODIFICATION OF STARCH-BASED PLATFORM

5.1. Introduction 94

5.2. Materials and Methods 100

5.2.1. Materials 100

5.2.2. Gelatinization of SBP 101

5.2.3. Determination of the effect of employing polyvalent cationic salts as crosslinking agents in improving the performance of the SBP 103

5.2.3.1. Determination of the drug entrapment potential 103

5.2.3.2. Determination of the drug release behaviour of cationically crosslinked SBP 103

5.2.4. Pilot study to elucidate the effect of ECH, Glut and STMP on the functional characteristics of the SBP 104

5.2.4.1. Preparation of crosslinked SBP 104

5.2.4.1.1. Preparation of ECH-crosslinked SBP 104

5.2.4.1.2. Preparation of Glut-crosslinked SBP 104

5.2.4.1.3. Preparation of STMP-crosslinked SBP 104

5.2.4.2. Entrapment of drug into modified SBP 105

5.2.4.3. Elucidation of extent of drug entrapment 105

5.2.4.4. Comparative *in vitro* drug release from pre-crosslinked and unmodified SBPs 105

5.2.5. Covalent crosslinking of SBP with ECH 106

5.2.5.1. Determination of the effect of ECH concentration on the crosslinking of SBP in a range of gelatinization mediums 106

5.2.5.2. Determination of hydration time and crosslinking time required for most favorable covalent ECH-crosslinking of the SBP 106

5.2.5.3. Determination of the effect of ECH-crosslinking on the functional characteristics of the SBP employing DPH as the model drug 107

5.2.5.3.1. Drug entrapment and determination of DPH entrapment efficiency . 107

5.2.5.3.2. Elucidation of the *in vitro* DPH release behavior of ECH-crosslinked SBP 108

5.2.5.4. Determination of the effect of ECH-crosslinking on the functional characteristics of the SBP employing captopril as the model drug ... 108

5.2.5.4.1. Determination of the effect of concurrent drug-loading and modifications of the SBP 108

5.2.5.4.1.1. Drug entrapment and determination of extent of captopril entrapment 108

5.2.5.4.1.2. Comparative *in vitro* captopril release behavior from ECH crosslinked and unmodified SBPs 109

5.2.5.4.2. Determination of the effect of step-wise drug-loading, controlled gelatinization and subsequent ECH crosslinking 109

5.2.5.4.2.1. Preparation of drug-loaded SBP 109

5.2.5.4.2.2. Modification of drug-loaded SBP 109

5.2.5.4.2.3. Elucidation of extent of drug entrapment 109

5.2.5.4.2.4. Comparative *in vitro* captopril release behavior of the post drug entrapment modified SBPs 110

5.2.5.4.3. Determination of the effect of drug-loading on pre-modified SBP..... 110

5.2.5.4.3.1. Preparation of pre-modified SBP 110

5.2.5.4.3.2. Drug entrapment into pre-modified SBP 110

5.2.5.4.3.3. Elucidation of extent of drug entrapment 111

5.2.5.4.3.4. Comparative *in vitro* drug release behavior of pre-modified drug-loaded SBP formulations 111

5.2.5.5. Determination of the effect of oxidation and crosslinking on the performance of SBP 111

5.2.5.5.1. Preparation of pre-oxidized SBP 111

5.2.5.5.2. Drug entrapment and crosslinking within the pre-oxidized SBP 111

5.2.5.5.3. Elucidation of extent of drug entrapment 112

5.2.5.5.4. Comparative *in vitro* drug release behavior of pre-oxidized drug-loaded SBPs 112

5.3. Results and Discussion 113

5.3.1. Effect of gelatinization on the stability of the SBP 113

5.3.2. Effect of crosslinking using polyvalent cationic salts 116

5.3.2.1. Effect of crosslinking using polyvalent cationic salts on the drug entrapment of the SBP 116

5.3.2.2. Effect of crosslinking using polyvalent cationic salts on the *in vitro* drug release behavior of the SBP 117

5.3.3. Effect of crosslinking using ECH, Glut and STMP 118

5.3.3.1. Effect of crosslinking on the hydration and drug entrapment of the SBP 118

5.3.3.2. Effect of crosslinking on the *in vitro* drug release behavior of the SBP 119

5.3.4. Effect of covalent ECH-crosslinking on the performance of the SBP 120

5.3.4.1. Effect of ECH concentration on the hydration of the SBP 120

5.3.4.2. Effect of hydration time and crosslinking time on the hydration of the SBP 121

5.3.4.3. Effect of hydration time and crosslinking time on the functional characteristics of SBP employing DPH as the model drug 122

5.3.4.3.1. Effect of hydration time and crosslinking time on the DPH entrapment 122

5.3.4.3.2. Drug release behavior of DPH from modified SBP 123

5.3.4.4. Effect of hydration time and crosslinking time on the functional characteristics of SBP employing captopril as the model drug 124

5.3.4.4.1. Effect of concurrent gelatinization and ECH-crosslinking on the functional characteristics of the SBP 124

5.3.4.4.2. Effect of step-wise drug-loading, gelatinization and crosslinking on the functional characteristics of the SBP 125

5.3.4.4.3. Effect of pre-modification on the functional characteristics of SBP 126

5.3.5. Effect of periodate oxidation on the functional characteristics of SBP employing captopril as the model drug 128

5.4. Concluding Remarks 132

CHAPTER 6

EMPLOYMENT OF AN ALKALI STABLE MODEL DRUG FOR THE DEVELOPMENT OF THE MULTIPARTICULATE ORAL DRUG DELIVERY SYSTEM

6.1. Introduction 134

6.2. Materials and Methods 135

6.2.1. Materials 135

6.2.2. Construction of calibration curves 135

6.2.3. Determination of the effects of concurrent modification and drug entrapment on the functional characteristics of the SBP 136

6.2.3.1. Preparation of modification solutions 136

6.2.3.1.1. Preparation of alkaline alcohol solution 136

6.2.3.1.2. Preparation of oxidizing solution 136

6.2.3.1.3. Preparation of covalent crosslinking solution 136

6.2.3.1.4. Preparation of ionic crosslinking solution 136

6.2.3.2. Preparation of drug solutions 136

6.2.3.3. Preparation of oxidized SBP 137

6.2.3.4. Concurrent modification and drug entrapment of the SBP 137

6.2.3.5. Determination of the *in vitro* drug release behavior of SSZ-loaded SBP 138

6.2.4. Determination of the effects of consolidated pre-modifications on the functional characteristics of the SBP 138

6.2.4.1. Preparation of modification solutions 138

6.2.4.1.1. Preparation of alkaline alcohol solution 138

6.2.4.1.2. Preparation of oxidizing solution 138

6.2.4.1.3. Preparation of covalent crosslinking solution 139

6.2.4.1.4. Preparation of ionic crosslinking solution 139

6.2.4.2. Preparation of drug solution 139

6.2.4.3. Preparation of various modified SBPs 139

6.2.4.3.1. Preparation of pre-oxidized SBP 139

6.2.4.3.2. Preparation of alkali pre-gelatinized SBP 139

6.2.4.3.3. Preparation of ECH-crosslinked pre-gelatinized SBP 140

6.2.4.3.4. Preparation of ionic crosslinked pre-gelatinized SBP 140

6.2.4.3.5. Preparation of covalent crosslinked pre-oxidized SBP 140

6.2.4.3.6. Preparation of ionic crosslinked pre-oxidized SBP 140

6.2.4.4. Drug entrapment into modified SBPs 141

6.2.4.5. Secondary crosslinking of drug-loaded SBPs 141

6.2.4.5.1. Preparation of double covalent crosslinked drug-loaded SBP 141

6.2.4.5.2. Preparation of double ionic crosslinked SBP 141

6.2.4.6. Determination of the extent of drug entrapment into consolidated pre-modified SBP 141

6.2.4.7. Determination of the *in vitro* drug release behavior of consolidated pre-modified SBPs 142

6.2.5. Determination of the effect of Drug-Loading Time and secondary Crosslinking Time on the performance of pre-gelatinized covalent crosslinked SBP 143

6.2.5.1. Preparation of pre-gelatinized crosslinked SBPs 143

6.2.5.2. Drug-loading and secondary crosslinking of SBP 143

6.2.5.3. Determination of the extent of drug entrapment into consolidated double covalent crosslinked SBP 144

6.2.5.4. Determination of the effect of DLT and secondary CLT on the *in vitro* drug release behavior of double covalent crosslinked SBPs 144

6.3. Results and Discussion 144

6.3.1. Calibration curves of SSZ in simulated physiological fluids 144

6.3.2. Effect of concurrent modification and drug entrapment on the functional characteristics of the SBP 145

6.3.2.1. Effect of concurrent modification on the drug entrapment potential of the SBP 145

6.3.2.2. *In vitro* SSZ release from concurrently modified and drug-loaded SBPs 147

6.3.3. Effect of consolidated modification on the functional characteristics of the SBP .. 149

6.3.3.1. Effect of consolidated modification on the drug-loading potential of the SBP 149

6.3.3.2. Effect of consolidated pre-modification on the *in vitro* drug release behavior of SBP 151

6.3.4. Effect of DLT and secondary CLT on the functional characteristics of the pre-gelatinized ECH-crosslinked SBP 152

6.3.4.1. Effect of DLT and secondary CLT on the drug entrapment of double crosslinked SBP 152

6.3.4.2. Effect of DLT and secondary CLT on the *in vitro* drug release behavior of double ECH-crosslinked SBP 154

6.4. Concluding Remarks 155

CHAPTER 7

OPTIMIZATION OF DOUBLE CROSSLINKED, SULFASALAZINE-LOADED STARCH-BASED PLATFORM

7.1. Introduction 157

7.2. Optimization of functional characteristics of the SBP utilizing a Face Centred Central Composite Design 158

7.2.1. Materials 158

7.2.2. Preparation of covalent crosslinked SBP 158

7.2.3. Implementation and analysis of FCCCD 159

7.2.3.1. Generation of a FCCCD and subsequent analysis 159

7.2.3.2. Drug entrapment into experimental design formulations 161

7.2.3.3. *In vitro* drug release behavior from experimental design formulations 161

7.2.3.4. Elucidation of mechanism of drug release of the design formulations 163

7.2.3.4.1. Zero-order release model 164

7.2.3.4.2. First order release model 164

7.2.3.4.3. Higuchi model 164

7.2.3.4.4. Korsmeyer-Peppas model 165

7.2.3.4.5. Hixson-Crowell model 166

7.2.3.5. Evaluation of the similarity of the drug release profiles 170

7.2.3.6. Comparative analysis between experimental and predicted values for the design generated SBP formulations 171

7.2.3.7. Analysis of Face Centred Central Composite Design 173

7.2.3.7.1. Residual analysis 173

7.2.3.7.2. Response analysis of DEE for SSZ-entrapped SBP 176

7.2.3.7.3. Response analysis of MDT for SSZ-entrapped SBP..... 177

7.2.4. Response optimization of the double crosslinked SSZ loaded SBP 177

7.3. Evaluation of the Characteristics of the Optimized Double ECH-Crosslinked SBP 178

7.3.1. Materials and Methods..... 178

7.3.1.1. Materials 178

7.3.1.2. Determination of the SSZ entrapment potential of the optimized double crosslinked SBP..... 178

7.3.1.3. Microscopic analysis of the surface and core of the optimized SBP ... 179

7.3.1.4. Scanning Electron Microscopy analysis of the surface and core of the optimized SBP..... 179

7.3.1.5. Analysis of the surface area and porosity of the optimized SBP 179

7.3.1.6. *In vitro* drug release behavior from the optimized SBP 182

7.3.1.7. Determination of extent of hydration and erosion of SBP matrix during drug release from the optimized SBP 182

7.3.1.8. Determination of the drug release kinetics and similarity of the optimized SBP..... 182

7.3.2. Results and discussion describing the characteristics of optimized double ECH-crosslinked SBP..... 182

7.3.2.1. Drug entrapment efficiency of optimized SBP..... 182

7.3.2.2. SEM imaging demonstrating the effect of optimization on the structure of the SBP 183

7.3.2.3. Effects of optimization on the surface area and porosity of the SBP... 184

7.3.2.4. Effect of optimization on the *in vitro* drug release behavior of the SBP 192

7.3.2.5. Drug release kinetics of optimized SBP 195

7.4. Concluding Remarks 197

CHAPTER 8

IN VIVO ASSESSMENT OF OPTIMIZED SULFASALAZINE-LOADED STARCH-BASED PLATFORM IN THE LARGE WHITE PIG MODEL

8.1. Introduction 198

8.2. Materials and Methods 202

8.2.1. Materials 202

8.2.2. Preparation of optimized SBP for application as the MODDS 202

8.2.3. Comparison of *in vitro* SSZ release from the MODDS and Salazopyrin® tablets 203

8.2.4. Experimental subjects, habituation and living conditions 203

8.2.5. Surgical insertion of a chronic jugular catheter 204

8.2.6. Intragastric dose administration 208

8.2.7. Blood sampling and plasma storage procedure 209

8.2.8. Determination of the *in vivo* drug release behavior of SSZ from Salazopyrin® tablets and MODDS 209

8.2.8.1. Development of a method for sample analysis employing Ultra Performance liquid chromatography 209

8.2.8.1.1. Equipment employed for Ultra Performance liquid chromatography analysis 210

8.2.8.1.2. Priming of pumps for Ultra Performance liquid chromatography analysis 210

8.2.8.1.3. Derivatization of 5-ASA to N-acetyl-5-ASA 211

8.2.8.1.4. Determination of UPLC parameters for adequate separation of SSZ, 5-ASA and N-Acetyl-5-ASA 212

8.2.8.2. Selection of a suitable method of deproteinization and drug extraction from plasma for UPLC analysis 212

8.2.8.2.1. Solid phase extraction 213

8.2.8.2.2. Liquid-liquid extraction 215

8.2.8.3. Preparation of analytical standards for the calibration series 216

8.2.8.4. UPLC analysis of drug release after the *in vivo* administration of Salazopyrin® and the MODDS 217

8.3. Results and Discussion 217

8.3.1. Comparative *in vitro* drug release behavior of Salazopyrin® tablets and the MODDS 217

8.3.2. Effect of habituation, catheterization, dosing and blood sampling 218

8.3.3. *In vivo* analysis of plasma samples subsequent to administration of Salazopyrin®tablets and the MODDS 219

8.3.3.1. Derivatization of 5-ASA to N-acetyl 5-ASA 219

8.3.3.2. Validation of developed method for UPLC analysis of plasma samples 220

8.3.3.3. Deproteinization and drug extraction 222

8.3.4. Calibration curves constructed for the quantitative analysis of SSZ, 5-ASA and N-Acetyl-5-ASA in plasma 224

8.3.5. *In vivo* drug release behavior of SSZ from Salazopyrin® tablets and MODDS 225

8.4. Concluding Remarks 228

CHAPTER 9

CONCLUSIONS AND RECOMMENDATIONS

9.1. Conclusions 229

9.2. Recommendations 231

REFERENCES..... 232

APPENDICES

APPENDIX A 269

Abstracts of Conference Proceedings

APPENDIX B.....275

Abstracts of Papers Published/Submitted

APPENDIX C.....277

Animal Ethics Clearance

LIST OF FIGURES

Figure 1.1: Structure of the human small intestine *(Adapted from Porth, 2007).* 1

Figure 1.2: Biopharmaceutics Classification System (BCS) *(Adapted from Custodio et al., 2008).* 2

Figure 1.3: Mechanisms of drug absorption in the GIT. *(Adapted from Gaucher et al, 2007).* 3

Figure 1.4: Schematic map of the dissertation. 23

Figure 2.1: Representation of the structures of (a) amylose and (b) amylopectin. 26

Figure 2.2: Digital images depicting (a) 2g SMP and (b) 2g TMP. 38

Figure 2.3: Microscopic depiction of (a1) SMP surface, (a2) SMP core (b1) TMP surface and (b2) TMP core. 39

Figure 2.4: SEM imaging of (a1) SMP surface, (a2) SMP core (b1) TMP surface and (b2)TMP core (magnifications in figures a1-b2 were: Q1=500X; Q2=1000X; Q3=3000X; Q4=5000X). 40

Figure 2.5: Comparative FTIR spectra of soluble starch, SMP and TMP. 42

Figure 2.6: Standard curve of amylose content vs. absorbance depicting average amylose content of SMP (n=3, SD≤2.235%) and TMP (n=3, SD≤3.128%). 43

Figure 2.7: Effect of hydration time on (a) Degree of swelling and (b) extent of erosion of SBPs in water, pH 1.2 and pH 6.8. (n=3 in all instances). 44

Figure 2.8: Typical Force vs. Time graph to determine the resilience of SBPs. 45

Figure 2.9: Effect of hydration on the resilience of (a) SMP (b) TMP as a function of hydration time (n=5 in all instances). 46

Figure 2.10: Typical Force vs. Distance graph to determine the deformation energy and hardness of SBPs. 47

Figure 2.11: Effect of hydration on the deformation energy of (a) SMP (b) TMP as a function of hydration time (n=5 in all instances). 47

Figure 2.12: Effect of hydration on the hardness of (a) SMP (b) TMP as a function of hydration time (n=5 in all instances). 48

Figure 2.13: Calibration curves of DPH in (a) SGF and (b) SIF. 48

Figure 2.14: *In vitro* drug release profiles of (a) SMP and (b) TMP in simulated physiological fluids (n=3 in all instances). 50

Figure 3.1: Schematic representation of design point of a 3-Factor, 3-level (3^3) Box-Behnken statistical design. 52

Figure 3.2: Chemical structure of diphenhydramine. 53

Figure 3.3: Effect of (a) DLT, (b) DT (c) drug solution volume and (d) [DPH] on the QDE of SBP with the inserts in (c) and (d) depicting the effects of drug solution volume and [DPH] respectively on the DEE of the SBP. (n=3 in all instances) 61

Figure 3.4: DEE vs. QDE of design generated SBP formulations. 63

Figure 3.5: Regression plots comparing experimental and fitted values ±95% confidence interval for QDE of the SBP formulations. 63

Figure 3.6: Effect of design variables (a) [DPH], (b) DLT and (c) DT on the mass gain of SBP as a result of drug entrapment. 64

Figure 3.7: Residual plots for QDE (mg). 65

Figure 3.8: Main effects plots of (a) DLT, (b) DT and (c) [DPH] on the QDE of the SBP. 67

Figure 3.9: Variable interaction plots of the QDE of the SBP. 69

Figure 3.10: Correlation of QDE with [DPH] and DLT utilizing (a) Response surface plot and (b) contour plot. 70

Figure 3.11: Correlation of QDE with [DPH] and DT utilizing (a) Response surface plot and (b) contour plot. 70

Figure 3.12: Correlation of QDE with DLT and DT utilizing (a) Response surface plot and (b) contour plot. 70

Figure 3.13: Optimization plot of the SBP indicating optimal factors, factor levels and desirability (D) for the optimal formulation. 71

Figure 3.14: DEE and QDE of optimized DPH-loaded SBP (n=3). 72

Figure 3.15: Comparative *in vitro* drug release of pre-optimized DPH loaded SBP (n=3). 73

Figure 4.1: Relationship between the principle determinants of blood pressure. 76

Figure 4.2: Chemical structure of propranolol HCl. 77

Figure 4.3: Chemical structure of captopril. 78

Figure 4.4: Chemical structure of furosemide. 79

Figure 4.5: Schematic representation of experimental apparatus. 83

Figure 4.6: UV spectrum of propranolol. 86

Figure 4.7: UV spectrum of captopril. 86

Figure 4.8: UV spectrum of furosemide. 87

Figure 4.9: UV spectrum of acetone. 87

Figure 4.10: UV spectrum of furosemide dissolved in acetone. 88

Figure 4.11: Calibration curve of propranolol HCl in (a) SIF and (b) SGF. 89

Figure 4.12: Calibration curve of captopril in (a) SIF and (b) SGF. 89

Figure 4.13: Calibration curve of furosemide in (a) SIF and (b) SGF. 90

Figure 4.14: Effect of hydration potential on drug entrapment efficiency of the SBP (n=3 in all instances). 92

Figure 4.15: *In vitro* Drug release profiles of viable formulations in (a) SIF and (b) in SGF (n=3 in all instances). 93

Figure 5.1: Structure of sodium (meta)periodate. 95

Figure 5.2: Periodate facilitated oxidation of starch. 95

Figure 5.3: Chemical structure of crosslinking agents (a) divalent and trivalent cationic salt, (b) sodium trimetaphosphate, (c) glutaraldehyde and (d) epichlorohydrin. 96

Figure 5.4: Polyvalent cationic crosslinking of starch using the example of calcium hydroxide. 97

Figure 5.5: STMP-facilitated crosslinking of starch. 98

Figure 5.6: ECH-facilitated crosslinking of starch. 99

Figure 5.7: Glut-facilitated crosslinking of starch. 100

Figure 5.8: Drug entrapment efficiency of salt crosslinked SBP (n=3 in all instances). 116

Figure 5.9: Drug release profiles of salt-crosslinked SBP in (a) SGF and (b) SIF (n=3 in all instances). 117

Figure 5.10: Comparative drug release profiles of crosslinked SBP in (a) SGF and (b) SIF (n=3 in all instances). 120

Figure 5.11: Effect of ECH concentration on the hydration potential of SBP (n=3 in all instances). 121

Figure 5.12: Correlation between hydration capacity and DPH entrapment of modified SBP (n=3 in all instances). 123

Figure 5.13: Comparative drug release of DPH from modified SBP in (a) SGF and (b) SIF (n=3 in all instances). 124

Figure 5.14: Effect of concurrent drug-loading and crosslinking of SBP on (a) the drug entrapment and (b) the *in vitro* drug release behavior of captopril (n=3 in all instances). 125

Figure 5.15: Effect of initial drug-loading followed by gelatinization and subsequent crosslinking of SBP on (a) the drug entrapment and (b) the drug release behavior of captopril (n=3 in all instances). 126

Figure 5.16: Effect of pre-modification of SBP on drug entrapment in different drug solution media (n=3 in all instances). 127

Figure 5.17: Effect of pre-modification on drug release behavior of SBP drug-loaded in (a) water-drug solution and (b) alkaline alcohol drug solution (n=3 in all instances). 128

Figure 5.18: Effect of oxidation and subsequent cross inking on the structural integrity and drug entrapment efficiency of the SBP (n=3 in all instances). 130

Figure 5.19: Effect of oxidation and subsequent crosslinking on the hydration capacity and drug-loading potential of the SBP (n=3 in all instances). 130

Figure 5.20: Effect of oxidation and subsequent crosslinking of the SBP on the drug release behavior of captopril in (a) SGF and (b) SIF (n=3 in all instances). 131

Figure 6.1: Chemical structure of sulfasalazine. 134

Figure 6.2: Schematic representation of resultant concurrently modified and SSZ-loaded SBPs. 138

Figure 6.3: Schematic representation of the consolidated modification and drug-loading of the SBPs. 142

Figure 6.4: Calibration curves of SSZ in (a) SIF and (b) in SGF. 144

Figure 6.5: Comparative effect of modification on the hydration and erosion of (a) previously unmodified and (b) pre-oxidized SBP during drug entrapment (n=3 in all instances). 146

Figure 6.6: Comparison of modifications on the drug entrapment of previously unmodified and pre-oxidized SBP (n=3 in all instances). 147

Figure 6.7: Effect of modifications on the comparative SSZ release behavior of (a) previously unmodified and (b) pre-oxidized SBP in SGF and SIF (n=3 in all instances). 149

Figure 6.8: Comparative effect of consolidated modification on the drug-loading potential of SBP (n=3 in all instances). 150

Figure 6.9: Comparative *in vitro* drug release behavior of consolidated pre-modified SBPs (n=3 in all instances). 152

Figure 6.10: Effect of (a) drug-loading time and (b) secondary crosslinking time on the drug entrapment of double covalent crosslinked SBPs (n=3 in all instances). 153

Figure 6.11: Effect of (a) drug-loading time and (b) secondary crosslinking time on the *in vitro* drug release behavior of double covalent crosslinked SBPs (n=3 in all instances). 155

Figure 7.1: General process involved in statistical optimization. 157

Figure 7.2: Schematic representation of design points for the 3^2 factor FCCCD. 160

Figure 7.3: Composite drug release profiles (a-d) of design generated double crosslinked SBP formulations in SGF and SIF ((n=3 in all instances)). 163

Figure 7.4: Regression plots comparing experimental and fitted values ±95% confidence interval for a) DEE and b) MDT. 172

Figure 7.5: Residual plots for (a) DEE and (b) MDT. 174

Figure 7.6: Correlation of DEE with DLT and CLT utilizing (a) Response surface plot and (b) contour plot. 176

Figure 7.7: Correlation of DEE with DLT and CLT utilizing (a) Response surface plot and (b) contour plot. 177

Figure 7.8: Optimization plots of the SBP indicating optimal factors, factor levels and desirability. 178

Figure 7.9: SEM imaging of optimized SBP (a) surface and (b) core and unmodified SBP (c) surface and (d) core (magnifications in figures a1-b2 were: Q1=500X; Q2=1000X; Q3=3000X; Q4=5000X). 184

Figure 7.10: IUPAC classification of adsorption isotherms (adapted from Siminiceanu *et al.,* 2008; Bawa *et al.,* 2011). 185

Figure 7.11: IUPAC classification of hysteresis (adapted from Siminiceanu *et al.,* 2008; Bawa *et al.,* 2011). 186

Figure 7.12: Depiction of surface area and porosity of optimized SBP with (a) Linear isotherm, (b) t-Plot, (c) pore volume distribution according to pore size with respect to (c1) adsorption branch and (c2) desorption branch and (d) pore area distribution according to pore size with respect to (d1) adsorption branch and (d2) desorption branch. 190

Figure 7.13: Depiction of surface area and porosity of unmodified SBP with (a) Linear isotherm, (b) t-Plot, (c) pore volume distribution according to pore size with respect to (c1) adsorption branch and (c2) desorption branch and (d) pore area distribution according to pore size with respect to (d1) adsorption branch and (d2) desorption branch. 191

Figure 7.14: *In vitro* drug release profiles of optimized SBP (a) sequentially and (b) separately magnified (b1) SGF phase with microscopic image of surface of SBP and (b2) SIF phase with microscopic image of core of SBP (n=3 in all instances). 194

Figure 7.15: Microscopic images (10X magnification) of (a) the surface and (b) the core of unmodified SBP. 194

Figure 7.16: Degree of hydration and erosion of optimized SBP during drug release (n=3 in all instances). 197

Figure 8.1: Schematic depiction of the pharmacokinetics of SSZ. 200

Figure 8.2: Schematic overview of *in vivo* animal study. 201

Figure 8.3: Digital images depicting (a) habituation and hand feeding process and (b) individual pens. 204

Figure 8.4: Digital images depicting (a) intramuscular administration of Buprenorphine and Carpofen, (b) intubation of the pig (c) maintenance of anesthesia, (d) monitoring of temperature, blood pressure and pulse, (e) shaving of the hair around the neck area and (f) the disinfection of the skin in preparation for surgical insertion of chronic jugular catheter. 205

Figure 8.5: Digital images depicting the surgical insertion of chronic jugular catheter procedure which included (a) isolation of jugular vein via blunt dissection, (b) the 7-French gauge double lumen 35cm catheter, (c) the surgical insertion of the catheter into the jugular vein, (d) subcutaneous tunneling of the catheter an exit point cranial to the dorsal aspect of the scapula using a trocar, (e) suturing of the externalized injection ports of the catheter and (f) suturing of the incision wound. 207

Figure 8.6: Digital images depicting (a) the intragastric tube, (b) administration of anesthetics and (c) dosing during the intragastric dose administration process. 208

Figure 8.7: Digital images depicting (a) the disinfection and (b) the flushing of catheter ports during blood sampling. 209

Figure 8.8: Chemical reaction for the synthesis of N-acetyl 5-ASA. 211

Figure 8.9: Schematic overview of the SPE procedure. 214

Figure 8.10: Schematic overview of the LLE procedure. 216

Figure 8.11: Comparative *in vitro* drug release behavior of SSZ from Salazopyrin® EN and the MODDS (n=3 in all instances). 218

Figure 8.12: Chromatograms illustrating the retention time peaks of a) 5-ASA (RT=1.1928) and b) N-Acetyl-5-ASA (RT=1.9269). 220

Figure 8.13: Chromatogram illustrating the retention time peak of SSZ (RT=2.4951 minutes). 220

Figure 8.14: Chromatogram illustrating the separation of the retention time peaks of (A) 5-ASA (RT=1.1928 minutes), (B) N-Acetyl-5-ASA (RT=1.9269 minutes) and (C) SSZ (RT=2.4951 minutes). 221

Figure 8.15: Chromatogram illustrating the retention time peak INH (RT=1.0151 minutes). 221

Figure 8.16: Chromatogram illustrating the separation of the retention time peaks of (A) 5-ASA (RT=1.2623 minutes), (B) N-Acetyl-5-ASA (RT=2.0235 minutes) and (C) SSZ (RT=2.6266 minutes) in the presence of (D) INH (RT=0.9961 minutes). 222

Figure 8.17: Chromatogram illustrating the separation of the retention time peaks of (A) 5-ASA (RT=1.1866 minutes), (B) N-Acetyl-5-ASA (RT=2.0228 minutes) and (C) SSZ (RT=2.6310 minutes) and (D) INH (RT=0.9961 minutes) subsequent to plasma extraction. 223

Figure 8.18: Plasma calibration curves of a) SSZ, b) 5-ASA and c) N-Acetyl-5-ASA. 224

Figure 8.19: Comparative plasma SSZ concentration profiles of the MODDS and Salazopyrin (n=5 in all instances). 226

Figure 8.20: Comparative plasma drug concentration profiles of a) 5-ASA and b) N-Acetyl-5-ASA (n=5 in all instances). 227

Figure 8.21: Comparison of the composite SSZ plasma concentrations due to release from the MODDS and Salazopyrin® (n=5 in all instances). 228

LIST OF TABLES

Table 1.1:	Surface areas of the various regions of the GIT	2
Table 1.2:	Average residence time of food in various areas of the GIT	4
Table 1.3:	Hormones involved in appetite and satiation	6
Table 2.1:	Parameters for analysis of the resilience of SBPs	35
Table 2.2:	Parameters for the analysis of hardness and deformation energy of the SBPs	35
Table 2.3:	Relative size and mass of SBPs	38
Table 3.1:	Formulation variable limits and responses with objective	56
Table 3.2:	Experimental matrix generated by Box-Behnken statistical design	57
Table 3.3:	Drug entrapment of Box-Behnken DOE SBP formulations	62
Table 3.4:	ANOVA table depicting regression coefficients for QDE (mg) with accompanying p-values	66
Table 4.1:	JNC VI Criteria for Classification of Blood Pressure	75
Table 4.2:	Preparation of drug solutions	83
Table 4.3:	Minimum quantity of SBP required for *in vitro* drug release studies	85
Table 4.4:	Maximum excitation wavelength of drugs	89
Table 4.5:	Efficiency of SBP to entrap drugs with varying physicochemical properties	91
Table 5.1:	Conditions employed for controlled gelatinization of SBP	102
Table 5.2:	Preparation of drug crosslinking-drug solutions	103
Table 5.3:	Drug-loaded SBP quantities to be used for *in vitro* drug release study	105
Table 5.4:	Constitution of alkaline alcohol gelatinization mediums	106

Table 5.5: Determination of favorable hydration and crosslinking times in various gelatinization media 107

Table 5.6: Drug-loading and crosslinking time for DPH study 108

Table 5.7: Conditions employed for the entrapment of drug into oxidized SBP 112

Table 5.8: Effect of controlled gelatinization 115

Table 5.9: Effect of crosslinking of SBP on the hydration and drug entrapment 118

Table 5.10: Effect of hydration time and crosslinking time on the hydration of the SBP 122

Table 6.1: Variation of Drug-Loading Time and secondary Crosslinking Time 143

Table 7.1: Independent variable limits and desired responses of (3^2) FCCCD 159

Table 7.2: Design matrix for independent variables generated by the 3^2 factor FCCCD for double crosslinked SSZ-loaded SBP 160

Table 7.3: Measured responses for experimental SBP formulations 162

Table 7.4: Interpretation of $\boldsymbol{n}$ value with regard to the mechanism of drug release from delivery systems with differing geometries 166

Table 7.5: *In vitro* SSZ release kinetics of experimental formulations in SGF 168

Table 7.6: *In vitro* SSZ release kinetics of experimental formulations in SIF 168

Table 7.7: *In vitro* SSZ release kinetics of experimental formulations sequentially in SGF and SIF 169

Table 7.8: Difference and similarity factors of the SSZ release profiles of the experimental formulations 171

Table 7.9: ANOVA analysis indicated estimated regression coefficients and P-values for DEE and MDT 175

Table 7.10: Parameters employed for degassing and analysis of SBP samples 180

Table 7.11: Comparative DEE of predicted, experimental and scale up optimized formulations 183

Table 7.12: Effect of optimization on the surface area SBP 189

Table 7.13: Effect of optimization on the porosity of the SBP 189

Table 7.14: *In vitro* SSZ release kinetics of optimized SBP in SGF 196

Table 7.15**:** *In vitro* SSZ release kinetics of optimized SBP in SIF 196

Table 7.16: *In vitro* SSZ release kinetics of optimized SBP sequentially in SGF and SIF 196

Table 8.1: Parameters employed in the gradient elution UPLC method for the separation of SSZ, 5-ASA and N-Acetyl-5-ASA 212

Table 8.2: Recovery of analytes subsequent to various deproteinization and extraction methods 223

LIST OF EQUATIONS

Equation 2.1: Determination of Degree of Swelling of the SBP 33

Equation 2.2: Determination of Degree of change in mass of the SBP 33

Equation 2.3: Elucidation of the Resilience of the SBP 34

Equation 2.4: Detemination of the Drug Entrapment Efficiency of the SBP 37

Equation 3.1: Complete Regression Equation Representing the Relationship Between the Independent Variables and the QDE Response 66

Equation 4.1: Elucidation of the Quantity of Drug-Loaded SBP Required for *In Vitro* Drug Release Studies 84

Equation 7.1: Elucidation of the Time at which 50% of Drug is Released by Utilizing the Korsmeyer-Peppas Model 161

Equation 7.2: Quantification of the *In Vitro* Drug Release Employing the Model Independent Aproach of Mean Dissolution Time 161

Equation 7.3: Determination of the Fractional Drug Release According to the Zero Order Release Model 164

Equation 7.4: Determination of the Fractional Drug Release According to the First Order Release Model 164

Equation 7.5: Linearization of the First Order Release Model to determine the First Order Release constant and burst release 164

Equation 7.6: Determination of the Fractional Drug Release According to the Higuchi Model 165

Equation 7.7: Determination of the Fractional Drug Release According to the Korsmeyer-Peppas Model 165

Equation 7.8: Linearization of the Korsmeyer-Peppas Model to Determine the Experimental Constant and Diffusion Constant 166

Equation 7.9: Determination of the Fractional Drug Release According to the Hixson and Crowell Model 166

Equation 7.10: Elucidation of the Similarity of the Drug Release Profiles 170

Equation 7.11: Elucidation of the Difference of the Drug Release Profiles 170

Equation 7.12: Complete Regression Equation Representing the Relationship Between the Independent Variables and the DEE Response 176

Equation 7.13: Complete Regression Equation Representing the Relationship Between the Independent Variables and the MDT Response 176

Equation 7.14: Determination of the Total Surface Area of the SBP Employing the Brunauer-Emmett-Teller Method 180

Equation 7.15: Relationship Between the Partial Pressure, Monolayer Capacity of the Adsorbate and the Enthalpy of Adsorption in the First Adsorbed Layer 181

Equation 7.16: Calculation of the Enthalpy of Adsorption in the First Adsorbed Layer 181

Equation 7.17: Calculation of the Monolayer Capacity of the Adsorbate 181

Equation 7.18: Determination of Specific Surface Area Relating to the Quantity of SBP tested 181

Equation 8.1: Elucidation of the Peak Analyte:INH ratio in Water 214

Equation 8.2: Elucidation of the Peak Analyte:INH ratio in Plasma 214

Equation 8.3: Determination of the Extent of Analyte Recovery During Plasma Extraction 214

CHAPTER 1
RATIONALE FOR THE DESIGN AND DEVELOPMENT OF A STARCH-BASED MULTIPARTICULATE ORAL DRUG DELIVERY SYSTEM

1.1. Background into the Anatomy and Physiology of the GIT and Bioavailability of Orally Administered Drugs

The oral route presents the most convenient (Sugawara *et al.*, 2005; Scholz *et al.*, 2008) and the most widely used route (Gan *et al.,* 1997; Kimura and Higaki, 2002; Masaoka *et al.,* 2006; Streubel *et al.,* 2006; Mconnel*,* 2008; Custodio *et al.,* 2008) by which drugs can be delivered to the systemic circulation as the anatomy and physiology of the gastrointestinal tract (GIT) are favorable for absorption (Helliwell, 1993; Balimane *et al.,* 2000). The GIT is an open-ended hollow muscular tube that is broadly divided into the mouth, pharynx, esophagus, stomach, small intestine, large intestine, rectum and anus (Helliwell, 1993; DeSesso and Jacobson, 2001; Porth, 2007).

Even though absorption occurs throughout the GIT, the small intestine remains the area where the most substantial absorption occurs (Masaoka *et al.,* 2006). In addition to the high vascularization, the small intestine consists of a single columnar epithelium lining (enterocytes) with an extensively large surface area due to folds, depressions and villi (DeSesso and Jacobson, 2001; Macdonald and Monteleone, 2005). The surface area is further increased by the presence of microvilli on the enterocytes (Swenson and Curatolo, 1992). Figure 1.1 depicts the structure of the small intestine. In addition, Table 1.1 outlines the surface areas of different regions of the GIT.

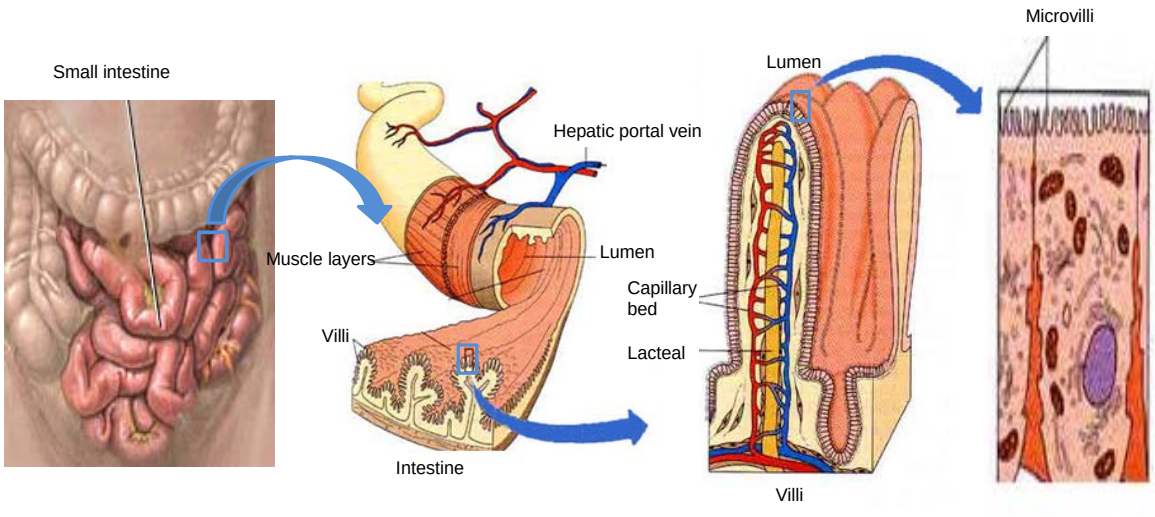


Figure 1.1: Structure of the human small intestine *(Adapted from Porth, 2007).*

Table 1.1: Surface areas of the various regions of the GIT

Region	Absolute surface area (m^2)	Relative surface area (m^2)
Body	1.8	-
Stomach	0.053	0.029
Small intestine	200	111
Large intestine	0.35	0.19

Adapted from DeSesso and Jacobson, 2001

The bioavailability of orally administered drugs is intrinsically related to the rate and extent of drug absorption from the lumen of the GIT (Custodio *et al.,* 2008). Absorption occurs as a result of drug passing from the lumen through the mucosa and into the systemic circulation. For this to occur, the drug must have sufficient solubility and stability within the gastrointestinal (GI) fluids and must be capable of permeating through the wall of the GIT (Swenson and Curatolo*,* 1992; Ezra and Golomb*.,* 2000; Davis*.,* 2005; Custodio *et al.,* 2008). Based on the permeability and solubility of the drug, the Biopharmaceutics Classification System (BCS) categorizes drugs into one of four classes, Class 1–Class 4, as depicted in Figure 1.2.

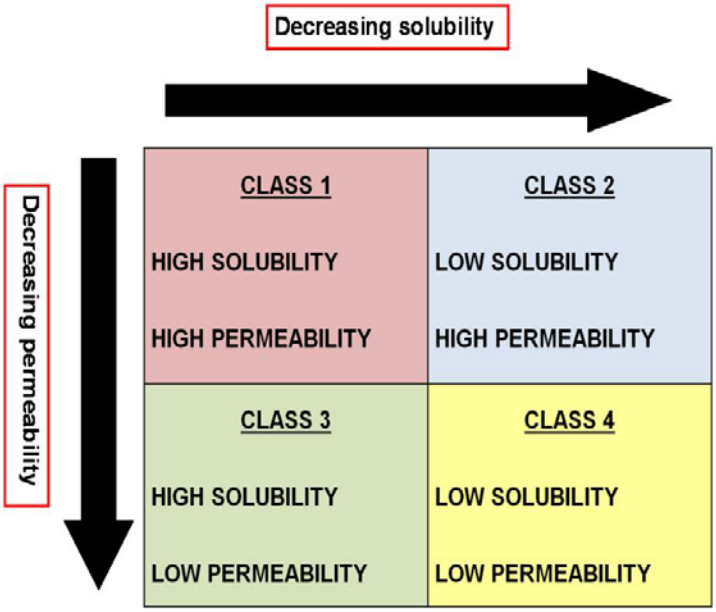


Figure 1.2: Biopharmaceutics Classification System (BCS) (*Adapted from Custodio et al., 2008).*

The solubility and stability of drugs within the GIT are influenced by both the physicochemical properties of the drug, which include the pKa; intrinsic solubility; surface charge; hydrophilicity; degradation potential and pH sensitivity (Sugawara *et al.,* 1998; Guo and Shen, 2004; Bhattachar *et al.,* 2006; Custodio *et al.,* 2008), as well as the environment of the GIT which varies according to region with regard to pH; luminal enzyme presence; fluid volume and bacterial colonization (Davis, 2005; Custodio *et al.,*

2008; McConnell, 2008). The intestinal wall provides a complex and highly dynamic barrier to the absorption of drugs (Gan *et al.,* 1997). This is due to the hydrophobic nature of the membranes of the enterocytes, site specific location of drug transporters, presence of efflux transporters such as P-glycoproteins and the presence of tight junctions between these epithelial cells, which maintains the integrity of the GIT epithelial lining (McConnell, 2008).

There are two basic routes by which drugs may be absorbed namely, transcellular and paracellular transport as depicted in Figure 1.3. In the transcellular route, drug is absorbed by moving through the enterocytes via simple diffusion, facilitated transport, active transport and pinocytosis (Ezra and Golomb, 2000; DeSesso and Jacobson, 2001; Escuder-Gilabert *et al.,* 2003; McConnell, 2008). In the paracellular route, drug is absorbed via small water filled channels called aquaporins situated within the tight junctions between epithelial cells. However, only molecules which are hydrophilic and small i.e. those up to molecular weight of 150g.mol^{-1}, can pass be absorbed via the paracellular route (Ezra and Golomb, 2000; Salama *et al.,* 2004).

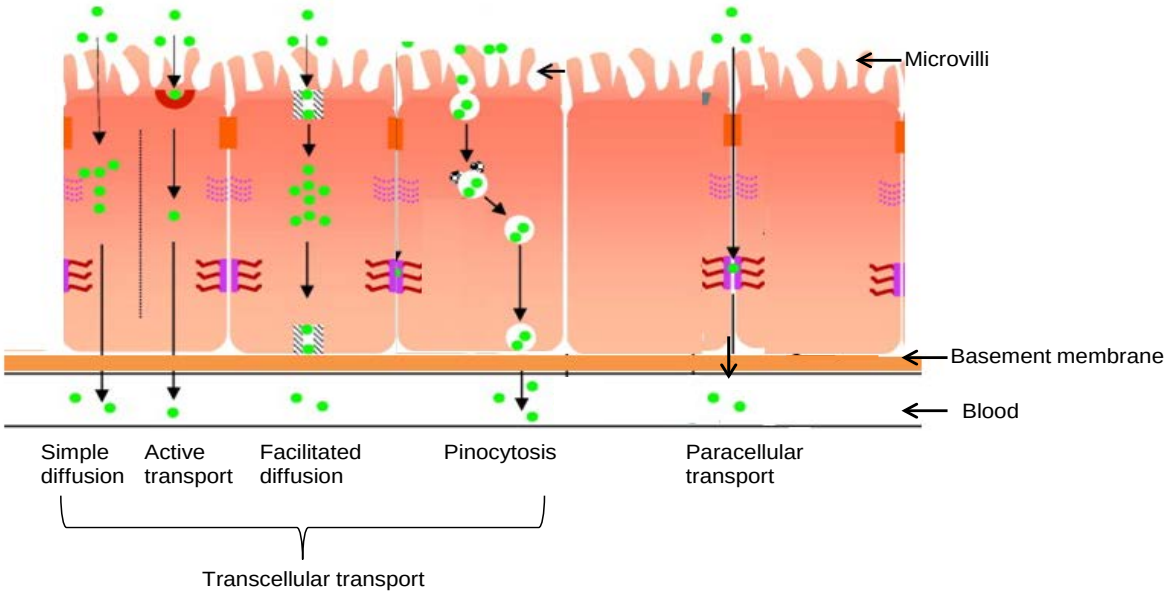


Figure 1.3: Mechanisms of drug absorption in the GIT. *(Adapted from Gaucher et al, 2007).*

The GIT, as mentioned previously, is a muscular tube, the function of which is the movement of food matter from the mouth to the anus. The motility of the GIT is dependent on vagal stimulation of the smooth muscle, activity of hormones, e.g. gastrin, disease state of the GIT and the presence of food within the GIT. The transit time of a dosage form through the different regions of the GIT has drastic consequences on the

bioavailability of the drug. This is especially true in cases where the solubility and stability of the drug is affected and where the drug has specific absorption sites (Robinson and Gauger, 1986; Fukudu *et al.,* 2006; Hoffman and Qadri, 2006; Sungthongjeen *et al.,* 2007). The GI transit times of a dosage form through different regions of the GIT is depicted in Table 1.2.

Table 1.2: Average residence time of food in various areas of the GIT

Gastrointestinal region	Mean residence time
Mouth	Seconds to minutes
Esophagus	Seconds
Stomach	~1-2 hours
Small intestine	~3 hours
Large intestine	~20 hours

Adapted from Balimane et al., 2000 and Davis, 2005

The bioavailability of drugs is further dependent on the extent of their metabolism prior to reaching the systemic circulation. Factors that affect metabolism include the drugs' susceptibility to cytochrome (CYP) enzymes in the GIT wall, the blood supply to the liver via the hepatic portal vein and the susceptibility of the drugs to hepatic metabolism. Drugs that are particularly lipophilic are more susceptible to the enzymatic metabolism and may thus display an inferior bioavailability (Lin and Lu, 1997). However, via the lymphatic vessels contained within the villi of the GIT, there exists a means by which very lipophilic drugs may avoid the first-pass hepatic metabolism resulting in enhanced bioavailability (Gershkovich and Hoffman, 2005; Yáñez *et al.,* 2011*).* There is therefore a need for drug delivery mechanisms that overcome GIT motility issues and which circumvent or reduce the extent of first-pass metabolism and thus lead to superior bioavailability and improved therapeutic outcomes.

1.2. Effects of Foods and Specific Macronutrients on the Physiology of the GIT

The breakdown of complex food molecules into their simpler constituents and the subsequent absorption of these nutrients is a normal physiological function of the GIT. Macronutrients in foods can be broadly categorized into three main groups viz. lipids, proteins and carbohydrates, each of which has a specific function within the body (Englyst and Hudson, 1996; Raybould, 1999; French and Cecil, 2001). The breakdown of these molecules occurs separately through unique processes, and the presence of both the parent molecules and breakdown products within the GIT may influence the physiology of the GIT (Charman *et al.,* 1997; Raybould, 1999).

Ingestion of food results in the stimulation of GI secretions and thus an increase in the volume of luminal fluids. This results in a greater ability for the nutrients to dissolve and thus be absorbed. Furthermore, these secretions alter the pH of the GIT with the effect of this alteration dependent on the region where the secretion occurs. For example, the presence of food in the mouth causes the release of saliva, which has a pH of 6.75, and within the stomach, the parietal cells secrete hydrochloric acid, which drastically lowers the pH to approximately 1.2. In the small intestine, the acidic chyme from the stomach interacts with bile salts and bile acids that are released from the gall bladder and pancreatic juices and bicarbonate that are released from the pancreas. The amount of these secretions depends on the relative acidity of the chyme and this interaction causes a partial neutralization of the chyme (Charman *et al.,* 1997).

The presence of food in the stomach reduces the motility of the GIT to allow the ingested food to mix with the gastric secretions and undergo adequate breakdown and digestion. Food also inhibits the housekeeping Migrating Myoelectric Complex (MMC) wave that is responsible for clearing out the undigested material during the fasted state (Davis, 2005; McConnell, 2008). The slowing down of gastric motility allows for increased time at the absorption sites facilitating improved nutrient absorption (Digenis *et al.,* 1977; O'Reilly *et al.,* 1984; Sangeker *et al.,* 1987; Digenis *et al.,* 1990; Davis, 2005). In addition to the secretion of saliva, food within the oral cavity stimulates the secretion of various juices within the GIT. This is known as the orosensory response and is dependent on the taste and palatability of the food. Thus, carbohydrates, lipids and proteins induce this response to different degrees. The orosensory response further affects the rate of gastric emptying and plays an important role in satiation (French and Cecil, 2001).

Food results in the release of many peptides that are involved in appetite and satiation (Karhunen *et al.,* 2008). Ghrelin, a peptide secreted most abundantly in the fundus of the stomach and the duodenum, stimulates the appetite. The secretion of ghrelin is inhibited by fatty acids of chain length greater than 12 carbons, carbohydrates and milk-based proteins. Meat-based proteins and short-chain fatty acids either have no effect or may increase ghrelin secretion (Vallejo-Cremades *et al.,* 2004). Cholecystokinin (CCK), a peptide released in the proximal intestine, stimulates satiation and decreases food intake. All the macronutrients stimulate its release but lipids and proteins have a greater effect than carbohydrates. Glucose-dependent insulinotropic polypeptide (GIP) induces satiation and its effects are most pronounced by fats and carbohydrates with little effect observed in the presence of proteins. Glucagon-like peptide 1 (GLP-1) is co-released with GIP and thus demonstrates the same effects as GIP. However, proteins induce its secretion to the

largest extent followed by carbohydrates and lastly lipids (Blom *et al.,* 2006; Andrews *et al.,* 2007; Pilichiewicz *et al.,* 2007; Karhunen, *et al.,* 2008).

Peptide YY (PYY), a gut hormone released by the intestine, stomach and pancreas, is involved in the gut-brain axis and stimulates satiation and insulin secretion. All macronutrients stimulates its release although different studies have displayed contrasting degrees of stimulation by carbohydrates, proteins and lipids (Karhunen *et al.,* 2008, Torres *et al.,* 2009; Clegg *et al.,* 2012; Holzer *et al.,* 2012). CCK, GIP and PYY all have a role to play in the ileal brake mechanism, which slows down gastric emptying and intestinal motility. Insulin, a major anabolic hormone and energy regulator is secreted in response to food in the GIT. Only simple monomeric molecules, the final digestion product of food breakdown, stimulate its release with short chain fatty acids and amino acids only stimulating its release in the presence of glucose. Pancreatic polypeptide (PP) is a gut hormone released from the pancreas in response to ingestion of food and functions to stimulates satiation and reduce appetite and food intake with all macronutrients stimulating its release (Batterham *et al.,* 2003; Karhunen *et al.,* 2008; Holzer *et al.,* 2012). A summary of the hormones involved in appetite and satiation is depicted in Table 1.3.

Table 1.3: Hormones involved in appetite and satiation

Peptide	Primary function	Secondary function	Effect of macronutrients on secretion of GI hormones		
			Carbohydrates	Proteins	Lipids
Ghrelin	Stimulates appetite	Increase motility Decrease insulin secretion	Inhibits	Stimulates and inhibits	Stimulates and inhibits
CCK	Stimulates satiation	Slows gastric emptying Stimulates ileal brake	Stimulates	Stimulates	Stimulates
GIP	Stimulates satiation	Increases insulin secretion	Stimulates	Stimulates	No effect
GLP-1	Stimulates satiation	Increases insulin secretion Stimulates ileal brake	Stimulates	Stimulates	Stimulates
PYY	Stimulates satiation	Increases insulin secretion Stimulates ileal brake	Stimulates	Stimulates	Stimulates
Insulin	Stimulates satiation	Energy intake regulation	Stimulates	Stimulates	Stimulates
PP	Stimulates satiation	Energy intake regulation Decrease gastric emptying	Stimulates	Stimulates	Stimulates

Where CCK denoted Cholecystokinin, GIP denoted Glucose-dependent insulinotropic polypeptide, GLP-1 denoted Glucagon-like peptide 1, PYY denoted Polypeptide YY and PP denoted Pancreatic Polypeptide

Furthermore, food stimulates an increase in blood and lymphatic flow to the GIT, which results in the absorbed nutrients being transported away from the absorption site thus maintaining sink conditions (Charman *et al.,* 1997). The individual nutrients also have specific effects on the physiology of the GIT.

1.2.1. Effect of lipids on the physiology of the GIT

Lipids and lipid breakdown products which include triglycerides, diglycerides, monoglycerides, glycerol and free fatty acids stimulate the release of CCK, which mediates the release of bile from the gall bladder and pancreatic enzymes from the pancreas (Charman *et al.,* 1997; McLaughlin *et al.,* 1999; Matzinger *et al.,* 2000). These compounds also stimulate the secretion of phospholipids and cholesterol into the GIT, both of which are important for the digestion and absorption of lipids (Porter and Charman, 2001).

Dietary fats and partially digested lipids, particularly long chain (≥12 carbons) fatty acids, delay gastric emptying and have been shown to reduce the motility of the GIT by a phenomenon known as the ileal brake (Davis, 2005). This feedback mechanism, which relies on stimulation of sensors in the intestinal wall by GI peptides, allows for increased digestion and absorption time in the proximal GIT by delaying gastric emptying and slowing peristalsis (Raybould, 1999; Dobson and Jacobson, 2000; Gentilcore, *et al.,* 2006). The effect of lipids on the secretion of GI fluids and motility can be both direct (through mechanisms not established) and indirect (as a result of gastrointestinal regulatory peptides).

Lipid digestion products interact with the GI membrane where they act as permeability enhancers and facilitate absorption of nutrients. The lipids that enter the enterocytes influence intestinal efflux proteins and stimulate lymphatic absorption and transport which results in higher plasma concentrations of lipids and other nutrients (Porter and Charman, 2001).

1.2.2. Effect of proteins on the physiology of the GIT

Among the macronutrients, proteins exert the greatest effect on satiation (French and Cecil, 2001; Blom *et al.,* 2006; van Erk *et al.,* 2006). This is because of increased amino acid concentration in the GIT. Proteins release CCK, which slows down gastric emptying rate, as well as other gut hormones that regulate physiological GI processes.

1.2.3. Effect of carbohydrates on the physiology of the GIT

Carbohydrates are polymers that consist of anywhere between one and hundred monomeric sugar units. Oligosaccharides are composed of 3-20 units and their presence in the GIT enhances the metabolism of lipids and other carbohydrates. Non-digestible oligosaccharides decrease colonic pH; stimulate the proliferation of colonic commensals thus promoting fermentation of foods and enhancement in the absorption of certain minerals (Roberfroid and Slavin, 2000; Mussatto and Mancilha, 2007).

Non-digestible starch and oligosaccharides, resistant starch and sugar alcohols that reach the colon alter the absorption of nutrients and the motility of the GIT (Salminen *et al.,* 1998). These molecules elicit their effect due to their physicochemical properties that include viscosity-enhancing effects, osmotic effects and water holding capacity (Cloetens *et al.,* 2008). Lactulose, gums and pectin absorb water from the GIT and swell causing an increase in pressure on the GI walls thus stimulating peristalsis. The increased motility may result in reduced contact time of nutrients with their absorption site. These substances additionally increase the viscosity of the luminal fluids and may impair the diffusion of entrapped nutrients to the mucosa. This, together with the greater motility of the GIT, results in a diminished absorption of food (Schuster-Wolff-Bühring *et al.,* 2010).

Carbohydrates exert a much more marked effect on satiation than lipids (French and Cecil, 2001; van Erk *et al.,* 2006). Glucose in the small intestine stimulates the release of CCK but to a lesser degree than lipids and proteins (Pilichiewicz *et al.,* 2007). Glucose in the proximal intestine slows down gastric emptying by inhibiting antral and duodenal pressure waves and by increasing pressure at the pyloric sphincter (Pilichiewicz *et al.,* 2007).

1.3. Effects of Concurrent Administration of Food and Drug Formulations

The food-induced alterations of the physiology of the GIT have implications for the bioavailability of many drugs and thus knowledge of such changes is important in establishing the bioavailability and subsequent efficacy of a drug and/or a dosage form when co-administered with food. Additionally food-drug and food-excipient interactions may have a further influence on the effectiveness of a dosage form from both a safety and efficacy viewpoint (Custodio *et al.,* 2008). Food-drug interactions may be a result of physicochemical interactions between food components and/or food induced GI secretions and the drugs and/or drug delivery systems. These interactions may be

beneficial, detrimental or have no effect on the bioavailability and subsequent clinical efficacy of the drug (Sakuma *et al.,* 2007).

Food and their breakdown products have the ability to increase the bioavailability of drugs when co-administered. This phenomenon is attributed to an enhancement in the permeability of the GI epithelial lining and is often observed with medium chain glycerides and N-acyl-amino acids e.g. N-acyl-glycine and N-acyl-alanine (Swenson and Curatolo, 1992). The mechanisms by which these substances increase permeability relate to interactions with the paracellular pathways as well as through interactions with transport proteins located on the cell membranes. Besides acting as permeability enhancers, lipids interact with bile salts and thus increase the effective luminal solubility of drugs, which allow them to be absorbed. They further influence intestinal efflux proteins and stimulate lymphatic absorption and transport of the drugs thus maintaining sink conditions ultimately resulting in increased bioavailability of drugs (Porter and Charman, 2001).

The presence of food in the stomach delays gastric motility and may thus lead to an improvement in bioavailability of drugs (Davis, 2005). This is due to an increase in the time available for adequate solubilization of drug within the GI fluids and an increase in time at the absorption sites. With regard to this, the concurrent administration of food with drugs displaying a narrow absorption window may theoretically increase the bioavailability of these drugs. Propranolol, a drug displaying a narrow absorption window, and hydralazine are examples of drugs that achieve higher bioavailability when administered with food (Winstanley and Orme, 1989). Other important examples of the enhancing effect on the absorption of food include griseofulvin and nitrofurantoin, which show low bioavailability in the fasted state and substantial increase in absorption when administered with a fatty meal. Fatty foods increase the solubilization of griseofulvin while the increased bioavailability of nitrofurantoin is due to slowing down of gastric motility (Winstanley and Orme, 1989).

On the other hand, many drugs show negative food-drug interactions. A typical example is seen with biphosphonates where the oral bioavailability is low and is further reduced by the presence of food in the GIT. This reduction could be due to food-facilitated decrease in the solubility of biphosphonates or inhibition of its paracellular absorption. Certain products such as orange juice and caffeine decrease bioavailability of biphosphonates. Furthermore, calcium, iron and magnesium, which are found in various foods, are believed to form complexes with biphosphonates, which further retards its absorption (Ezra and Golomb, 1999). Another example was found in the work of Digenis and co-

workers (1990) who demonstrated that food reduced the peak plasma concentration, bioavailability and time to peak plasma concentration of erythromycin base when given within 2 to 4 hours of a meal.

Recently, Sommers and co-workers (1984) showed that alcohol and caffeine, which are often consumed with meals, have both an effect on absorption, as seen with the biphosphonates, as well as on the pharmacological effects of drugs. Examples of these effects are evident by the increased risk of GI complications associated with concurrent administration of NSAIDS and alcohol (Neutel and Appel, 2000); increased central nervous system depression with alcohol and benzodiazepine use (Lau and Falk, 1991) and synergistic impairment of motor function resulting from caffeine and midazolam co-administration (Lau and Falk, 1991).

Lastly, there are drug formulations that are not affected by the presence of food, either with regard to bioavailability or to their pharmacodynamics. This was shown by Kenyon and co-workers (1995) who developed a sustained release formulation for the NSAID, naproxen, in which the bioavailability of the drug was not affected by the presence of food.

1.4. Employment of Macronutrients in Drug Delivery

1.4.1. Employment of lipids in drug delivery

Lipids in the forms of cholesterol, triglycerides, monoglycerides, fatty acids, micro-emulsions and lecithin to name a few have been used extensively as drug delivery devices or adjuncts to such devices. The major use of lipids as drug carriers stem from their ability to improve the solubilization potential of poorly water-soluble drugs thereby, enhancing the drugs' *in vivo* formulation characteristics (Chen *et al.,* 2008). The absorption of such formulations is further enhanced by the stimulation of lymphatic transport whereupon the lipid-based formulations' distribution may be facilitated by lipoproteins within the body (Chen *et al.,* 2008; Mconnel, 2008). Furthermore, lipid breakdown products within the intestine act as permeation enhancers and thus offer a further advantage to their use in drug delivery (Swenson and Curatolo, 1992).

Liposomes are common lipid-based formulations and are used in applications as complex as gene delivery. These formulations are composed of drug-loaded vesicles that are soluble in biological fluids. Weiner (1989) conducted a complete review of the characterization, compatibility and use of liposomes in the administration of peptides.

Mishima (2008) described the development of soy lecithin liposomes by the supercritical technique with the employment of the anti-fungal drug, miconazole, as the model drug. Optimization of drug entrapment was discussed without any clinical data being included. Grigoriev and Miller (2008) formulated drug carrying emulsion droplets with impressive stability, even in the presence of the destabilizing drug, indomethacin. This was achieved by incorporating anionic phospholipids and medium chain triglycerides as binary mixtures into the interfacial films, which resulted in very large negative zeta potentials thus stabilizing the formulation.

Nnamani and co-workers (2010) conducted an investigation using three different lipid matrices consisting of two natural homolipids from *Capra hircus* (goat fat) and *Bovine Spp*. (tallow fat) and one semi-synthetic lipid (Softisan® 142) separately structured with Phospholipon® 90G (P90G) as a potential drug delivery system for poorly water-soluble drugs. They analyzed the different lipid matrices by differential scanning calorimetry (DSC) and measured the enthalpies of the lipid matrices permitting them to conclude that the natural lipids with an enthalpy of $-2.813 mW.mg^{-1}$ favored drug-loading of some poorly water-soluble drugs more than the semi-synthetic lipids.

1.4.2. Employment of proteins and peptides in drug delivery

Proteins are known to be complex structures possessing hydrophilic and hydrophobic groups and this feature is exploited in the stabilization of emulsions. Peptides interact with each other to form an interfacial film, which may protect drug-loaded emulsions from enzymatic degradation by sterically hindering access of the enzymes to the drug particles (Grigoriev and Miller, 2008).

The development of intravaginal drug delivery systems using polypeptides as drug carriers has recently received immense attention due to their biodegradable nature and non-toxic degradation products. Leong and Langer (1987) reviewed the use of poly(glutamic) acid as a pendant delivery system to be used as a contraceptive device as well as to treat certain cancers by conjugation with a drug. As a contraceptive device, it showed release for 4 months in rats and as a cancer therapy, it demonstrated superior cell growth suppression compared to the drug alone. Similarly, formulations containing copolymers of glutamic acid and ethylglutamate have shown controlled release of levonorgestrel for up to 8 months (Leong and Langer, 1987).

In a different study conducted by Jin and Kim (2008), oppositely charged gelatin and ethylcellulose was combined to form a complex coacervate gel and further co-formulating

the complex coacervate with thermo-reversible polymers for the delivery of biomacromolecules. The combination of complex coacervate and thermo-reversible polymer demonstrated synergistic effects on the *in situ* gel depot formation and release rates of model proteins incorporated within the gel matrix. Gels indicated sustained release patterns of the protein over 25 days with minimal initial bursts. Stable complex coacervate formations between the gelatin protein and oppositely charged polyelectrolytes depending on their isoelectric points were critical to achieve sustained protein release from the *in situ* gel depot. These protein-based systems demonstrate a potential for efficient protein drug delivery, in terms of high protein loading, sustained protein release, ease of administration, and an aqueous environment without toxic organic solvents (Jin and Kim, 2008).

Recently there has also been advancement in preparing microgels and microcapsules using proteins and peptides for drug delivery. Microgels are lightly crosslinked gel particles with an ability to change their volume drastically in response to changes in their environment, which include pH, ionic strength, temperature, presence of specific ions and other compounds, redox conditions, or through external fields. This enables microgels to incorporate host molecules through various mechanisms and subsequently release the entrapped molecule in response to specific stimuli. The host molecules in these protein microgels include drugs, nutraceuticals, proteins, peptides and other biomacromolecular drugs. Compared to microgels, microcapsules consist of a shell, formed by incorporating peptides and alternating cationic and anionic polyelectrolytes, and a core containing the drug either in aqueous solution or in its solid state. Due to this lack of connectivity throughout the particle, microcapsules do not generally display abrupt volume transitions as seen in microgels, and controlling drug release is achieved by controlling shell permeability to incorporated drugs. The review conducted by Bysell and co-workers (2011) discussed the different characteristic of microgels and microcapsules and positively emphasizes their use in protein and peptide-based drug delivery systems.

1.4.3. Employment of carbohydrates in drug delivery

Polysaccharides are polymers that are natural or semi-synthetic and include starches, alginates, cellulose derivatives, dextrans, gelatin, pectin, chitosan, poly(acrylic acids) and xanthan gum (Helliwell, 1993). Polysaccharides have been applied extensively in drug delivery due to their natural origin, low cost, biocompatibility and ability to be easily modified. Their ability to act as drug carriers is influenced by their charge, molecular weight, structural composition and branching and have been employed in the delivery of drugs ranging from small molecules to large proteins (Pasut and Veronese, 2007).

1.4.3.1. Employment of cellulose in drug delivery

Cellulose is a polysaccharide that makes up the cell walls of plants and is indigestible by humans due to the absence of the enzyme responsible for its breakdown in the GIT. Cellulose displays very hydrophobic behavior but can be chemically modified to alter its physical properties. Medically, cellulose and its analogues have been used in applications such as wound healing products, controlled drug delivery and bone scaffolding technology (Levy *et al.,* 2004).

Sodium carboxymethyl cellulose (CMC), a modified cellulose derivative, has been used to deliver spermicides to the vagina due to its mucoadhesive properties (Valenta, 2005). Other cellulose derivatives such methylcellulose (MC), hydroxypropyl cellulose (HPC) and hydroxypropylmethyl cellulose (HPMC) have been employed as mucoadhesive polymers for the delivery of a wide range of antimicrobials to the vaginal tract. Valenta (2005) further described the use of these polymers for the delivery of anticancer agents as well as prostaglandins for the induction of uterine contractions.

The mucoadhesive characteristics displayed by cellulose derivatives was the basis for employing CMC by Ugwoke and co-workers (2000) as an intranasal drug delivery system employing apomorphine as the model drug. Apomorphine is usually used as a subcutaneous injection in the treatment of Parkinson's disease but has to be administered often due to its short half-life. The CMC intranasal system developed displayed a bioavailability comparable to the conventional treatment in addition to maintaining plasma concentrations. However, the intranasal route and the sustained release simplified dosing and provided a less invasive route of delivery.

Surelease® is a coating material that is composed of ethylcellulose and amylose and has been found to provide very specific colonic drug release (Leong *et al.*, 2002; McConnell, 2008). Lin and co-workers (2002) utilized ethylcellulose in the formulation of compression-coated tablets and found that the size of the ethylcellulose particles played an important role in the physical characteristics of the tablets. Further studies were conducted on these tablets in combination with various other polymers and osmotic agents in an attempt to develop a time-controlled delivery device. They further found that in addition to ethylcellulose, the concentration of osmotic agent in the formulation played an important role in the lag phase and thus on the control of drug release (Lin *et al.,* 2002).

1.4.3.2. Employment of chitosan in drug delivery

Chitosan is a derivative of chitin, a natural polymer found in the exoskeletons of crustaceans, and is composed of N-acetyl-glucosamine and N-d-glucosamine monomers (Senel and McClure, 2004; Mishima, 2008; Springate *et al.,* 2008). Chitosan has been shown as a promising candidate for use in drug delivery due to its biocompatibility, biodegradability and lack of toxicity (Mi *et al.,* 2002). There have been several reported uses of chitosan in delivering genes to the body via complexation, thus enabling the control of their release *in vivo* (Mishima, 2008; Springate *et al.,* 2008). Senel and McClure (2004) reviewed the veterinary use of chitosan and described the advantages of its use in applications from wound healing to vaccine delivery.

Pharmaceutically, the cationic form of chitosan has been shown to possess the ability to adhere to the mucous membranes of animals (Davis, 2005). Crcarevska and co-workers (2008) made use of this physical property and designed a microparticulate colonic drug delivery system composed of chitosan and calcium alginate. The system possessed bioadhesive capability and furthermore, the microparticles were coated with Eudragit® S100 that ensured the system only adhered to the colonic mucosa. Budesonide, a corticosteroid, was used as the model drug and displayed favorable entrapment and release profiles.

Furthermore, due to its cationic nature and presence of hydroxyl, carboxylic and amino groups, chitosan has been employed as a mucoadhesive material for vaginal delivery of various drugs. Impressively, these functional groups can be further modified in order to enhance the physicochemical properties while retaining the biocompatibility and biodegradation of chitosan (Sajomsang *et al.*, 2009). Modified chitosan also possesses the ability to control the rate of drug release and its intrinsic antimicrobial properties against *Candida albicans*, makes its use in vaginal drug delivery systems even more advantageous (Valenta, 2005).

The flexibility of chitosan is further demonstrated by its use as a coating material and absorption enhancer (Salama *et al.,* 2004; Davis, 2005). Yu and co-workers (2008) used chitosan to reinforce alginate microparticles that further acted to retard and sustain the release of 5-fluorouracil and tegafur from both an injectable and oral delivery system. Mi and co-workers (2002) developed an intramuscular sustained release delivery system composed of Chitosan-genipin crosslinked microspheres and found minimal inflammation at the injection site. The microparticles showed very promising release and degradation profiles (Mi *et al.,* 2002). In addition to microparticles, Dung and co-workers (2007)

developed chitosan nanoparticles containing antisense oligonucleotides and applied it to the treatment of periodontal disease. The released oligonucleotides were stable enough for 12 hours under the 20% saliva solution and suggest that the sustained release of oligonucleotide from chitosan nanoparticles may be suitable for the local therapeutic application in periodontal diseases.

An osmotically active colonic drug delivery system using chitosan was also developed by Liu and co-workers (2007). This system was enteric coated which prevented acid breakdown and contained a semi-permeable membrane that permitted fluid entry into the delivery system into the colon and was specifically broken down by colonic microorganisms thus facilitating release of the model drug, budesonide, at a controlled rate up to 24 hours. Transdermal cosmetic patches for the delivery of tamarind fruit extracts were also developed where the polymeric matrix of the patch was formulated by crosslinking chitosan with various starches at different ratios. The entrapment and release data obtained from these formulations varied considerably (Viyoch *et al.,* 2003; Viyoch *et al.,* 2005; Boriwanwattanarak *et al.,* 2008).

1.4.3.3. Employment of various starches in drug delivery

Starch, a mixture composed mainly of highly branched amylopectin and linear chains of amylose is one of the most abundant food sources in the world and its importance is emphasized by its utilization as the staple diet of many populations. Starches are biodegradable, biocompatible, widely available and cost-effective which make them attractive candidates to be employed in novel drug delivery systems (Muadklay and Charoenrein, 2008). Furthermore, starches can be modified and are thus available in numerous forms and compositions allowing them to be utilized for various applications within the pharmaceutical industry (Tuovinen *et al.*, 2004).

Based on these advantages, starch has been used in pharmaceutical applications ranging from use as basic excipients in formulations to advanced applications such as in orthopedic implants, bone tissue scaffolding technology, micro-spherical nasal and parenteral devices and mucoadhesive buccal drug delivery systems (Hamdi *et al.,* 1998; Geresh *et al.,* 2004; Levy *et al.,* 2004; Balmayor *et al.,* 2008). Glucose, the monomeric moiety of starch polymers, has been used to enhance drug delivery as demonstrated by its incorporation in a gastrointestinal insulin delivery formulation (Leong and Langer, 1987). Starches obtained from various plants sources contain different ratios of amylose and amylopectin resulting in varying physicochemical properties and thus different pharmaceutical applications (Oh *et al.,* 2008).

1.4.3.3.1. Pea starch

Milojevic (1996) developed a starch-based coating derived from pea starch amylose for the delivery of drugs to the colon. The release of drug from the system was accomplished by means of bacterial metabolism of the starch-based coating within the colon. A similar study was conducted by Wilson and Basit (2005) to explore the utility of the coating for colonic targeting of single unit tablet systems. Amylose from pea starch was combined with the water-insoluble polymer, ethylcellulose, with 5-amino salicylic acid employed as the model drug. Drug release was facilitated by bacterial digestion of the amylose component of the film coat producing pores for drug diffusion. These studies indicated that pea starch amylose coated tablet formulations were promising methods for drug delivery to the colon (Milojevic, 1996; Wilson and Basit. 2005).

In a recent investigation surveyed by Bialleck and Rein (2011), spherical starch pellets were directly produced using hot-melt extrusion and die-face pelletization. Pellets were produced utilizing pea starch, four different active ingredients (ibuprofen, paracetamol, phenazon and tramadol-HCl) and various additives with the drug either dispersed or dissolved in the starch melt. The resulting pellets exhibited good mechanical stability, low porosity and small surface areas. Pellets with a very narrow particle size distribution and particle sizes even in the micron scale were produced. The pellets could be dispersed and was deemed well suited for use in pediatrics and geriatrics (Bialleck and Rein, 2011).

1.4.3.3.2. Maize/ corn starch

Chen and co-workers (2007) developed a tablet coating utilizing acetylated maize starch for the delivery of porcine serum albumin. The coating showed a good degree of swelling and hydration and was resistant to degradation in the proximal GIT. The coating displayed good albumin release in the colon, and was thus proposed to be used for colonic delivery of macromolecules (Chen *et al.,* 2007).

Balmayor and co-workers (2008) developed corn starch-polycaprolactone microparticles for the delivery of dexamethasone to bones. The system relied on enzymatic degradation by α-amylase and lipase for release of drug and showed only 48% drug release after 30 days. Ameye and co-workers (2001) made use of waxy corn starch and rice starch to synthesize starch-*g*-poly(acrylic acid) copolymers and starch/poly(acrylic acid) mixtures in order to deliver proteins via the oral route. These modified starches had an inhibitory effect on trypsin and bound divalent Calcium and Zinc ions thus displaying potential to be used in drug delivery (Ameye *et al.,* 2001).

Silva and co-workers (2005) developed corn starch-polylactic acid microparticles that were non-cytotoxic and possessed the ability to release corticosteroids for up to 30 days. The mechanism of drug release from the microparticles was attributed to initial hydration and thereafter to matrix erosion. A sustained release drug formulation by etherification of high amylose corn starch was developed by Nabais and co-workers (2007). Addition of sodium chloride to the formulation substantially improved the integrity of the tablet in acidic medium and provided an almost linear drug release profile. Brouillet and co-workers (2007) used a similar approach employing corn starch and developed a starch-based excipient as a spray drying coating. This coating formed a gel layer on the surface of the tablet and displayed almost linear drug release that was based on diffusion of drug out of the tablet.

1.4.3.3.3. Potato starch

Starch capsules made from potato starch have been developed and show characteristics similar to those of gelatin capsules but possess the added advantage of being a non-animal derived material. Other advantages include greater stability against moisture, pH independent dissolution as well as a greater potential to be enteric coated (Vilivalam *et al.,* 2000).

Te Wierik and co-workers (1997) developed an excipient for the controlled release of drugs from tablets by enzymatically degrading pregelatinized potato starch. The resultant tablets' porosity and ability to control drug release could be manipulated to achieve specific drug release profiles. Tuovinen and co-workers (2004) used potato starch in an acetylated form in order to formulate microparticles with calcein as a model drug. This modification to the starch caused reduced swelling and enzymatic breakdown. Thus, the incorporation of α-amylase into the system was used to induce the degradation of the starch microparticles and ultimately facilitate the release of calcein from the formulation.

1.4.3.3.4. Tapioca starch

Native and modified tapioca starches are natural biopolymers widely used as fillers, binders and disintergrants for tablet production (Casas *et al.*, 2009). Various studies suggest that hydrocolloids modify gelatinization and retrogradation behaviors of starch, which contribute to the thickening and stabilizing effects and texture of tapioca starch. This interaction results in gels, pastes and thickened mixtures of tapioca starch which can be employed in pharmaceutical applications such as emulsifiers and creams (Ratnayake and Jackson 2006; Sae-kang and Suphantharika, 2006).

Atichokudomchaia and Varavinita (2002) performed a study that suggested that tablets prepared from acid-modified crosslinked tapioca starch were superior to those prepared from acid-modified tapioca starch. In a further study, Atichokudomchaia and co-workers (2004) discovered that the acid-modified tapioca starches could potentially be used as a tablet filler in the direct compression process as the acid modification increased the mechanical strength of tablets.

Tapioca starch graft copolymers was studied by Casas and co-workers (2009) to determine the drug release of systems prepared with EMA copolymers as matrix-forming materials and anhydrous theophylline as model drug. All tablets behaved as inert matrices controlling drug release mainly by diffusion.

1.4.3.3.5. Sago starch

Over the past decade, sago starch has been studied for potential applications in the controlled release of therapeutic agents. Tay and co-workers (2012) synthesized water-soluble crosslinked starch-maleate monoester gel particles from native sago starch using nontoxic precipitating media (ethanol, propan-2-ol, or butan-1-ol). They showed potential utility of starch-maleate gel particles as drug delivery carriers in biomedical applications.

Sago starch is an interesting substrate for the production of cyclodextrans (CD), which are important modified polysaccharides due to its unique hydrophobic interior cavity and hydrophilic exterior. CD can encapsulate hydrophobic organic substances and aid its solubilization in water, which is useful in pharmaceutical applications (Singh *et al.*, 2004). In a study surveyed by Singhal and co-workers (2008) it was found that modified sago starch was more useful than native starch as modification lead to higher retrogradation resulting in the formation of a long cohesive gel with increased syneresis. Modifying sago starch can be done by crosslinking the sago starch, which reinforced the granule of starch to be more resistant towards acidic medium, heat and shearing, while hydroxypropylation improves its freeze-thaw or cold storage stability, which can assist in improving the delivery method of certain drugs. Sago starch can also be modified by acid hydrolysis at an ambient temperature to form highly crystalline starch, which increases the hardness of the tablet (Singhal *et al.*, 2008).

Sago starch can also be employed as a flavor-encapsulating agent. To achieve this, sago starch is hydrolyzed partially by thermostable α-amylase, and then reacted with stearic acid to give pregelatinized hydrolyzed sago starch stearate, which can be used as an encapsulating agent for both water-soluble and water-insoluble flavors. Capsules

produced from sago starch have been used successfully to protect various entities such as living microbes or enzymes against the effect of the environment or the intestine during drug delivery (Singhal *et al.*, 2008). Sago starch has been used as a tablet binder in certain formulations and evaluation of the binding property of sago starch in comparison with various commercial binders such as corn starch, tapioca starch, pregelatinized starches and polyvinylpyrrolidone showed sago starch to prolong the disintegration by ~19.3 min as compared to about 5 min for other samples (Singhal *et al.*, 2008).

Absorbents including ampholytic, anionic, cationic, nonionic and zwitterionic polymers are used in medicine and in drug delivery, where water absorbency or water retention is important. In a study conducted by Lutfor and co-workers (2001), a series of poly(hydroxamic acid) absorbent from poly(methyl acrylate) (PMA) grafted sago starch had been prepared, which contained various concentrations of sago starch. They studied the swelling behavior of these absorbents in distilled water and various salt solutions to investigate the absorbent properties of sago starch and grafted sago starch in order to determine its applicability to medical wound dressings and drug delivery patches.

Nanoparticles and their application in drug delivery has been a dynamic field of research due to their unique ability to target the specific region of interest. Various synthesis methods have been attempted to prepare nanoparticles from starch or starch derivatives. Due to its simplicity and reproducibility, the nano-precipitation technique has been explored for the preparation of synthetic polymer nanoparticles such as poly(lactic acid) (PLA) and poly(lactic-co-glycolic acid) (PLGA) nanoparticles. Chin and co-workers (2011) reported on the synthesis of starch nanoparticles with controllable particle sizes from native sago starch using the nano-precipitation method. Starch nanoparticles were instantaneously produced in this one-step precipitation process with controllable particle size and shape obtained by optimizing the precipitation conditions, which included the rate of starch precipitation and the use of surfactants during precipitation.

In all of the above-mentioned applications, native or modified starches in the form of powders have been used. However, sago and tapioca starches are commercially available as food grade pearls/pellets and by using these starches in this form, offer a novel means to develop a Multiparticulate Oral Drug Delivery System (MODDS). Thus, in the development of the MODDS proposed in this dissertation, evaluation of the commercially available Starch-Based Multiparticulates will be carried out to determine the Starch-Based Multiparticulates with the greatest potential to be used as the Starch-Based Platform (SBP) in the MODDS. Furthermore, a suitable model drug will be determined

and application of various modification techniques to the SBP, while still maintaining the multiparticulate nature of the SBP, will be performed in order to enhance functionality of the SBP and thus the efficacy of the model drug incorporated into the MODDS.

1.5. Rationale and Motivation for the Study

The rationale for using the Starch-Based Multiparticulates derived from tapioca and sago as the drug delivery platform in the MODDS is that it eliminates the process and cost associated with formulation of a core from which drug would be released. The wide availability and low cost of the SBP offer an added advantage to their use (Muadklay and Charoenrein, 2008). The SBP also offers physicochemical and physicomechanical characteristics that are favorable to the development of a MODDS with the inherent ability to hydrate, swell and float in gastric juices. The MODDS will be composed of natural materials primarily starch which makes the formulation biocompatible and biodegradable as the GIT contains enzymes such as amylase which naturally metabolizes starch (Muadklay and Charoenrein, 2008). Furthermore, the natural functionality of the SBP will be improved by accentuating its pore forming, gel forming and swelling abilities to facilitate drug incorporation into the SBP. The SBP can be modified in various ways to improve its stability, drug loading potential as well as drug release characteristics. All of these factors offer novelty and advantageous outcomes and thus promote the use of these SBPs as the platform in a MODDS.

1.6. Aim and Objectives

This study aimed to develop a drug delivery system prepared primarily from commercially available food grade starch, obtained from tapioca and/or sago to be administered as multiparticulates via the oral route in order to improve the therapeutic outcomes of drugs currently available.

In order to achieve the above-mentioned aim, the following objectives have been outlined:

1) To elucidate the physicochemical and physicomechanical properties, including structure; morphology; hydration capacity; and functional characteristics such as drug-loading and control of drug release, of the tapioca and sago multiparticulates in order to establish an optimal SBP choice.
2) To select suitable model drugs with different BCS classifications for employment within the MODDS.

3) To determine the modification techniques which impart the most advantageous properties onto the SBP.
4) To optimize a method of incorporating adequate quantities of the model drug into the SBP and establishing the mechanisms through which drug will be released.
5) To conduct *in vitro* studies in order to evaluate drug release and integrate the SBP into an appropriate MODDS.
6) To conduct *in vivo* studies on a suitable animal model in order to predict the bioavailability and clinical efficacy of the newly developed MODDS.

1.7. Overview of the Dissertation

Chapter one introduces oral drug delivery along with the anatomy and physiology of the GIT in relation to drug absorption. The effect of food on the functioning of the GIT is then explained and further extrapolated onto the effect of concurrent food and drug administration. Thereafter, a brief literature survey into the use of various food macromolecules in development of drug delivery systems is presented leading to the rationale for the work detailed in this dissertation.

Chapter two contains the characterization and comparison of tapioca and sago multiparticulates. Furthermore, in this Chapter, determination of the functional characteristics of each SBP is conducted and the optimal SBP for the study is selected.

Chapter three establishes the effects of various processing variables on the drug entrapment capacity of the chosen SBP which included volume of drug solution, swelling time, concentration of drug solution, drying temperature and temperature of drug solution and sets limits for each variable. The variables that elicit a major effect when altered are then used in a Box-Behnken design of experiments to determine the optimum conditions for maximized drug entrapment. The optimized drug-loaded SBP is then formulated and its functional characteristics evaluated.

Chapter four describes the evaluation of the MODDS for potential as a multidrug carrier in the treatment of hypertension, employing the model drugs captopril, furosemide and propranolol. The functional characteristics of the SBP with regard to each of the drugs are evaluated for application and further development of the MODDS. Furthermore, the potential for the SBP to serve as a universal drug carrier was evaluated as these model drugs exhibit varying physicochemical characteristics and different BCS classifications.

Chapter five describes the various modification techniques and combinations of certain modifications that were evaluated in order to confer the best structural and functional characteristics onto the SBP. Furthermore, in this Chapter captopril (and to a lesser extent diphenhydramine) was employed as the model drugs for the study in order to determine their suitability for use within the SBP.

Chapter six discusses variations of the specific modifications attempted on the SBP in Chapter five employing sulfasalazine (SSZ) as the model drug due to the chemical instability of captopril and diphenhydramine in the modification media. Thereafter the optimum combination of modifications was selected and variables for statistical optimization were determined.

Chapter seven describes the optimization of the formulation parameters utilizing a full factorial surface response Face Centered Central Composite Design of experiments owing to the presence of no more than 2 processing variable parameters. The design was analyzed and the optimized formulation was prepared and characterized to elucidate the structural and functional characteristics of the SBP.

Chapter eight contains the *in vivo* analysis of the optimized SBP as the MODDS in the large white pig model, and comprises of descriptions of blood sampling, dose administration, drug extraction and ultra pressure liquid chromatography techniques developed. Furthermore, the *in vivo* drug release behavior of the MODDS was elucidated and compared to the commercially available SSZ formulation, Salazopyrin®.

Chapter nine provides the conclusions derived from this study and recommendations for future work.

A map illustrating the development the MODDS entailed in this dissertation is depicted in Figure 1.4.

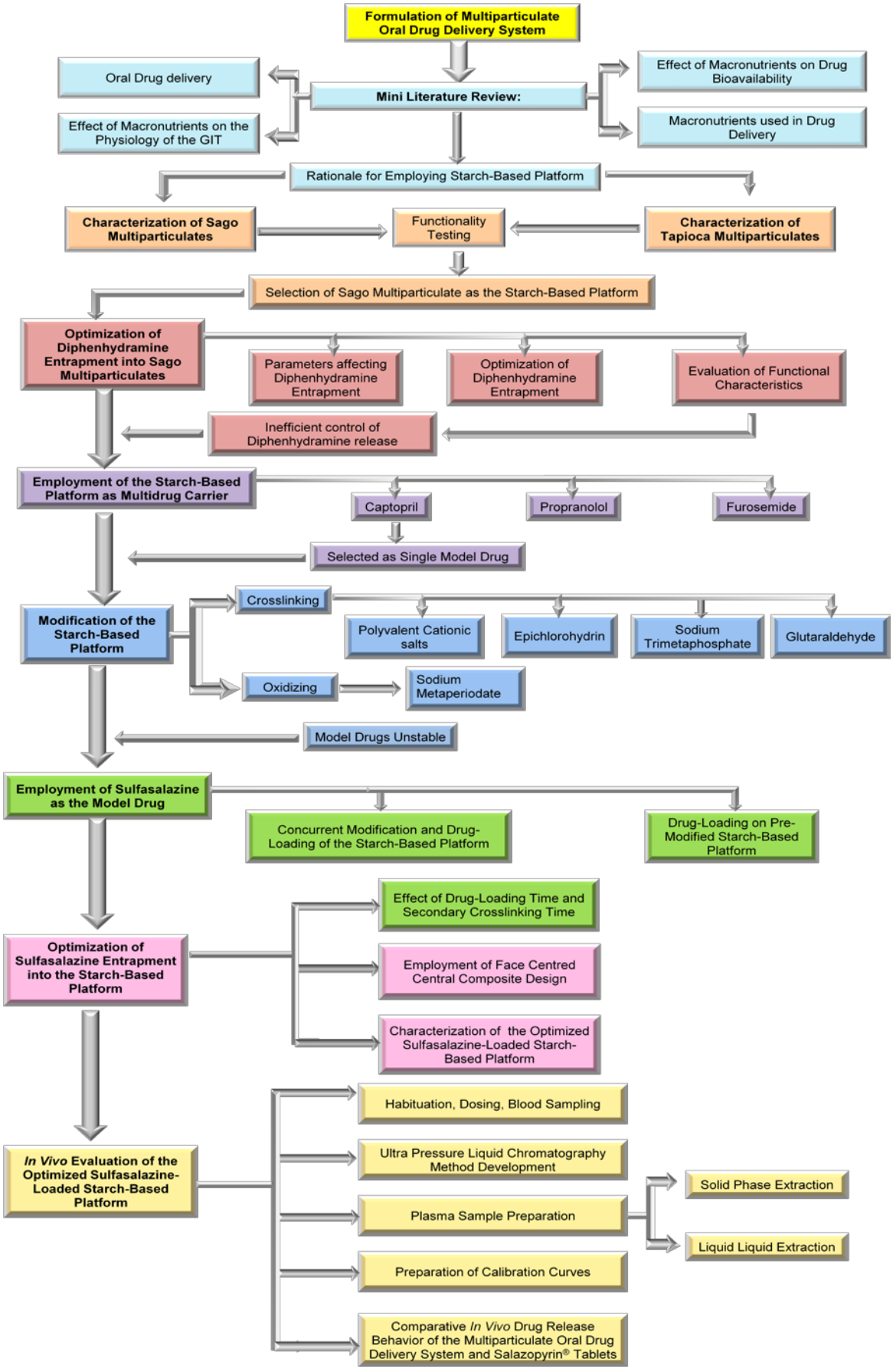


Figure 1.4: Schematic map of the dissertation.

CHAPTER 2
CHARACTERIZATION OF SAGO AND TAPIOCA MULTIPARTICULATES AND ELUCIDATION OF THEIR POTENTIAL APPLICATION AS A PLATFORM FOR MULTIPARTICULATE ORAL DRUG DELIVERY

2.1. Introduction

Oral drug delivery, although being the most convenient and widely used method of delivering drugs, does have its setbacks. These include drug solubility and kinetics, stability of drugs and drug delivery system at varying physiological conditions and site-specific drug absorption (Helliwell, 1993; Escuder-Gilabert *et al.,* 2003; Neuhoff *et al.,* 2005; Chavanpatil *et al.,* 2006; Streubel *et al.,* 2006; Sakuma *et al.,* 2007). In addition, natural physiological activities, disease induced alterations to the gastrointestinal tract (GIT) and presence of food within the GIT may affect the absorption, bioavailability and ultimately the efficacy of drugs (Ezra and Golomb, 2000; Crowley and Martin, 2004; Fukuda *et al.,* 2006; Sakuma *et al.,* 2007).

In order to overcome these setbacks, drugs are formulated within controlled release drug delivery systems, which enhance their bioavailability, maintain effective drug concentrations in the blood and possess the ability to provide site specific delivery to treat local GIT disorders (Chavanpatil *et al.*, 2006; Hoffman and Qadri, 2006; Sungthongjeen *et al.,* 2007; Crcarevska *et al.,* 2008). This facilitates superior clinical outcomes as patient compliance may be improved through simpler dosage regimens and fewer dose related side-effects (Helliwell, 1993; Streubel *et al.,* 2002; Jain *et al.,* 2005; Nevsten *et al.,* 2005; Chavanpatil *et al.,* 2006; Streubel *et al.,* 2006).

However, specialized controlled release drug delivery systems have their disadvantages, as the formulation process may be lengthy, expensive and difficult to reproduce on a large scale (Streubel *et al.,* 2002; Jain *et al.,* 2005; Streubel *et al.,* 2006). Biocompatibility and biodegradation, which are crucial to the success of these systems as they may form the basis for drug release and excretion (Peppas, 1992; Liu *et al.,* 2007; Crcarevska *et al.,* 2008), presents a challenge as many synthetic polymers employed within controlled release drug delivery systems may not be broken down nor excreted to a sufficient extent (Jain *et al.,* 2005).

A multiparticulate drug delivery system comprises of many discrete units, each loaded with a fraction of the total dose and each possessing the ability to release entrapped drug independently (Borgquist *et al.,* 2004; Frenning *et al.,* 2005). Controlling the release from each subunit allows diverse applications within a single dosage form. The multiparticulate drug delivery system may consist of multiparticulates containing different drug moieties and can therefore be used to treat more than one disease state or can provide multiple drug therapies required in some diseases, thus decreasing the pill burden in various disease states. Each subunit group may be programmed with varying release characteristics such as immediate release, pH responsiveness and sustained drug release, which can be used to ensure targeted drug delivery, enhanced therapeutic activity, and reduced side-effects (Carell *et al.,* 1997; Asghar and Chandran, 2006; Dey *et al.,* 2008; Phale and Gothoskar, 2011).

Additional advantages over conventional (i.e. monolithic) drug delivery systems include more reproducible pharmacokinetic behavior and lower intra- and inter-subject variability, which may lead to predictable bioavailability of drugs. There is also a reduced likelihood of dose dumping as the malfunction of a subunit only affects the performance of that particular subunit, whereas in the monolithic dosage form, a complete system failure is observed (Streubel *et al.,* 2002; Borgquist *et al.,* 2004; Nevsten *et al.,* 2005; Asghar and Chandran, 2006; Bardonnet *et al.,* 2006; Dey *et al.,* 2008; Phale and Gothoskar, 2011). Furthermore, multiparticulate systems can be formulated as tablets or encapsulated, enteric coated and formulated as pH and/or enzyme responsive and can thus be functionalized to deliver drugs throughout the GIT or at particular sites in the GIT as required for the treatment of specific conditions.

Starch is one of the most abundant food sources in the world and its importance is emphasized by its utilization as the staple diet of many populations (Vermeylen *et al.,* 2004; Galland *et al.,* 2007; Iida *et al.,* 2008). Starch is found in the form of semi-crystalline granules in different parts of plants (Katopo *et al.,* 2002; Mukerjea *et al.,* 2007) and is composed mainly of mixture of two polysaccharide polymers, amylose and amylopectin. The linear chains (α-(1-4) glycosidic bonds) of amylose (Figure 2.1a) accounts for the amorphous characteristics while the highly-branched amylopectin (α-(1-6) glycosidic bond branches of the α-(1-4) chains) (Figure 2.1b) accounts for the crystalline structure of starch (Vermeylen *et al.,* 2004; Mukerjea *et al.,* 2007; Brouillet *et al.,* 2008). Starches obtained from various plants contain different amylose:amylopectin ratios and thus exhibit varying physicochemical and physicomechanical properties (Lawal, 2004; Mukerjea *et al.,* 2007; Lesmes *et al.,* 2008; Oh *et al.,* 2008; Singhal *et al.,* 2008; Almeida *et al.,* 2010).

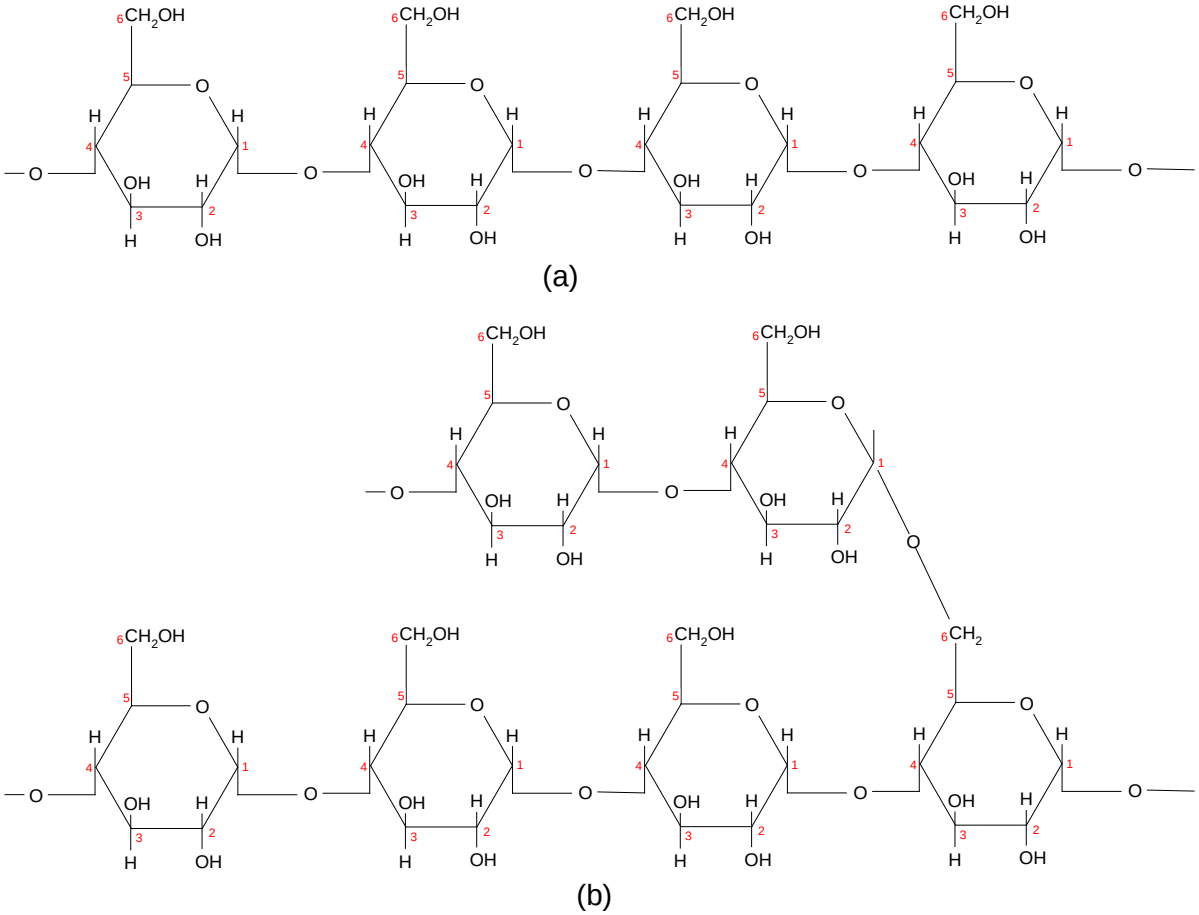


Figure 2.1: Representation of the structures of (a) amylose and (b) amylopectin.

Sago starch is found in the pith of the sago palm (*Metroxylon sagu*) and is indigenous to South East Asia and Oceanic regions (Muhammad *et al.,* 2000; Danjaji *et al.,* 2002). Sago starch is composed of approximately 25-30% amylose (Ahmad *et al.,* 1999; Muhammad *et al.,* 2000; Singhal *et al.,* 2008) and is used for various applications in the food, petroleum, textile and pharmaceutical industries. In these applications, sago starch is predominantly used in the powdered form (Muhammad *et al.,* 2000; Danjaji *et al.,* 2002). In the past few decades, the processing and refinement of sago starch has improved and has thus replaced other traditionally used starches in certain applications. Furthermore, sago starch has advantageous properties in that it has a low gelatinization temperature with gelatinization occurring easily and the ability to be modified to suit specific applications (Maaruf *et al.,* 2001). However, sago starch is also produced as pearls/pellets that are utilized in the food industry.

Tapioca starch, also known and cassava starch (Temsiripong *et al.,* 2005; Pongsawatmanit *et al.,* 2006; Lertworasirikul, 2008) is obtained from the roots/tubers of the cassava plant (*Manihot esculenta Crantz*). Cassava is cultivated in tropical areas in Africa, Brazil, Asia and Latin America and account for a large percentage of food calories

consumed in these areas (Fama *et al.,* 2007; Flores *et al.,* 2007). The literature describes tapioca starch as composed of between 17% and 32% amylose depending on the region and processing of the tubers with bitter and sweet varieties identified according to palatability with both types requiring a degree of processing in order to be consumed (Atichokudomchai *et al.,* 2004; Adebowale *et al., 2006;* Fama *et al.,* 2007; Itthisoponkul *et al.,* 2007; Oluwole *et al.,* 2007; Rao and Tattiyakul, 2007; Casas *et al.,* 2010). Its use is increasing due low production costs compared to other starch sources and is principally used in the form of a powder/flour. The food, paper and textile industries employ tapioca (Lee *et al.,* 2007) as it displays good pasting properties with clear gelatinization and high viscosity (Temsiripong *et al.,* 2005, Pongsawatmanit *et al.,* 2006; Muadklay and Charoenrein, 2008) while it is utilized in the pharmaceutical industry as a tablet filler. Analogous to sago starch, tapioca starch is also produced as pearls or pellets for use in the food industry (Pongsawatmanit *et al.,* 2007).

During the production of pearls of both sago and tapioca, moisture as well as heat is used which causes a degree of gelatinization of the starches (Collado and Corke, 1998; Maaruf *et al.,* 2001; Singhal *et al.,* 2008). These pearls can be seen as natural Starch-Based Multiparticulates (SBM) and, in addition to their biocompatibility and biodegradation, they exhibit physicochemical and physicomechanical properties that allow them to hydrate, swell and undergo modifications, which favor their employment as Starch-Based Platforms (SBP) for drug delivery (Tuovinen *et al.,* 2004). Furthermore, the wide availability and low cost of both tapioca and sago SBPs offer an added advantage for their use (Muadklay and Charoenrein, 2008) as it eliminates the process and cost associated with formulation of a core for the Multiparticulate Oral Drug Delivery System (MODDS) from which drug would be released.

Starches obtained from different botanical sources contain varying quantities of intrinsic polymers, i.e. amylose and amylopectin, and thus exhibit varying characteristics. The ratio of intrinsic polymers within the SBPs was important to determine as it affects the physicochemical and physicomechanical properties of the SBPs and would thus affect both the formulation and performance of the MODDS. Thus in this Chapter, characterization of the overall structure of both the sago multiparticulates and tapioca multiparticulates, as well as determination of the ratio of amylose and amylopectin within both SBPs, was undertaken. Furthermore, studies pertaining to the functionality of the MODDS were conducted in order to ascertain the behaviors of each of the SBPs and to ultimately select the most appropriate SBP for application in the MODDS.

2.2. Materials and Methods

2.2.1. Materials

Sago Multiparticulates (SMP, food grade) and Tapioca Multiparticulates (TMP, food grade) were purchased from KOO South Africa (Tiger Brands Ltd., Bryanston, Johannesburg, South Africa) and were used as the Starch-Based Platforms (SBP). Amylose and amylopectin, iodine powder (I_2, Mw=253.81g.mol^{-1}) and potassium iodide (KI, 166.00g.mol^{-1}) were purchased from Aldrich® (Sigma-Aldrich Inc., St. Louis, USA). Sodium hydroxide (NaOH, Mw=40.00g.mol^{-1}), potassium dihydrogen orthophosphate (KH_2PO_4, Mw=136.08g.mol^{-1}), sodium chloride (NaCl, Mw=58.44g.mol^{-1}) and n-Propanol (99%$^{v}/_{v}$, Mw=60.10g.mol^{-1}) were purchased from Saarchem-Holpro Analytic (Pty) Ltd., (Krugersdorp, Johannesburg, South Africa) and was of analytical grade. Hydrochloric acid (HCl, 32%$^{v}/_{v}$) and Dimethyl Sulphoxide (DMSO, 99%$^{v}/_{v,}$ Mw=78.13g.mol^{-1}) were purchased from Merck (Pty) Ltd. (Modderfontein, Johannesburg, South Africa). Diphenhydramine (DPH, Mw=291.82g.mol^{-1}, solubility>100mg.mL^{-1} in water at 21.5°C) was purchased from Aldrich® (Sigma-Aldrich Inc., St. Louis, USA) and used as the model drug. Deionized water, purified by a MilliQ Millipore water purification system (Milli-Q, Millipore, Billerica, MA, USA), was used throughout the study. All other reagents were of analytical grade and all products were used as received.

2.2.2. Determination of the size and morphology of the SBPs

The size, surface structure and network density of the SBPs influence their ability to bind with polymers and drug molecules and influence the way in which the SBPs interact with biological fluids. In addition, these factors and especially the size of the SBPs, have a direct impact on the type of MODDS that could ultimately be formulated and was thus important to determine in the initial formulation processes.

2.2.2.1. Gravimetric analysis of the SBPs

Single SBP samples (n=100) of both sago and tapioca were removed from the packaging and analyzed gravimetrically using a digital electronic mass balance and the average SBP mass was calculated.

2.2.2.2. Macroscopic analysis of to determine the relative size of the SBPs

Macroscopic analysis of both SBPs was conducted in order to gain insight into the general shape and proportional size of the SBPs. SMP and TMP samples (2g) were accurately weighed using a digital electronic mass balance and analyzed under no magnification.

2.2.2.3. Light microscopic analysis to determine the morphology of the SBPs

Light microscopic analysis was conducted on an Olympus® Stereo Microscope (Model SZX-D2-200) fitted with an Olympus® SZX-TR30 camera (Tokyo, Japan) in order to gain a more accurate size measurement and examine the shape of the SBPs more closely. Single SBP samples (n=100) of both sago and tapioca were removed from packaging and immediately placed under light microscope. The surfaces of the SBPs were visually analyzed for size, shape and contours at magnifications that suited SMP and TMP and the average size of both SBPs was then calculated. In addition, transverse sections through the core of the SBPs were prepared and microscopically analyzed to gauge the internal morphological structure of the SBPs.

2.2.2.4. Scanning Electron Microscopy to determine the intrinsic structure of the SBPs

In order to obtain a more descriptive view of the structure and morphology of the SBPs, scanning electron microscopy (SEM) was performed on single SBP samples and on the transverse sections of both SMP and TMP. SBP samples were firmly mounted on aluminium stubs with carbon tape and gold sputter coated with argon gas whilst under a vacuum of 0.1Torr using a SPI-MODULE™ Sputter Coater and SPI-MODULE™ Control (SPI Supplies, Division of Structure Probe Inc., West Chester, PA, USA). Each sample required 4.5 minutes of coating at 90-second intervals to ensure complete coverage of the sample, which minimized sample activation during viewing. Subsequent viewing was performed at various magnifications under the Phenom™ desktop scanning electron microscope (FEI Company™, Hillsboro, OR, USA).

2.2.3. Fourier Transform Infrared Analysis to determine structure of the SBPs

Fourier Transform Infrared (FTIR) spectroscopy, which allows detection of vibrational frequencies of chemical functional groups in response to infrared light, was used to determine the polymeric backbone of both SBPs. Analysis was conducted using a FTIR spectrometer (Nicolette Impact 400 D FT-IR Spectrometer, ThermoFisher Scientific, Germany) and interferograms were translated via the mathematical technique of Fourier Transformation before being presented as an infrared spectrum, which plots transmittance versus wavenumber. The resultant spectra were compared to elucidate if structural differences between the SBPs were present. In addition, the spectra of the SBPs were compared to soluble starch powder to determine the degree of morphological change imparted onto the SBPs during formulation into multiparticulates.

2.2.4. Colorimetric determination of intrinsic polymer ratio of the SBPs

For the past seven decades, many different methods have been employed in determining amylose content as a means of determining the amylose to amylopectin ratio within starches. These include, but are not limited to, differential scanning calorimetry (DSC), FTIR spectroscopy, nuclear magnetic resonance (NMR) spectrosocopy, high pressure size exclusion chromatography, rheological methods, X-ray diffraction and most notably and commonly the amylose complexation of iodine (Matheson, 1971; Tikuisis, 1993; Ge´rard *et al.,* 2001; Noosuk *et al.,* 2003; Charoenkul *et al.,* 2006; Zhu *et al.,* 2008). The affinity of iodine to complex the linear amylose chains have been explored by many researchers who have proposed different techniques to employ this phenomenon in determining the amylose content of starches. These include gravimetric analysis of precipitated iodine-amylose complexes, as well as potentiometric, amperometric titrations and spectrophotometric methods (Ge´rard *et al.,* 2001; Charoenkul *et al.,* 2006; Almeida *et al.,* 2010).

The rationale for utilizing the colorimetric/spectrophotometric method was based on the characteristic blue color observed in the amylose-iodine complex as compared to the reddish-purple color produced by amylopectin-iodine complex (Bourn and Peat, 1949). In addition to the visible difference in color, the amylose-iodine complex absorbs ultraviolet (UV) light at higher wavelengths (λmax=580-720nm) as compared to amylopectin-iodine complex which has a λmax of 520-540nm (Knutson, 1986; Ge´rard *et al.,* 2001; Fitzgerald *et al.,* 2009; Almeida *et al.,* 2010). However, ~6% of the absorbance at λmax=600nm can be attributed to the end chains of amylopectin branches and the effect of lipids and proteins bound to starch and thus has to be taken into account in determining amylose content of starch (Knutson, 1986; Ge´rard *et al.,* 2001; Fitzgerald *et al.,* 2009).

2.2.4.1. Preparation of solutions for colorimetric analysis of SBPs

n-Propanol (75%$^{v}/_{v}$) solution was prepared by adding 150mL n-propanol (99%$^{v}/_{v}$) into a 200mL volumetric flask and making up to 200mL with deionized water. This solution was stored at 25±1°C until used.

Iodine solution (0.0025M I_2:0.0065M KI) was prepared by dissolving 0.1079g KI in 10mL deionized water in a 100mL volumetric flask and thereafter completely dissolving 0.0315g I_2 in this solution. The solution was then made up to 100mL and stored at 4°C in an amber bottle away from light.

2.2.4.2. Preparation of a standard amylose curve and determination of amylose content in the SBPs

Amylose:amylopectin blends (1g) were prepared by triturating accurately measured quantities of amylose and amylopectin to achieve amylose proportions ranging between 0% amylose (100% amylopectin) and 100% amylose (0% amylopectin). Samples of each amylose:amylopectin blend (20mg) was accurately weighed and placed into a round bottom screw-cap tube fitted with Teflon-faced rubber liner in a cap. DMSO (90%, 8mL) was then added to the sample and mixed vigorously with a vortex mixer (Vortex-Genie 2, Scientific Industries Inc., Bohemia, NY, USA) for 2 minutes. The tube was then heated for 25 minutes in a shaker bath maintained at 85°C and rotating at 50rpm after which it was allowed to cool until room temperature (~25°C) was reached and then diluted to 25mL with deionized water. A sample of this solution (1ml) was placed in a volumetric flask and made up to 50mL with 5mL iodine solution and 44mL deionized water. The mixture was then shaken vigorously for 2 minutes and then allowed to develop color at 25°C for 30 minutes. The absorbance of the colored solution was then determined using a UV spectrophotometer (diode array UV spectrophotometer, Specord 40, Analytik Jena AG, Jena) programmed at 600nm for analysis (WinASPECT® Spectroanalytical Software, Analytik Jena AG, Jena). The absorbance of each amylose:amylopectin blend was used to construct a standard %amylose vs. absorbance curve in order to determine the amylose content of the SBPs.

The amylose content of the SBPs was determined using the method of Hoover and Ratnayake (2001) with minor modifications. SMP and TMP samples (10g) were separately ground in a coffee grinder for 2 minutes in order to form a homogenous powder. Powdered SBP (5g) was accurately weighed and placed into a cellulose extraction thimble and the mouth covered with a cotton wool plug. Lipids were extracted using 120mL n-propanol (75%$^{v}/_{v}$) with a heating mantle for 7 hours in a Soxhlet extractor and the lipid free starch was air dried within the thimble for 12 hours. The starch was then removed and oven dried at 30°C for 24 hours.

Powdered SBP samples (20mg) were subjected to the same treatment as described for the amylose:amylopectin blends used to construct the standard curve and the amylose content of both SBPs was calculated using the standard curve. The study was conducted in triplicate (n=3).

2.2.5. Gravimetric analysis to determine the hydration capacity and erosion behavior of the SBPs in water and simulated biological fluids

The principal mechanisms by which the MODDS was aimed to function were by way of hydration and erosion. *In vitro* hydration of the SBP was the mechanism by which drug entrapment may be achieved and both *in vivo* hydration and erosion of drug-loaded SBP may be exploited to facilitate drug release. These studies were performed to establish optimal conditions to achieve the desired extent of hydration and erosion. Additionally, the stability and effectiveness of the SBP within the GIT was assessed by exposing the SBP to conditions that simulate those in which it will be subjected to *in vivo.*

2.2.5.1. Preparation of hydration and erosion media

2.2.5.1.1. Deionized water

Deionized water, purified by a MilliQ Millipore water purification system (Milli-Q, Millipore, Billerica, MA, USA), was used as the primary hydration media.

2.2.5.1.2. Simulated gastric fluid

Simulated Gastric Fluid (SGF) was prepared according to the method described in the USP (USP 33, 2009). NaCl (2g) was accurately weighed and dissolved in 100mL de-ionized water. Concentrated HCl was then added to the solution in a drop wise manner until the desired solution pH was reached. The solution was then made up to 1000mL using de-ionized water. A total of 7mL HCl was required to achieve a pH of 1.2.

2.2.5.1.3. Simulated intestinal fluid

Simulated Intestinal Fluid (SIF) was prepared according to the method described in the USP (USP 33, 2009). A 0.1M solution of sodium hydroxide was prepared by accurately weighing 4g NaOH and dissolving it in 100mL de-ionized water and thereafter made up to 1000mL using de-ionized water. A potassium dihydrogen phosphate solution was prepared by accurately weighing and dissolving 13.6g of KH_2PO_4 in 100mL de-ionized water and made up to 1000mL using de-ionized water. Adequate quantities of the two solutions were combined until a pH of 6.8 was obtained.

2.2.5.2. Determination of the effect of drug-loading and drug release media on the hydration and erosion of the SBPs

Separate SMP and TMP samples (2g) were accurately weighed using an analytical mass balance. These SBP samples were separately immersed into each of the hydration media prepared in Section 2.2.5.1 (20mL) and allowed to hydrate for 0.5, 1, 2, 3, 4, 6, 8, 10, 12, 16, 20 and 24 hours in a shaker bath maintained at 25°C and rotating at 50rpm. At each

time point, the hydrated SBPs were carefully removed from the hydration media, lightly blotted with tissue paper to remove excess moisture, placed onto glass petri dishes and immediately weighed. The extent of hydration of the SBP samples was calculated gravimetrically using Equation 2.1.

$$DOS = \frac{M_h - M_r}{M_r} \text{ X } 100 \qquad \textbf{\textit{Equation 2.1}}$$

Where:
DOS= *Degree of swelling (%)*
M_h= *Hydrated mass of SBP (g)*
M_r= *Mass of dried SBP (g)*

The hydrated SBPs were then allowed to air dry until constant mass was achieved (~8 hours). During the drying process, the SBPs were physically separated using a flat-ended metal spatula. Once dried, the SBPs were weighed and extent of erosion within the hydration media was calculated gravimetrically using Equation 2.2. The study was conducted in triplicate (n=3).

$$DCM = \frac{M_d - M_0}{M_0} \text{X}100 \qquad \textbf{\textit{Equation 2.2}}$$

Where:
DCM= *Degree of change in mass (%)*
M_d= *Mass of dried SBP (g)*
M_0= *Original mass of SBP (g)*

2.2.6. Buoyancy studies to elucidate the potential of the SBPs to act as a gastro-floatable MODDS

The SBP may be employed as a swellable and floatable gastro-retentive MODDS due to its intrinsic physicochemical properties. Thus, the effectiveness as a gastro-retentive MODDS was dependent on the ability of the SBP to remain buoyant in gastric fluid. Samples (2g) of both SBPs were accurately weighed and subjected to buoyancy studies, which was conducted on a USP rotating paddle apparatus (USP 33, 2009) using SGF as the dissolution medium. The time interval between the introduction of the SBP into the dissolution medium and its rise to the top of the medium was recorded as the buoyancy lag-time and the duration of floatation of the SBPs was determined visually and recorded.

2.2.7. Textural analysis to elucidate the effect of hydration on the mechanical behavior of the SBPs

Physicomechanical properties such as resilience, deformation energy and hardness are influenced by the hydration state of particles and this in turn leads to altered performance of drug delivery systems. It was thus important to elucidate the effect of hydration on the physicomechanical properties of both SBPs in order to select an appropriate SBP for use in the MODDS.

2.2.7.1. Determination of the effect of hydration on the resilience of both SBPs

SMP samples (n=35) were divided into 7 subsets, each containing 5 SMP. Each subset was then placed into 5mL deionized water with the exception of subset 1, which was used to determine the resilience of non-hydrated SMP. Subsets 2-7 were allowed to hydrate for 1, 4, 8, 12, 18, 24 hours respectively. After the appropriate hydration time for particular subset had elapsed, the SMP was removed from the hydration medium, lightly blotted with tissue paper to remove excess moisture and allowed to dry on a petri dish at 25°C for 2 minutes. TMP was subjected to the same treatment as described for SMP.

Resilience analysis, using a calibrated Textural Profile Analyzer (*TA.XT.plus Texture Analyser*, Stable Microsystems®, Surrey, UK) fixed with a 50kg load cell and 36mm cylindrical steel probe, was then performed in accordance with the parameters set out in Table 2.1. Data acquisition was performed at 200 points.sec^{-1} via Texture Exponent for Windows software, Version 3.2. Force vs. Time textural profiles were generated and the resilience of the matrix was calculated as the ratio of the area under the curve (AUC) or work done by the SBP on the probe after the maximum decompressive force was reached to the AUC or work done by the probe on the matrix up to the maximum compressive force as depicted in Equation 2.3.

$$RES = \frac{AUC_{2-3}}{AUC_{1-2}} \text{X}100 \qquad \textbf{\textit{Equation 2.3}}$$

Where:
RES= *Resilience (%)*
AUC_{1-2}= *Area under the curve 1-2 (N.sec)*
AUC_{2-3}= *Area under the curve 2-3 (N.sec)*

Table 2.1: Parameters for analysis of the resilience of SBPs

Parameter	Value
Return distance	10mm
Return speed	5mm/sec
Contact force	10g
Test mode	Compression
Pre test speed	1mm/sec
Test speed	0.5mm/sec
Post test speed	10mm/sec
Target mode	Strain
Distance	9%
Trigger type	Auto-force
Trigger force	0.05N
Break mode	Off
Stop plot at	Start position
Tare mode	Auto
Control oven	Disabled

2.2.7.2. Determination of the effect of hydration on the hardness and deformation energy of both SBPs

The method for determining the deformation energy and hardness of the SBPs was the same as that followed in determining their resilience with a few alterations. These included the substitution of the probe with a 2mm flat-ended cylindrical steel probe and the changing the equipment testing parameters to those portrayed in Table 2.2. Additionally, Force vs. Distance textural profiles were generated by the integrated software with the deformation energy of the SBPs calculated as the area under the Force vs. Distance curve ($N.mm^{-1}$) and SBP hardness determined by calculating the slope of the Force vs. Distance curve (N.mm).

Table 2.2: Parameters for the analysis of hardness and deformation energy of the SBPs

Parameter	Value
Return distance	10mm
Return speed	5mm/sec
Contact force	10g
Test mode	Compression
Pre test speed	1mm/sec
Test speed	0.5mm/sec
Post test speed	10mm/sec
Target mode	Distance
Distance	1mm
Trigger type	Auto-force
Trigger force	0.05N
Break mode	Off
Stop plot at	Start position
Tare mode	Auto
Control oven	Disabled

2.2.8. Determination of the functional characteristics of SMP and TMP for employment as the platform in the MODDS

2.2.8.1. Construction of calibration curves for DPH in SGF and SIF

Stock solutions of DPH were prepared by accurately weighing and dissolving 100mg DPH in 100mL SGF and separately in 100mL SIF (SGF and SIF was prepared as described in Section 2.2.5.1). 6-fold serial dilutions were then performed on each stock solution and the absorbance of each dilution (SGF concentrations: 0-0.335mg.mL^{-1} and SIF: 0-0.680mg.mL^{-1}) was determined with a UV spectrophotometer (diode array UV spectrophotometer, Specord 40, Analytik Jena AG, Jena) at the maximum absorbance wavelength of DPH (λmax=254nm). Calibration curves were then constructed by plotting the observed absorbance on the y-axis against its corresponding concentration (mg.mL^{-1}) on the x-axis. All intercepts were set at 0 and the R^2 values were determined to be 0.9983 and 0.9994 in SGF and SIF respectively.

2.2.8.2. Drug entrapment employing the highly water-soluble model drug, DPH

2.2.8.2.1. Drug entrapment into the SBPs

DPH solution (150mg.mL^{-1}) was prepared by accurately weighing and dissolving 9g DPH in 20mL deionized water and making up this solution to 60mL using deionized water. SMP and TMP samples (2g) were accurately weighed using an analytical mass balance, placed into drug solution (10mL) and allowed to hydrate for 4 hours in a shaker bath maintained at 25°C and rotating at 50rpm.

2.2.8.2.2. Elucidation of extent of drug entrapment

The drug-loaded SBPs were then removed from the drug solution, lightly blotted with tissue paper to remove excess moisture and thereafter weighed. The extent of hydration of the SBP samples was calculated gravimetrically using Equation 2.1. The drug-loaded SBPs were then placed onto petri dishes and air dried until constant mass was achieved (~8 Hours). During the drying process, the SBP were physically separated using a flat-ended metal spatula. Once dried, the drug-loaded SBPs were weighed and samples (1g) were homogenized in 10mL SIF for 120 seconds. The homogenized suspension was then made up to 500mL with SIF maintained at 100ºC, stirred and allowed to cool to approximately 30ºC. Three 10mL samples from the cooled suspension were then centrifuged at 3000rpm using rotor 3 (Optima® LE-80K, Beckman, USA) for 90 minutes. The supernatant was removed and thereafter filtered through a 0.45µm Millipore filter. The filtered samples were then analyzed using UV spectroscopy and the calibration curves constructed in Section 2.2.8.1 at a λmax=254nm to determine the drug content within the SBPs. The content of the three samples were then averaged. The Drug

Entrapment Efficiency (DEE) of both SMP and TMP was calculated according to Equation 2.4. The study was conducted in triplicate (n=3).

$$DEE = \frac{Y_E}{Y_T} \text{X}100 \qquad \textbf{\textit{Equation 2.4}}$$

Where:
DEE*= Drug entrapment efficiency (%)*
Y_E*= Experimental yield (mg)*
Y_T*= Theoretical yield (mg)*

2.2.8.3. In vitro drug release study to determine the ability of SMP and TMP to control the release of DPH in simulated biological fluids

The *in vitro* drug release studies were performed on the drug-loaded SBPs using a USP 33 dissolution apparatus II, rotating paddle apparatus, (Caleva Dissolution Apparatus, Model 7ST) (Caleva Ltd., Sturminster Newton, Dorset, England). Separate drug-loaded SMP and TMP samples (containing 50mg DPH) were accurately weighed and placed separately into SIF (900mL) or SGF (900mL). Formulations were placed below a steel mesh assembly within each vessel to protect the SBPs from breakdown due to contact with the rotating paddle. The media were maintained at 37±0.5°C and rotated at 50rpm. Samples (5mL) were manually withdrawn at predetermined time intervals over a 12-hour period and replenished with fresh buffer in order to maintain sink conditions. The absorbance values were measured using UV spectroscopy at λmax=254nm and fractional drug release was calculated using the predefined calibration curves (Section 2.2.8.1). The study was conducted in triplicate (n=3).

2.3. Results and discussion

2.3.1. Comparison of the size and morphology of SMP and TMP

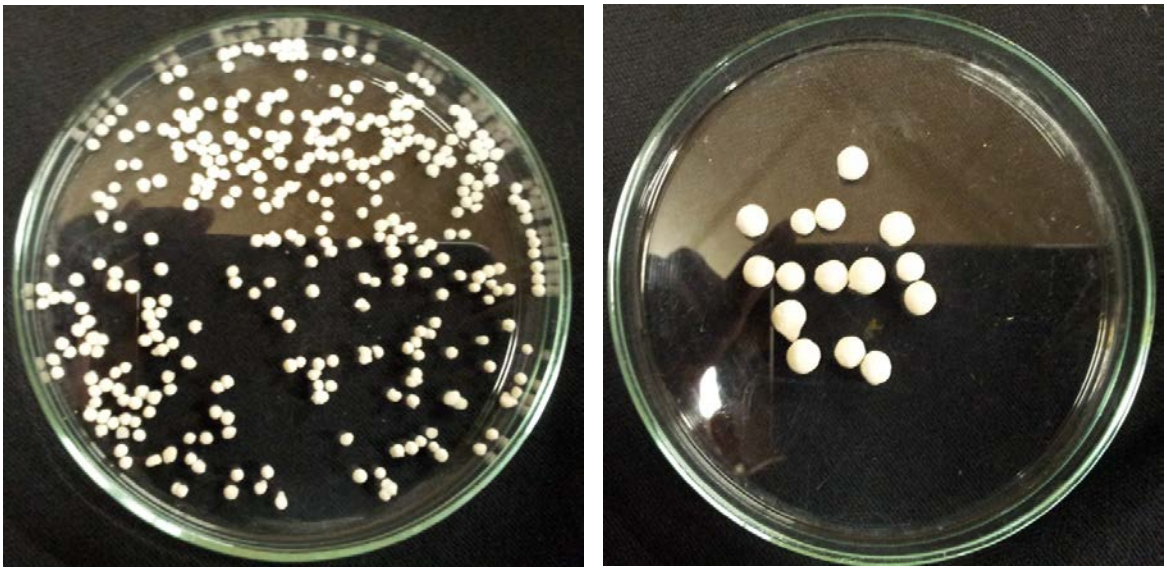
2.3.1.1. General and microscopic morphology of the SBPs

Figure 2.2 compares the general shape and size of SMP and TMP with both SBPs exhibiting a generally spherical shape when observed from afar. TMP demonstrated a diameter that was approximately 5 times larger than that of SMP and contained approximately 10 times the mass of SMP as illustrated in Table 2.3. The density difference between the SBPs could be due to differences in intrinsic polymer ratios or processing parameters in formulating the multiparticulates.

Table 2.3: Relative size and mass of SBPs

SMP		TMP	
Mass (mg)	**Size (mm)**	**Mass (mg)**	**Size (mm)**
0.0116± 0.0013	1.65± 0.23	0.1278± 0.0144	8.43± 0.76

Where SMP denoted Sago Multiparticulates, TMP denoted Tapioca Multiparticulates (n=100 in all instances)



(a) (b)

Figure 2.2: Digital images depicting (a) 2g SMP and (b) 2g TMP.

Upon closer inspection, it was observed that both SBPs are not exactly spherical but display contours on their surfaces a depicted in Figure 2.3a. Additionally, Figure 2.3a showed that at slight magnification, the surface appearance and structure of the SBPs are very similar which could be attributed to similar production methods and intrinsic polymer compositions. However, when examining the core structure (Figure 2.3b), TMP displays a more porous network with large gaps between the granule clusters, which could be attributed to the size of the multiparticulates and may possibly indicate increased fragility compared to SMP.

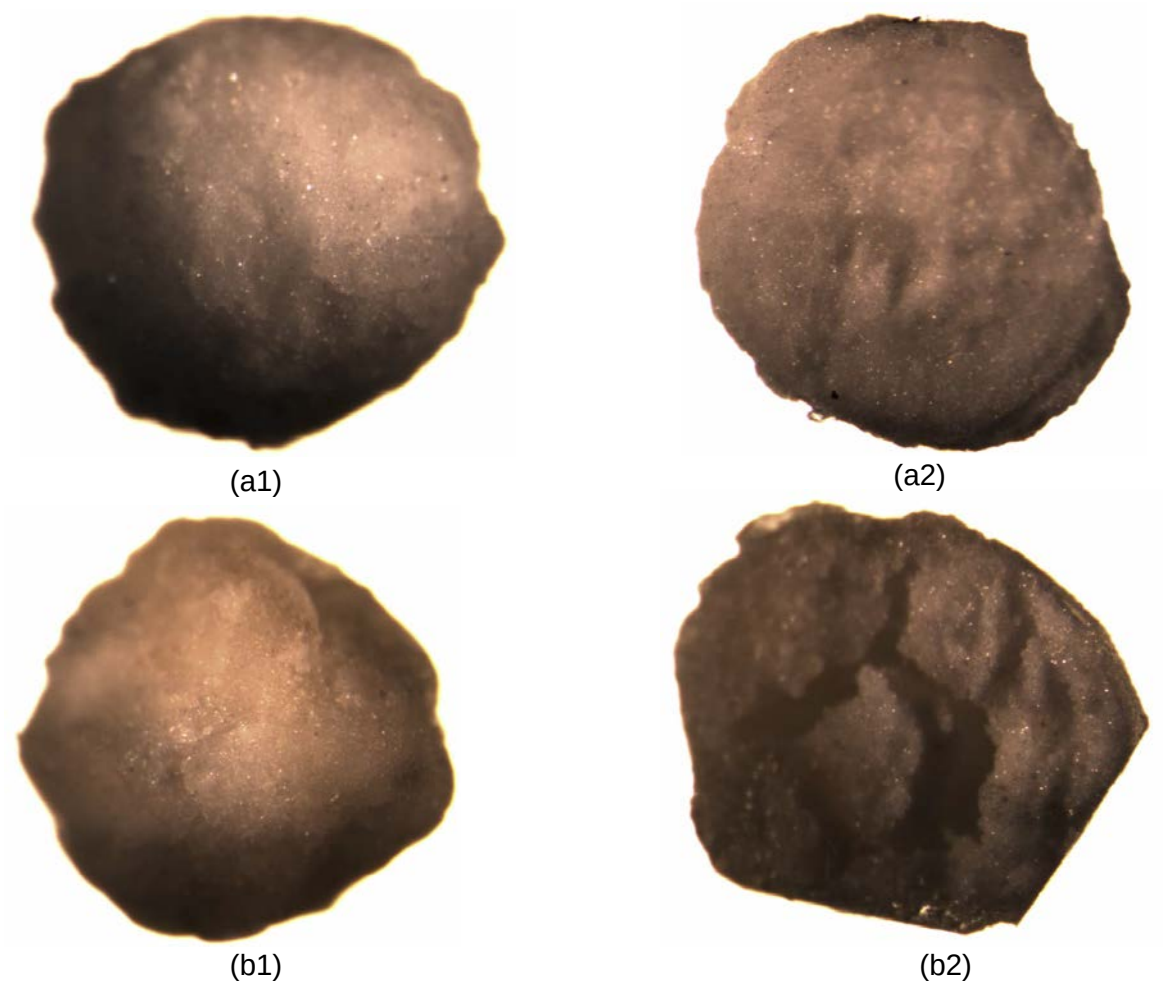


Figure 2.3: Microscopic depiction of (a1) SMP surface, (a2) SMP core (b1) TMP surface and (b2) TMP core.

2.3.1.2. SEM imaging of intrinsic structure of the SBPs

SEM imaging of the surface (Figure 2.4a1) and transverse section through the core (Figure 2.4a2) of the SMP portrayed these SBPs as comprising of many smaller composite particles. These particles were determined to be individual native starch granules containing amylose and amylopectin. At lower magnifications, the granules were perceived to be regularly shaped with comparable sizes. However, upon viewing at higher magnifications, the granules depicted inconsistent shapes with varying sizes which ranged between 20µm and 80µm. SMP further demonstrated a porous nature, as spaces between individual granules as well as between clusters of granules were present, which could permit swelling and expansion of the granules during hydration and drug-loading. Comparison between the core and surface at high magnification showed little difference but at lower magnifications, the surface appeared to be more continuous with granules tending to merge into each other. This could be a result of process parameters and gelatinization during formulation of sago starch into SMP.

When analyzing the SEM images of the TMP (Figure 2.4b1 and Figure 2.4b2), analogous observations to those of SMP were made including the presence of composite granules, the size of the granules and the merging of granules at the surface. The gelatinization and merging of surface granules was clearly demonstrated at high magnifications in Figure 2.4b1. However, compared to SMP, larger spaces between intrinsic granules as well as between granule clusters were observed. This was consistent with the observation made during the light microscopy described in Section 2.3.1.1 and while these voids could encourage hydration and drug entrapment, they may have indicated structural instability of TMP.

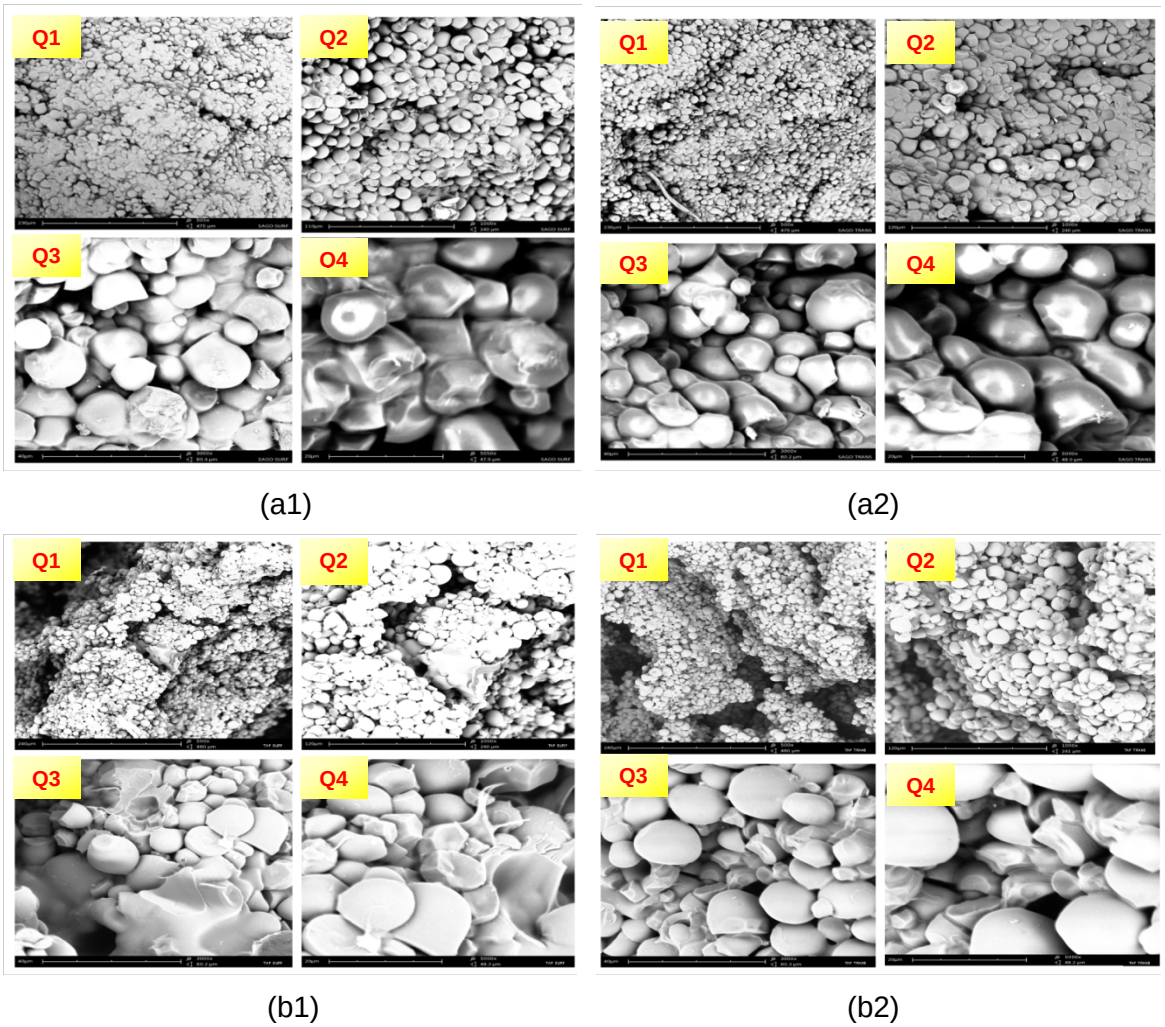


Figure 2.4: SEM imaging of (a1) SMP surface, (a2) SMP core (b1) TMP surface and (b2) TMP core (magnifications in figures a1-b2 were: Q1=500X; Q2=1000X; Q3=3000X; Q4=5000X).

2.3.2. Comparative FTIR representation of structure of SMP, TMP and soluble starch

Figure 2.5 depicted the FTIR spectrum of soluble starch which displayed bands that were characteristic of the functional groups and structure of starch. The broad band between 3070cm^{-1} and 3600cm^{-1} was due to the hydrogen-bonded OH groups that contribute to the complex vibrational stretches associated with free intermolecular and intramolecular bound OH groups, which make up the gross structure of starch. In addition, intensity of this band was attributed to OH bonding due to water within the starch structure. The peaks found in the band between 3010cm^{-1} and 2849cm^{-1} were characteristic of CH and CH_2 stretches associated with the ring methane hydrogen atoms while CH_2 and CH bending was illustrated by the peaks in the band between 1301cm^{-1} and 1486cm^{-1}. The bands between 1639cm^{-1} and 1659cm^{-1} and between 1200cm^{-1} and 1287cm^{-1} were associated with C-OH interactions and were representative of bound water within the starch. The prominent band between 958cm^{-1} and 1190cm^{-1} was composed of C–C, C–O and C-OH stretching and vibrations of the polysaccharide backbone and the bands <900cm^{-1} were indicative of the polymeric skeletal backbone of starch and include, C-O-C modes, effects of α(1-4) linkages between glucose monomers and out of phase OH bending (Galat, 1980; Iizuka and Aishima, 1999; Bernazzani *et al.,* 2008; Rajan *et al.,* 2008; Kumari and Rani, 2011; Apopei *et al.,* 2012).

Figure 2.5 additionally compared the FTIR spectra of SMP and TMP and further compared these spectra to the FTIR spectrum of soluble starch powder in order to elucidate the structural alterations of starch imparted during multiparticulate formation. Both SBPs displayed almost identical FTIR spectra, which alluded to the SBPs eliciting very similar intrinsic structures and polymer compositions. However, minor differences in band intensities between 3070cm^{-1} and 3600cm^{-1} and between 3010cm^{-1} and 2849cm^{-1} and shifted water bands between 1597cm^{-1} and 1722cm^{-1} were noted. This could be due to slight differences in structural polymer composition and water content within the SBPs. However, FTIR was limited in terms of quantification and could not be used to quantify the amylose and amylopectin content within SMP and TMP accurately.

When comparing the SBPs to starch, shifting, appearance and disappearance of peaks between 940cm^{-1} and 590cm^{-1} and between 1301cm^{-1} and 1486cm^{-}1, as well decrease in the intensity of the band between 3010cm^{-1} and 2849cm^{-}1 was observed. This indicated that structural changes to the skeletal polymeric backbone had taken place during production of the multiparticulates. Furthermore, there was a decrease in intensity of the bands between 3070cm^{-1} and 3600cm^{-1}; between 1639cm^{-1} and 1659cm^{-1} and between

1200cm^{-1} and 1287cm^{-1}, which indicated decreased OH bonding and thus loss of intrinsic water within both SBPs (Shey *et al.,* 2006; Kumari and Rani, 2011). This phenomenon, in addition to the increased intensity of the band between 958cm^{-1} and 1190cm^{-1} alluded to the possible gelatinization of the SBPs during production (Iizuka and Aishima, 1999). Thus, it was concluded that production of SMP and TMP resulted in slight alterations to the morphology of the native sago and tapioca starches.

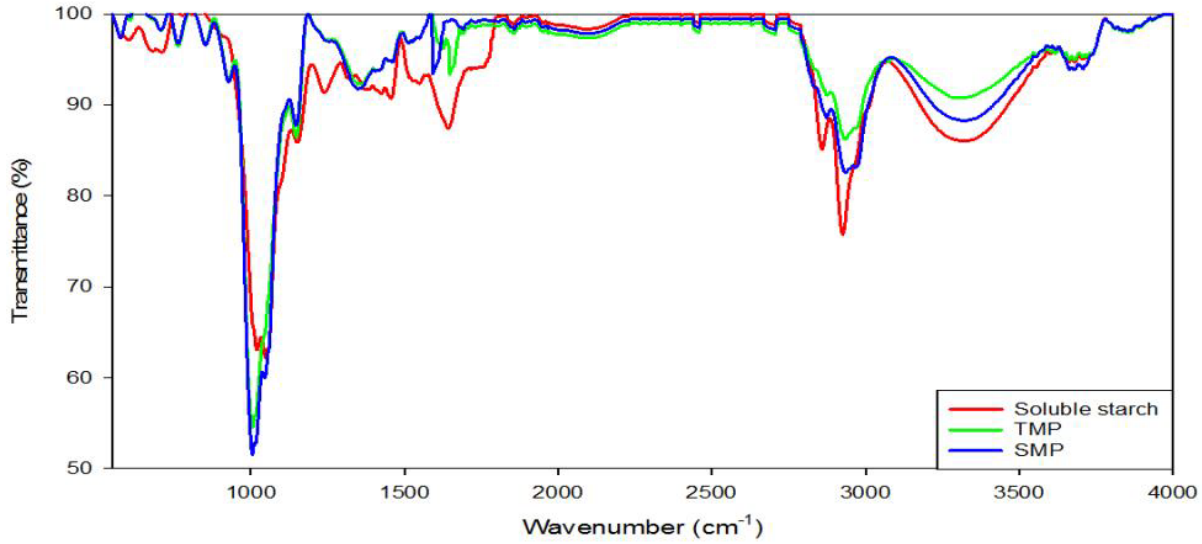


Figure 2.5: Comparative FTIR spectra of soluble starch, SMP and TMP.

2.3.3. Colorimetric ratio of amylose and amylopectin within SBPs

The standard curve of %amylose depicted in Figure 2.6 displayed good linearity with an R^2=0.9945. The amylose-iodine complex is known to display λmax at higher wavelengths compared to the amylopectin-iodine complex. However, end chain branching of amylose and the amylopectin-iodine complex do absorb UV light at 600nm to a small extent and thus accounts for the fraction (~6%) of the actual absorbance observed at 600nm (Fitzgerald *et al.,* 2009). This fraction explained the inability of the y-intercept of the standard curve to pass through the origin and allowed for more accurate determination of the amylose content in starches. Thus, the standard curve constructed was found to be suitable for the quantification of amylose content within the SBPs.

Upon analyzing the SMP samples (Figure 2.6), it was found that the amylose content of SMP was 29.125±2.235%, which was similar to the values stated in the literature (Ahmad *et al.,* 1999; Muhammad *et al.,* 2000; Singhal *et al.,* 2008). The same finding was observed with TMP (Figure 2.6) which displayed amylose content of 22.252±3.128% which was congruent to the values stated in the literature (Atichokudomchai *et al.,* 2004; Fama *et al.,* 2007; Itthisoponkul *et al.,* 2007; Rao and Tattiyakul, 2007; Casas *et al.,*

2010). However, slight alterations to the structure of the starches during production of SMP and TMP were found as discussed in the FTIR and SEM analysis of the SBPs. Presence of these alterations could imply slightly different amylose and amylopectin content within the SBPs compared to their native starches and could have accounted for the relatively large standard deviations observed in Figure 2.6.

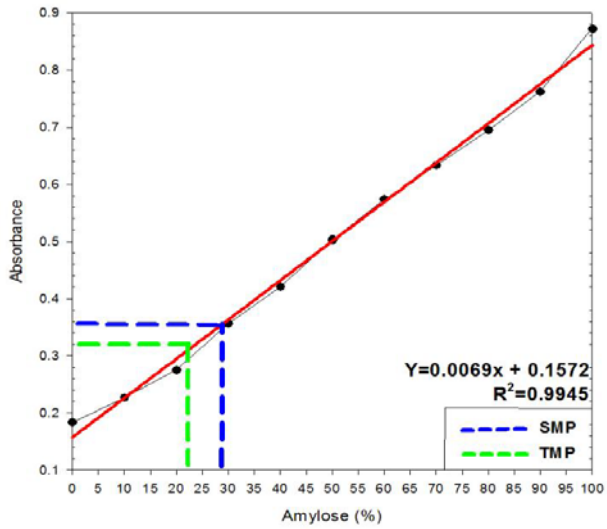


Figure 2.6: Standard curve of amylose content vs. absorbance depicting average amylose content of SMP (n=3, SD≤2.235%) and TMP (n=3, SD≤3.128%).

2.3.4. Effect of drug-loading and dissolution media on the hydration and erosion of the SBPs

The SBPs displayed the ability to immediately imbibe each of the hydration mediums when submerged. This was represented as the sharp rise in the degree of swelling in the initial half hour (Figure 2.7a). Thereafter hydration continued over the next few hours until a plateau was reached at approximately 4 hours in each hydration medium. During the plateau phase, an equilibrium of sort was established and minimal further hydration occurred. In SIF, the curve displayed a slight rising slope with increased hydration time and this was attributed to alkali-induced gelatinization of the SBPs. This observation was further substantiated by Figure 2.7b, which showed increased erosion of SBPs as the pH of the media was increased.

Furthermore, increase in hydration time resulted in higher degrees of erosion due to increase penetration and interaction of the mediums with the SBPs. Therefore, Figure 2.7a and Figure 2.7b demonstrated that swelling and erosion of the SBP were dependent on both the medium in which they were hydrated and the time spent within the hydration medium. Additionally, increasing the pH of the hydration medium resulted in increased hydration and increased erosion of the SBPs.

Comparison between SBPs showed that TMP underwent a superior hydration but was more prone to disintegration than SMP. During the study, a larger number of TMP did not remain as intact multiparticulate units as compared to SMP. Quantitatively, this finding was illustrated by Figure 2.7b as TMP showed a greater extent of erosion in each of the hydration media. The greater instability could be attributed to the size and internal structure of TMP as explicated in FTIR and SEM analysis. There was also a much higher inter-batch variability with TMP as was observed from the large standard deviations in Figure 2.7a and Figure 2.7b which suggested that more unpredictable results could be obtained when employing TMP in the MODDS. Thus, in addition to the hydration medium and hydration time, the type of SBP was important with SMP displaying more favorable characteristics than TMP.

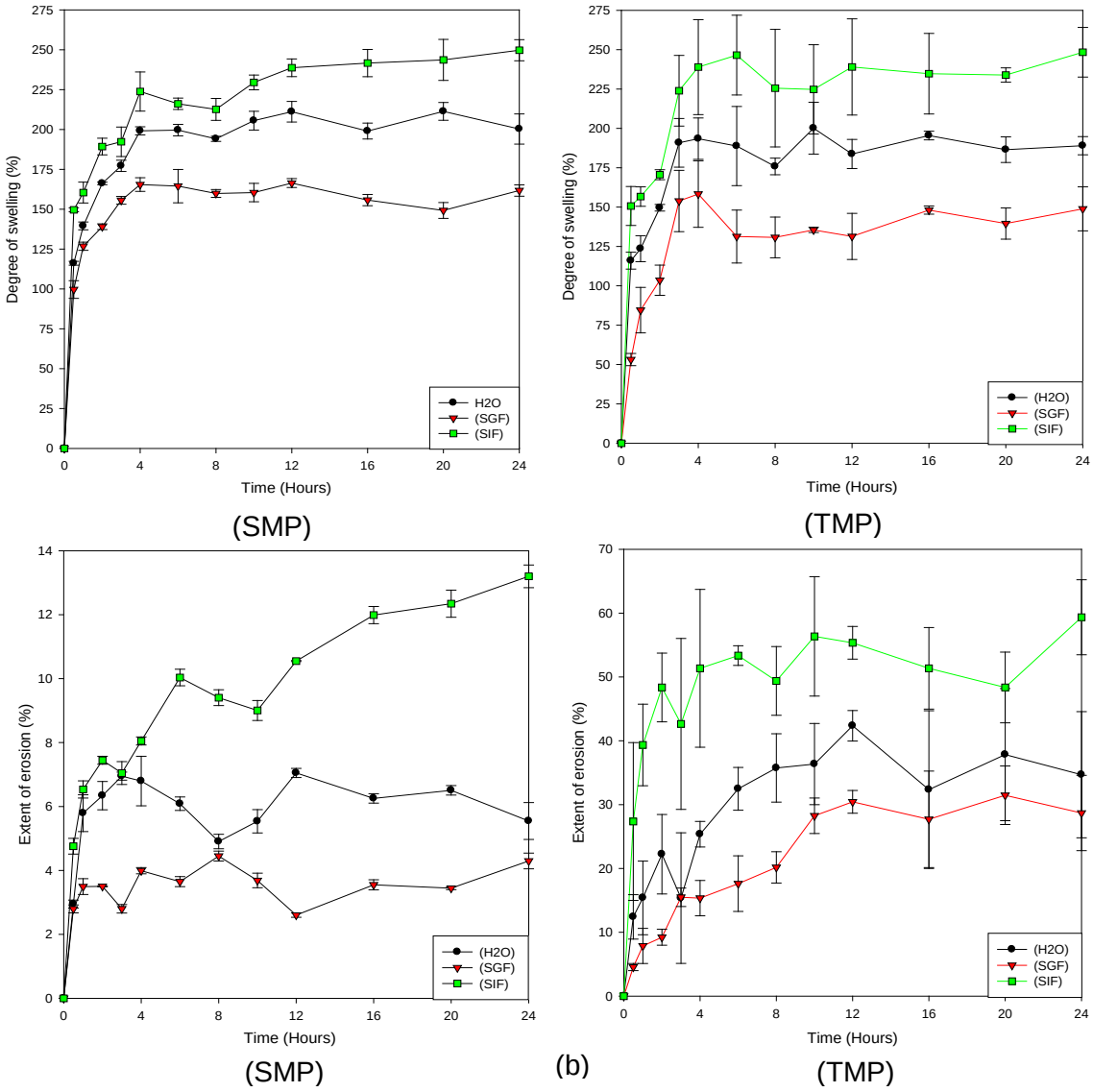


Figure 2.7: Effect of hydration time on (a) Degree of swelling and (b) extent of erosion of SBPs in water, pH 1.2 and pH 6.8. (n=3 in all instances).

2.3.5. Potential of the SBP to be employed as a buoyant MODDS

Neither the small SMP nor the larger TMP displayed any buoyancy in SGF. Both SBPs immediately sank upon contact with the dissolution medium and remained rooted to the bottom of the vessel throughout the duration of the study. The increased mass during hydration could have been a buoyancy prohibiting factor but essentially both SBPs lacked the potential to be employed as a gastro-floatable MODDS unless further modifications were imparted onto them.

2.3.6. Effect of hydration on the mechanical behavior of the SBPs

Figure 2.8 depicted the typical Force vs. Time graph used for the determination of SBP resilience**.** The resilience of non-hydrated SMP was low (~20%) and displayed a relatively small decrease of approximately 15% upon hydration with an inversely proportional relationship to the degree of hydration as depicted in Figure 2.9a. In contrast, non-hydrated TMP demonstrated excellent resilience (~125%) which could be due to the voids in its internal structure, which facilitated a degree of movement of the granules within the TMP during compression and allowed TMP to display characteristics that were more elastic. However, upon hydration the resilience of TMP decreased by ~85% and the effect of further hydration was minimal (Figure 2.9b). The decrease in resilience of the SBPs could be attributed to water entering the SBP and loosening intrinsic bonds thus causing the SBP to be more spongy and softer. However, SMP was able to maintain much more of its structural integrity and thus, portrayed a greater hydrated resilience than TMP.

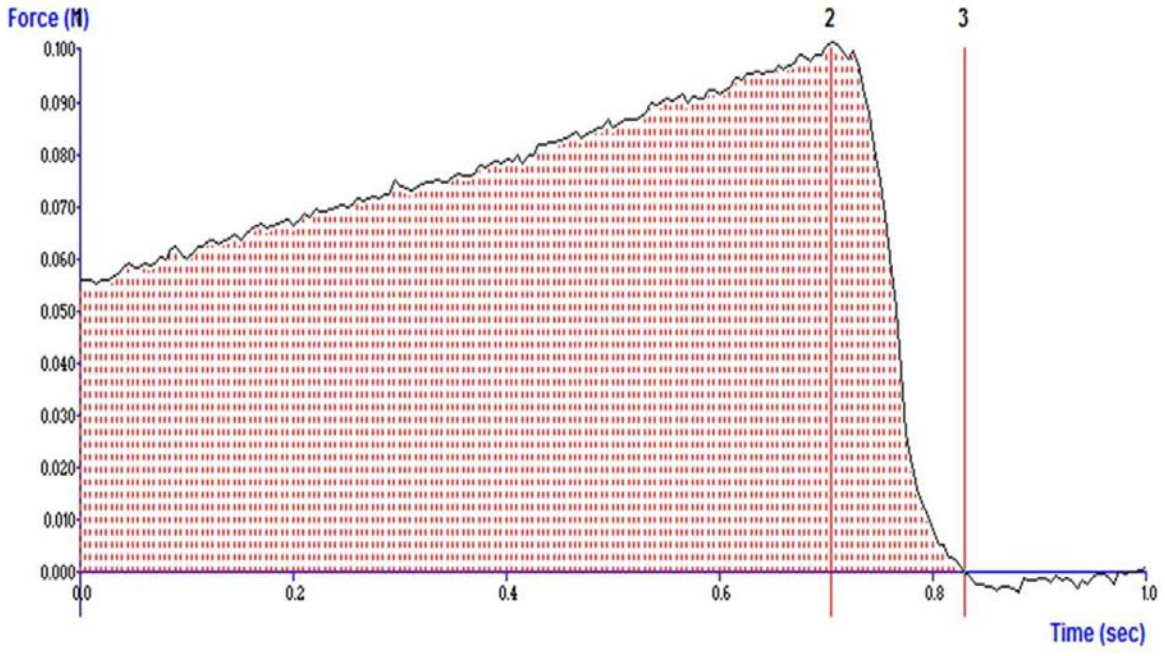
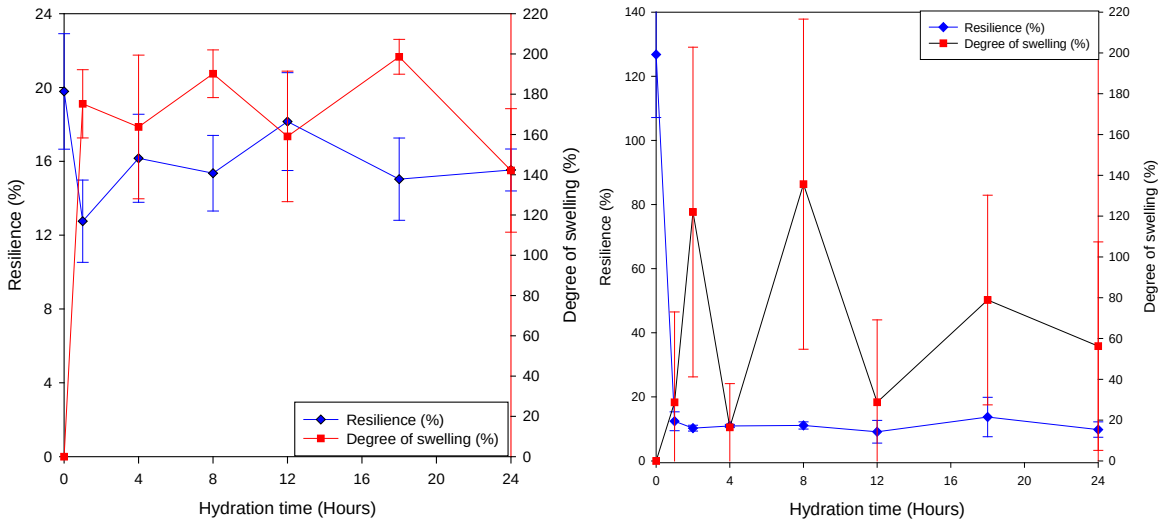


Figure 2.8: Typical Force vs. Time graph to determine the resilience of SBPs**.**



(a) (b)

Figure 2.9: Effect of hydration on the resilience of (a) SMP (b) TMP as a function of hydration time (n=5 in all instances).

Figure 2.10 depicted the typical Force vs. Distance graph used for the determination of SBP deformation energy and SBP hardness. SMP and TMP showed very similar non-hydrated deformation energy values of ~20N.mm (Figure 2.11a and Figure 2.11b) and hardness values of ~55N/mm (Figure 2.12a and Figure 2.12b). However, the deformation energy and hardness of both SBPs showed a drastic decline to below 1N.mm and 1N.mm^{-1} respectively upon hydration. These parameters showed consistent values of ~0.0776N.mm for deformation energy and ~0.222N/mm for hardness throughout the hydration processes. Thus, hydration did influence the textural profile in terms of hardness and deformation energy of the SBPs, but the time and degree of hydration had no influence on their deformation energy and hardness.

Single SBP hydration displayed very contrasting effects on SMP and TMP with SMP displaying fairly constant hydration patterns compared to the erratic hydration behavior observed in TMP as illustrated in Figure 2.9, Figure 2.11 and Figure 2.12. The inconsistent hydration of TMP could be attributed to its instability and resultant disintegration that made obtaining intact hydrated TMP samples very difficult. The results from this study showed that SMP were more stable compared to TMP. The deformation energy and hardness behavior of SMP resembled that of TMP but differed considerablely with regard to resilience. This could be as a result of the smaller size and internal structure of SMP and favored its use in developing the MODDS.

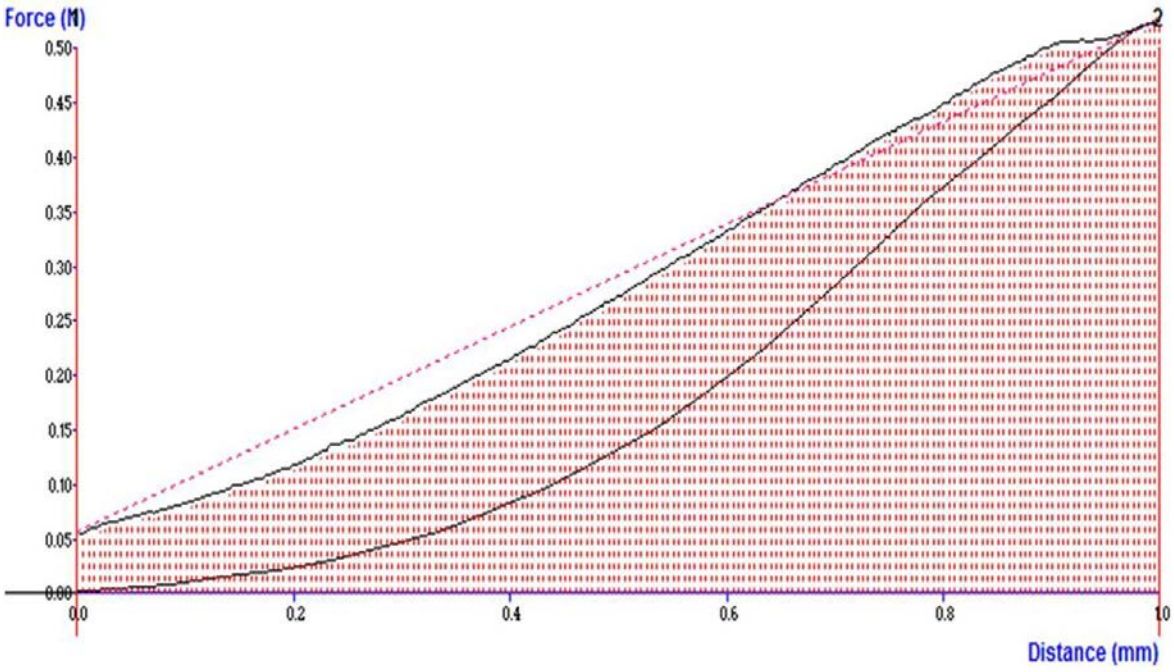


Figure 2.10: Typical Force vs. Distance graph to determine the deformation energy and hardness of SBPs.

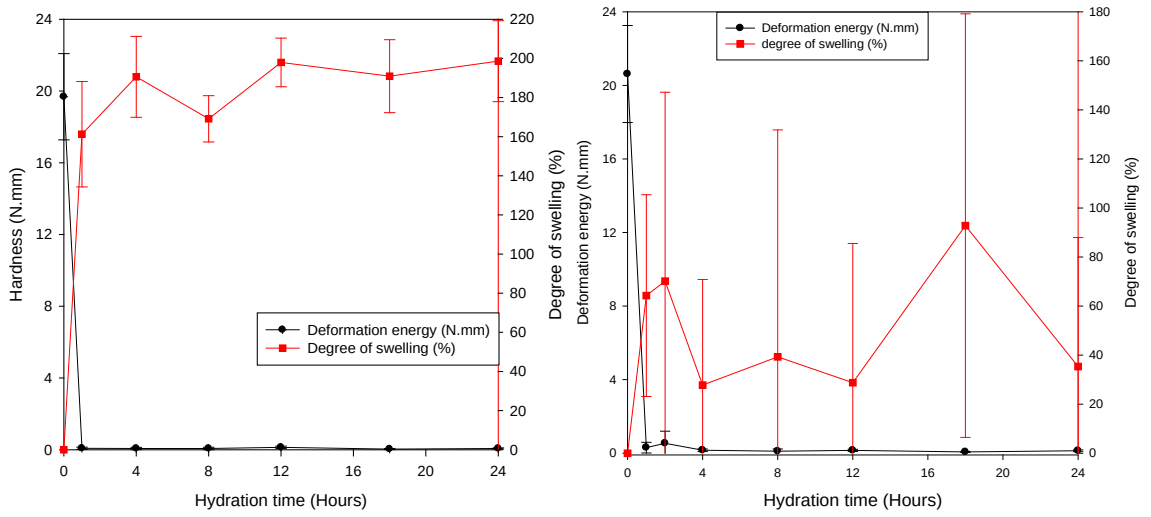
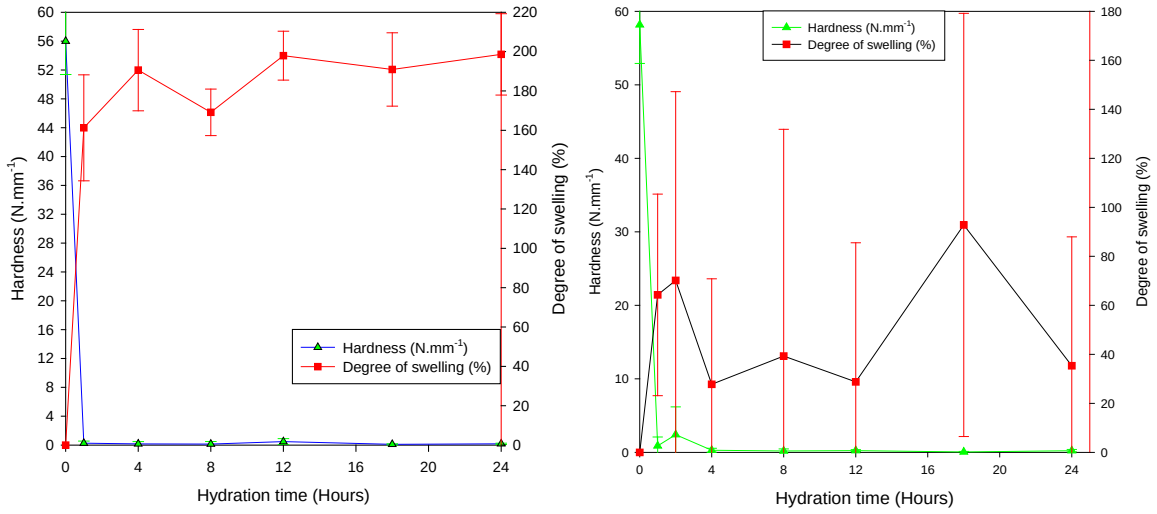


Figure 2.11: Effect of hydration on the deformation energy of (a) SMP (b) TMP as a function of hydration time (n=5 in all instances).



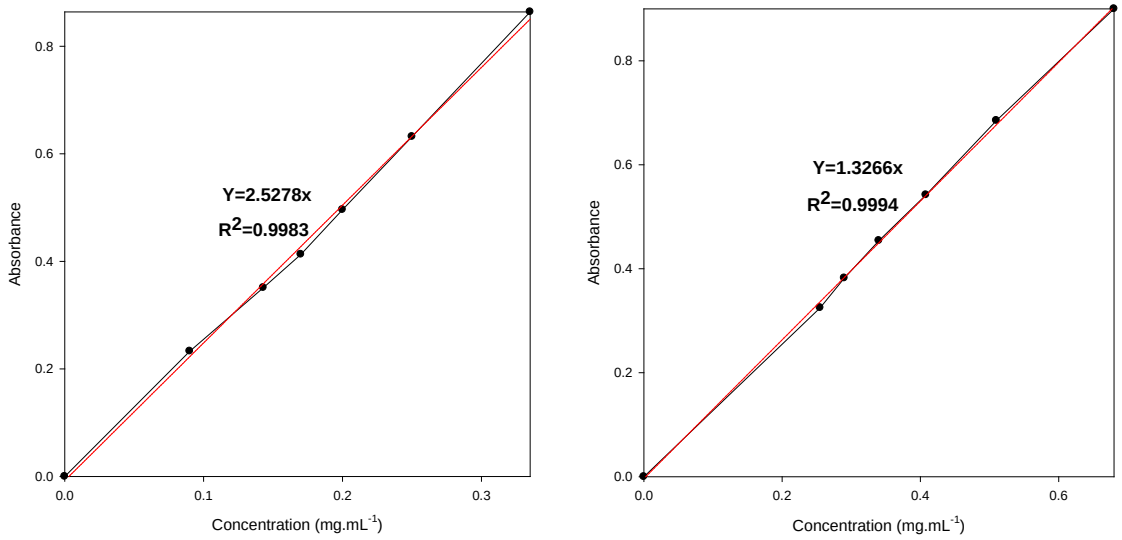
(a) (b)

Figure 2.12: Effect of hydration on the hardness of (a) SMP (b) TMP as a function of hydration time (n=5 in all instances).

2.3.7. Functional characteristics of the SBPs

2.3.7.1. Calibration curves of DPH in SGF and SIF

The calibration curves prepared displayed good linearity in both SGF (Figure 2.13a) and SIF (Figure 2.13b) with R^2 values of 0.9983 and 0.9994, respectively and was thus deemed appropriate to be used in quantifying the drug entrapment and drug release characteristics of the SBPs in these simulated biological fluids.



(a) (b)

Figure 2.13: Calibration curves of DPH in (a) SGF and (b) SIF.

2.3.7.2. Comparative DPH entrapment of the SBPs

Drug entrapment data showed SMP was able to entrap 546.452±15.546mg of DPH (DEE~36%, n=3), as compared to the 382.789±62.465mg of DPH (DEE~26%, n=3) entrapped by TMP. The experimental yield or Quantity of Drug Entrapped (QDE) was satisfactory for both SBPs, however, the results showed that SMP had a greater drug-loading potential than TMP and was thus more suited for use within the MODDS. It must be noted that TMP disintegrated to a greater extent during the drug entrapment study and thus resulted in a lower dried mass, which could have decreased its experimental yield and may be a further contributing factor to the large standard deviation observed with TMP. The DEE of both SBPs was low and this could be attributed to saturation of SBPs with DPH within the drug solution with the concentration of drug solution prepared at a high level (150mg.mL^{-1}) and the volume of drug solution used (10mL) was large. Reducing either or both of the above-mentioned factors was postulated to result in an improved DEE without necessarily increasing the QDE within the SBPs.

2.3.7.3. In vitro DPH release characteristics of SBPs

DPH release from both SMP (Figure 2.14a) and TMP (Figure 2.14b) showed a complete burst effect in both SGF and SIF. This burst effect was depicted by the steep rise in fractional drug release within the first 30 minutes followed by a plateau representing no further drug release for the remainder of the study. This could be due to DPH merely forming weak interactions with the surface of the starch granules with no substantial bond formation between functional group of DPH and SBP polymers. Comparison of the drug release profiles of SMP and TMP demonstrated almost identical DPH release behavior in both physiological fluids, which indicated a lack of superiority in controlling drug release by either SBP. This finding could be explained by the similarity in structure of both SBPs that resulted in neither of the SBPs possessing advantageous characteristics over the other with regard to retarding drug release. Even though FTIR and SEM analysis of the SBPs showed slight modification to the native sago and tapioca starch during multiparticulate formation, the modifications were not major and thus the drug release results obtained from the SBPs were comparable to the findings of Zhu and Bertoft (1997) and Pereswetoff-Morath (1998) which showed that native starches did not retard drug release sufficiently and could be attributed to the substantial hydration of starches. Thus modification of the SBPs may be crucial in developing a controlled release MODDS.

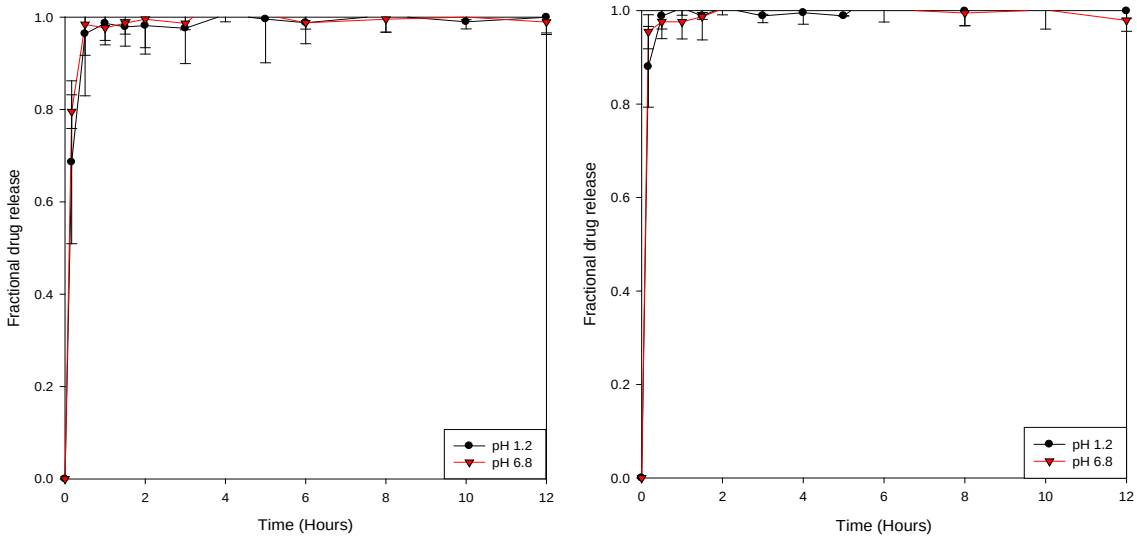


Figure 2.14: *In vitro* drug release profiles of (a) SMP and (b) TMP in simulated physiological fluids (n=3 in all instances).

2.4. Concluding Remarks

The studies demonstrated that SMP and TMP were very similar in structure but differed substantially with regard to stability when hydrated. Both SBPs were able to imbibe water and thus hydration could be used as a primary means of drug entrapment. TMP disintegrated to a larger extent during drug entrapment and displayed an inferior DEE to SMP. This lack of stability could be attributed to the larger size and spaces between the granules and granule clusters of TMP. Both SBPs showed a burst release and neither SBP was able to control drug release nor displayed any buoyancy and further enhancements to the SBPs will have to be explored to achieve a greater degree of control over drug release. SMP, due to its greater stability and greater QDE, was chosen as the SBP to be used in the development of the MODDS. The DEE of the SMP was low and could be improved by decreasing volume or drug concentration of the drug solution. Furthermore, the most favorable conditions encouraging drug entrapment must be elucidated in order to achieve the optimum DEE.

CHAPTER 3
OPTIMIZATION OF ENTRAPMENT OF DIPHENHYDRAMINE EMPLOYING THE BOX-BEHNKEN RESPONSE SURFACE METHODOLOGY

3.1. Introduction

Studies performed in Chapter 2 suggested that Tapioca Multiparticulates (TMP) displayed inferior stability and lower drug entrapment capacity compared to Sago Multiparticulates (SMP) and thus SMP was chosen as the Starch-Based Platform (SBP) to be utilized in the development of the Multiparticulate Oral Drug Delivery System (MODDS). Thus, from this point forward, the term SBP will refer to the particular use of SMP. In order to achieve optimum drug entrapment within the SBP, formulation parameters (variables) which exert a significant effect on drug entrapment need to be established. Determining the effect of individual independent variables on a response requires the use of large amount of materials, resources and time and does not provide information regarding the effects of interactions between the variables on the measured response (Pan *et al.,* 2008; Ray *et al.,* 2009; Dziczkowski and Soucek, 2012). The incidence of variable interactions is common and thus this approach could lead to inaccurate interpretation of the results and the likelihood of erroneous optimization (Pan *et al.,* 2008; Ray *et al.,* 2009).

Thus, in order to overcome this predicament simultaneous determination of the direct effects, pair-wise interaction effects and curvilinear variable effects of the independent variables is required and can be provided by statistical-based design of experiments (Mohajeri *et al.,* 2010; Dziczkowski and Sourcek, 2012). The most common statistical-based design of experiments is Response Surface Methodology (RSM) and involves statistical experimental designs, multiple regression analysis, and mathematical optimization algorithms for seeking the optimum formulation under a set of constrained conditions (Guo *et al.,* 2009; Badkar *et al.,* 2010).

The Box-Behnken Design (BBD) of experiments is one of many RSM designs employed, and is based upon the combination of two-level factorial designs and incomplete block designs with a minimum requirement of 3 factors (variables) each varied at 3 levels (Sheriff *et al.,* 2008; Ray *et al.,* 2009). The BBD differs from the other RSM designs in that this particular design uses points midway along the cube edge instead of eight corner points. The BBD is spherical, virtually rotatable and requires fewer experiments than other RSM designs (Ray *et al.,* 2009, Dziczkowski and Sourcek, 2012). A 3-Factor, 3-level (3^3)

BBD produces 13 distinct experimental design points, 12 of which are midway along the cube edge and 1 at the centre point as depicted in Figure 3.1. The centre point is replicated three times in order to compute an estimate of the error resulting in a total of 15 experimental runs (Sheriff *et al.,* 2008).

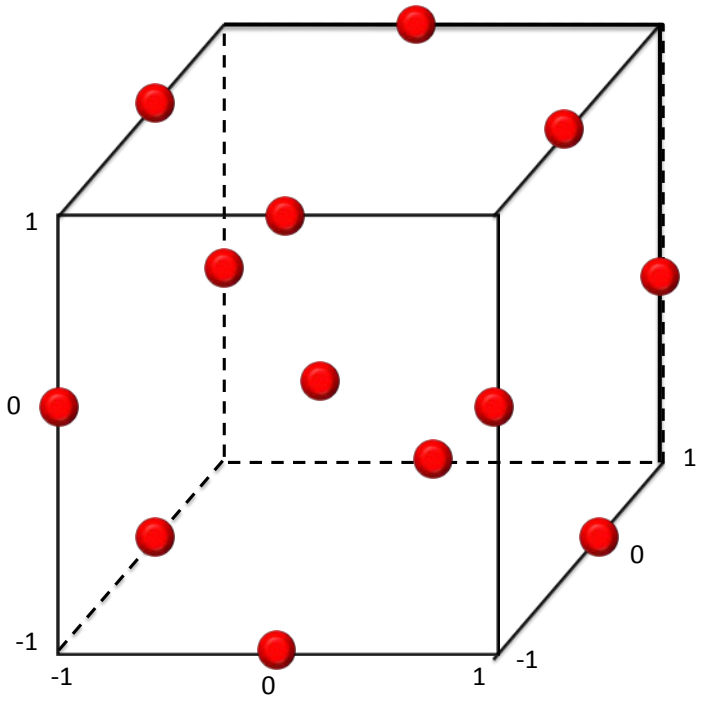
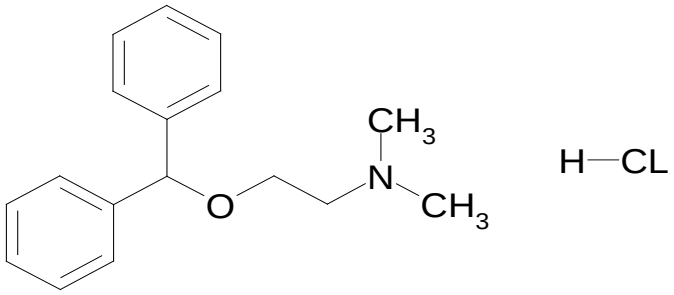


Figure 3.1: Schematic representation of design point of a 3-Factor, 3-level (3^3) Box-Behnken statistical design.

Diphenhydramine (DPH) is a first generation ethanolamine-derivative antihistamine and is commonly formulated as a hydrochloride salt (Carlson *et al.,* 2000; Kotwal *et al.,* 2007; Nandgude *et al.,* 2008; Mishra *et al*, 2010; Hung *et al.,* 2011). DPH occurs as a white, odorless, crystalline powder that slowly darkens on exposure to light. DPH has a pK_a of ~9 and is highly water soluble and freely soluble in alcohol (Mizuuchi *et al.,* 1999; Kotwal *et al.,* 2007; USP 33). The chemical structure of DPH is depicted in Figure 3.2. When taken orally, DPH is rapidly absorbed with an onset of action ~15 to 45 minutes post ingestion and peak effect occurs within 1 hour. Half-life of DPH ranges between 1-4 hours with the drug extensively protein bound. DPH is comprehensively metabolised in the liver and excreted as degradation products in the urine within 24 hours (Drugbank, 2012*).*



2-(Diphenylmethoxy)-*N*,*N*-dimethylethanamine hydrochloride

Figure 3.2: Chemical structure of diphenhydramine.

DPH exerts its pharmacological action by competitively inhibiting the binding of histamine to histamine (H1) receptors and thereby reduces smooth-muscle contraction in the respiratory and gastrointestinal tracts; pruritus; sneezing by sensory-nerve stimulation; vasodilation and vascular permeability (Galeotti *et al.,* 2003; Jeffery and Lytle-Saddler, 2008; Thormann *et al.,* 2011). In addition, DPH also exerts local anaesthetic properties and noteworthy anticholinergic effects which can result in adverse side effects such as dry mouth, throat and nose, thickening of mucus in the nose, throat and bronchi, tachyarrhythmias, hallucinations, urinary retention, blurred vision and sedation (Al-Baggou' and Mohammad, 1999; Carlson *et al.,* 2000; Thakur *et al.,* 2005; Thormann *et al.,* 2011). However, these anticholinergic effects may be clinically useful in treating mild insomnia and extrapyramidal effects in certain medical conditions (Thakur *et al.,* 2005). Thus, DPH is used to treat allergies, motion sickness, nausea and vomiting, mild insomnia and mild Parkinson's disease (Moraes *et al.,* 2004; Thakur *et al.,* 2005, Kotwal *et al.,* 2007; Hung 2011; Mehta *et al.,* 2011; Thormann *et al.,* 2011; Drugbank, 2012).

In this Chapter, DPH was selected as the model drug and process variables that affected its entrapment into the SBP were quantified. Furthermore, a BBD was implemented, which enabled the examination of the relationship between the drug entrapment response and the set independent process variables identified. This ultimately allowed the optimization of the levels of each process variable in order to maximize the drug entrapment within the SBP.

3.2. Materials and Methods

3.2.1. Materials

Sago Multiparticulates (SMP, food grade) was purchased from KOO South Africa (Tiger Brands Ltd., Bryanston, Johannesburg, South Africa). Diphenhydramine (DPH, Mw=291.82g.mol^{-1}, solubility>100mg.mL^{-1} in water at 21.5°C), was purchased from Aldrich® (Sigma-Aldrich Inc., St. Louis, USA) and used as the model drug. All other materials and chemicals used were as described in the Chapter 2.

3.2.2. Pre-formulation studies to determine variable parameters which influence drug entrapment of the SBP

3.2.2.1. Swelling time

It was established in Chapter 2, Section 2.2.5 that the SBP was able to imbibe water and this feature was used as a mechanism of entrapping drug within the SBP. It was further observed that the SBP could only absorb a limited quantity of water and that additional time spent within the hydration medium had little effect on the hydration capacity of the SBP. Since hydration is a mechanism of drug entrapment, it was important to determine the degree to which hydration influenced the Quantity of Drug Entrapped (QDE) of the SBP. DPH solution (150mg.mL^{-1}) was prepared by dissolving 40.5g DPH in 270mL deionized water. SBP samples (2g) were placed into DPH solution (10mL) and allowed to hydrate and entrap drug for 1, 2, 4, 8, 12, 18, 24, 36 and 48 hours under constant stirring at 50rpm in a shaker bath maintained at 25°±1C. After the predetermined time, the sample set was removed and the drug content of the SBP was determined as described in Chapter 2, Section 2.2.8.2.2.

3.2.2.2. Drying temperature

Applying heat to hydrated SBP was employed to increase the rate of dehydration of the SBP. The increased dehydration rate was postulated to improve QDE by inducing more rapid contraction of bonds between the starch polymers resulting in quicker expulsion of water and retention of drug within the core of the SBP. However, a drawback which discouraged the use of heat to dehydrate the SBP was the extensive gelatinization potential of the hydrated SBP which resulted in loss of drug-loaded SBP during drying. It was thus vital to determine the heat range that could be applied to dry the SBP without inducing noteworthy gelatinization and altering the multiparticulate nature of the SBP. DPH solution (150mg.mL^{-1}) was prepared by dissolving 27.0g DPH in 180mL deionized water. SBP samples (2g) were placed into DPH solution (10mL) and allowed to hydrate and entrap drug for 4 hours under constant stirring at 50rpm in a shaker bath maintained

at 25±1°C. The SBP samples were then removed and the drug content of the SBP was determined as described in Chapter 2, Section 2.2.8.2.2. The only alteration in the method was the drying conditions which were changed from air drying to the being convection dried in a laboratory oven maintained at either 15°C, 25°C, 40°C, 50°C, 60°C or 70° to elucidate the effect of drying temperature on the QDE of the SBP.

3.2.2.3. Volume of drug solution

As described in Chapter 2, Section 2.3.7.2, the volume of drug solution was another factor that would affect the Drug Entrapment Efficiency (DEE) and QDE of the SBP, and therefore determining the effect of volume change was an important step in determining optimum drug entrapment conditions. DPH solutions (150mg.mL^{-1}) of individual volumes 3mL, 5mL, 7mL and 10mL were prepared by accurately weighing and dissolving 1.35g, 2.25g, 3.15g, and 4.5g of DPH in 9mL, 15mL, 21mL and 30mL deionized water, respectively. SBP samples (2g) were placed into a DPH solution and allowed to hydrate and entrap drug for 4 hours under constant stirring at 50rpm in a shaker bath maintained at 25°±1C. Thereafter the sample sets were removed from the drug solution and the drug content of the SBP was determined as described in Chapter 2, Section 2.2.8.2.2.

3.2.2.4. Concentration of drug solution

The DEE of the SBP in Chapter 2, Section 2.3.7.2 was low in contrast to the QDE displayed by the SBP. This observation could be due to high concentration of DPH in the drug solution that resulted in saturation of DPH within the SBP and thus lead to wastage of excess drug. It was therefore important to determine the effect of drug solution concentration on both the DEE and QDE within the SBP. DPH solutions of concentrations 25mg.mL^{-1}, 50mg.mL^{-1}, 100mg.mL^{-1}, 150mg.mL^{-1} and 200mg.mL^{-1} were prepared by accurately weighing 0.75g, 1.5g, 3.0g, 4.5g and 6.0g of DPH, respectively, and dissolving each in 30mL deionized water. SBP samples (2g) were placed into a DPH solution (10mL) and allowed to hydrate and entrap drug under constant stirring at 50rpm in a shaker bath maintained at 25°±1C. Thereafter the sample sets were removed from the drug solution and the drug content of the SBP was determined as described in Chapter 2, Section 2.2.8.2.2.

3.2.2.5. Temperature of drug solution

Upon heating of starch in aqueous medium, the bonds between the starch molecules relax to a greater extent allowing the starch to achieve an increased hydration capacity and undergo gelatinization. This phenomenon was true for the SBP, and allowed a greater quantity of drug solution to enter and be retained by the SBP, thus increasing the

drug-loading capacity of the SBP. Therefore, it was crucial to elucidate the effects of hydration temperature on the drug entrapment of the SBP. DPH solution (150mg.mL^{-1}) was prepared by dissolving 13.5g DPH in 90mL deionized water. SBP samples (2g) were placed into a DPH solution (10mL) and allowed to hydrate and entrap drug for 4 hours in a shaker bath maintained at either 10°C, 25°C or 50°C under constant stirring at 50rpm. Thereafter the sample set was removed and the drug content of the SBP was determined as described in Chapter 2, Section 2.2.8.2.2.

Note: All drug solutions prepared were initially dissolved in an appropriate quantity of deionized water to ensure complete dissolution of DPH and thereafter made up to the required quantity as stated in each section. Furthermore, the quantity of each drug solution prepared in Section 3.2.2 was sufficient to conduct all studies mentioned in triplicate (n=3).

3.2.3. Optimization of the drug entrapment conditions utilizing a Box-Behnken design of experiments

3.2.3.1. Generation of a design of experiments through a BBD and subsequent testing

Preliminary drug entrapment investigations revealed that altering three processing conditions namely, hydration time within drug solution/Drug Loading Time (DLT); concentration of drug solution ([DPH]); and Drying Temperature (DT), greatly affected both the QDE and DEE within the SBP. It was also observed that hydration temperatures above 25°C resulted in decreased SBP stability and was thus kept constant at 25°C. The volume of drug solution used only affected the DEE, as the theoretical yield was altered with changing solution volume and very little effect on the QDE (experimental yield) as explicated by Equation 2.4. Thus, the hydration volume was kept constant at 5mL. The upper and lower limits of the variable conditions were determined as 4-24 hours, 50-150mg.mL^{-1} and 25-50°C for DLT, [DPH] and DT respectively, as depicted in Table 3.1.

Table 3.1: Formulation variable limits and responses with objective

Independent variables	**Upper limit**	**Lower limit**	**-**
[DPH] (mg.mL^{-1})	50	150	
DLT (Hours)	4	24	-
DT (°C)	25	50	-
Response	**Upper limit**	**Lower limit**	**Objective**
QDE (mg)	300	470	maximize

Where [DPH] denoted the concentration of Diphenhydramine in the hydration medium, DLT denoted the Drug-Loading Time, DT denoted the Drying Temperature and QDE denoted the Quantity of Drug Entrapped within the SBP

Based on the constraints for the variable conditions, a 3-Factor, 3-level (3^3) Box-Behnken statistical design on MINITAB®, (V14, Minitab, USA) was employed that generated 15 experimental formulations as illustrated in Table 3.2. These formulations were prepared and subsequently assessed to quantify the DPH entrapped within the SBP.

Table 3.2: Experimental matrix generated by Box-Behnken statistical design

Formulation	[DPH] ($mg.mL^{-1}$)	DLT (Hours)	DT (°C)
1	100	24	25
2	50	24	37.5
3	150	14	25
4	100	14	37.5
5	100	4	50
6	100	24	50
7	50	14	50
8	150	24	37.5
9	50	4	37.5
10	50	14	25
11	100	14	37.5
12	100	14	37.5
13	150	4	37.5
14	150	14	50
15	100	4	25

Where [DPH] denoted the concentration of Diphenhydramine in the hydration medium, DLT denoted the Drug-Loading Time and DT denoted the Drying Temperature

3.2.3.2. Determination of drug content and entrapment efficiency

Drug entrapment was conducted as described in Chapter 2, Section 2.2.8.2.1 employing the respective processing conditions generated by the design and described in Table 3.2 using 5mL drug solution and maintained at 25°C. Determination of the extent of drug entrapment was conducted as described in Chapter 2, Section 2.2.8.2.2.with convection drying undertaken in a laboratory oven.

3.2.3.3. Optimization of the formulation parameters

Following analysis of the experimental formulations and generation of the polynomial equation relating the dependent and independent variables, the formulation process was optimized under constrained conditions for the measured response of QDE. Equation solving for optimization of the formulation process was performed to obtain the levels of independent variables, which would achieve the desired drug entrapment (i.e. maximization of the QDE within the SBP) on MINITAB®, (V15, Minitab Inc, Pennsylvania, USA).

3.2.3.4. Determination of the in vitro drug release behavior of optimized DPH-loaded SBP

Drug-loaded SBP was formulated according to the optimized conditions established and the quantity of optimized DPH-loaded SBP containing 50mg DPH was determined, accurately weighed and subjected to *in vitro* drug release studies as described in Chapter 2, Section 2.2.8.3.

3.3. Results and Discussion

3.3.1. Effect of variable parameters on the drug entrapment of the SBP

Figure 3.3a demonstrated that hydration of the SBP increased sharply during the first 4 hours within the hydration medium after which SBP hydration remained fairly constant until 24 hours at which point maximum SBP hydration of 249.570±4.3546% was observed. Beyond 24 hours, decrease in the Degree of Swelling (DOS) of the SBP was noticed and this alluded to saturation in hydration capacity at 24 hours and possible erosion of the SBP with further time within the hydration medium. Figure 3.3a further illustrated a close correlation between the hydration capacity and the drug-loading potential of the SBP. This was clearly evident as the QDE curve very closely followed the DOS curve as a function of time. Due to the acceptable QDE values (520.2870±6.3155mg) after 4 hours within drug solution, the 4-hour time point was selected as the lower limit for DLT.

After 24 hours within drug solution, the QDE of the SBP was 549.0384±5.3565mg, which was slightly lower than the maximum QDE (562.7664±7.3563mg DLT=18 hours), and thereafter the QDE decreased substantially in accordance with the decreasing DOS. This could be due to increased disintegration of the SBP within the drug solution which resulted in a decrease in physical SBP available to entrap DPH and was evident by the lower drug-loaded SBP mass recovered after drying. Therefore, the upper limit for DLT was chosen as 24 hours.

Figure 3.3b illustrated the effect of DT on the drug entrapment potential of the SBP. At low DT (15°C), the SBP displayed low QDE values (367.5299±6.2450mg) but as heat was applied to the hydrated SBP, quicker bond contraction within the SBP was evident which lead to increased drug entrapment and quicker drying time. The lower limit for DT was thus selected as 25°C. The applied heat also caused gelatinization of the SBP, which further enhanced the QDE, but only up to 50°C at which point QDE was 557.3735±8.3585mg. Thereafter the gelatinization of the SBP became excessive and

caused SBP mass loss through attachment of the gelatinized surfaces to the surface of the petri dish and flat-ended metal spatula during separation. The loss of SBP mass resulted in decreased QDE and thus the upper limit of DT was determined to be 50°C.

The volume of drug solution used affected both the QDE and the DEE of the SBP (Figure 3.3c). At the low drug solution volume of 3mL, the SBP demonstrated low QDE (416.469±8.878mg) which correlated to the low DOS (151.499±10.348%) displayed by the SBP. This was due to the SBP completely imbibing the drug solution without saturating the hydration potential of the SBP and implied that an insufficient volume of drug solution was used. When placed in drug solution volumes between 5mL and 10mL, the SBP exhibited steady DOS values ranging between 221.349% and 246.569%, with excess solution remaining within the experimental apparatus. This suggested that saturation of the hydration potential of the SBP was achieved. The constant DOS translated into relatively constant QDE values ranging between 509.486mg and 555.866mg.

The effect of drug solution volume on DEE was more pronounced as increasing the volume resulted in a steady decrease in DEE as depicted in the insert in Figure 3.3c. This, coupled with the constant QDE, implied greater wastage of drug with no enhanced drug-loading at higher drug solution volumes. Thus, it was concluded that the drug solution volume was to be maintained at 5mL to ensure adequate hydration and maximize DEE with minimal drug wastage.

The effect of [DPH] had minimal effect on the hydration capacity as the SBP displayed relatively constant DOS (~235±10%) at all [DPH] utilized in the study, but had a marked effect on the QDE and DEE of the SBP as illustrated in Figure 3.3d. The general trend observed in the study showed that as the [DPH] within the hydration medium increased, the QDE of the SBP increased. This was attributed to increase drug content within the hydration medium that allowed increased interaction between the SBP and DPH molecules and which resulted in a greater ability of the SBP to entrap DPH. This observation was true up to [DPH] of 150mg.mL^{-1} after which the QDE remained constant, which alluded to saturation of drug within the SBP. Thus, 150mg.mL-1 was chosen as the higher limit of [DPH] to be used in optimizing drug entrapment.

The effect of [DPH] on the DEE of the SBP was illustrated in the insert of Figure 3.3d. When [DPH] was below 50mg.mL^{-1} displayed very low QDE (<200mg per 2g SBP) and the associated DEE was low as well (32.184±0.938% at [DPH] = 25mg.mL^{-1}). This was

attributed to the very low drug content within the hydration solution that caused inadequate interaction between SBP and DPH molecules. At 50mg.mL^{-1}, the QDE was greater than 200mg (220.6456±5.8760mg) and the DEE was the highest (44.1291±1.1752%) which suggested increased SBP-DPH interactions with the least degree of drug wastage and was thus chosen as the lower limit of [DPH] to be used in optimizing drug entrapment. Upon further [DPH] increases, saturation of the SBP with DPH occurred and further wastage of drug, which resulted in the lower DEE. The decreased DEE was related to the increased drug content within the hydration medium and thus the higher predicted yield illustrated by Equation 2.4.

Manipulating the temperature at which drug entrapment occurred showed destructive effects on the SBP. As the temperature was increased, the SBP was able to imbibe more drug solution but displayed decreased mechanical stability. At even higher temperatures, the SBP began to gelatinize and coalesce to form a large starchy mass that was impossible to separate into distinct particles. Furthermore, loss of SBP mass upon drying due to sticking of the coalesced mass was an added deterrent for the use of heat during the drug-loading process. It was therefore decided to keep the hydration temperature constant at 25°C throughout future studies.

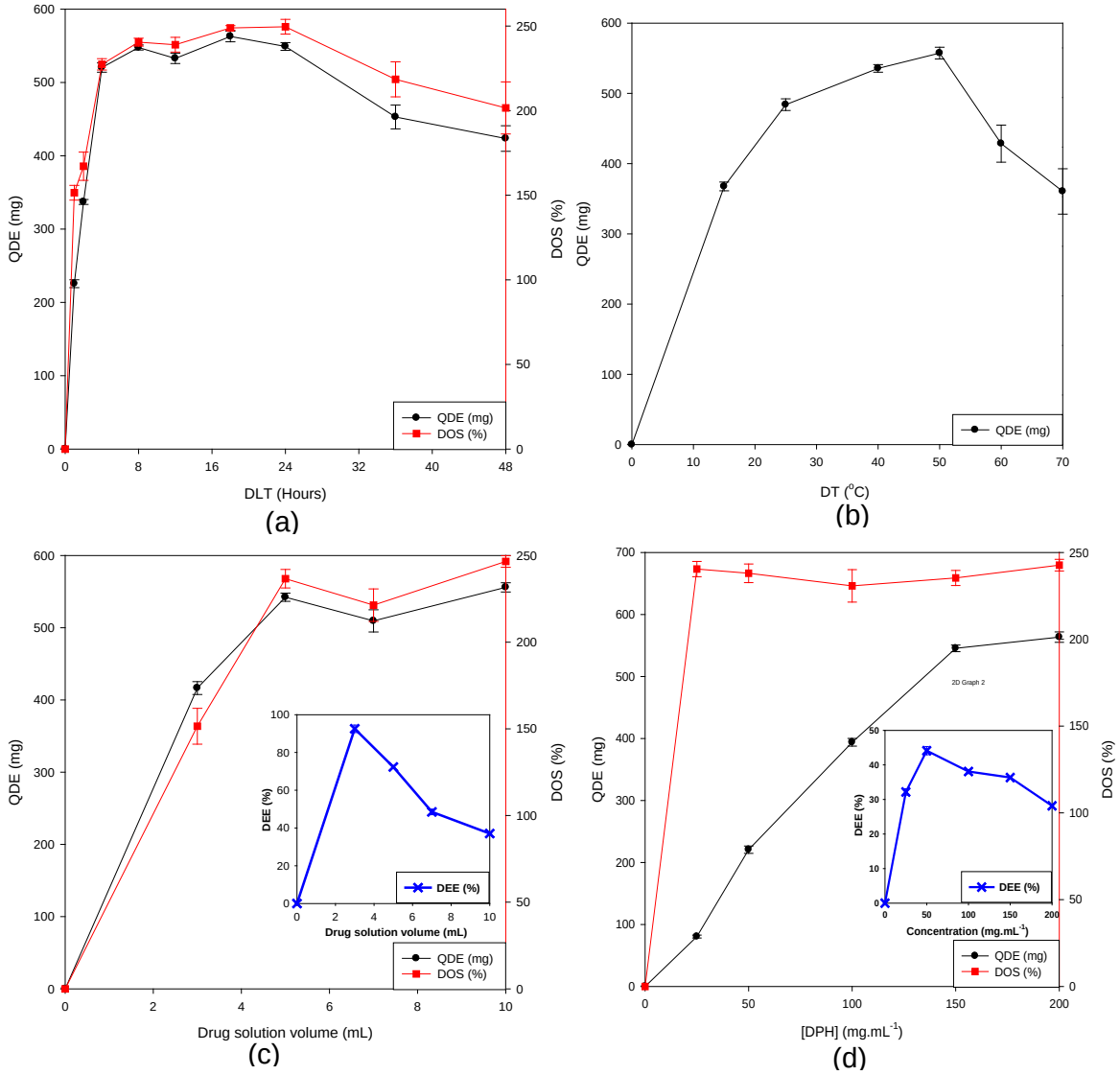


Figure 3.3: Effect of (a) DLT, (b) DT (c) drug solution volume and (d) [DPH] on the QDE of SBP with the inserts in (c) and (d) depicting the effects of drug solution volume and [DPH] respectively on the DEE of the SBP. (n=3 in all instances).

3.3.2. Measured responses for the experimentally synthesized SBP formulations

The measured responses obtained for the experimentally synthesized SBP are depicted in Table 3.3 and Figure 3.4. Formulations with low [DPH] (Formulations 2, 7, 9 and 10) displayed high DEE values (79.614-92.951%) but relatively low QDE vales (199.036-232.387mg). this was in contrast to the high QDE values (395.498-547.240mg) and relatively low DEE values (52.733-72.965%) demonstrated by formulations with high [DPH] (Formulations 3, 8, 13 and 14) as depicted in Table 3.3 and Figure 3.4. The DEE in these formulations was due to the theoretical yield value represented in Equation 2.4.

DLT showed varying results on the QDE and DEE of the SBP with 14 hours being in most cases the best DLT. The composite formulation parameters affected the hydration in different ways and thus did not correlate well with the QDE as was seen in preliminary studies. The influence of DT was most pronounced at higher temperatures, which suggest a beneficial thermal alteration of the structure of the SBP, thus causing drug to be more adequately incorporated into the SBP. The mass gained by the SBP correlated well with the QDE values which indicated that the mass gained during drug-loading was largely due to drug incorporation into the SBP. The mass gain however was slightly lower than the quantity QDE and this difference could be attributed to a minor erosion of the SBP during hydration. In the context of these SBP formulations, the QDE was viewed as more important than the DEE as the QDE would affect the actual size of the dosage form and thus the QDE was utilized as the response for which the SBP drug entrapment would be optimized.

Table 3.3: Drug entrapment of Box-Behnken DOE SBP formulations

Formulation	Mass gain (mg)	DOS (%)	QDE (mg)	DEE (%)
1	0.352	236.342	388.364	77.673
2	0.173	240.750	232.378	92.951
3	0.420	205.245	484.158	64.554
4	0.282	234.238	402.976	80.595
5	0.335	195.349	351.642	70.328
6	0.244	231.456	407.938	81.588
7	0.067	238.106	219.256	87.703
8	0.280	208.908	395.498	52.733
9	0.046	211.407	199.036	79.614
10	0.144	239.787	229.977	91.991
11	0.312	234.327	418.774	83.755
12	0.285	240.363	375.626	75.125
13	0.357	189.492	427.372	56.983
14	0.403	208.974	547.240	72.965
15	0.302	204.671	344.891	68.978

Where DOS denoted the Degree of Swelling, QDE denoted the Quantity of Drug Entrapped and DEE denoted the Drug Entrapment Efficiency

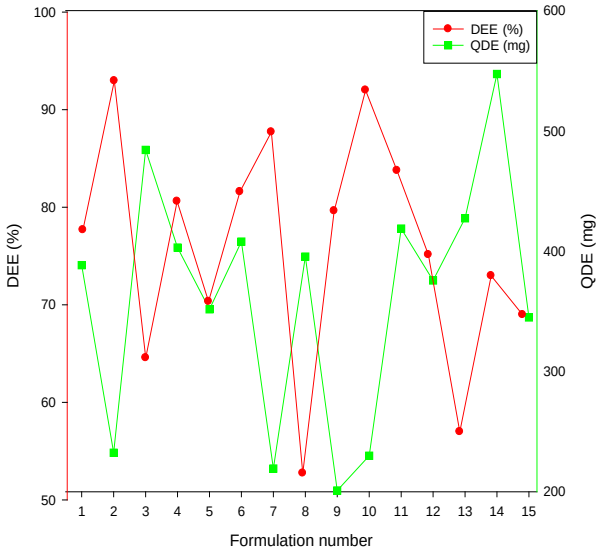


Figure 3.4: DEE vs. QDE of design generated SBP formulations.

3.3.3. Comparative analysis between experimental and predicted values for the design generated SBP formulations

Experimental results of each of the design formulation were plotted against the design predicted value for the response QDE together with the lower and upper 95% predicted confidence limits as illustrated in Figure 3.5. The resultant R^2 of 95.3% demonstrated that a good correlation between the experimental and predicted values was achieved. In addition, when compared to the 95% predicted confidence limits, it was observed that all experimental values for QDE fell within this range thus authenticating the BBD used.

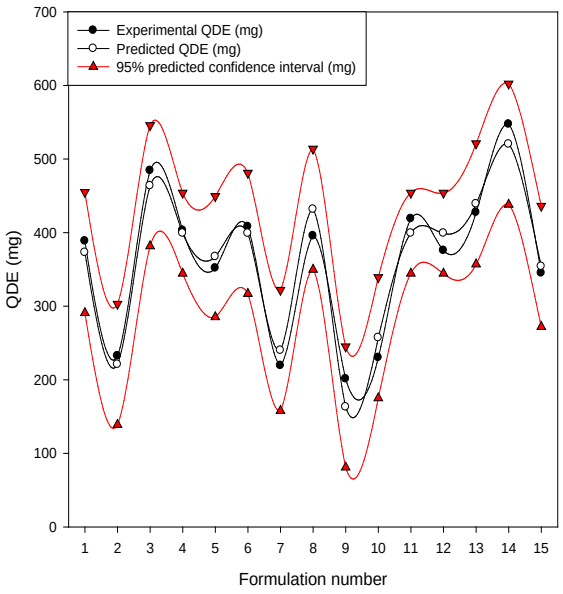


Figure 3.5: Regression plots comparing experimental and fitted values ±95% confidence interval for QDE of the SBP formulations.

3.3.4. Effect of independent variables on the mass gain of the SBPs

Figure 3.6 showed the average effect of each independent variable of the design on the mass gain of the design formulations. It was observed that [DPH] and DT displayed linear correlation with mass gain with R^2 values of 0.9672 and 0.9891 respectively and that DLT displayed no correlation with mass gain (R^2=0.0242). DLT did however affect the QDE and the lack of mass gain could be attributed to increased erosion experienced by the SBP with DLT. The most pronounced singular effect on mass gain was elicited by [DPH] with the mass gain showing correlation to the QDE of the SBP.

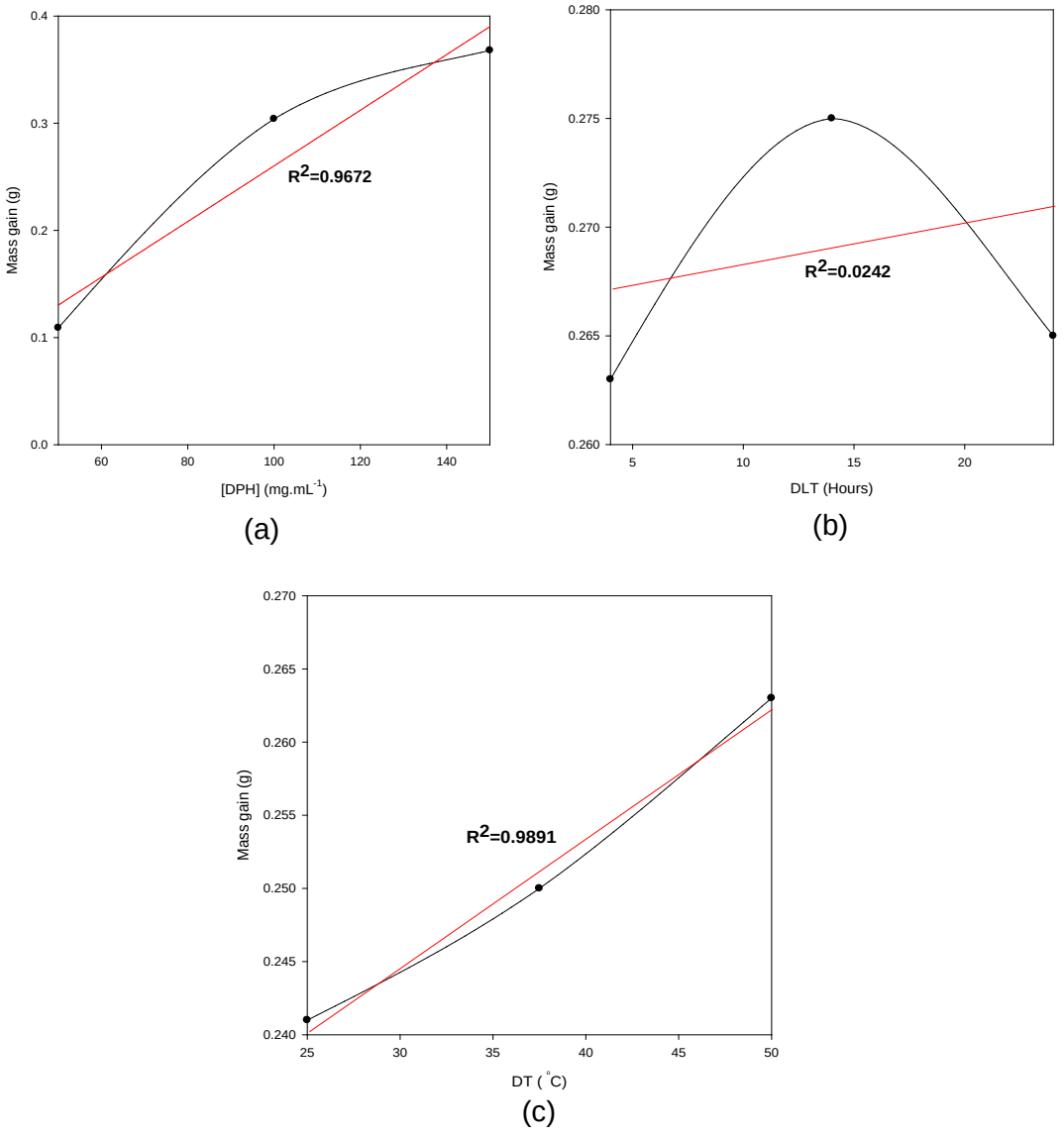


Figure 3.6: Effect of design variables (a) [DPH], (b) DLT and (c) DT on the mass gain of SBP as a result of drug entrapment.

3.3.5. Analysis of the Box-Behnken Design

3.3.5.1. Analysis of residuals generated by experimental design formulations

Diagnostic residual analysis of the BBD was conducted in order to evaluate the suitability and robustness of the design (Figure 3.7). Smaller residuals values indicated less variance and higher design accuracy and were thus a desired outcome for the design. Analysis of the normal probability plot of the residuals showed that the residuals fell on a straight line and thus confirmed the normal distribution of data for QDE. The residuals versus fitted plot for DQE showed randomly scattered residual data points around the horizontal line (residual=0), which indicated constant variance. The residuals and standardised residuals indicated that all experimental values were adequately fitted by the response surface model with no outliers, denoted by standardised residuals >2, detected. The histogram of the residuals for DEE confirmed the normal distribution with the mean at zero and constant variance. Analysis of the residuals versus the order of the data was used to identify non-random error for experimental QDE runs. This QDE plot showed a both positive (clustering of Formulations 1-4) and negative correlation indicated by rapid changes in the signs (-/+) of the subsequent consecutive residuals.

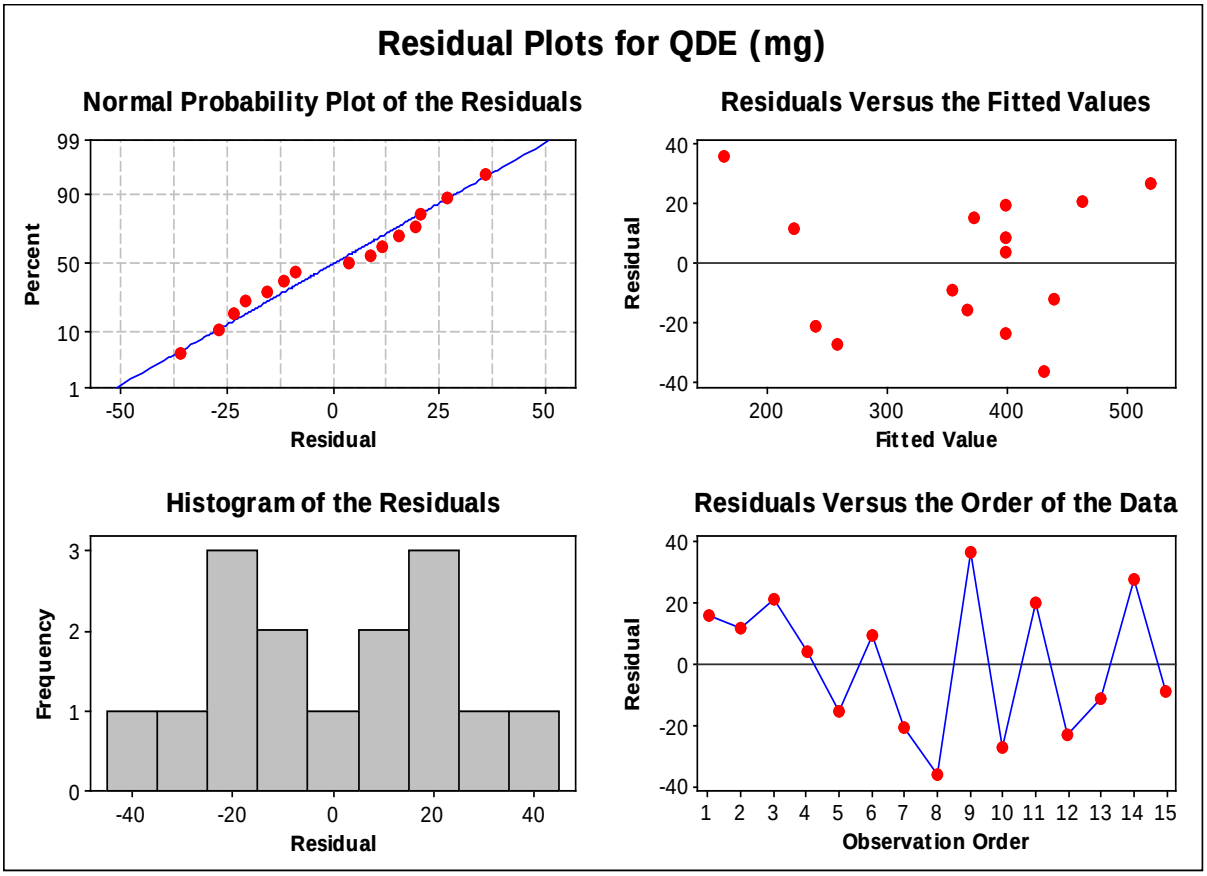


Figure 3.7: Residual plots for QDE (mg).

The analysis of variance for the QDE model (Table 3.4) demonstrated that the terms [DPH], DLT, DT, DT x DT, [DPH] x DT and DLT x DT had a positive correlation with QDE and that the terms [DPH] x [DPH], DLT x DLT and [DPH] x DLT displayed a negative correlation with QDE. The positive and negative correlations implied than an increase in these terms would result in an increase and decrease in QDE, respectively. The ANOVA table further showed that the [DPH] concentration had the largest and most significant effect on the QDE of the SBP (coefficient=121.703 and $p<0.05$) with the effect of the remainder of the terms being much less significant ($p>0.05$). This was congruent to the mass gain of the SBP, which showed that [DPH] elicited the greatest effect on the QDE of the SBP. In its entirety, the regression model exhibits a significant effect on QDE, denoted by the regression $p<0.05$, and fitted the model adequately with the lack of fit $p>0.05$ and R^2=95.3% thus affirming the robustness of the design.

Table 3.4: ANOVA table depicting regression coefficients for QDE (mg) with accompanying p-values

Term	Coefficient	P-value
Regression	-	0.011
Constant	399.125	0.000
[DPH]	121.703	0.000
DLT	12.655	0.300
DT	9.836	0.506
[DPH] x [DPH]	-44.303	0.098
DLT x DLT	-41.252	0.119
DT x DT	15.335	0.576
[DPH] x DLT	-16.304	0.294
[DPH] x DT	18.451	0.386
DT x DLT	3.206	0.875
Lack of fit	-	0.183

Where [DPH] denoted the concentration of Diphenhydramine in the hydration medium, DLT denoted the Drug-Loading Time and DT denoted the Drying Temperature

The complete regression equation representing the relationship between the independent variables and the QDE response was described by Equation 3.1:

QDE = 399.125 + 121.703 x [DPH] + 9.836 x DT + 12.655 x DLT - 44.303 x [DPH] x [DPH] – 41.252 x DLT x DLT + 15.335 DT x DT - 16.304 x [DPH] x DLT + 18.451 x [DPH] x DT + 3.206 x DT x DLT ***Equation 3.1***

3.3.5.2. Determination of the main effects on QDE of SBPs

The main effects plots showed that a decrease in QDE is produced when DLT was either <or> 14 hours (Figure 3.8a) and an increase in QDE is produced when DT was either <or> 37°C (Figure 3.8b). The 15mg increase observed when lowering DT compared to 30mg increase when elevating the DT showed that increasing DT was the superior process modification. However, altering the DLT and DT produced a mere 50mg and 30mg change in QDE values was thus deemed insignificant (DLT p=0.300, and DT p=0.506) in affecting the QDE of the SBP (Table 3.4). When analyzing the main effect plot of [DPH] (Figure 3.8c), it was observed that increasing the [DPH] from 50mg.mL^{-1} to 150mg.mL^{-1} increased the QDE of the SBP. In contrast to DLT and DT, altering the [DPH] had a profound and significant effect on QDE (QDE increase of ~230mg and p=0.000) (Table 3.4) and was thus concluded to be the main effect on the QDE of the SBP.

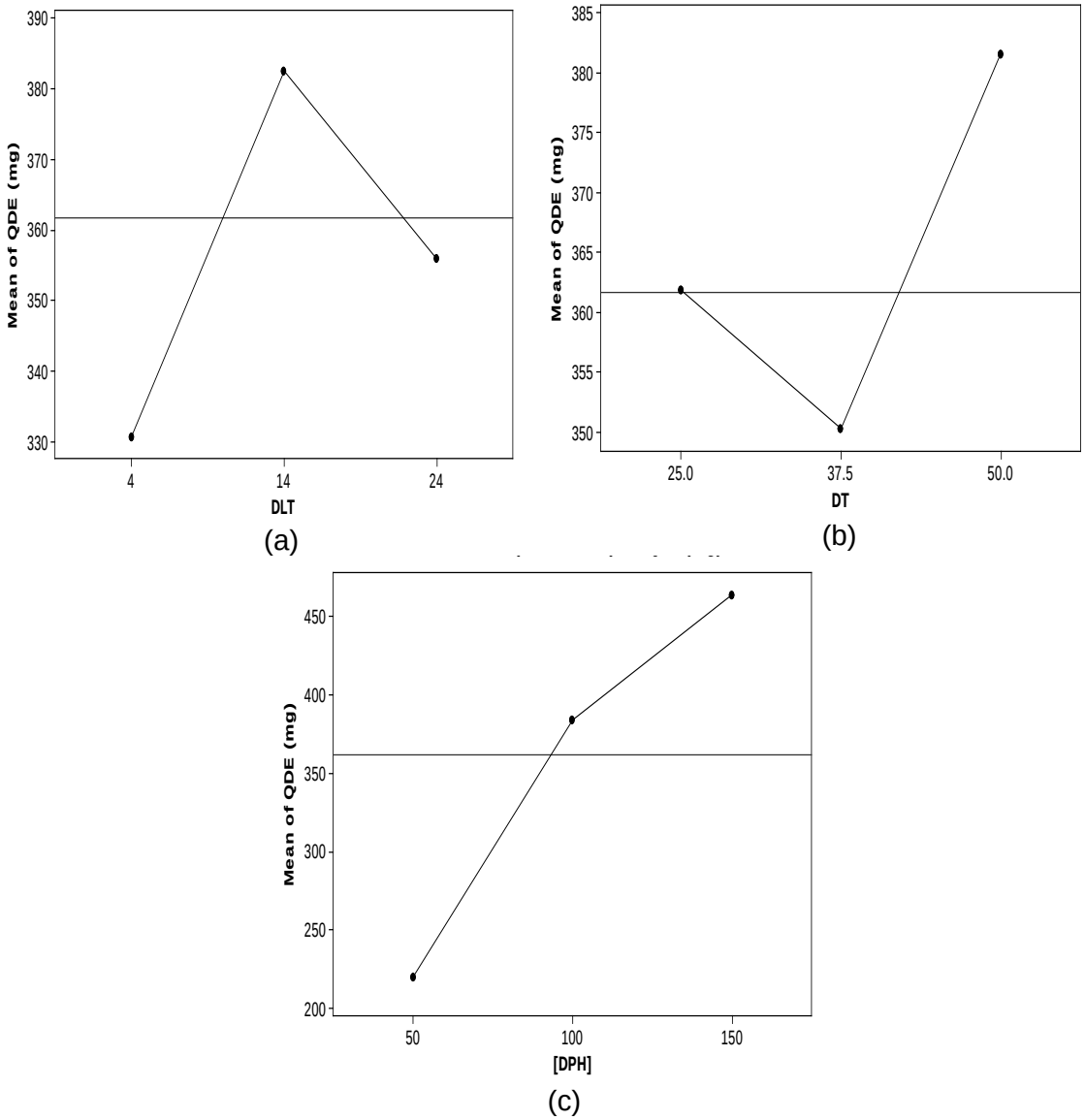


Figure 3.8: Main effects plots of (a) DLT, (b) DT and (c) [DPH] on the QDE of the SBP.

3.3.5.3. Determination of the interactions between independent variable on the QDE of the SBP

Figure 3.9 demonstrated the effect of independent variable interactions on the QDE of the SBP. At low and medium hold values of [DPH], altering the DLT had no significant impact on QDE whereas at the high holding value of [DPH] (i.e. DPH=150mg.mL^{-1}), increasing DLT up to 14 hours increased QDE and further increases in DLT beyond 14 hours decreased QDE of the SBP. Inversely, when DLT was held constant, altering [DPH] showed a positive effect by increasing the QDE as [DPH] was increased at the low and medium hold values for DLT and demonstrated a plateau as [DPH] increased beyond 100mg.mL^{-1}. The resultant model interaction between [DPH] and DLT was judged to be insignificant with p=0.294 (Table 3.4).

With regard to effect of altering DT at low and at medium hold values for [DPH], QDE values showed no significant change. However, upon comparison to the high hold value for [DPH], QDE decreased as the DT increased from 25ºC to 37.5ºC and thereafter QDE increased as DT increased further. When [DPH] was altered at steady DT values, the same effect was observed as was seen when altering [DPH] values at constant DLT values. However, the plateau was demonstrated by the medium hold value (DT = 37.5ºC) instead of the high value demonstrated by DLT. The resultant model interaction between [DPH] and DLT was judged to be insignificant with p=0.386 (Table 3.4).

When DLT values were held constant, Interactions between DT and DLT were analogous to those observed between [DPH] and DT at constant [DPH] values where no impact on QDE was observed by increasing DT at low and medium DLT hold values and QDE increased as DT was either <or> 37ºC at the high DLT hold value. Upon altering DLT values at constant DT values, profiles similar to those observed between [DPH] and DLT at constant [DPH] values were produced. However, the decrease in QDE as DLT was either <or> 14 hours was observed in the medium hold value of 37ºC and not the high hold value as was the case with the [DPH]-DLT interaction. Holistically, the interactions between DT and DLT was the least significant for the regression model as p=0.875 (Table 3.4).

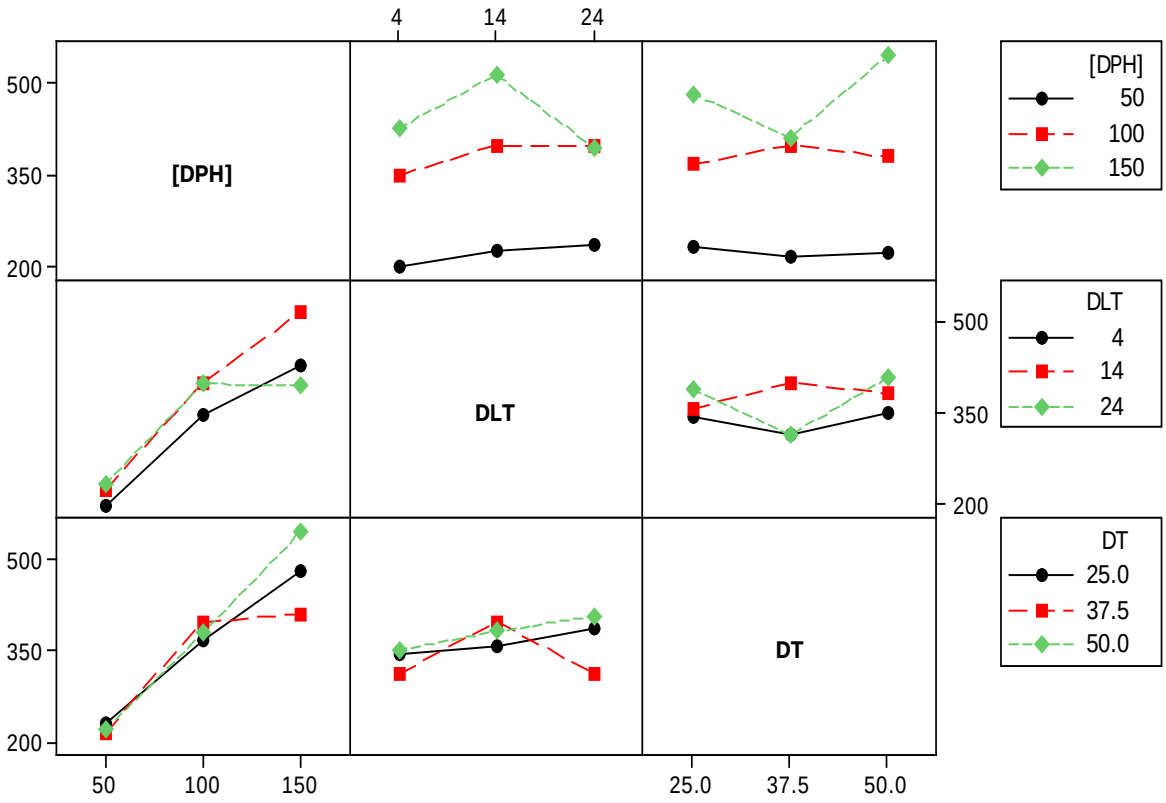
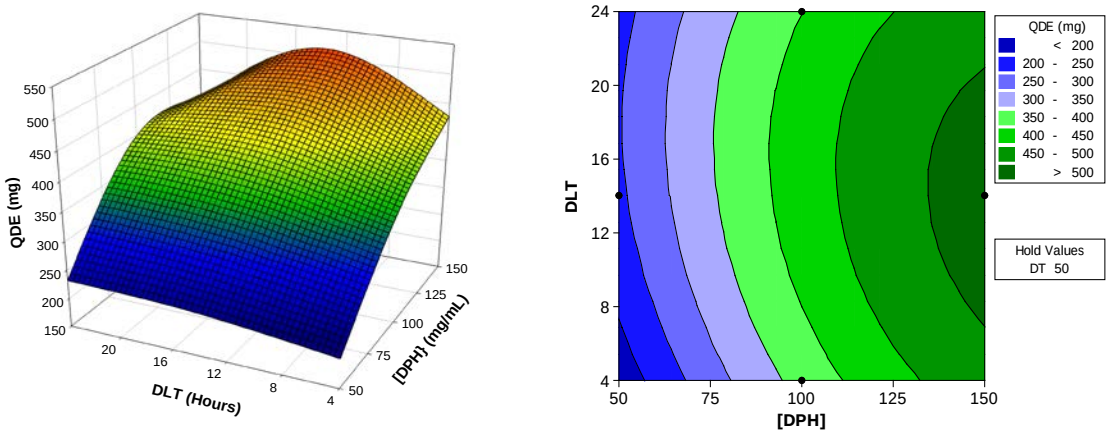


Figure 3.9: Variable interaction plots of the QDE of the SBP.

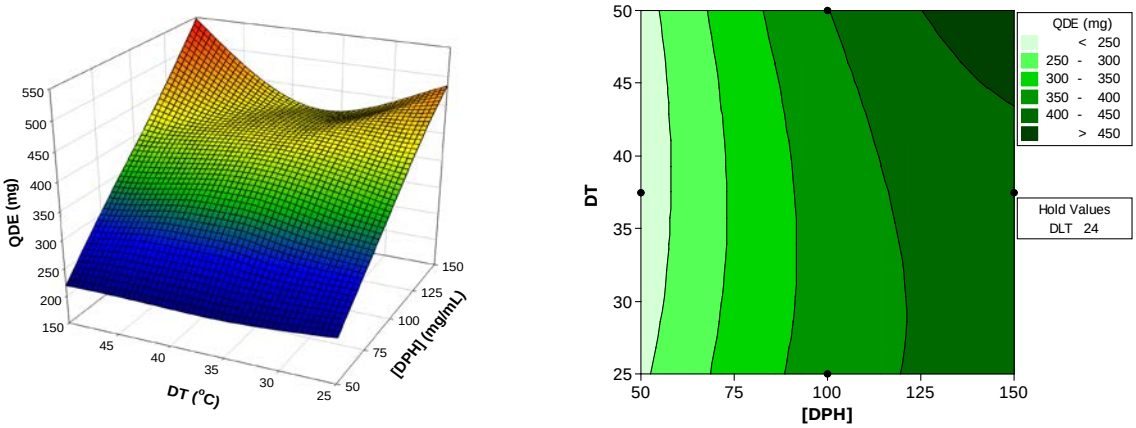
3.3.5.4. Response Analysis of QDE of the DPH-loaded SBP

Each of the factors, quantity of drug within solution ([DPH]); the amount of time exposed to drug solution (DLT); and the effect of heat during drying (DT), affected the QDE of the SBP in specific ways. Figure 3.10a and Figure 3.10b showed that QDE portrayed a positive correlation with DLT up to ~14 hours and thereafter a negative correlation until 24 hours as depicted by the increase and subsequent decrease in QDE as the DLT was increased. On the other hand, [DPH] and DT portrayed a completely positive correlation to QDE. Thus, when analyzing the combined effect of two of the variables (at the high hold values for the third independent variable) on QDE, it was observed in Figure 3.10a and Figure 3.10b that highest QDE (QDE>500mg) was obtained by maintaining [DPH] above 130mg.mL^{-1} and allowing drug-loading to proceed for 8 <DLT< 20 hours. Furthermore, Figure 3.11a and Figure 3.11b showed that maintaining [DPH] above 130mg.mL^{-1} and DT above 43°C produced the highest QDE values (QDE>450mg). Additionally, Figure 3.12a and Figure 3.12b demonstrated that highest QDE values (QDE>520mg) resulted from restricting drug-loading (8 <DLT< 20 hours) and increasing the DT beyond 45°C. Thus, it was deduced that medium drug-loading times coupled with high drug concentrations and increased heat exposure during drying afforded the greatest QDE on the SBP.



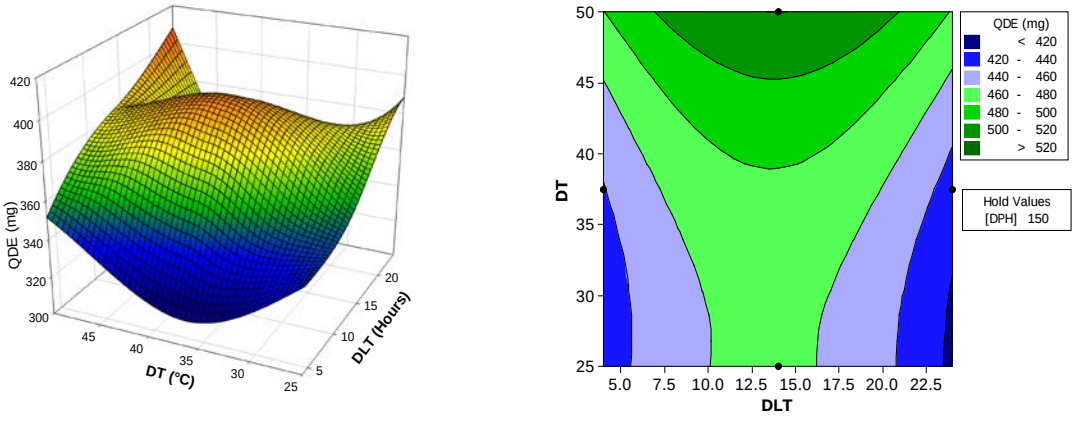
(a) (b)

Figure 3.10: Correlation of QDE with [DPH] and DLT utilizing (a) Response surface plot and (b) contour plot.



(a) (b)

Figure 3.11: Correlation of QDE with [DPH] and DT utilizing (a) Response surface plot and (b) contour plot.



(a) (b)

Figure 3.12: Correlation of QDE with DLT and DT utilizing (a) Response surface plot and (b) contour plot.

3.3.6. Response optimization

The outcomes from each of the 15 experimental formulations were statistically analyzed on MINITAB®, (V15, Minitab Inc, Pennsylvania, USA) and response optimization procedure was used to obtain the optimized levels of the independent variables, viz. [DPH], DLT and DT. A single optimum formulation was generated following constrained optimization of QDE, which maximized the QDE of the SBP with a statistical desirability of 1. The optimized levels of the independent variables, the goal for the response, the predicted response, y, at the current factor settings, as well as the desirability score are depicted in Figure 3.13.

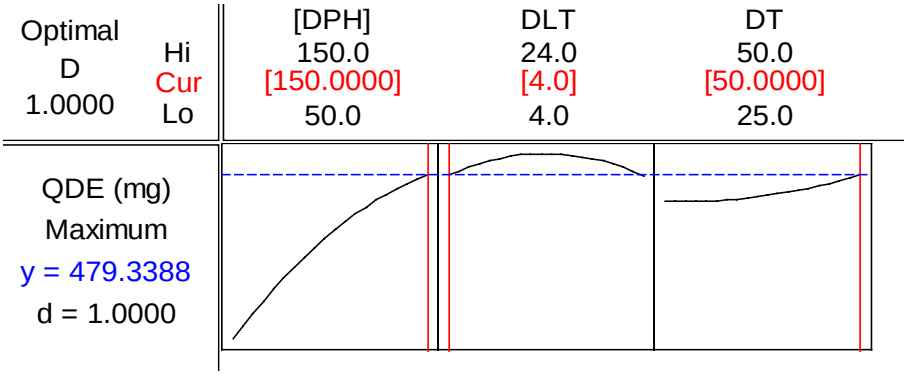


Figure 3.13: Optimization plot of the SBP indicating optimal factors, factor levels and desirability (D) for the optimal formulation.

The optimized DPH-loaded SBP were prepared by accurately weighing SBP samples (2g) and submerging them into 5mL DPH solution (150mg.mL^{-1}) maintained at 25±1°C. The SBP was allowed to hydrate and entrap drug for 4 hours under constant stirring at 50rpm in a shaker bath and upon removal from the drug solution, convection dried in a laboratory oven maintained at 50°C until constant mass was attained (~2 hours). Figure 3.14 illustrated the DEE and QDE of the SBPs after being subjected to the optimum drug entrapment conditions and further compared the experimental results to that predicted by the optimization plot. The QDE of the SBP was 455.158±12.5997mg which translated into a DEE of 59.354±0.8400% (n=3) which was slightly lower than the predicted value but still displayed close correlation to the predicted value (R^2=0.945) and thus validated the optimization process employed.

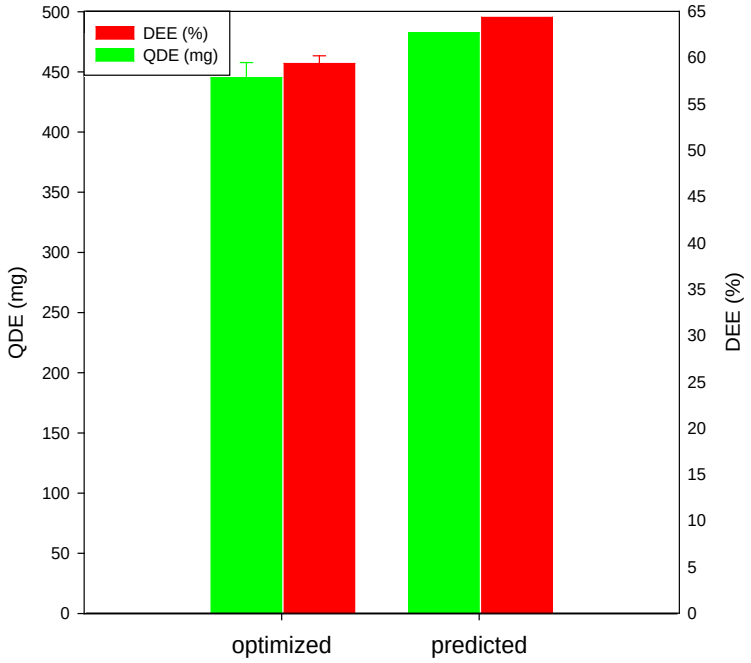


Figure 3.14: DEE and QDE of optimized DPH-loaded SBP (n=3).

3.3.7. *In vitro* drug release behavior of optimized DPH-loaded SBP

The drug release profiles of the optimized DPH-loaded SBP demonstrated a burst release within the first 30 minutes in both Simulated Gastric Fluid (SGF) and Simulated Intestinal Fluid (SIF) as depicted in Figure 3.15. This burst accounted for ~90% of the drug contained within the SBP, which was unsatisfactory for a controlled drug delivery system. Explications of the drug release behavior was as described in Chapter 2, Section 2.3.7.3 as only drug entrapment conditions had been optimized in this Chapter with no enhancements to the control of drug release attempted. The SBP may have to be modified or incorporated into a coating in order to better control drug release. In addition, the possibility of drug inappropriateness must be considered and could be as a result of solubility, stability or general incompatibility of DPH with the SBP, in which case an alternate drug be considered for incorporation within the SBP.

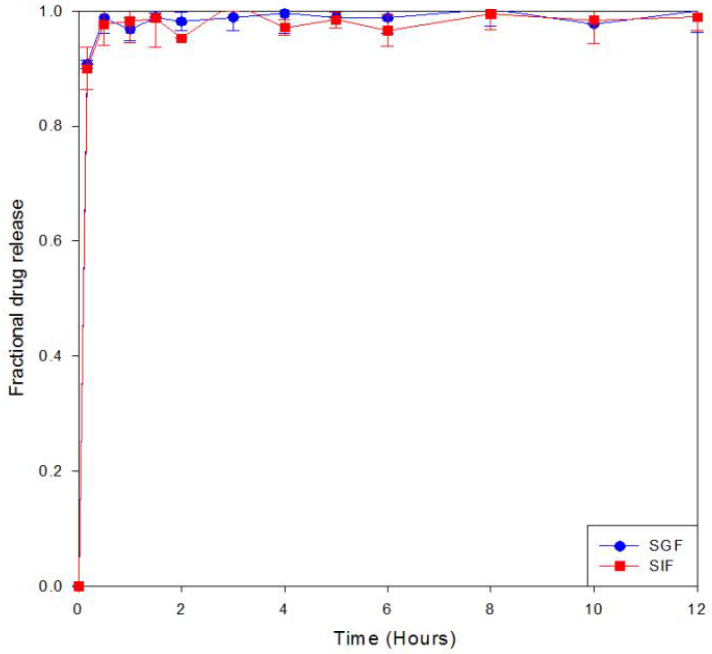


Figure 3.15: Comparative *in vitro* drug release from the optimized DPH-loaded SBP (n=3).

3.4. Concluding Remarks

Manipulation of the various processing parameters showed that hydration time, drying temperature and DPH concentration within the drug solution had pronounced effects on the drug entrapment of the SBP. Volume of drug solution had no impact on the QDE of the SBP and high drug solution volumes resulted in wastage of drug during the entrapment process. Finally, increasing the temperature of drug solution during drug entrapment resulted in instability of the SBP. Thus, while drug solution volume and drug-loading temperature was kept constant, DLT, [DPH] and DT were varied in order to maximize the drug entrapment of the SBP.

In order to standardize the determining factor of drug entrapment of the SBP, QDE was chosen as the response as it ultimately affected size and content of MODDS. Testing of the experimental formulations showed good correlation to the predicted values and all experimental values fell within the 95% confidence limit of the predicted values. Analysis of the design showed that [DPH] concentration has the largest and most significant effect on the QDE of the SBPs while, in its entirety, the regression model generated by the BBD exhibited a significant effect on QDE. Analysis of residuals showed normal distribution of data for QDE and was adequately fitted by the response surface model and thus authenticated the BBD used.

Formulation of the optimized DPH-loaded formulation showed that experimental drug entrapment demonstrated good correlation to the predicted value and thus validated the optimization process employed. Drug release profile displayed poor control by the SBP as ~90 of the drug was released as a burst effect and thus DPH may not be an ideal model drug due its high solubility and physicochemical characteristics. Furthermore, the MODDS was postulated to incorporate multiple drugs and thus drugs with varying characteristics need to be examined for their potential to be incorporated into the SBP.

CHAPTER 4
ELUCIDATION OF THE ABILITY OF THE STARCH-BASED PLATFORM TO ENTRAP AND CONTROL THE RELEASE OF VARIOUS DRUGS

4.1. Introduction

Although displaying very good diphenhydramine (DPH) entrapment, the complete inability of the sago Starch-Based Platforms (SBP) to control the release of DPH was seen as cause for change of the model drug in the development of the Multiparticulate Oral Drug Delivery System (MODDS). Furthermore, the MODDS was postulated to incorporate and deliver multiple drugs in a single dosage form in order to lessen the pill burden experienced by patients with conditions requiring multiple drug therapy. A typical example of such a condition is hypertension.

Hypertension is a common disorder and affects ~20% of the world's population (Elliot, 2006; Yavagal *et al.,* 2011). This global epidemic of high blood pressure is expected to shift the burden of disease so that heart disease will become the most common cause of death worldwide by the year 2025. The estimated cost of hypertension and its treatment in USA alone in 2006 was $63.5 billion. Worldwide the cost was six times above that value, and included costs associated with lifestyle modifications and drug treatment (Yavagal *et al.,* 2011).

Hypertension is now generally defined as a blood pressure (BP) of more than 140/90 mmHg (Elliot, 2006) and according to the guidelines published in Seventh Report of the Joint National Committee on *Prevention, Detection, Evaluation, and Treatment of High Blood Pressure* (JNC VI, 2004), the averaged clinic reading of systolic pressure of 140mmHg or higher and/or diastolic pressure of 90mmHg or higher on two consecutive clinic visits are now considered as treatment-requiring hypertension. The criteria for classifying hypertension according to the JNC VI were depicted in Table 4.1.

Table 4.1: JNC VI Criteria for Classification of Blood Pressure

Category	SP (mmHg)	DP (mmHg)
Normal	<120	<80
Pre-hypertension	120–139	80–89
Hypertension, Stage 1	140–159	90–99
Hypertension, Stage 2	≥160	≥100

Where SP denoted Systolic blood Pressure and DP denoted Diastolic blood Pressure

The prevalence of hypertension in the community can be attributed to many factors including age, ethnicity, genetic predisposition, smoking, obesity, dyslipidaemia, type-2 diabetes mellitus, high salt intake diets, alcohol use and certain medications (Lalouel, 1995; Reis *et al.,* 2000; Beevers *et al.,* 2001; Elliot, 2006). Development of atherosclerosis, ischemic heart diseases, stroke, cardiac failure and renal failure, which result in decreased quality of life and increased mortality, are direct consequences of hypertension and provide a rationale for the emphasis on its treatment (Aronow *et al.,* 2011; Stewart *et al.,* 2011).

Although single drug treatments are applicable in certain cases, structured management of hypertension and pharmacological studies showed the benefits of greater BP control with combination anti-hypertensive therapy (Stewart *et al.,* 2011). Drug treatments for hypertension focus on correcting the three principle determinants of BP, which include peripheral vascular resistance, stroke volume and heart rate (Beevers *et al.,* 2001; Kopp, 2005). Figure 4.1 provides a simplified inter-relating mechanism by which these principle determinants provide BP homeostasis, although it must be noted that various other factors and organs do have an influence on BP. The aims in the treatment of hypertension are to both lower BP and maintain the BP at the lowered level with minimal fluctuation. The latter therapeutic outcome is seldom achieved as many drugs display low oral bioavailability and require frequent dosing in order to eliminate the peak-trough cycle and achieve a stable plasma concentration, which is essential in maintaining the desired therapeutic effect. The side-effects and complex dosing regimens may cause poor patient compliance and may ultimately lead to therapeutic failure (Pandit *et al.,* 2006).

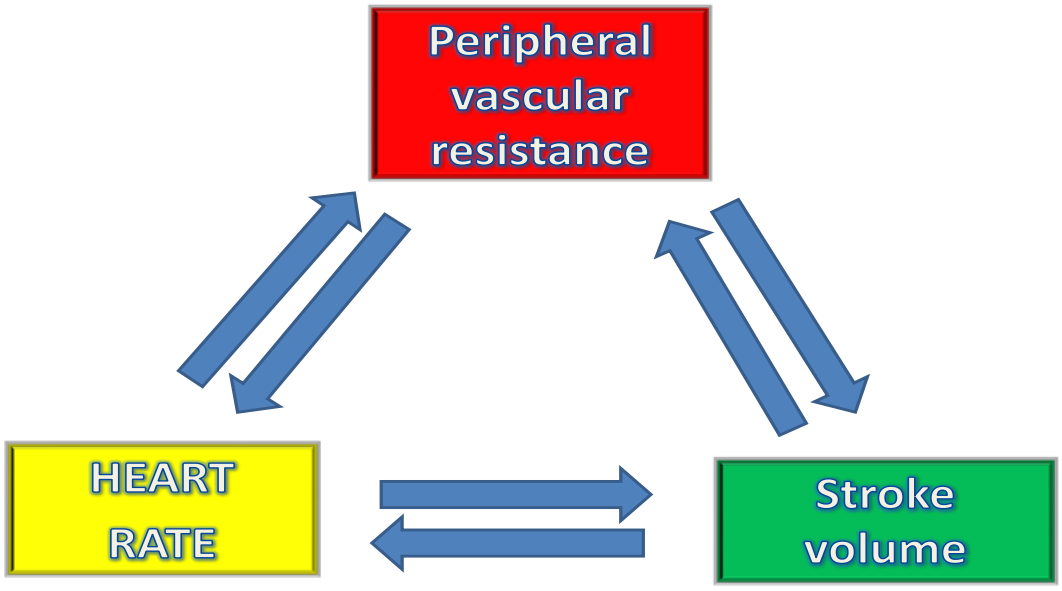
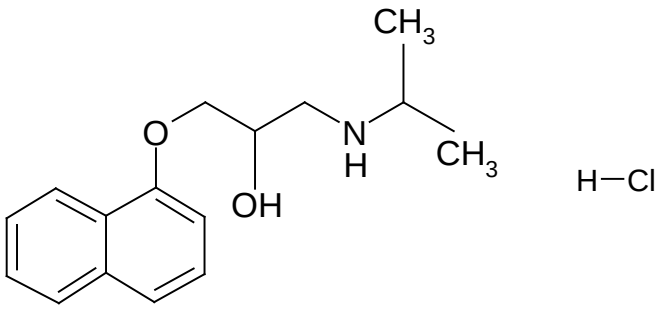


Figure 4.1: Relationship between the principle determinants of blood pressure.

An example of a multidrug treatment which addresses the three principle determinants of BP comprises the use of beta-blockers which reduce sympathetic stimulation of the heart and thus reduce heart rate; Angiotensin Converting Enzyme (ACE) inhibitors which reduce peripheral vascular resistance and diuretics which decrease fluid volume and thus stroke volume (Reis *et al.*, 2000; Beevers *et al.,* 2001, Kopp, 2005).

Propranolol, commonly formulated as a hydrochloride salt, is a synthetic competitive beta-adrenergic receptor-blocker and is a stereoscopic molecule composed of an S(-)-enantiomer and an R(+)-enantiomer (Uwai *et al.,* 2005; Lee *et al.*, 2010; Drugbank, 2012). Propranolol, and in particular the S(-)-enantiomer which is one hundred times more potent than the R(+)-enantiomer, inhibits sympathetic stimulation of the heart thereby reducing the heart rate and ultimately the BP (Kiriyama *et al.,* 2008). In addition, propranolol is used to treat anxiety, tremors, angina, arrhythmias, treat or prevent heart attack, and to reduce the severity and frequency of migraine headaches (Sica and Gehr, 2007). Dosages vary between 10mg and the maximum daily dose of 640mg depending on the condition and its severity (Davis, 2007).

According to the BCS classification, propranolol is a class I drug with high solubility and high permeability but displays site-specific absorption (Lindenberg *et al.,* 2004; Davis, 2005). Propranolol, with a plasma half-life of ~4 hours, is highly lipophilic and almost completely absorbed after oral administration with peak blood concentrations occurring approximately 6 hours after administration (Lawrence and Lawrence, 2005; Bashir and Nanjundaswamy, 2009; Drugbank, 2012). Propranolol is highly protein bound and excreted in the kidney following metabolism in the liver (Wu *et al.,* 2001; Kiriyama *et al.,* 2008). The chemical structure of propranolol hydrochloride is depicted in Figure 4.2.

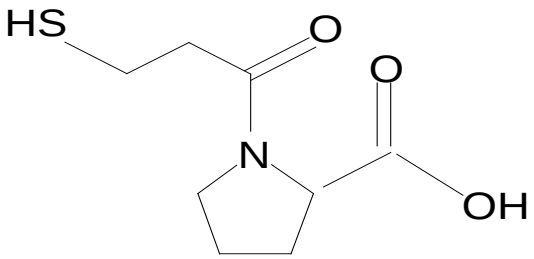


(±) -1-Isopropylamino-3-(1-naphthyloxy)-2-propanol

Figure 4.2: Chemical structure of propranolol HCl.

Captopril is a specific competitive inhibitor of ACE, the enzyme responsible for the conversion of angiotensin I to angiotensin II and thus decreases the vasocontrictive effect of angiotensin II resulting in lower total peripheral resistance. Captopril is therefore used in the treatment of hypertension and exerts its pharmacological antihypertensive effect in an indirect manner (Sica and Gehr, 2007; Bakris, 2010). According to the Biopharmaceutical Classification System (BCS) classification, captopril is a class III drug with high solubility and low permeability (Lindenberg *et al.,* 2004). The low permeability could be attributed to the narrow absorption window displayed by captopril with the presence of food in the stomach further decreasing its absorption by ~25-30% (Davis, 2005; Vijayaraghavan and Deedwania, 2011, Drugbank, 2012).

Captopril, with a plasma half-life of ~2 hours, is administered at doses ranging between 25mg and 150mg 2-3 times daily depending on patient response, and is rapidly absorbed following oral administration with peak blood levels reached approximately 1 hour after administration (Rahman *et al.,* 2005; Davis, 2007; Vijayaraghavan and Deedwania, 2011, Drugbank, 2012). Approximately 25-30% of the circulating drug is plasma-bound with 95% of the administered dose eliminated in the urine within 24 hours. The structure of captopril is depicted in Figure 4.3.



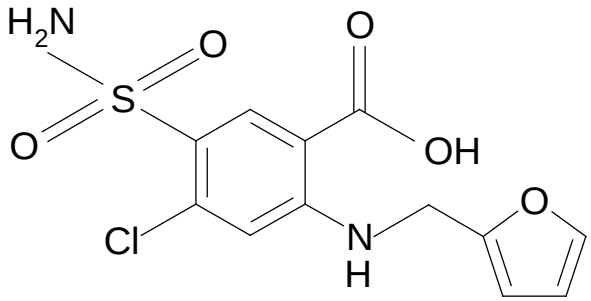
***N*-[(S)-3-Mercapto-2-methylpropionyl]-L-proline**

Figure 4.3: Chemical structure of captopril.

Furosemide is an anthranilic acid derivative-loop diuretic, which is indicated to treat fluid retention in hypertension alone or in combination with other antihypertensive drugs (Ponto and Schoenwald, 1990; Goto *et al.,* 2010; Drugbank, 2012; Ranjbar *et al.,* 2012). Furosemide blocks the sodium-potassium-chloride co-transporter (NKCC2) in the thick ascending limb of the loop of Henle thus preventing sodium reabsorption resulting in water being retained in the nephron and subsequently excreted (Ponto and Schoenwald, 1990; Goto *et al.,* 2010; Zvonar et al., 2010; Laulicht *et al.,* 2011; Drugbank, 2012; Wang *et al.,* 2012). Furosemide thus lowers blood pressure by lowering decreasing stroke volume and reducing the load on the heart. In addition, furosemide exerts its action on the

proximal and distal tubules of the nephron and is thus a potent diuretic used to treat oedema in people with congestive heart failure, liver disease, or kidney disorders such as nephrotic syndrome (Ai *et al.,* 2003; Sica and Gehr, 2007; Zvonar *et al.,* 2010; Laulicht *et al.,* 2011; Ranjbar *et al.,* 2012).

According to the BCS classification, furosemide is a class IV drug with low solubility and low permeability, which could be attributed to site-specific absorption and level of protonation (Lindenberg *et al.,* 2004; Davis, 2005; Laulicht *et al.,* 2011). The dose of furosemide ranges from 20mg up to 600mg daily depending on the severity of the oedema (Davis, 2007). Upon oral administration, furosemide, with a peak plasma half-life of ~2 hours, reaches peak concentration after 1 hour, is highly protein bound and is excreted mainly unchanged via the kidneys where it exerts its pharmacological action (Zvonar *et al.,* 2010; Laulicht *et al.,* 2011). The structure of furosemide is depicted in Figure 4.4.



4-Chloro-*N*-furfuryl-5-sulfamoylanthranilic acid

Figure 4.4: Chemical structure of furosemide.

Thus in this Chapter, propranolol, captopril and furosemide were evaluated for use as model drugs in the development of the MODDS. The maximum absorbance wavelengths (λmax) and functional characteristics for each drug were determined and their potential for use within the MODDS, either singularly or simultaneously, was elucidated. In addition, a novel experimental apparatus, employed to facilitate adequate circulation of the experimental fluids encompassing the SBP while avoiding inadvertent collisions between the SBP and stirring mechanism, was designed and implemented.

4.2. Materials and Methods

4.2.1. Materials

Propranolol HCl (Mw=295.80g.mol^{-1}, solubility >50 mg.mL^{-1} in water with heat), captopril (Mw=217.29g.mol^{-1}, solubility ~160mg.mL^{-1} in water at 25°C) and furosemide (Mw=330.74g.mol^{-1}, solubility <0.1mg.mL^{-1} in water at 30°C) were acquired from Sigma-Aldrich, (Sigma-Aldrich Inc., St. Louis, USA) and were used as received. Acetone (99%$^{v}/_{v}$, Mw=58.08g.mol^{-1}) and sodium hydroxide (NaOH, Mw=40.00g.mol^{-1}) was purchased from Merck (Pty) Ltd. (Modderfontein, Johannesburg, South Africa) and was of analytical grade. Ethanol (99%$^{v}/_{v}$, Mw=46.07g.mol^{-1}) was purchased from Saarchem (Wadeville, Gauteng, South Africa) and was of analytical grade. Deionized water, purified by a MilliQ Millipore water purification system (Milli-Q, Millipore, Billerica, MA, USA), was used throughout the study. All other reagents utilized were as described in Chapter 2.

4.2.2. Determination of the maximum absorbance wavelengths (λmax) of drugs employed in this phase of the study

Simulated Intestinal Fluid (SIF) (prepared as described in Chapter 2, Section 2.2.5.1.3) was filtered through a 0.45µm Millipore filter and inserted into the UV spectrophotometer (diode array UV spectrophotometer, Specord 40, Analytik Jena AG, Jena) in order to zero the baseline value of the UV spectrophotometer at all wavelengths between 200nm and 600nm. This procedure was conducted prior to UV analysis (WinASPECT® Spectroanalytical Software, Analytik Jena AG, Jena) of each drug used in the study.

4.2.2.1. Determination of the maximum absorbance wavelength (λmax) of propranolol

Propranolol solution was prepared by accurately weighing and dissolving 6.436mg propranolol in 100mL SIF. A sample (4mL) of this solution was filtered through a 0.45µm Millipore filter and inserted into the UV spectrophotometer. The UV spectrum of propranolol that was produced was then analyzed and the wavelength at which maximum absorbance occurred (λmax) was determined. The experimental λmax was then compared to the literature to confirm the λmax obtained.

4.2.2.2. Determination of the maximum absorbance wavelengths (λmax) of captopril

Captopril solution was prepared by dissolving 1.286g captopril in 100mL SIF and then subjected to the same procedure as described in, Section 4.2.2.1 in order to determine the λmax of captopril.

4.2.2.3. Determination of the maximum absorbance wavelength (λmax) of furosemide

A saturated furosemide solution was prepared by dissolving 50mg furosemide in 100mL SIF and subjected to vacuum filtering using 0.22µm pore size Cameo Acetate membrane filter (Millipore Co., Bedford, Massachusetts). The filtered solution was then subjected to UV analysis and the λmax of furosemide was determined as described in, Section 4.2.2.1.

Due to the lack of solubility of furosemide in water, furosemide would initially have to be dissolved in acetone. Thus, in order to elucidate the absorbance spectrum of acetone, an acetone solution was prepared by dissolving 1mL acetone in 100mL SIF and then subjected to the same procedure as described in, Section 4.2.2.1. Acetone/SIF ($1\%^{v}/_{v}$) solution was prepared by adding 1mL acetone to a volumetric flask and making up to 100mL with SIF. Furosemide/acetone solution was prepared by dissolving 1.8mg furosemide in 1mL acetone. This solution was then placed into a volumetric flask and made up to 100mL using SIF. Dilution of this solution was achieved by adding an aliquot (5mL) to 45mL acetone/SIF ($1\%^{v}/_{v}$) solution. UV analysis was conducted on the diluted solution as described in Section 4.2.2.1 in order to determine the λmax of furosemide in the presence of acetone.

4.2.3. Construction of calibration curves in SIF and SGF for each drug

4.2.3.1. Construction of calibration curves for propranolol

Stock solutions of propranolol were prepared by accurately weighing 6.3mg and 5.48mg propranolol and dissolving in 100mL SIF and Simulated Gastric Fluid (SGF) respectively (SGF and SIF prepared as described in Chapter 2, Section 2.2.5.1.2 and Section 2.2.5.1.3 respectively). 5-fold serial dilutions were then performed on each stock solution and the absorbance of each diluted solution determined with a UV spectrophotometer (diode array UV spectrophotometer, Specord 40, Analytik Jena AG, Jena) at the maximum absorbance wavelength of propranolol selected. Calibration curves were then constructed by plotting the observed absorbance on the y-axis against its corresponding concentration ($mg.mL^{-1}$) on the x-axis with all intercepts set at 0.

4.2.3.2. Construction of calibration curves for captopril

Stock solutions of captopril were prepared by accurately weighing 10.5mg and 7.0mg captopril and dissolving in 250mL SIF and SGF, respectively (SGF and SIF prepared as described in Chapter 2, Section 2.2.5.1.2 and Section 2.2.5.1.3 respectively). 5-fold serial dilutions were then performed on each stock solution and the absorbance of each diluted solution determined with a UV spectrophotometer (diode array UV spectrophotometer,

Specord 40, Analytik Jena AG, Jena) at the maximum absorbance wavelength of captopril. Calibration curves were then constructed by plotting the observed absorbance on the y-axis against its corresponding concentration ($mg.mL^{-1}$) on the x-axis with all intercepts set at 0.

4.2.3.3. Construction of calibration curves for furosemide

Stock solutions of furosemide were prepared by accurately weighing and dissolving 1.5mg of furosemide in 1mL acetone and subsequently making this solution up to 100mL with SIF and SGF, respectively (SGF and SIF prepared as described in Chapter 2, Section 2.2.5.1.2 and Section 2.2.5.1.3 respectively). 5-fold serial dilutions using acetone/SIF ($1\%^{v}/_{v}$) solution were then performed on each stock solution and the absorbance of each diluted solution determined with a UV spectrophotometer (diode array UV spectrophotometer, Specord 40, Analytik Jena AG, Jena) at the maximum absorbance wavelength of furosemide selected. Calibration curves were then constructed by plotting the observed absorbance on the y-axis against its corresponding concentration ($mg.mL^{-1}$) on the x-axis with all intercepts set at 0.

4.2.4. Determination of the potential of the SBP to entrap drugs displaying varying physicochemical properties

4.2.4.1. Description of experimental apparatus

The experimental apparatus depicted in Figure 4.5 was designed in order to facilitate adequate circulation of the experimental fluids encompassing the SBP while avoiding inadvertent collisions between the SBP and stirring mechanism. The experimental apparatus consisted of a cylindrical re-sealable transparent exterior vessel, a cylindrical porous interior partitioning vessel fitted to the base at the centre the exterior vessel and an electric magnetic stirring device fitted with heat and speed controls. The SBP was placed into the void between the exterior vessel and interior vessel with experimental solution, which was allowed to flow freely between interior and exterior vessels, while a magnetic stirrer bar was placed into the interior vessel to facilitate circulation of experimental solution. Importantly, the pores in the partitioning vessel were large enough to facilitate movement of experimental solutions but small enough to prevent entry of SBP into the partitioning vessel. The temperature and speed of stirring was controllable and the re-sealable lid on the exterior vessel allowed for modifications of the experimental solutions if necessary.

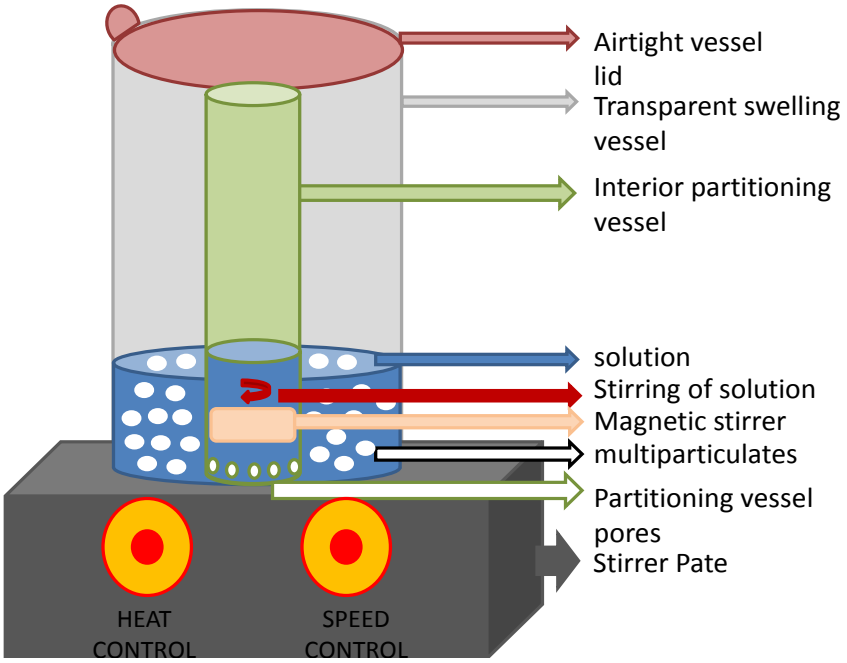


Figure 4.5: Schematic representation of experimental apparatus.

4.2.4.2. Drug entrapment within the SBP

Drug solutions of the three model drugs, propranolol, captopril and furosemide, of various concentrations were prepared as depicted in Table 4.2 and placed into experimental apparatuses. SBP samples (2g) were accurately weighed using an analytical mass balance and placed into a drug solution. The SBP samples were then allowed to hydrate and entrap drug for 4 hours in an experimental apparatus (Figure 4.5) maintained at 25±1°C and stirred at 50rpm. The study was conducted in triplicate (n=3).

Table 4.2: Preparation of drug solutions

Formulation	Drug	Q_{Drug} (mg)	Solvent medium	$Q_{Solvent}$ (mL)	[Drug solution] ($mg.mL^{-1}$)
1	Propranolol	100	Water	10	10
2	Propranolol	500	Water	10	50
3	Propranolol	750	Water	10	75
4	Propranolol	100	Ethanol	10	10
5	Propranolol	150	Ethanol	10	15
6	Propranolol	200	Ethanol	10	20
7	Propranolol	500	Ethanol	10	50
8	Captopril	750	Water	10	75
9	Furosemide	500	Acetone	10	50
10	Furosemide	750	Acetone	10	75
11	Furosemide	2	Water	10	0.2
12	Furosemide	375	Acetone + Water (5:5)	10	37.5

Where Q_{Drug} denoted the quantity of drug, $Q_{Solvent}$ denoted the quantity of solvent and [Drug solution] denoted the concentration of drug solution employed.

4.2.4.3. Elucidation of extent of drug entrapment

The drug-loaded SBP samples were then removed from the experimental apparatus, lightly blotted with tissue paper to remove excess moisture and thereafter weighed. The extent of hydration of the SBP during drug-loading was calculated gravimetrically using Equation 2.1. The drug-loaded SBP samples were then placed onto glass petri dishes and into a laboratory oven maintained at 50°C, and thereafter allowed to convection dry until constant mass was achieved. During the drying process, the SBP particles were physically separated using a flat-ended metal spatula.

Once dried, the drug-loaded SBP samples were weighed and a sample (1g) was homogenized in 10mL deionized water for 120 seconds. The homogenized suspension was then made up to 500mL with SIF maintained at 100ºC, stirred manually and allowed to cool to approximately 30ºC. Three 10mL aliquots from the cooled suspension were then centrifuged (Optima® LE-80K, Beckman, USA) using rotor 3 at 3000rpm for 90 minutes. The supernatant was removed and thereafter filtered through a 0.45µm Millipore filter. The filtered samples were then analyzed using UV spectroscopy at wavelengths specified in Table 4.2 and then averaged to determine the drug content within the SBP. The above-mentioned method was employed for propranolol and captopril. With regard to furosemide-loaded SBP, samples (1g) were homogenized in acetone/SIF ($1\%^{v}/_{v}$) solution in order to solubilize furosemide and then made up to 500mL using acetone/SIF ($1\%^{v}/_{v}$) maintained at 100°C. Thereafter the same procedure as for propranolol and captopril was employed to determine the furosemide content of the SBP.

4.2.5. Determination of the *in vitro* drug release behavior from the SBP

Based on the results from the drug entrapment study, the quantity of SBP containing the minimum quantity of drug used in commercial formulations for each drug was calculated according to Equation 4.1 and subjected to identical *in vitro* drug release tests. The Quantity of Drug Entrapped (QDE) by the SBP dictated the viability of using the prepared formulations and was depicted in Table 4.3.

$$B_r = \frac{D_r}{F_{Bd}} \mathrm{X} B_d \qquad \textbf{Equation 4.1}$$

Where:
B_r= *Quantity of drug-loaded SBPs required (g)*
D_r= *Quantity of drug required (mg)*
F_{Bd}= *Quantity of drug contained in dried SBPs (mg)*
B_d= *Quantity of dried SBPs (g)*

Table 4.3: Minimum quantity of SBP required for *in vitro* drug release studies

Formulation	Q_d (mg)	Q_{SBP} (g)	Viability
1	10	0.378	Positive
2	10	0.091	Positive
3	10	0.075	Positive
4	10	6.503	Negative
5	10	8.471	Negative
6	10	8.647	Negative
7	10	1.165	Negative
8	25	0.124	Positive
9	20	3.894	Negative
10	20	2.609	Negative
11	20	578.502	Negative
12	20	1.406	Negative

Where Q_d denoted the Quantity of drug required and Q_{SBP} denoted the Quantity of SBP required

Separate drug-loaded SBP samples, ascertained to be viable for *in vitro* drug release studies and as depicted in Table 4.4, were accurately weighed and subjected to the same process as described in Chapter 2, Section 2.2.8.3. UV analysis was carried out at the wavelengths depicted in Table 4.2 and the fractional drug release from each SBP formulation was determined using the predefined calibration curves prepared in Section 4.2.3. The study was conducted in triplicate.

4.3. Results and Discussion

4.3.1. Maximum absorbance wavelength (λmax) of various drugs employed in this phase of the study

The UV spectrum of propranolol was depicted in Figure 4.6 and displayed two separate λmax values at 289nm and a series of peaks between 210nm and 245nm. In previous work undertaken by Reyes and co-workers (2008) and Bashir and Nanjundaswamy (2009) on propranolol, the λmax value of 289nm was used and was thus employed in UV spectrometric analysis of propranolol in this study.

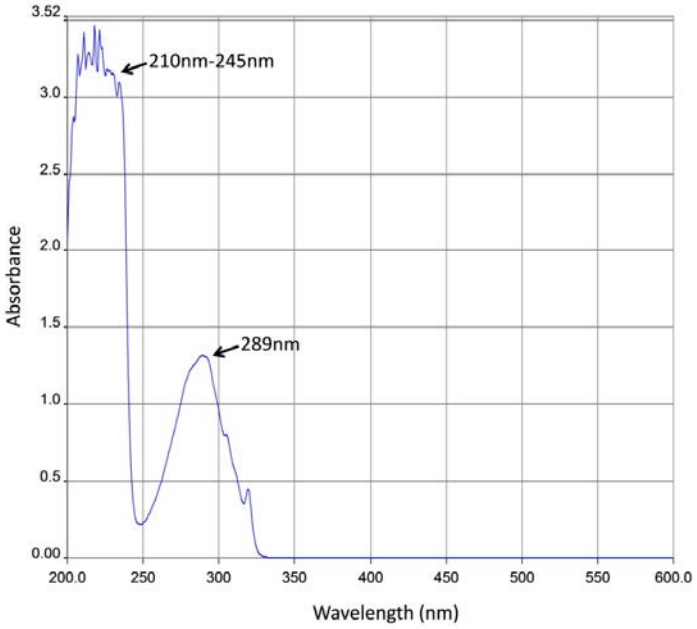


Figure 4.6: UV spectrum of propranolol.

The UV spectrum of captopril was depicted in Figure 4.7 and showed a single λmax peak at 214nm. There was no consistent λmax value found in the literature but the experimental value obtained was close to the 210nm value stated by Ivanovic and co-workers (2004). Other values found in the literature included 200nm, 214nm, 220nm, and 246nm by Brittain and co-workers (1990), Hillaert and co-workers (1999), the Japanese Pharmacopeia (1999) and Amini and co-workers (1999) respectively. The value of 214nm obtained experimentally fitted within this range and was therefore used in UV spectrometric analysis of captopril in this study.

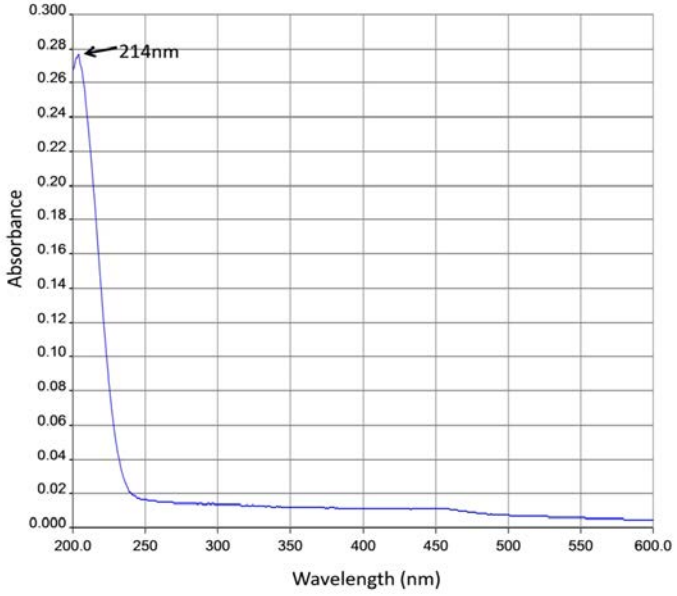


Figure 4.7: UV spectrum of captopril.

The UV spectrum of furosemide was depicted in Figure 4.8 and showed 3 distinctive absorbance maxima at wavelengths of 229nm, 274nm and 330nm with the literature describing λmax= 274nm as the most common for analysis of furosemide (Iannuccelli *et al.,* 2000; Jouyban-Gharamaleki *et al.,* 2001; Cho *et al.,* 2005). When analyzing the UV spectrum produced by acetone depicted in Figure 4.9, a series of peaks with close proximity to each other in the vicinity of 255nm-280nm was observed.

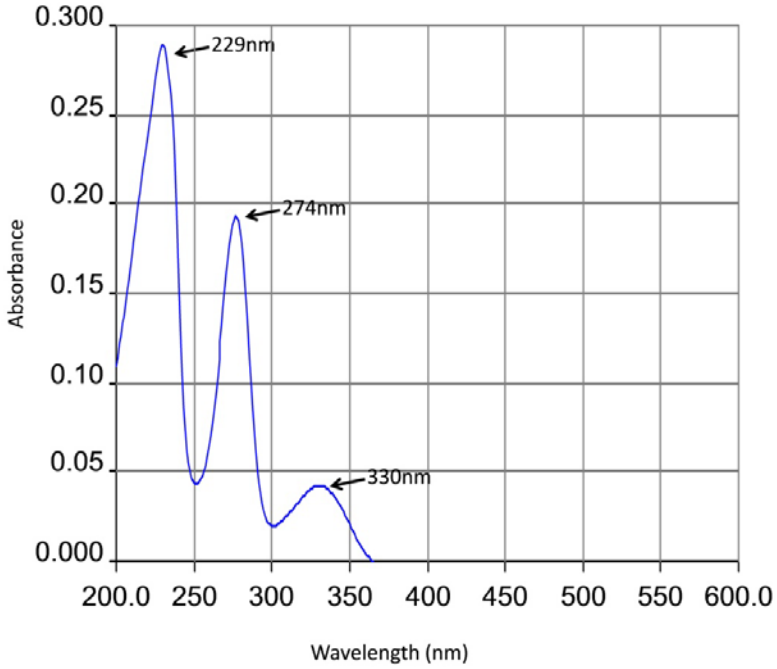


Figure 4.8: UV spectrum of furosemide.

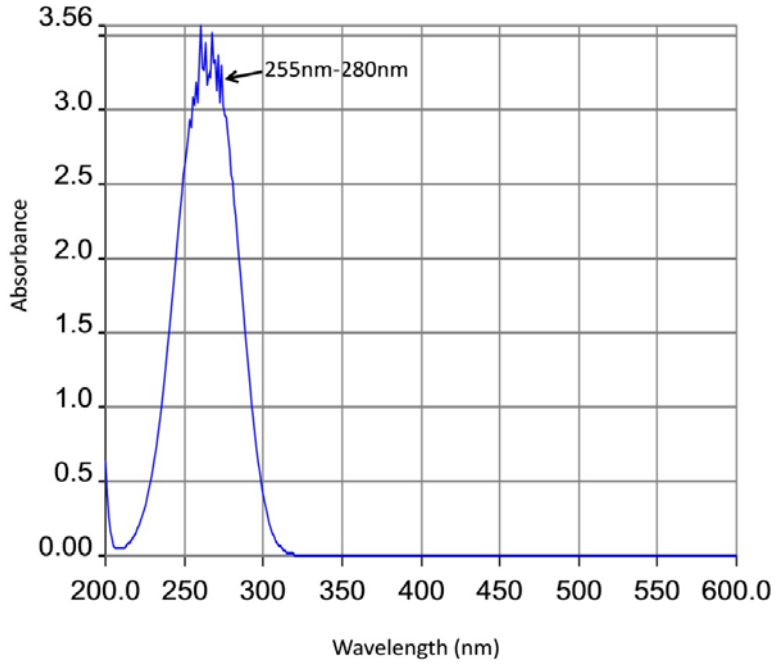


Figure 4.9: UV spectrum of acetone.

Thus, when furosemide was dissolved in acetone and analyzed via UV spectroscopy, the absorbance maxima at 274nm overlapped with the peaks indicative of acetone, which could lead to inaccurate quantification of furosemide and thus could not be used in the study (Figure 4.10). However, Figure 4.10 demonstrated that the λmax at 330nm and 229nm remain unaffected when furosemide was dissolved in acetone. The absorbance of furosemide was greatest at 229nm in both Figure 4.8 and Figure 4.10 and this was confirmed by the study conducted by Cruz and co-workers (1979) which discussed the analysis of furosemide at λmax of 230nm and 274nm. Thus λmax=229nm obtained from the UV spectrum was employed in UV spectrometric studies on furosemide.

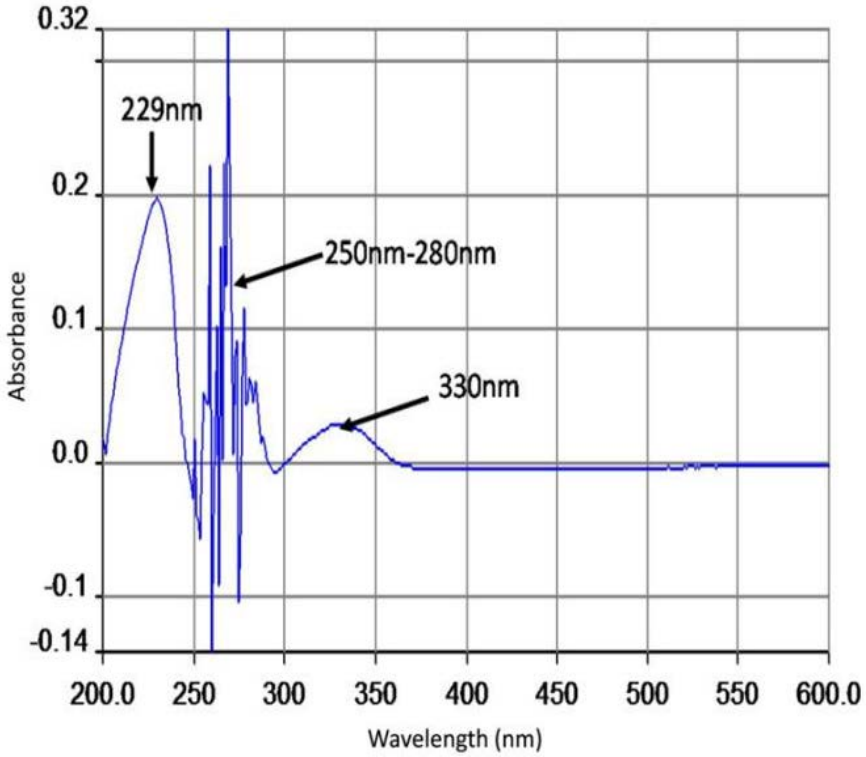


Figure 4.10: UV spectrum of furosemide dissolved in acetone.

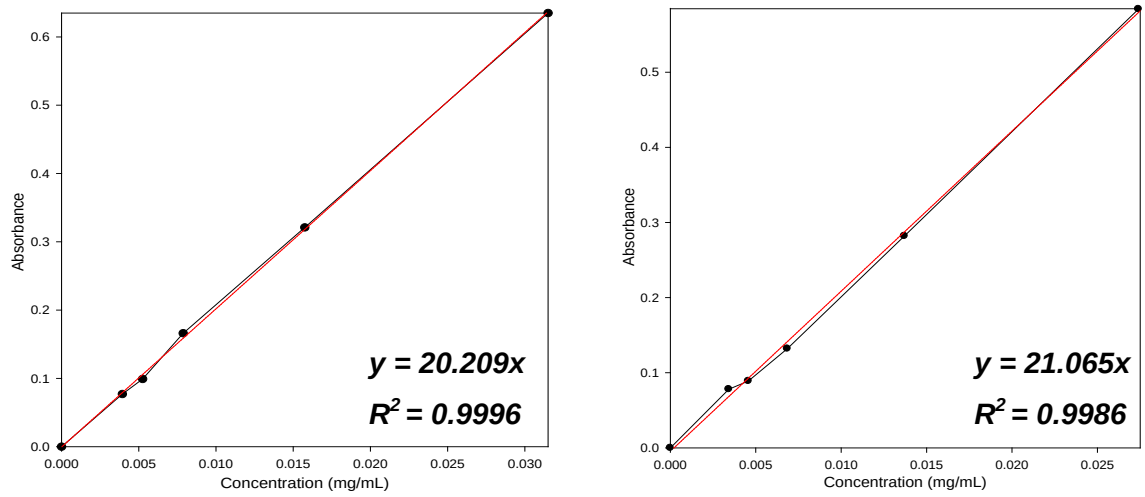
4.3.2. Calibration curves of the various drugs in simulated fluids

The linear range of the calibration curves with its corresponding R^2 value for each drug in both SIF and SGF was summarized in Table 4.4. Each of the calibration curves constructed display good linearity with R^2 values greater than 0.99 as illustrated in Figure 4.11, Figure 4.12 and Figure 4.13, and the equations derived from these curves was therefore used in analysis of these drugs in both SIF and SGF.

Table 4.4: Maximum excitation wavelength of drugs

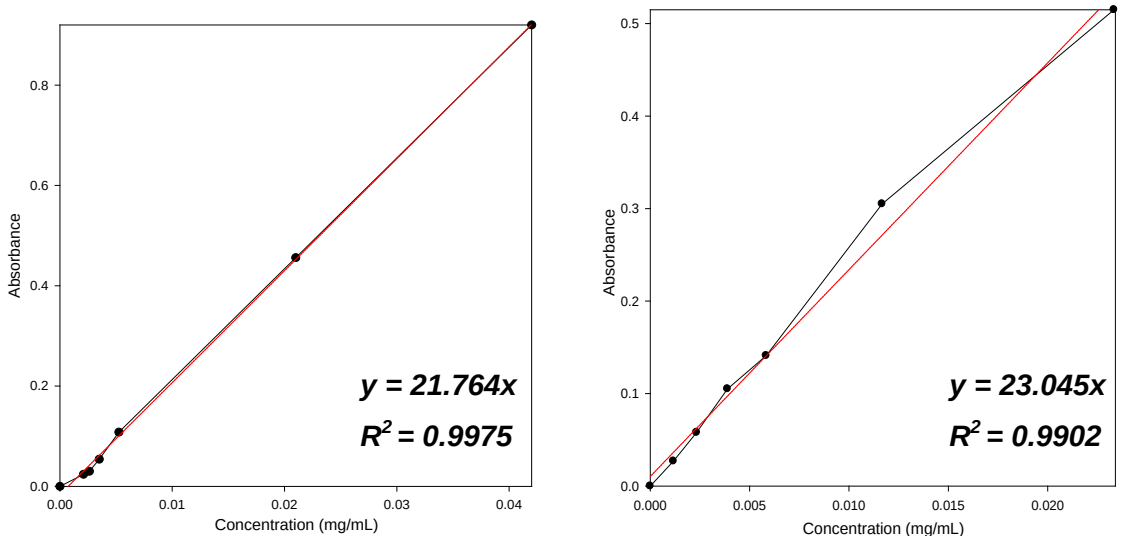
Drug	Simulated fluid	Standard concentrations ($mg.mL^{-1}$)	Λmax (nm)	R^2
Propranolol	SIF	0 – 0.0315	289	0.9996
Captopril	SIF	0 – 0.0420	214	0.9975
Furosemide	SIF	0 – 0.0074	229	0.9966
Propranolol	SGF	0 – 0.0274	289	0.9986
Captopril	SGF	0 – 0.0233	214	0.9902
Furosemide	SGF	0 – 0.0103	229	0.9978

Where SIF Denoted Simulated Intestinal Fluid and SGF denoted Simulated Gastric Fluid



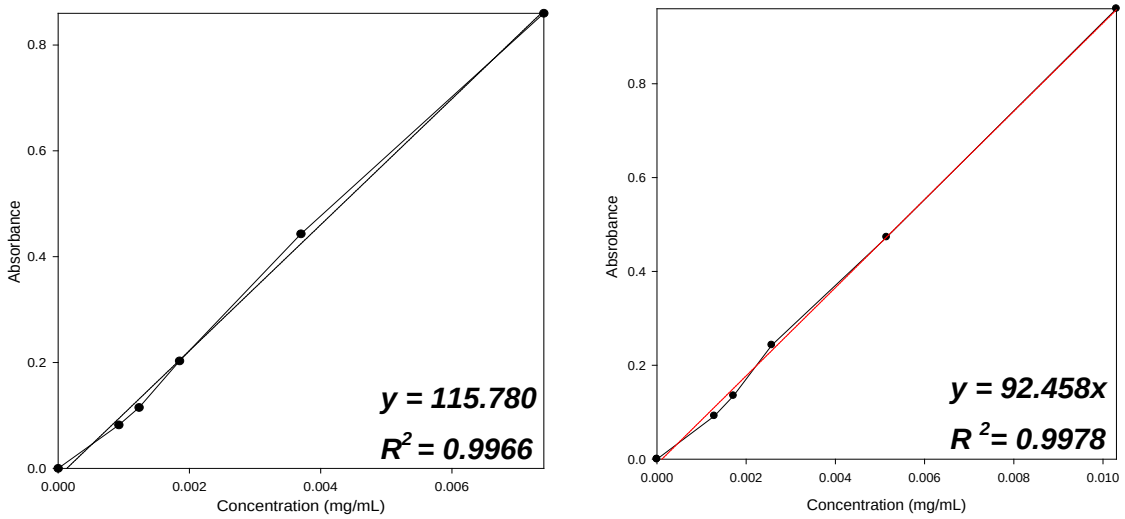
(a) (b)

Figure 4.11: Calibration curve of propranolol HCl in (a) SIF and (b) SGF.



(a) (b)

Figure 4.12: Calibration curve of captopril in (a) SIF and (b) SGF.



(a) (b)

Figure 4.13: Calibration curve of furosemide in (a) SIF and (b) SGF.

4.3.3. Entrapment and drug content of SBP

The results from the drug entrapment study were portrayed in Table 4.5 and Figure 4.14. During drug-loading, it was observed that the SBP underwent negligible hydration in non-aqueous medium (acetone or ethanol) as observed from the Degree of Swelling (DOS) values which ranged between 12% and 36%. Conversely, SBP hydration in water was excellent with DOS values ranging between 195% and 242%. The co-solvent mixture composed of water and acetone displayed DOS of only ~47.5%. The effect of hydration had a marked effect on the DEE as the curves displayed good correlation (R^2=85.62%).

Thus, it was observed that when propranolol was dissolved in water, the QDE of the SBP was good (242.180±4.182mg, n=3) and increased as the concentration of propranolol increased. However, the Drug Entrapment efficiency (DEE) decreased as more drug molecules remained within the drug-loading medium. In the non-aqueous medium, ethanol, drug entrapment with propranolol was minimal (QDE=2.335±1.742mg, n=3) and increasing the drug concentration within the drug-loading medium had a negligible effect on the propranolol entrapment of the SBP (maximum QDE=17.660±1.6062mg, n=3).

In the case of the very water-soluble drug, captopril, a single formulation based on the optimized drug-loading concentration (Chapter 3, Section 3.3.6) was used due to the high water-solubility of the drug and no other drug-loading medium was employed. Captopril demonstrated excellent hydration potential (DOS=223.972±8.490%, n=3) and as a result displayed the greatest QDE and DEE (460.8572±10.387mg and 61.4476±1.385%, respectively, n=3).

Furosemide was observed to be the anomaly in Figure 4.14 as it portrayed excellent hydration potential in aqueous medium (DOS=195.205±8.534%, n=3) and very low drug entrapment DEE=3.46±0.342% (n=3). This can be attributed to the very low water-solubility of furosemide, which prevented the transfer of drug into the SBP. Furosemide within the non-aqueous medium, acetone, behaved in a similar manner to propranolol in ethanol resulting in very low QDE and DEE which did not improve upon increasing the drug concentration of the drug-loading medium (maximum QDE=15.568±7.152mg and DEE=3.462±0.342%, n=3). When furosemide was dissolved in the water/acetone co-solvent, the drug entrapment was increased (QDE=29.024±24.113mg, n=3). A possible explanation for this effect was that the aqueous component was allowed to hydrate the SBP and in the process towed the drug containing non-aqueous component that resulted in drug entering the SBP. However, the increase was minimal as the SBP achieved DEE of 7.739±6.42% (n=3).

Table 4.5: Efficiency of SBP to entrap drugs with varying physicochemical properties

Formulation	DOS (%)	QDE (mg)	DEE (%)
1	208.576 ±5.959	53.686 ±6.384	53.686 ±6.384
2	242.527 ±7.446	242.180 ±4.182	48.436 ±0.836
3	212.869 ±6.909	295.902 ±23.079	39.453 ±3.077
4	13.120 ±2.259	3.120 ±3.832	3.120 ±3.832
5	11.883 ±0.916	2.369 ±0.327	1.579 ±0.218
6	12.589 ±0.252	2.335 ±1.742	1.167 ±0.871
7	36.360 ±4.653	17.660 ±1.606	3.532 ±0.212
8	223.972 ±12.49	460.857 ±10.382	61.447 ±1.385
9	8.107 ±5.385	10.328 ±5.177	2.065 ±1.035
10	8.402 ±3.330	15.568 ±7.152	2.075 ±0.953
11	195.205 ±8.532	0.069 ±0.002	3.462 ±0.342
12	47.550 ±2.253	29.024 ±24.11	7.739 ±6.429

Where DOS denoted the Degree of Swelling, QDE denoted the Quantity of Drug Entrapped and DEE denoted the Drug Entrapment Efficiency (n=3 in all instances)

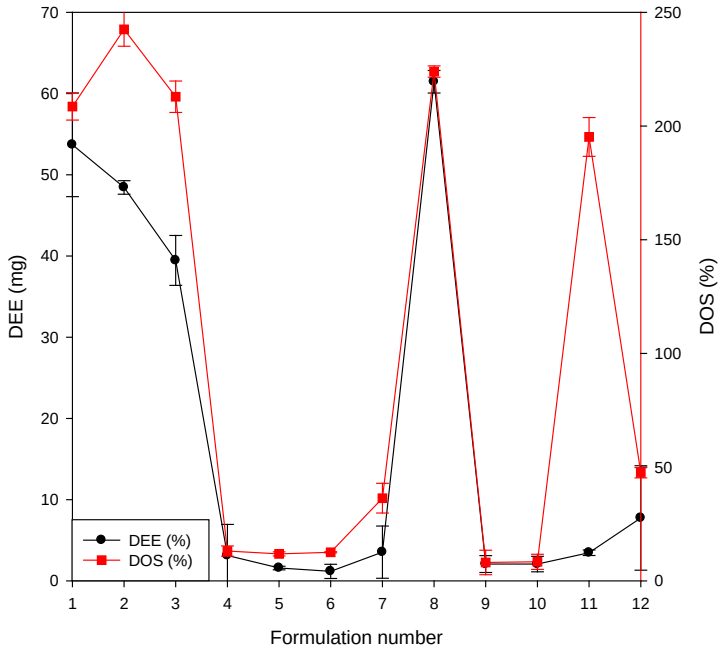


Figure 4.14: Effect of hydration potential on drug entrapment efficiency of the SBP (n=3 in all instances).

4.3.4. *In vitro* drug release characteristics of the SBP loaded with model drugs

The QDE of the SBP with regard to each formulation in Section 4.3.3 dictated the viability of the corresponding drug-loaded SBP formulation to undergo *in vitro* drug release studies. Due to the low drug content and the high quantity of drug-loaded SBP required, Formulations 4, 5, 6, 7, 9, 10, 11 and 12 were excluded from *in vitro* the drug release studies. Therefore, only Formulations 1, 2, 3 (containing propranolol) and Formulation 4 (containing captopril) was assessed.

The SBP showed an inability to control the release of the entrapped drugs in both SIF and SGF. This was depicted in Figure 4.15 where a burst effect that resulted in >90% of drug being released within the first hour within both dissolution media was observed. However, during the *in vitro* drug release study, the SBP remained intact with minimal disintegration observed. A possible explanation for the release behavior could be that the drug entrapped was merely adsorbed onto the surface and not incorporated into the structure of the SBP and was thus easily removed when the SBP were exposed to the dissolution media. The postulated mechanism of drug release was simple diffusion into the aqueous dissolution media in which both drugs have a very appreciable solubility. Therefore, modifications of the SBP must be undertaken in order to control the release of the entrapped drug.

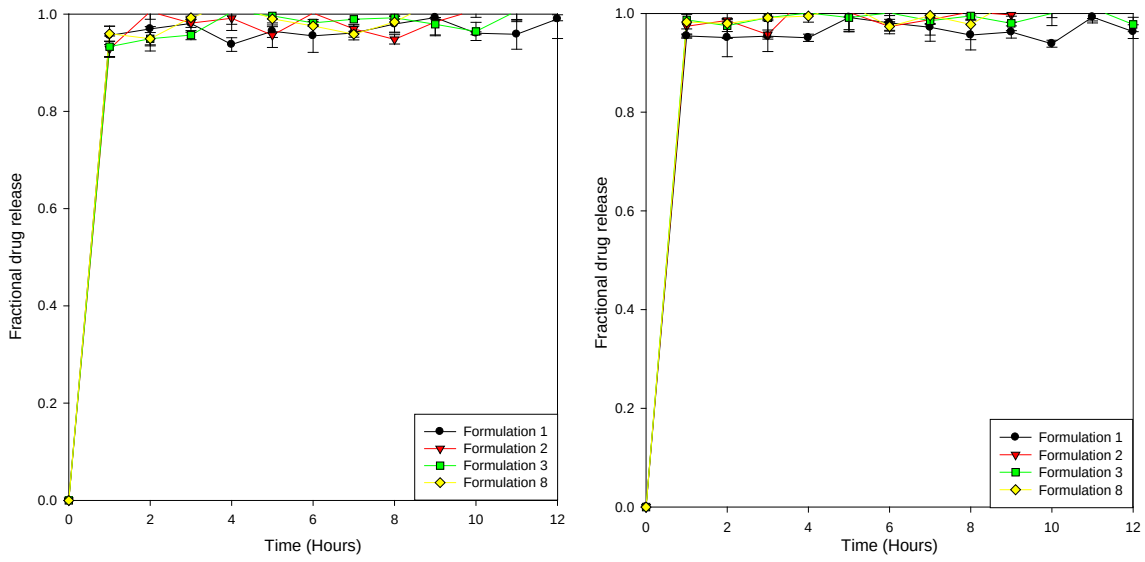


Figure 4.15: *In vitro* drug release profiles of viable formulations in (a) SIF and (b) in SGF (n=3 in all instances).

4.4. Concluding Remarks

The λmax was determined as 289nm, 214nm and 229nm for propranolol, captopril and furosemide, respectively. The λmax obtained for each of the drugs are in close agreement with the λmax values found in the literature and was thus employed for analysis of these drugs. The potential of a medium to hydrate the SBP was a crucial aspect in the drug-loading process. The aqueous medium was observed to be most suited to this process and thus only drugs with good water-solubility may be employed where hydration is the key mechanism utilized for drug-loading. Thus, furosemide due to its very low water solubility could not be utilized as a model drug for the type of application being attempted.

Drug entrapment results showed that the SBP was able to entrap propranolol in aqueous medium but not to an extent that encouraged its use in the development of the MODDS. In contrast, captopril displayed excellent drug entrapment which could be due its high water solubility. However, the SBP could not control the *in vitro* drug release of any of the drugs. Therefore, based on the drug entrapment, a multidrug formulation was deemed unfeasible and captopril was selected as the model drug for the development of the MODDS. Due to the ineffective control of drug release, modifications to the structure of the SBP must be attempted in order to improve the drug release behavior of the SBP.

CHAPTER 5
IMPROVEMENT OF THE FUNCTIONAL CHARACTERISTICS BY WAY OF MODIFICATION OF STARCH-BASED PLATFORM

5.1. Introduction

Preliminarily studies have shown that the Starch-Based Platform (SBP) derived from sago was able to incorporate drugs by means of hydration but displayed inadequate control of drug release. This was similar to the findings of Zhu and Bertoft (1997) and Pereswetoff-Morath (1998) which showed that native starches did not retard drug release sufficiently with the phenomenon attributed to the substantial swelling and degradation of the starches in the drug release mediums. As the SBP is composed of starch, inducing modifications by means of gelatinization, oxidation and crosslinking may improve the stability and functional characteristics of the SBP (Karim *et al.,* 2008; Xiao *et al.,* 2011).

Gelatinization of starch is a well-documented phenomenon and applied in various industries to enhance the properties of the starch. Gelatinization is the disruption of molecular orders and breaking of intermolecular bonds within the starch granule and results in irreversible changes to the structure and properties of the starch granule (Maaruf *et al.,* 2001; Lida *et al.,* 2008; Oh *et al.,* 2008). The principle approaches of inducing gelatinization of starch are by application of heat during starch hydration and by placing starch into aqueous alkali medium (Wootton and Ho, 1989; Ragheb *et al.,* 1995; Ratnayake and Jackson, 2009; Nor Nadiha *et al.,* 2010). However, during preliminary studies conducted, the use of heat proved unsuccessful due to the lack of control of gelatinization, which resulted in structural instability of the SBP with deformation and mass loss occurring and was thus not pursued in subsequent studies.

In the case of the use of alkali hydroxides, the literature and preceding studies conducted have shown that the presence of NaOH induced gelatinization and an increase in the NaOH concentration resulted in progressive gelatinization to the extent of solubilization of the SBP at high NaOH concentrations (Karim *et al.,* 2008). In contrast, the use of ethanol displayed a tendency to inhibit the hydration of the SBP and in so doing inhibited the subsequent gelatinization of the SBP. Thus, the employment of ethanol proved to elicit a protective effect by maintaining the shape and size of the SBP and was postulated to confer a controlling effect on the alkali-induced gelatinization of the SBP.

Oxidized starch has been prepared with several different techniques in order to provide biocompatible and biodegradable polymers. One method involves the use of sodium (meta)periodate (Figure 5.1) in acidic pH which breaks the cyclic structure of the glucose monomers and produces highly reactive aldehyde groups within the starch molecule. Periodate oxidation is very selective and affects carbon atoms C2 and C3 on the glucose ring resulting in a dialdehyde starch which is able to crosslink intramolecularly and intermolecularly with other starch chains by means of hemiacetal and acetal formation (Veelaert *et al.,* 1994; Christensen *et al.,* 2001; Wongsagon *et al.,* 2005). Figure 5.2 depicts the periodate-facilitated formation of dialdehyde starch with approximately one mol sodium (meta)periodate required to oxidize one mol of anhydrous glucose units. Oxidation imparts different physicochemical and physicomechanical properties compared to native unmodified starches and coupled with its increased reactivity, the oxidized starch lends itself to further modifications and use as a functional polymer in drug delivery systems.

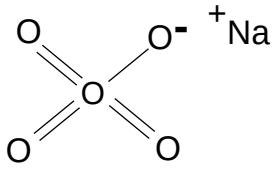


Figure 5.1: Structure of sodium (meta)periodate.

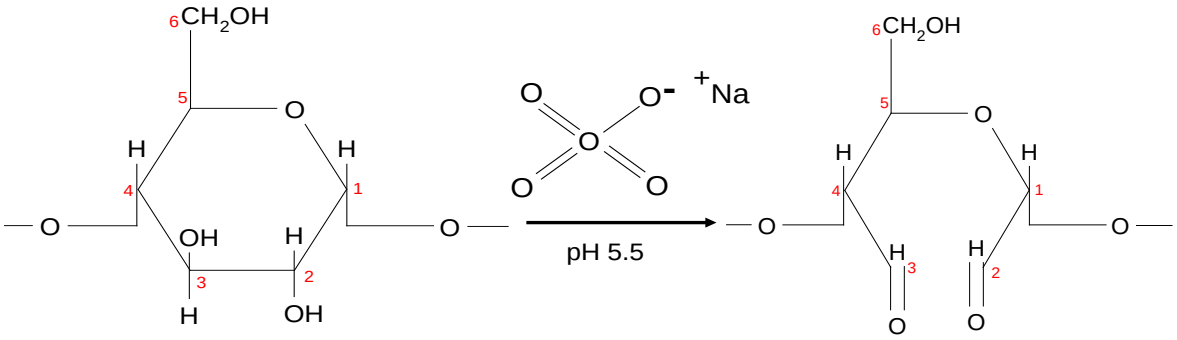
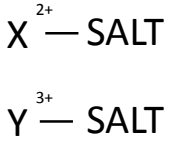


Figure 5.2: Periodate facilitated oxidation of starch.

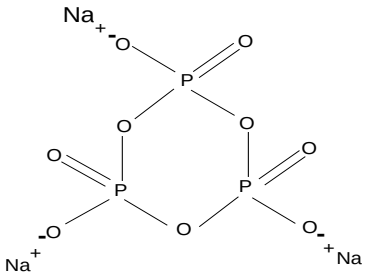
Crosslinking of starches is a method that has been employed for decades and is accomplished by modifications and linkages between hydroxyl groups contained in amylose and amylopectin (Gui-Jie *et al.,* 2006). The crosslinking can occur between amylose and amylopectin, between individual amylose chains and between separate amylopectin molecules (Hamerstrand, 1960). Many different crosslinking agents have been employed, e.g. polyvalent cationic salts (Figure 5.3a) and Sodium Trimetaphosphate (STMP) (Figure 5.3b), which act as ionic crosslinkers, and Glutaraldehyde (Glut) (Figure

5.3c) and Epichlorohydrin (ECH) (Figure 5.3d), which act as covalent crosslinkers. Thus, the various crosslinkers differ slightly in their mechanism and result in slightly different crosslinked end products. However, most crosslinkers employed act in alkaline medium with hydroxyl groups as the targets for crosslinking (Heeres *et al.,* 1998; Hamdi *et al.,* 1999). Any one of the available hydroxyl groups on the reacting glucose molecules (OH group on C2, C3 or C6) may be crosslinked and the resultant crosslinking further enhances the stabilizing effects of the already present hydrogen bonding (Jane *et al.,* 1992; Xiao *et al.,* 2012). The crosslinking of starches is known to confer increased resistance to heating, high pH and improves the structural stability of the starch (Xiao *et al.,* 2011). In addition, crosslinking affects the hydration, swelling, gelatinization and erosion of starch (Heeres *et al.,* 1998; Muhammad *et al.,* 2000; Xiao *et al.,* 2012) which may be advantageous in manipulating the mechanisms of drug entrapment and drug release when employing the SBP as a MODDS.



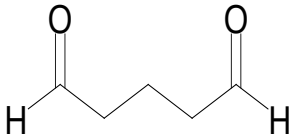
Polyvalent cationic species in salt form 1,3,5,2λ^5,4λ^5,6λ^5-

(a)



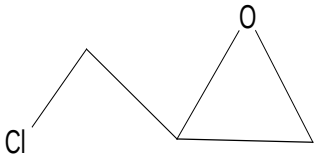
Trisodium 2,4,6-trioxido-trioxatriphosphinane 2,4,6-trioxide

(b)



1,5-Pentanedial

(c)



1-Chloro-2,3-epoxypropane

(d)

Figure 5.3: Chemical structure of crosslinking agents (a) divalent and trivalent cationic salt, (b) sodium trimetaphosphate, (c) glutaraldehyde and (d) epichlorohydrin.

Upon placing salts into solution, dissociation of the salt occurs releasing the ionic species' contained within the salt allowing them to interact with other molecules within the solution. In the case of cationic crosslinking of starch, polyvalent cations (carrying positive charge) interacts with the electron rich hydroxyl oxygen of the glucose monomers on the amylose and/amylopectin chains. The cationic species can interact with more than one glucose

monomer due to its polyvalent nature and thus facilitate intra or intermolecular crosslinking between the intrinsic starch polymer chains as depicted in Figure 5.4 (Chen *et al.,* 2009; Syed *et al.,* 2011; Keita and Imai, 2012). Furthermore, the anionic species of the salt influences the crosslinking environment and thus affects the extent to which crosslinking occurs. In addition, cations may only react with a single glucose monomer and may potentially react with nucleophilic groups within drug molecules or anionic drug molecules to facilitate drug absorption.

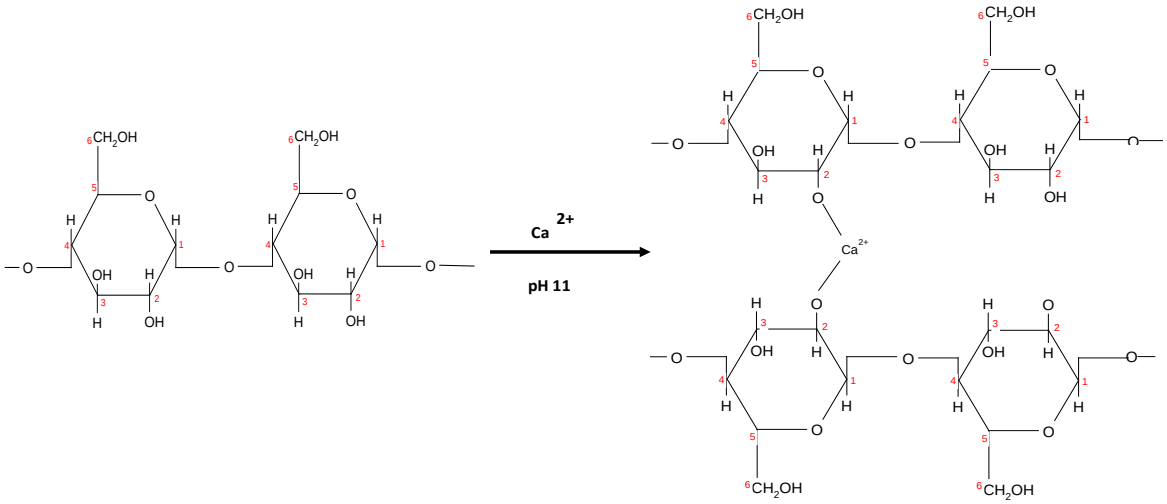


Figure 5.4: Polyvalent cationic crosslinking of starch using the example of calcium hydroxide.

STMP, the sodium salt of metaphosphoric acid, can be regarded as an inorganic ionic crosslinker as it introduces negatively charged phosphate ions into the solution, which then reacts with starch (Li *et al.,* 2009). The reactive species are the electron rich hydroxyl oxygen atoms of the glucose monomers and the electrophilic phosphorous atom in the crosslinker. The reaction proceeds stepwise with lineation of the cyclic STMP followed by bonding to a single starch molecule. Thereafter crosslinking takes place through binding of a second starch molecule to the same phosphorous atom in a manner identical to the bonding of the first starch molecule. The entire STMP-crosslinking reaction is depicted in Figure 5.5. Crosslinking using STMP is achieved through esterification with the crosslinked starch known as distarch phosphate (Lim and Seib 1993; Muhammad *et al.,* 2000; Gui-Jie *et al.,* 2006; Abbas *et al.,* 2010). The crosslinked starch that continues to carry an anionic charge may further interact with electrophilic groups within drug molecules or cationic drug molecules to facilitate drug absorption (Li *et al.,* 2009).

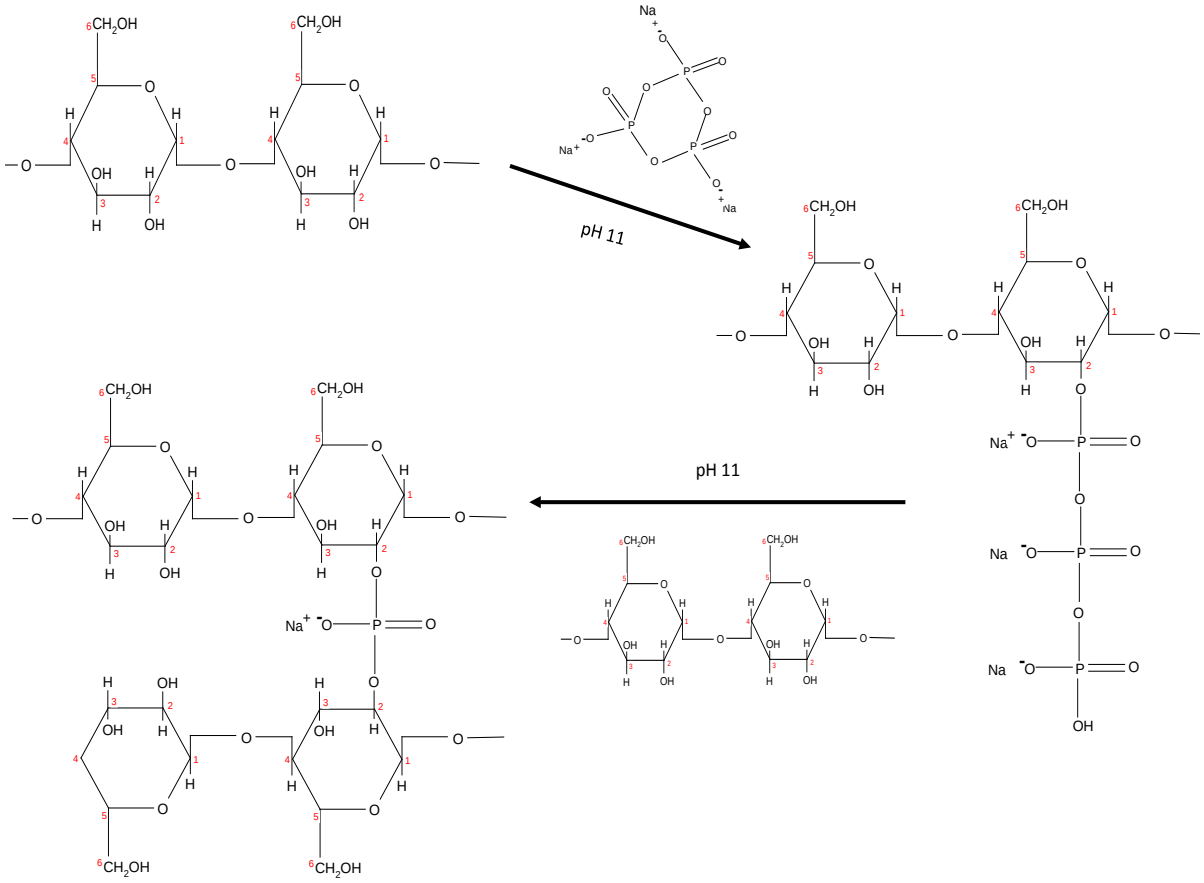


Figure 5.5: STMP-facilitated crosslinking of starch.

In contrast to STMP, ECH is regarded as an organic covalent crosslinker (Jane *et al.,* 1992; Hamdi *et al.,* 2001; Gui-Jie *et al.,* 2006; Xiao *et al.,* 2012). In alkaline medium, crosslinking follows a stepwise reaction process with the nucleophilic hydroxyl oxygen atom of the glucose monomers interacting with the electrophilic epoxy carbon atom (C3) of the crosslinker. The intermediate molecule, a monostarch glycerol, then forms a second reactive epoxide ring at the far end of the molecule (between C1 and C2) that interacts with a second starch molecule in a manner identical to the bonding of the first starch molecule. The entire ECH crosslinking reaction is depicted in Figure 5.6. Crosslinking using ECH is achieved through etherification with the crosslinked product known as distarch glycerol (Hamerstrand *et al.,* 1960; Heeres *et al.,* 1998).

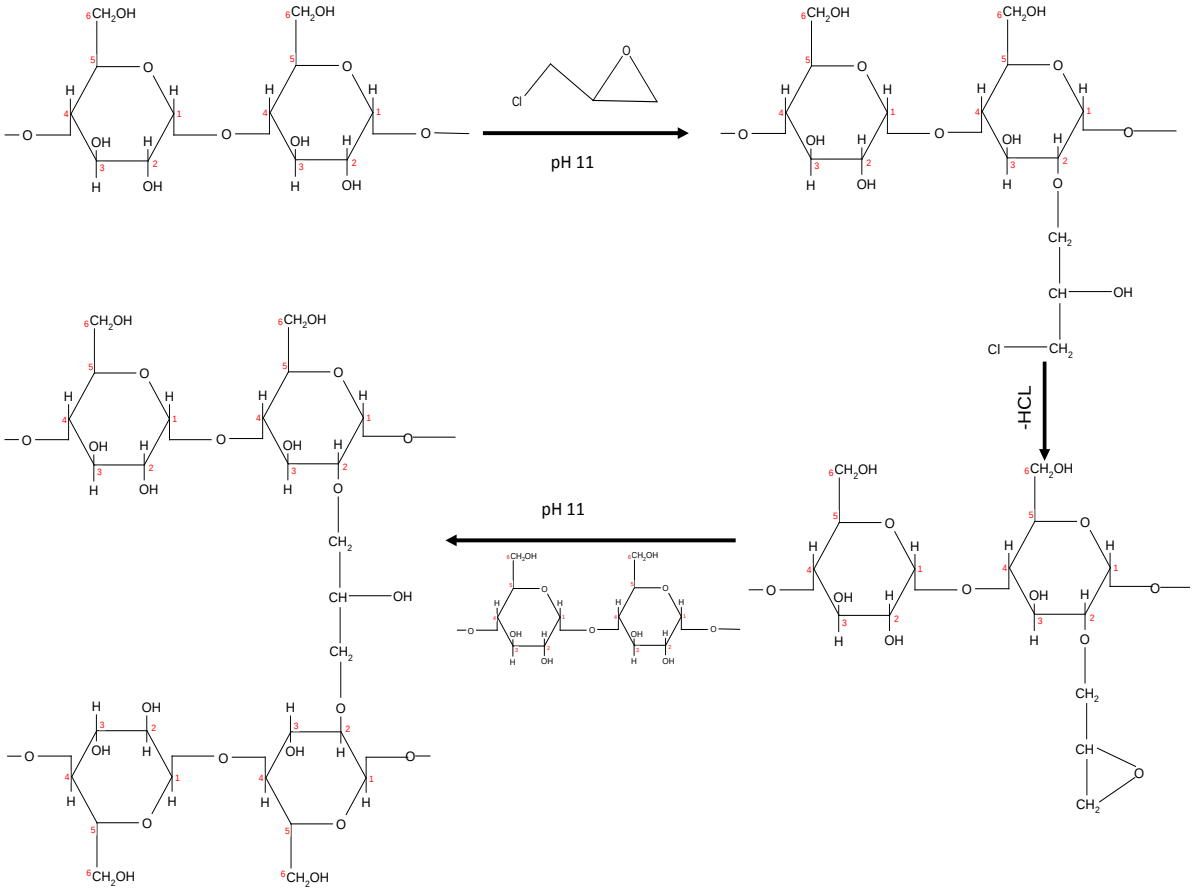


Figure 5.6: ECH-facilitated crosslinking of starch.

Glut is a dialdehyde crosslinking agent that has been used extensively in the crosslinking of polymers (Syed *et al.,* 2011). The crosslinking of intrinsic starch polymers with glut is achieved through the nucleophilic interactions of hydroxyl groups of the glucose monomers with the carbonyl groups contained in glut molecule to form hemi-acetal linkages as depicted in Figure 5.7. Due to the presence of two carbonyl groups on the glut molecule, glut can crosslink up to four hydroxyl groups either intramolecularly or intermolecularly and is thus regarded as a very strong crosslinking agent. (El-Tahlawy *et al.,* 2007; Pal *et al.,* 2008; Chen *et al.,* 2009; Syed *et al.,* 2011).

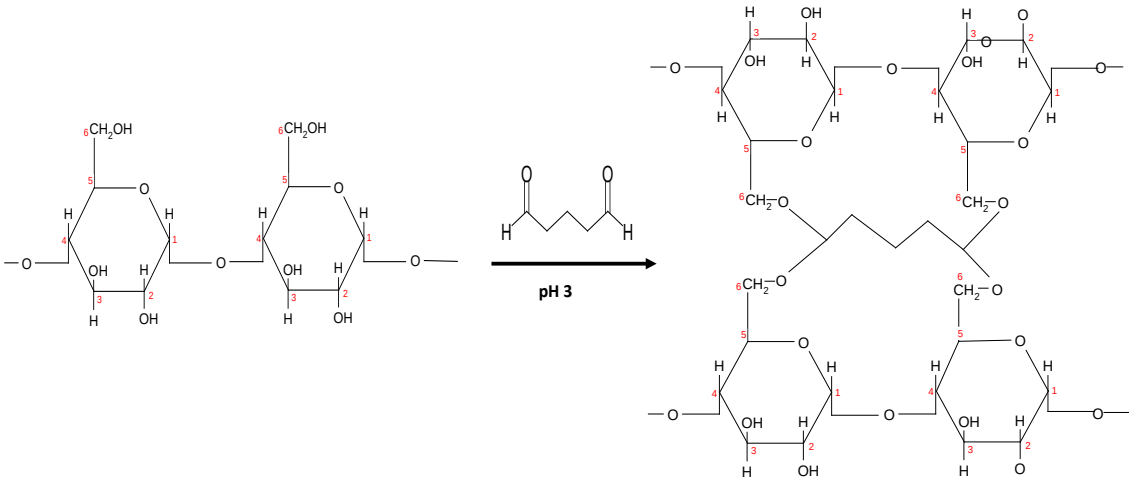


Figure 5.7: Glut-facilitated crosslinking of starch.

Due to the ability of starch to undergo various modifications, in this Chapter the various modifications that can be applied to starch will be attempted on SBP to improve the drug entrapment potential and enhance the drug release behavior of the SBP. Additionally, the modifications will be conducted in order to improve the structural integrity while maintaining the multiparticulate nature of the SBP.

5.2. Materials and Methods

5.2.1. Materials

Sago Multiparticulates (SMP, food grade) were purchased from KOO South Africa (Tiger Brands Ltd., Bryanston, Johannesburg, South Africa) and were used as the Starch-Based Platform (SBP). Captopril (Mw=217.29g.mol^{-1}, solubility ~160mg.mL^{-1} in water at 25°C) and Diphenhydramine (DPH, Mw=291.82g.mol^{-1}, solubility>100mg.mL^{-1} in water at 21.5°C) were acquired from Sigma-Aldrich (Sigma-Aldrich Inc., St. Louis, USA). Sodium hydroxide (NaOH, Mw=40.00g.Mol^{-1}), Barium chloride ($BaCl_2$, Mw= 208.23g.Mol^{-1}), Calcium chloride ($CaCl_2$, Mw=110.98g.Mol^{-1}), Aluminium chloride ($AlCl_3$, Mw=133.34g.Mol^{-1}), Aluminium oxide (Al_2O_3, Mw=101.961g.Mol^{-1}), Aluminium sulphate ($Al_2(SO_4)_3$, Mw=342.15g.Mol^{-1}), Magnesium chloride ($MgCl_2$, Mw=95.21g.Mol^{-1}), Barium sulphide (BaS, Mw= 69.39g.Mol^{-1}), Copper (II) hydroxide ($Cu(OH)_2$, Mw=97.56g.Mol^{-1}), Calcium lactate ($Ca(Lac)_2$, Mw=218.22g.Mol^{-1}), Magnesium hydroxide ($Mg(OH)_2$, Mw=58.32g.Mol^{-1}), Tin (II) chloride ($SnCl_2$, Mw=189.60g.Mol^{-1}), were purchased from Saarchem-Holpro Analytic (Pty) Ltd., (Krugersdorp, Johannesburg, South Africa) and were of analytical grade. Ethanol (99%$^{v}/_{v}$, analytical grade), Calcium hydroxide ($Ca(OH)_2$, Mw=74.093g.Mol^{-1}), Calcium gluconate ($Ca(Glu)_2$, Mw=430.373g.Mol^{-1}), Calcium sulphate ($CaSO_4$, Mw=136.14g.Mol^{-1}), Zinc sulphate ($ZnSO_4$, Mw=161.47g.Mol^{-1}), Aluminium

hydroxide ($Al(OH)_3$, Mw=78.00g.Mol^{-1}), were purchased from Merck (Pty) Ltd. (Modderfontein, Johannesburg, South Africa). Epichlorohydrin (ECH, Mw= 92.52g.mol^{-1}, 99%$^{v}/_{v}$) and Glutaraldehyde (Glut, Mw=100.12g.mol^{-1}, 30 %$^{v}/_{v}$) were purchased from Sigma-Aldrich (Sigma-Aldrich Inc., St. Louis, USA). Sodium trimetaphosphate (STMP, Mw=305.89, ≥96.0%$^{w}/_{w}$) was purchased from Aldrich (Sigma-Aldrich Inc., St. Louis, USA). Sodium (meta)periodate ($NaIO_4$, Mw=213.892g.mol^{-1}, 99%$^{w}/_{w}$) was purchased from Sigma-Aldrich, (Sigma-Aldrich Inc, Aston Manor, South Africa). All other materials and chemicals used were as describe in Chapter 2 and Chapter 3.

5.2.2. Gelatinization of SBP

Various ratios of ethanol, deionized water and NaOH solution (1M) were prepared as shown in Table 5.1 and placed into the experimental apparatus. To each solution, SBP samples (4g) were added and allowed to hydrate and gelatinize for 4 hours in an experimental apparatus maintained at 25±1°C and stirred at 50rpm. The gelled SBP samples were then removed, lightly blotted with tissue paper to remove excess surface moisture, weighed to determine the degree of swelling and then dried in a laboratory oven maintained at 50°C until constant mass was achieved. During the drying process, the SBP were moved around the petri dish using a flat-ended metal spatula to prevent cohesion of the gelled surfaces to adjacent SBP and the surface of the petri dish. The dried SBP were then weighed to determine the change in SBP mass during modification. The study was conducted in triplicate (n=3).

Table 5.1: Conditions employed for controlled gelatinization of SBP

Alcohol (%)	NaOH (mL)	EtOH (mL)	Water (mL)	Final volume (mL)	EtOH (%)	Water (%)	NaOH (%)
70	1	14	6	21	66.667	28.571	4.762
70	2	14	6	22	63.636	27.273	9.091
70	3	14	6	23	60.870	26.087	13.043
70	4	14	6	24	58.333	25.000	16.667
70	5	14	6	25	56.000	24.000	20.000
70	6	14	6	26	53.846	23.077	23.077
70	7	14	6	27	51.852	22.222	25.926
70	8	14	6	28	50.000	21.429	28.571
70	9	14	6	29	48.276	20.690	31.034
70	10	14	6	30	46.667	20.000	33.333
60	1	12	8	21	57.143	38.095	4.762
60	2	12	8	22	54.545	36.364	9.091
60	3	12	8	23	52.174	34.783	13.043
60	4	12	8	24	50.000	33.333	16.667
60	5	12	8	25	48.000	32.000	20.000
60	6	12	8	26	46.154	30.769	23.077
60	7	12	8	27	44.444	29.630	25.926
60	8	12	8	28	42.857	28.571	28.571
60	9	12	8	29	41.379	27.586	31.034
60	10	12	8	30	40.000	26.667	33.333
50	1	10	10	21	47.619	47.619	4.762
50	2	10	10	22	45.455	45.455	9.091
50	3	10	10	23	43.478	43.478	13.043
50	4	10	10	24	41.667	41.667	16.667
50	5	10	10	25	40.000	40.000	20.000
50	6	10	10	26	38.462	38.462	23.077
50	7	10	10	27	37.037	37.037	25.926
50	8	10	10	28	35.714	35.714	28.571
50	9	10	10	29	34.483	34.483	31.034
50	10	10	10	30	33.333	33.333	33.333
40	1	8	12	21	38.095	57.143	4.762
40	2	8	12	22	36.364	54.545	9.091
40	3	8	12	23	34.783	52.174	13.043
40	4	8	12	24	33.333	50.000	16.667
40	5	8	12	25	32.000	48.000	20.000
40	6	8	12	26	30.769	46.154	23.077
40	7	8	12	27	29.630	44.444	25.926
40	8	8	12	28	28.571	42.857	28.571
40	9	8	12	29	27.586	41.379	31.034
40	10	8	12	30	26.667	40.000	33.333
30	1	6	14	21	28.571	66.667	4.762
30	2	6	14	22	27.273	63.636	9.091
30	3	6	14	23	26.087	60.870	13.043
30	4	6	14	24	25.000	58.333	16.667
30	5	6	14	25	24.000	56.000	20.000
30	6	6	14	26	23.077	53.846	23.077
30	7	6	14	27	22.222	51.852	25.926
30	8	6	14	28	21.429	50.000	28.571
30	9	6	14	29	20.690	48.276	31.034
30	10	6	14	30	20.000	46.667	33.333

Where NaOH denoted sodium hydroxide solution (1M) and EtOH denoted ethanol (99%$^{v}/_{v}$)

5.2.3. Determination of the effect of employing polyvalent cationic salts as crosslinking agents in improving the performance of the SBP

5.2.3.1. Determination of the drug entrapment potential

Crosslinking drug solutions were prepared as depicted in Table 5.2 and aliquots (5mL) were placed into experimental apparatuses. SBP samples (2g) were accurately weighed using an analytical mass balance and submerged within crosslinking drug solutions. The SBP samples were then allowed to hydrate and crosslink for 4 hours in an experimental apparatus maintained at 25±1°C and stirred at 50rpm. Thereafter the drug-loaded ionically crosslinked SBP samples were removed, lightly blotted with tissue paper to remove excess moisture and weighed in order to determine the hydration of the ionically crosslinked SBP. The drug-loaded ionically crosslinked SBP samples were then convection dried in a laboratory oven maintained at 50°C. During the drying process, the ionically crosslinked SBP were physically separated using a flat-ended metal spatula to prevent adhesion to the adjacent SBP and the surface of the petri dish. The extent of drug entrapment was determined as previously described in Chapter 4, Section 4.2.4.3 and analyzed at a λmax=214nm. The study was conducted in triplicate (n=3).

Table 5.2: Preparation of drug crosslinking-drug solutions

XL salt	Cationic species and valency	$Q_{XL\ salt}$ (mg)	V_{DS} (mL)	[XL salt] ($\%^{w}/_{v}$)	[Captopril] ($mg.mL^{-1}$)
$BaCl_2$	Ba^{2+}	0.25	5	5	75
$CaCl_2$	Ca^{2+}	0.25	5	5	75
$AlCl_3$	Al^{3+}	0.25	5	5	75
$Ca(OH)_2$	Ca^{2+}	0.25	5	5	75
$Ca(Glu)_2$	Ca^{2+}	0.25	5	5	75
$CaSO_4$	Ca^{2+}	0.25	5	5	75
$ZnSO_4$	Zn^{2+}	0.25	5	5	75
$Al(OH)_3$	Al^{3+}	0.25	5	5	75
Al_2O_3	Al^{3+}	0.25	5	5	75
$Al_2(SO_4)_3$	Al^{3+}	0.25	5	5	75
$MgCl_2$	Mg^{2+}	0.25	5	5	75
BaS	Ba^{2+}	0.25	5	5	75
$Cu(OH)_2$	Cu^{2+}	0.25	5	5	75
$Ca(Lac)_2$	Ca^{2+}	0.25	5	5	75
$Mg(OH)_2$	Mg^{2+}	0.25	5	5	75
$SnCl_2$	Sn^{2+}	0.25	5	5	75

Where XL salt denoted the crosslinking salt employed, $Q_{XL\ salt}$ denoted the quantity of crosslinking salt required, V_{DS} denoted the Volume of drug solution *[XL salt] denoted the concentration of crosslinking salt and [Captopril] denoted the concentration of captopril*

5.2.3.2. Determination of the drug release behaviour of cationically crosslinked SBP

The quantity of each drug-loaded SBP required for the study was calculated using the results of the drug entrapment study and Equation 4.1. This quantity was accurately weighed and subjected to *in vitro* drug release studies. The *in vitro* drug release behavior

of each of the salt-crosslinked SBP formulations was determined as previously described in Chapter 4, Section 4.2.5 at λmax=214nm. The study was conducted in triplicate (n=3).

5.2.4. Pilot study to elucidate the effect of ECH, Glut and STMP on the functional characteristics of the SBP

5.2.4.1. Preparation of crosslinked SBP

5.2.4.1.1. Preparation of ECH-crosslinked SBP

Alkaline alcohol (40% EtOH: 5mL NaOH) solution was prepared by adding NaOH solution (1M, 25mL) to 100mL ethanol solution comprising 60mL ethanol and 40mL water. Aliquots (20mL) of this solution were accurately measured and placed into the experimental apparatuses. SBP samples (4g) were accurately weighed and submerged within the alkaline alcohol solution. ECH (99%$^{v}/_{v}$ 0.1mL) was then immediately added to the experimental apparatus and the SBP samples allowed to hydrate and covalently crosslink for 4 hours in an experimental apparatus maintained at 25±1°C and stirred at 50rpm. The SBP samples were then removed, lightly blotted with tissue paper to remove excess moisture and weighed in order to determine the hydration of the ECH-crosslinked SBP. The ECH-crosslinked SBP were then convection dried in a laboratory oven maintained at 50°C until constant mass was achieved. The mass of the dried ECH-crosslinked SBP were then determined gravimetrically.

5.2.4.1.2. Preparation of Glut-crosslinked SBP

An acidic hydration medium was prepared by dissolving 0.2g sodium chloride in 100mL deionized water and then adding HCl until the desired pH of 1.2 was attained (~0.7mL HCl). Aliquots (20mL) of this solution were accurately measured and placed into the experimental apparatuses. SBP samples (4g) were accurately weighed and submerged within the acidic hydration medium. Glut (0.1mL) was then immediately added to the experimental apparatus and the SBP samples were subjected to the same treatment as described in Section 5.2.4.1.1.

5.2.4.1.3. Preparation of STMP-crosslinked SBP

STMP solution (99%$^{w}/_{v}$) was prepared by accurately weighing and dissolving 9.90g STMP in 5mL deionized water and making this solution up to 10ML using deionized water. The same procedure as described in Section 5.2.4.1.2 was then employed with the STMP solution prepared used in place of ECH to facilitate ionic crosslinking.

5.2.4.2. Entrapment of drug into modified SBP

Drug solution (75mg.mL^{-1}) was prepared by accurately weighing and dissolving 6.75g captopril in 30mL deionized water and thereafter making up the solution to 90mL. Aliquots (10mL) of drug solution were accurately measured and placed into the experimental apparatus. ECH-crosslinked, Glut-crosslinked, STMP-crosslinked and unmodified SBP samples (2g) were accurately weighed, submerged within the drug solutions and allowed to hydrate and entrap drug for 4 hours in an experimental apparatus maintained at 25±1°C and stirred at 50rpm. A second set of ECH-crosslinked, Glut-crosslinked, STMP-crosslinked and unmodified SBP samples was subjected the same procedure with water used in place of drug solution (placebos). The study was conducted in triplicate (n=3).

5.2.4.3. Elucidation of extent of drug entrapment

The extent of drug entrapment was determined as previously described in Chapter 4, Section 4.2.4.3 and analyzed at a λmax=214nm.

5.2.4.4. Comparative in vitro drug release from pre-crosslinked and unmodified SBPs

The quantity of each drug-loaded SBP required for the study was dictated by the minimum quantity of drug used in commercial captopril formulations (i.e. 25mg) and was calculated using the results of the drug entrapment study and Equation 4.1 and depicted in Table 5.3. The required quantity of SBP was accurately weighed and subjected to *in vitro* drug release studies. The comparative *in vitro* drug release behavior of each of the SBP formulations was determined as previously described in Chapter 4, Section 4.2.5 at λmax=214nm. The quantity of placebo SBP required was equal to their analogous drug-loaded SBP and was subjected to identical *in vitro* drug release studies as the drug-loaded SBP. The study was conducted in triplicate (n=3).

Table 5.3: Drug-loaded SBP quantities to be used for *in vitro* drug release study

SBP formulation	Quantity of SBP required (g)
Drug-loaded ECH-crosslinked	0.082
ECH-crosslinked placebo	0.082
Drug-loaded Glut-crosslinked	0.222
Glut-crosslinked placebo	0.222
Drug-loaded STMP-crosslinked	0.109
STMP-crosslinked placebo	0.109
Drug-loaded unmodified	0.114
Unmodified placebo	0.114

Where SBP denoted Starch-Based Platform, ECH denoted Epichlorohydrin, Glut denoted Glutaraldehyde and STMP denoted Sodium Trimetaphosphate

5.2.5. Covalent crosslinking of SBP with ECH

5.2.5.1. Determination of the effect of ECH concentration on the crosslinking of SBP in a range of gelatinization mediums

Alkaline alcohol gelatinization media were prepared utilizing the EtOH: NaOH: water ratios depicted in Table 5.4. SBP samples (2g) were accurately weighed and placed into experimental apparatuses. Gelatinization media (10mL) were then placed simultaneously with various ECH volumes (0.05mL, 0.1mL, 0.3mL, 0.5mL, 0.7mL, 1mL) into the experimental apparatuses and allowed to crosslink for 4 hours while maintained at 25±1°C and stirred at 50rpm. The SBP samples were then removed, lightly blotted with tissue paper to remove excess moisture and weighed in order to determine the hydration potential of the crosslinked SBP. The ECH-crosslinked SBP were then dried in a laboratory oven maintained at 50°C, weighed and then visually analyzed to determine their structural integrity and feasibility for drug entrapment studies. The study was conducted in triplicate (n=3).

Table 5.4: Constitution of alkaline alcohol gelatinization mediums

Alkaline alcohol ratio (% EtOH: mL NaOH)	EtOH (mL)	Water (mL)	NaOH (mL)	Final volume	EtOH (%)	Water (%)	NaOH (%)
30:3	6	14	3	23	26.087	60.870	13.043
40:5	8	12	5	25	32.000	48.000	20.000
40:7	8	12	7	27	29.630	44.444	25.926

Where NaOH denoted sodium hydroxide solution (1M) and EtOH denoted ethanol (99%$^{v}/_{v}$)

5.2.5.2. Determination of hydration time and crosslinking time required for most favorable covalent ECH-crosslinking of the SBP

Alkaline alcohol gelatinization mediums were prepared utilizing the EtOH: NaOH: water ratios depicted in Table 5.4. SBP samples (2g) were accurately weighed and placed into experimental apparatuses. Gelatinization mediums (10mL) were then placed into experimental apparatuses and the SBP samples were allowed to gelatinize for a designated time (Table 5.5) at 25±1°C and stirring at 50rpm. Thereafter, ECH (1mL) was added to the experimental apparatus and the SBP was allowed to crosslink for a designated time (Table 5.5) at 25±1°C and stirring at 50rpm. The SBP samples were then removed, lightly blotted with tissue paper to remove excess moisture and weighed in order to determine the hydration potential of the crosslinked SBP. The ECH-crosslinked SBP were then convection dried in a laboratory oven maintained at 50°C, weighed and then visually analyzed to determine their structural integrity and feasibility for drug entrapment studies. The study was conducted in triplicate (n=3).

Table 5.5: Determination of favorable hydration and crosslinking times in various gelatinization media

Formulation	HT (Hours)	CT (Hours)	Total time (Hours)
1	4	0	4
2	2	0	2
3	1	0	1
4	0.5	0	0.5
5	0	2	2
6	0	1	1
7	2	2	4
8	1	2	3
9	0.5	2	2.5
10	1	1	2
11	0.5	1	1.5

Where HT denoted Hydration Time and CT denoted Crosslinking Time

5.2.5.3. Determination of the effect of ECH-crosslinking on the functional characteristics of the SBP employing DPH as the model drug

5.2.5.3.1. Drug entrapment and determination of DPH entrapment efficiency

Alkaline alcohol gelatinization media were prepared utilizing the EtOH: NaOH: water ratios depicted in Table 5.4. Drug solutions (100mg.mL^{-1}) were prepared by accurately weighing and dissolving 3g DPH in 20mL of each alkaline alcohol medium and then made up to 30mL with the respective alkaline alcohol. Aliquots of drug solution (10mL) were accurately measured and placed into the experimental apparatuses. SBP samples (2g) were then accurately weighed, submerged within drug solution and allowed to entrap drug for a designated time (Table 5.6) while maintained at 25±1°C and stirred at 50rpm. Thereafter ECH (0.1mL) was added to particular drug solutions and the drug-loaded SBP samples were allowed to crosslink for a designated time (Table 5.6) while maintained at 25±1°C and stirred at 50rpm. A comparative control drug solution was prepared by dissolving 3g DPH in 10mL deionized water (replacing the alkaline alcohol) and made up to 30mL with deionized water. SBP samples (2g) were then weighed and subjected to the formulation conditions described for Formulation 6 in Table 5.6. All the SBP samples were then removed and subjected to the same procedure as described in Section 5.2.5.2. The extent of drug entrapment was determined as previously described in Chapter 2, Section 2.2.8.2.2 at λmax=254nm and utilizing the pre-constructed calibration curve in Chapter 2, Section 2.2.8.1. The study was conducted in triplicate (n=3).

Table 5.6: Drug-loading and crosslinking time for DPH study

Formulation	Alkaline alcohol ratio (%EtOH: mL NaOH)	HT (Hours)	CT (Hours)	Total time (Hours)
1	40/5	2	2	4
2	40/5	4	2	6
3	40/7	1	1	2
4	30/3	4	2	2
5	30/3	4	0	4
6	0/0	4	0	4

Where NaOH denoted sodium hydroxide solution (1M) and EtOH denoted ethanol (99%$^{v}/_{v}$), HT denoted Hydration Time and CT denoted Crosslinking Time

5.2.5.3.2. Elucidation of the in vitro DPH release behavior of ECH-crosslinked SBP

The drug release behaviors of each of the crosslinked SBP formulations and unmodified formulation were determined as previously described in Chapter 2, Section 2.2.8.3 and utilizing the pre-constructed calibration curve in Chapter 2, Section 2.2.8.1.

5.2.5.4. Determination of the effect of ECH-crosslinking on the functional characteristics of the SBP employing captopril as the model drug

5.2.5.4.1. Determination of the effect of concurrent drug-loading and modifications of the SBP

5.2.5.4.1.1. Drug entrapment and determination of extent of captopril entrapment

Alkaline alcohol (40% EtOH: 5mL NaOH) was prepared as illustrated in Table 5.4. Drug solutions (75mg.mL^{-1}) were prepared by accurately weighing and dissolving 4.50g captopril in 20mL alkaline alcohol and then made up to 60mL using alkaline alcohol. Aliquots of drug solution (10mL) were accurately measured and placed into experimental apparatuses. SBP samples (2g) were then accurately weighed, submerged within drug solution maintained at 25±1°C, and allowed to entrap drug for 4 hours, under constant stirring at 50rpm. In a second formulation, ECH (0.1mL) was added to the drug solution after 2 hours of gelatinization and the drug-loaded SBP were allowed to crosslink for a further 2 hours at 25±1°C and stirring at 50rpm. A comparative control drug solution was prepared by accurately weighing and dissolving 2.25g captopril in 10mL deionized water (replacing the alkaline alcohol) and made up to 30mL with deionized water. The SBP samples (2g) for the control formulations were then accurately weighed submerged within drug solution maintained at 25±1°C, and allowed to entrap drug for 4 hours, under constant stirring at 50rpm. All the SBP formulations were then removed from the experimental apparatuses and subjected to the same procedure as described in Chapter 4, Section 4.2.4.2. The extent of drug entrapment was determined as previously described in Chapter 4, Section 4.2.4.3 at λmax=214nm utilizing the pre-constructed calibration curve in Chapter 4, Section 4.3.2. The study was conducted in triplicate (n=3).

5.2.5.4.1.2. Comparative in vitro captopril release behavior from ECH crosslinked and unmodified SBPs

The *in vitro* drug release behaviors of each of the SBP formulations prepared were determined as previously described in Chapter 4, Section 4.2.5 and utilizing the pre-constructed calibration curve in Chapter 4, Section 4.3.2. The study was conducted in triplicate (n=3).

5.2.5.4.2. Determination of the effect of step-wise drug-loading, controlled gelatinization and subsequent ECH crosslinking

5.2.5.4.2.1. Preparation of drug-loaded SBP

Drug solutions (75mg.mL^{-1}) were prepared by accurately weighing and dissolving 9g captopril in 20mL deionized water and then made up to 120mL using deionized water. Aliquots of drug solutions (10mL) were accurately measured and placed within the experimental apparatuses. SBP samples (2g) were then accurately weighed, submerged in drug solution maintained at 25±1°C, and allowed to entrap drug for 4 hours, under constant stirring at 50rpm.

5.2.5.4.2.2. Modification of drug-loaded SBP

The drug-loaded SBP samples were retained in the experimental apparatuses and an adequate quantity of concentrated alkaline alcohol solution was added to the produce a 40% EtOH: 5mL NaOH alkaline alcohol drug solution. ECH (0.1mL) was simultaneously introduced to this drug solution and these SBP samples were allowed to crosslink for 4 hours. In a second formulation, the drug-loaded SBP samples were allowed to gel for 2 hours prior to ECH being added and thereafter allowed to crosslink for 2 hours. In a third formulation, no ECH was added and the drug-loaded SBP samples were allowed to gel for 4 hours. In a fourth formulation, the control, the drug-loaded SBP samples were removed immediately after drug entrapment and were not subjected to further modification. In all circumstances, the solutions were maintained at 25±1°C, and stirred at 50rpm. The study was conducted in triplicate (n=3).

5.2.5.4.2.3. Elucidation of extent of drug entrapment

The extent of drug entrapment was determined as previously described in Chapter 4, Section 4.2.4.3 at λmax=214nm and utilizing the pre-constructed calibration curve in Chapter 4, Section 4.3.2. The study was conducted in triplicate (n=3).

5.2.5.4.2.4. Comparative in vitro captopril release behavior of the post drug entrapment modified SBPs

The drug release behaviors of each of the SBP formulations prepared were determined as previously described in Chapter 4, Section 4.2.5 and utilizing the pre-constructed calibration curve in Chapter 4, Section 4.3.2. The study was conducted in triplicate (n=3).

5.2.5.4.3. Determination of the effect of drug-loading on pre-modified SBP

5.2.5.4.3.1. Preparation of pre-modified SBP

Alkaline alcohol (40% EtOH: 5mL NaOH) was prepared as described in Table 5.4. SBP samples (3g) were accurately weighed and placed into the experimental apparatuses. Aliquots of the hydration medium (10mL) in conjunction with 0.1mL ECH were then added to the experimental apparatus and allowed to stir at 50rpm for 4 hours at a constant temperature of 25±1°C (Formulation 1). In a second formulation, the SBP samples were allowed to gel within the hydration medium for 2 hours prior to ECH being added and thereafter allowed to crosslink for 2 hours at 25±1°C under constant stirring at 50rpm (Formulation 2). In a third formulation, no ECH was added and the SBP samples were allowed to gel for 4 hours (Formulation 3). The SBP were then removed, lightly blotted with tissue paper to remove excess moisture and weighed in order to determine the hydration of the modified SBP samples. The SBP were then convection dried in a laboratory oven at 50°C. During the drying process, the SBP samples were physically separated using a flat-ended metal spatula and their texture analyzed. The dried modified SBP samples were then visually analyzed to determine their structural integrity and feasibility for drug entrapment studies.

5.2.5.4.3.2. Drug entrapment into pre-modified SBP

Alkaline alcohol (40% EtOH: 5mL NaOH) was prepared as depicted in Table 5.4. Drug solutions (75mg.mL^{-1}) were prepared by accurately weighing and dissolving 6.75g captopril in 20mL alkaline alcohol medium and then made up to 90mL using alkaline alcohol. A second drug solution was prepared in the similar manner with the only difference being the replacement of alkaline alcohol with deionized water. Aliquots of drug solution (10mL) were accurately measured and placed within experimental apparatuses. Once dry, samples (2g) of the modified SBP formulations prepared in Section 5.2.5.4.3.1 were accurately weighed, immersed in 10mL of a drug solution maintained at 25±1°C and stirred at 50rpm and allowed to entrap drug for 4 hours. The drug-loaded SBP samples were then removed, lightly blotted with tissue paper to remove excess moisture and weighed in order to determine the hydration potential of the modified SBP. The SBP were then convection dried in a laboratory oven maintained at 50°C and thereafter weighed.

5.2.5.4.3.3. Elucidation of extent of drug entrapment

The extent of drug entrapment was determined as previously described in Chapter 4, Section 4.2.4.3 at λmax=214nm and utilizing the pre-constructed calibration curve in Chapter 4, Section 4.3.2. The study was conducted in triplicate (n=3).

5.2.5.4.3.4. Comparative in vitro drug release behavior of pre-modified drug-loaded SBP formulations

The drug release behaviors of each of the modified SBP formulations prepared were determined as previously described in Chapter 4, Section 4.2.5 and utilizing the pre-constructed calibration curve in Chapter 4, Section 4.3.2. The study was conducted in triplicate (n=3).

5.2.5.5. Determination of the effect of oxidation and crosslinking on the performance of SBP

5.2.5.5.1. Preparation of pre-oxidized SBP

Oxidizing medium was prepared by dissolving 4.8g of sodium (meta)periodate in 45mL phthalate buffer pH4.6 (prepared as described in USP 33). Aliquots (10mL) of this oxidizing medium were placed separately into 4 experimental apparatuses. SBP samples (1.8g; 0.01M based on molecular mass of anhydrous glucose) were accurately weighed and submerged in the oxidizing medium within the experimental apparatuses. The SBP samples were allowed to oxidize under constant stirring at 50 rpm for 1.5 hours at a constant temperature of 25±1°C. Thereafter the oxidized SBP samples were removed from the oxidation medium, washed with 500mL deionized water to remove excess oxidizing agent, lightly blotted with tissue paper and subjected to drug entrapment.

5.2.5.5.2. Drug entrapment and crosslinking within the pre-oxidized SBP

Alkaline alcohol (40% EtOH: 5mL NaOH) was prepared as described in Table 5.4. Drug solutions (75mg.mL^{-1}) were prepared by accurately weighing and dissolving 750mg captopril in 30mL drug solution media as depicted in Table 5.7. Subsequent to their removal from the oxidation medium and washing, the oxidized SBP samples from Section 5.2.5.5.1 were immediately placed into 10mL drug solution, maintained at 25±1°C under constant stirring at 50rpm and allowed to hydrate and crosslink for the specified times depicted in Table 5.7.

Table 5.7: Conditions employed for the entrapment of drug into oxidized SBP

Formulation	Drug solution medium	[Captopril] ($mg.mL^{-1}$)	HT (Hours)	CT (Hours)	Total time (Hours)
1	Deionized water	75	4	0	4
2	Alkaline alcohol	75	4	0	4
3	Alkaline alcohol	75	0	4	4
4	Alkaline alcohol	75	2	2	4

Where [Captopril] denoted the concentration of captopril in the hydration medium, HT denoted Hydration Time and CT denoted Crosslinking time

5.2.5.5.3. Elucidation of extent of drug entrapment

The extent of drug entrapment was determined as previously described in Chapter 4, Section 4.2.4.3 at λmax=214nm and utilizing the pre-constructed calibration curve in Chapter 4, Section 4.3.2. The degree of change in mass during the drug entrapment procedure was calculated using Equation 2.2 while the extent of hydration of the SBP samples was calculated using Equation 2.1. The study was conducted in triplicate (n=3).

5.2.5.5.4. Comparative in vitro drug release behavior of pre-oxidized drug-loaded SBPs

The drug release behaviors of each of the pre-oxidized SBP formulations prepared were determined as previously described in Chapter 4, Section 4.2.5 with samples (5mL) withdrawn every 30 minutes over the first 2 hours and thereafter every hour over a 6 hour period and replenished with fresh buffer in order to maintain sink conditions. The study was conducted in triplicate (n=3).

5.3. Results and Discussion

5.3.1. Effect of gelatinization on the stability of the SBP

When submerged in 60% and 70% ethanol, hydration of the SBP was low and gelatinization was observed to be minimal (Table 5.8). Furthermore, the SBP retained their spherical structure, remained firm and did not disintegrate during the hydration process even with the addition of up to 10mL NaOH. Gelatinization during drying at 50°C was also minimal and the SBP were observed to be slightly sticky during the initial drying stages but were easy to separate from each other and the petri dish with minimal breakage and residue. The SBP formulations that exhibited this effect were confined to SBP exposed to higher NaOH concentrations (9-10mL NaOH). Thus, the protective effect of ethanol was most pronounced at the high ethanol concentration and overshadowed the gelatinization effect of NaOH.

When low volumes of NaOH (1mL-4mL) were added to 50% ethanol, the hydration and gelatinization behavior resembled that seen in 60% and 70% ethanol. A slight increase in gelatinization was observed when 5mL-6mL NaOH was added and this gelatinization was amplified during drying which caused the peripheries of the SBP to become sticky resulting in clumping. However, the SBP remained intact and were easy to separate after the initial stages of drying. Upon further addition of NaOH (up to 10mL), gelatinization increased and upon drying, the SBP began losing their structure and presented as translucent and jelly-like masses. Once dry, a gelled mass with glassy appearance was formed which was very difficult to remove from petri dish and thus had to be scraped off resulting in breakage of the SBP. Once removed, the SBP presented as glassy shavings and translucent glassy irregularly shaped spheres with very few intact SBP entrapped and minimal distinct separated SBP present.

In 40% ethanol, SBP exposed to 1mL-3mL NaOH and 4mL NaOH behaved similarly to SBP placed in 50% ethanol and exposed to 1mL-4mL NaOH and 5mL NaOH, respectively. Upon increasing NaOH to 5mL, the SBP displayed gelatinization within the hydration medium and the gelatinization increased with heat exposure during the initial stages of drying. However, the SBP clumps that formed during drying were easy to separate. Further increase in NaOH resulted in a gel mass forming within the hydration medium due to substantially increased gelatinization. Furthermore, there was an elevated viscosity of the hydration medium observed which was attributed to dissolution of the SBP within the hydration medium as the lower ethanol concentrations provided inadequate protective effects against NaOH induced gelatinization.

In 30% ethanol, the SBP behaved in a manner resembling that seen in 40% ethanol. However, a greater degree of swelling and subsequent gelatinization was observed. In addition, a decrease in structural stability of the SBP was noted and the peripheral gelling fronts in hydration medium were observed to penetrate deeper into the core of the SBP.

The hydration of the SBP increased as the quantity of NaOH increased. At lower ethanol: NaOH ratios, the SBP underwent gelatinization to a larger extent and become stickier in nature. In addition, the increase in the water: alcohol ratio of the hydration mediums increased the hydration of the SBP matrix and thus facilitated the action of NaOH to a larger extent and ultimately lead to clumping of the SBP. When the hydrated SBP were subjected to heat during the drying process, further gelatinization was observed resulting in attachment of SBP particles to adjacent SBP particles and the surface of the petri dish in which drying occurred. As a consequence, loss of gelatinized portions of the SBP occurred. After the initial drying phase, the tendency of the SBP to stick to each other decreased. A possible explanation for the increased gelatinization and sticking observed in the initial stages of drying was the faster evaporation rate of the highly volatile ethanol thus diminishing the protective effect conferred by the ethanol. The SBP formulations that underwent substantial hydration and those that underwent substantial gelatinization became fragile and unstable and were thus not viable for drug entrapment studies. The most advantageous combination for controlled gelatinization was found to be the ration 40% ethanol: 5mL NaOH.

Table 5.8: Effect of controlled gelatinization

Alcohol (%)	NaOH (mL)	DOS (%)	Std dev (%)	DCM (%)	Std dev (%)
70	1.000	38.066	3.148	-4.047	2.073
70	2.000	44.805	3.271	0.715	0.300
70	3.000	40.273	2.200	2.215	2.288
70	4.000	51.864	3.725	3.762	0.581
70	5.000	58.012	2.094	6.435	0.851
70	6.000	71.162	11.553	12.773	5.112
70	7.000	58.706	3.128	16.678	0.911
70	8.000	60.419	3.689	19.558	1.919
70	9.000	66.045	0.703	27.467	1.183
70	10.000	53.645	1.479	27.021	5.517
60	1.000	40.175	2.946	2.730	0.547
60	2.000	37.960	2.358	4.513	1.181
60	3.000	45.021	22.168	3.492	2.661
60	4.000	45.473	5.807	4.539	0.361
60	5.000	48.869	2.995	5.030	2.321
60	6.000	66.642	8.034	14.326	1.540
60	7.000	75.185	5.428	7.090	1.519
60	8.000	80.861	1.171	1.827	2.328
60	9.000	91.183	3.536	2.974	0.824
60	10.000	99.001	29.325	4.458	0.805
50	1.000	46.728	1.903	1.099	0.409
50	2.000	52.080	3.816	1.631	0.464
50	3.000	56.288	1.489	1.914	1.485
50	4.000	58.479	4.158	3.977	0.625
50	5.000	66.638	5.806	7.424	1.826
50	6.000	88.075	4.191	12.111	0.563
50	7.000	106.522	4.776	17.363	0.516
50	8.000	121.339	7.246	20.945	0.610
50	9.000	116.806	16.511	22.858	3.482
50	10.000	164.634	11.271	28.968	1.051
40	1.000	65.694	4.213	1.581	1.085
40	2.000	69.015	4.430	2.962	0.427
40	3.000	81.432	10.355	2.876	2.506
40	4.000	114.535	2.495	8.298	0.903
40	5.000	162.698	23.351	16.729	2.685
40	6.000	254.094	42.037	17.829	1.454
40	7.000	456.870	65.268	-3.911	7.717
40	8.000	528.640	19.591	-7.490	1.419
40	9.000	481.522	38.394	-17.778	8.111
40	10.000	504.156	19.419	-11.604	3.131
30	1.000	106.720	8.756	-0.183	0.464
30	2.000	154.185	22.281	-0.033	0.850
30	3.000	274.669	12.773	0.399	2.223
30	4.000	384.311	12.502	-8.347	2.284
30	5.000	578.211	12.124	-6.738	2.253
30	6.000	811.643	44.022	-23.032	10.786
30	7.000	770.439	41.572	-12.280	3.452
30	8.000	757.735	9.281	-8.080	1.404
30	9.000	715.495	38.816	-10.962	1.824
30	10.000	713.024	12.223	-8.969	2.783

Where NaOH denoted sodium hydroxide solution (1M), DOS denoted Degree of Swelling, Std Dev denoted the standard deviations and DCM denoted the Degree of Change in Mass (n=3 in all instances)

5.3.2. Effect of crosslinking using polyvalent cationic salts

5.3.2.1. Effect of crosslinking using polyvalent cationic salts on the drug entrapment of the SBP

Figure 5.8 showed that crosslinking utilizing polyvalent cationic salts resulted in a slight decrease in the Drug Entrapment Efficiency (DEE) of captopril compared to unmodified drug entrapment, except in the cases of barium sulphate and tin chloride where an increase in the DEE was observed. Furthermore, there was no trend observed with regard to either the cationic or the anionic component of the salts used. However, a clear distinction was seen when comparing the *in vitro* drug release profiles within Simulated Intestinal Fluid (SIF) Simulated Gastric Fluid (SGF) (Figure 5.9). In SIF, the salt-crosslinked SBP showed a complete burst release within the first hour for all the formulations regardless of the anionic or cationic species contained within the salt. However, in SGF, the crosslinked SBP showed an enhancement in controlling drug release. This observation could be due to increased gelatinization and solubilization of the crosslinked SBP at the higher pH of SIF resulting in increased exposure and subsequent dissolution of drug within SIF.

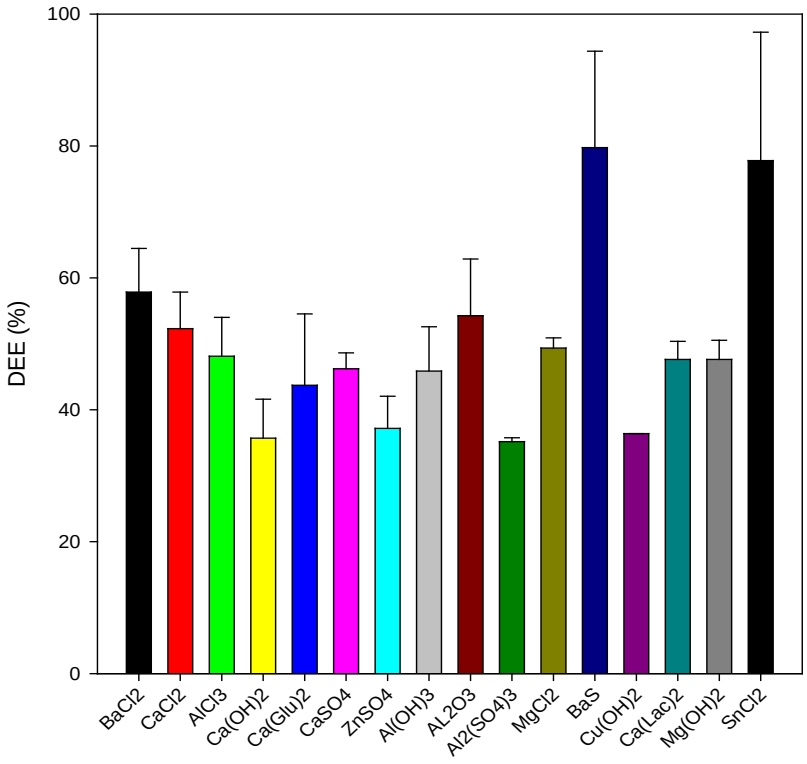
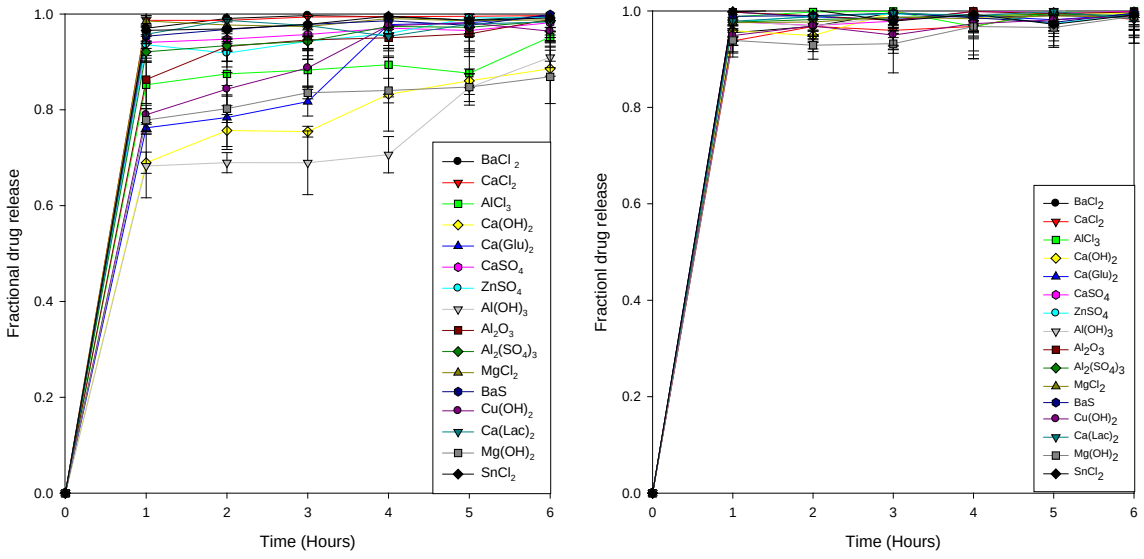


Figure 5.8: Drug entrapment efficiency of salt crosslinked SBP (n=3 in all instances)**.**

5.3.2.2. Effect of crosslinking using polyvalent cationic salts on the in vitro drug release behavior of the SBP

When elucidating the effect of the particular salts on the *in vitro* drug release behavior of the crosslinked SBP in SGF, it was observed that SBP which were crosslinked using salts containing a hydroxide as the anionic species displayed the ability to retard drug release to a much greater extent than other salts. A possible explanation of this observation was the alkalinization of the hydration medium due to the presence of hydroxide ions which caused increased gelatinization on starch SBP. This facilitated increased penetration of drug containing medium and simultaneous entrapment of drug within the gelatinized network through crosslinking. With regard to the cationic species, aluminium was observed to retard *in vitro* drug release to the greatest extent. This phenomenon could be attributed to its trivalent nature, which allowed more complex crosslinking of the drug-loaded SBP structure resulting in impeded penetration of dissolution medium within the SBP thus decreasing the release of drug from the SBP. Thus, it was observed that aluminium hydroxide, although having a moderate drug-loading potential, portrayed the most favorable drug release profile in SGF. However, further modifications or employment of other crosslinking agents may be necessary to retard drug release adequately in both SIF and SGF.



(a) (b)

Figure 5.9: Drug release profiles of salt-crosslinked SBP in (a) SGF and (b) SIF (n=3 in all instances).

5.3.3. Effect of crosslinking using ECH, Glut and STMP

5.3.3.1. Effect of crosslinking on the hydration and drug entrapment of the SBP

The Degree of swelling (DOS) and entrapment observed in unmodified SBP were very similar to values observed during the drug entrapment study in Chapter 4, Section 4.3.3, thus affirming the reproducibility of the drug entrapment method used for the study. With regard to the crosslinked SBP, Glut-crosslinking displayed a negative effect on the drug entrapment process as evident by the much lower DOS and drug entrapment when compared to unmodified SBP (Table 5.9). In contrast, ECH-crosslinking displayed an appreciable improvement in the drug entrapment process resulting in higher DEE values despite displaying a lower hydration capacity compared to the unmodified SBP. A possible explanation for the observed hydration effect could be the relative covalent crosslinking strength of the crosslinkers used with Glut being a much stronger crosslinker than ECH.

Therefore, the inhibition of hydration and subsequent drug entrapment experienced with Glut could be attributed to very strong intramolecular and intermolecular crosslinking of the SBP preventing adequate imbibition of hydration medium within the SBP. This effect was much less pronounced with ECH leading to improved stability while facilitating enhanced penetration of hydration medium into the SBP. The higher drug entrapment of ECH-crosslinked SBP compared to Glut-crosslinked SBP was a direct consequence of the hydration capacities of these SBP. However, the increase in drug entrapment values of ECH-crosslinked SBP compared to unmodified SBP could be attributed to interactions between the drug, ECH and the SBP facilitating enhanced incorporation of drug into the SBP.

Table 5.9: Effect of crosslinking of SBP on the hydration and drug entrapment

SBP	DOS (%)	Placebo DOS (%)	QDE (mg)	DEE (%)
ECH-crosslinked	195.356	183.466	530.760	70.768
Glut-crosslinked	153.039	128.536	206.67	27.556
STMP-crosslinked	249.412	234.705	417.443	55.659
Unmodified	218.608	197.255	436.845	58.246

Where SBP denoted Starch-Based Platform, DOS denoted the Degree of Swelling, QDE denoted the Quantity of Drug Entrapped and DEE denoted the Drug Entrapment Efficiency. (n=3 in all instances and Standard deviations were: DOS≤12.476%, Placebo DOS≤18.487%, QDE≤24.112mg, DEE≤3.596%)

Analysis of the effect STMP-crosslinking showed an increase in hydration potential with minimal effect on drug entrapment of the SBP (Table 5.9). The increase in hydration could be attributed to the increased stability imparted by STMP-crosslinking, which allowed the SBP to swell to a greater degree but STMP-drug-SBP interactions were not as prominent as seen with ECH-crosslinking leading to the lower observed DEE. A further observation was the greater DOS of drug-loaded SBP in comparison to their respective placebos. This may be a result of drug molecules penetrating the core of the SBP and disrupting intramolecular bonds within the SBP thus creating more space within the SBP for hydration medium to enter.

5.3.3.2. Effect of crosslinking on the in vitro drug release behavior of the SBP

Figure 5.10 illustrated that the various crosslinking methods applied to the SBP resulted in differing degrees of enhancement in the *in vitro* drug release behavior. The most outstanding feature was the improvement in control of the burst effect that was displayed by the unmodified SBP. This reduction was seen in both SIF and SGF although it was more pronounced in SGF and could be a direct result of the lower pH of SGF. Comparison of the effect of different crosslinking agents showed that drug release displayed similar profiles with none of the crosslinking agents employed demonstrating the ability to control drug release for a prolonged period. Covalent crosslinking showed superiority to ionic crosslinking as *in vitro* drug release from STMP-crosslinked SBP was complete within 4 hours in SGF and within 2 hours in SIF. Comparison between the covalent crosslinking agents demonstrated that Glut displayed slightly better control of drug release than ECH and retained a higher fraction of drug within the SBP after 12 hours in both SIF and SGF. The ability of Glut and ECH to completely impede the release of a fraction of drug could be due to the very strong crosslinking and incorporation of captopril within the core of the SBP.

Crosslinking improved the drug release behavior of the SBP but none of the crosslinking agents showed clear superiority in this aspect as could be seen by the similar drug release profiles that were obtained. STMP displayed the most inferior control of drug release and had an inconsequential effect on drug entrapment compared to the covalent crosslinking agents. The superior drug entrapment results, milder formulation conditions employed as well as the novelty in utilizing alkaline alcohol as both a crosslinking medium and a controlled gelatinization medium with the use of ECH offered obvious advantages over the use of Glut and thus ECH was chosen as the crosslinker to be employed in further studies.

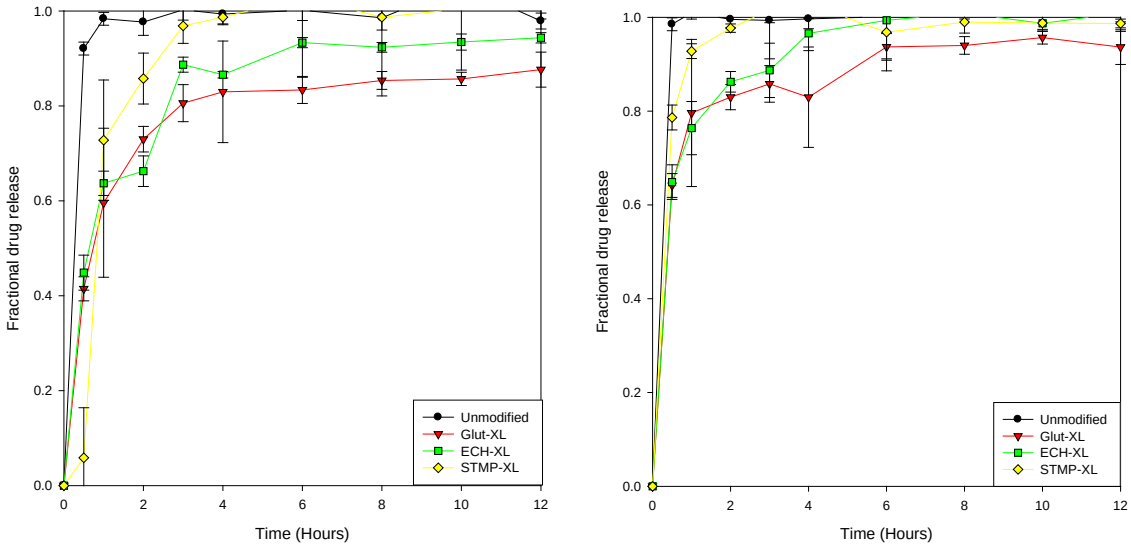


Figure 5.10: Comparative drug release profiles of crosslinked SBP in (a) SGF and (b) SIF (n=3 in all instances).

5.3.4. Effect of covalent ECH-crosslinking on the performance of the SBP

5.3.4.1. Effect of ECH concentration on the hydration of the SBP

Figure 5.11 showed that the addition of ECH decreased the DOS of the SBP. The extent of this decrease was not related to the quantity of ECH used as a 1% solution had comparable reduction in hydration to a 10% solution. ECH requires an alkaline medium in order crosslink starch and thus the use of NaOH served a dual role in establishing both an alkaline gelatinization medium as well as a suitable medium for ECH crosslinking to occur. The effect of the ECH in decreasing the DOS was due to increasing the structural integrity of the SBP by forming a more rigid crosslinked structure. Thus, water is not able to enter the freely between crosslinked areas of the SBP leading to decreased NaOH facilitated gelatinization. However, at higher NaOH concentrations, the effect of ECH was not able to prevail over the effect of NaOH leading to higher DOS and increased gelatinization. It was observed during the study that time within the hydration medium as well as within the crosslinking medium had an effect on the structural integrity of the SBP.

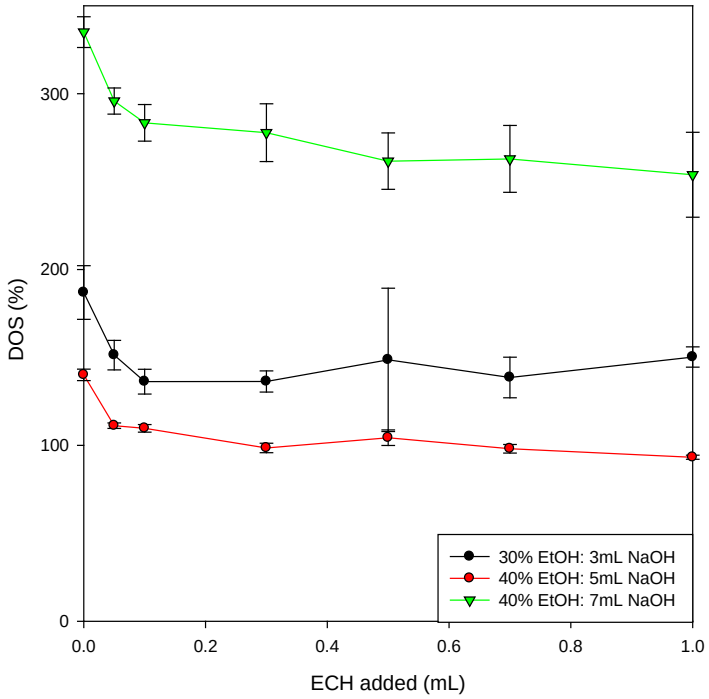


Figure 5.11: Effect of ECH concentration on the hydration potential of SBP (n=3 in all instances).

5.3.4.2. Effect of hydration time and crosslinking time on the hydration of the SBP

Table 5.10 demonstrated that hydration time and crosslinking time and the hydration medium affected the DOS of the SBP. The DOS was directly proportional to the hydration time and inversely proportional to the crosslinking time. This trend was evident at each of the alkaline alcohol: NaOH ratios employed and held true for SBP that was subjected to crosslinking subsequent to a degree of pre-hydration. The addition of ECH and the decrease in hydration time resulted in the SBP displaying an increased stability both during hydration and upon drying. Small SBP aggregates did form during drying process but were easily separated once dry with minimal structural breakdown. Although demonstrating greater hydration in both 30% EtOH: 3mL NaOH and 40% EtOH: 7mL NaOH hydration mediums, the structural stability of the SBP subjected to these hydration media were inferior to that displayed by SBP modified in 40% EtOH: 5mL NaOH solution. With regard to modification times, 2 hours of hydration followed by 2 hours of ECH crosslinking proved to produce the greatest SBP hydration and thus SBP samples modified according to these time parameters in 40% EtOH: 5mL NaOH was adjudged to result in SBPs displaying most beneficial functional and structural modifications.

Table 5.10: Effect of hydration time and crosslinking time on the hydration of the SBP

HT (Hours)	CT (Hours)	30% EtOH: 3mL NaOH		40% EtOH: 5mL NaOH		40% EtOH: 7mL NaOH	
		DOS (%)	Std Dev (%)	DOS (%)	Std Dev (%)	DOS (%)	Std Dev (%)
4	0	274.669	12.773	162.698	23.351	250.402	26.333
2	0	136.148	6.500	90.470	4.248	220.218	4.328
1	0	117.218	3.117	83.628	2.800	184.019	1.601
0.5	0	101.116	3.559	67.560	0.519	162.374	5.886
0	2	92.688	1.266	76.440	2.062	103.896	3.645
0	1	100.981	4.046	86.556	6.098	109.272	1.482
2	2	120.218	5.870	97.499	3.060	155.716	5.191
1	2	115.754	2.789	80.960	0.959	143.770	4.082
0.5	2	106.163	1.661	74.247	1.381	135.632	1.986
1	1	132.026	1.209	87.659	1.058	165.555	4.859
0.5	1	95.282	13.689	80.385	1.905	139.706	7.290

Where HT denoted Hydration Time, CT denoted Crosslinking Time, DOS denoted Degree of Swelling and Std Dev denoted the Standard Deviation (n=3 in all instances)

5.3.4.3. Effect of hydration time and crosslinking time on the functional characteristics of SBP employing DPH as the model drug

5.3.4.3.1. Effect of hydration time and crosslinking time on the DPH entrapment

Figure 5.12 showed that there was a close correlation between the hydration and the extent of drug entrapment in Formulations 1, 2, 4 and 6. When exposed to identical formulation compositions and crosslinking times, increasing the hydration time resulted in greater DOS and Quantity of Drug Entrapped (QDE) as is evident when compared Formulations 1 and 2. When the alcohol content of the hydration medium was decreased (while maintaining identical hydration and crosslinking times), the hydration and gelatinization of the SBP increased resulting in enhanced drug entrapment. This was clearly observed when comparison of Formulations 4 and 2 were made. When comparing Formulations 4 and 5, it was deduced that crosslinking reversed the hydration of the SBP as the DOS of Formulation 5 far surpassed that of Formulation 4 with the only difference between the formulations being the introduction of crosslinking in Formulation 4.

Formulations 3 and 5 displayed deviance from the trend seen in the other formulations, as the drug entrapment was much lower than the hydration would suggest. With regard to Formulation 3, the DOS was higher than Formulations 1, 2 and 4, which could be attributed to higher NaOH content (7mL), but exhibited the lowest drug entrapment of all the formulations in the study. It was postulated that the high pH induced by the additional NaOH resulted in DPH instability. Regarding Formulation 5, the hydration was the highest observed in the study, as the SBP was allowed to gelatinize without being retarded by

crosslinking and was thus expected to exhibit the greatest drug entrapment. However, this was not realized and the drug entrapment was only slightly greater than that observed in Formulation 4 which was crosslinked.

During analysis of Formulation 6 (control) and subsequent comparison to the other formulations in the study, it was found that a sizeable decrease in drug entrapment occurred in the presence of crosslinking medium. A possible explanation could be due to the resultant increase in structural rigidity of the crosslinked-SBP which inhibited the entrance of the drug containing hydration medium and which ultimately resulted in decreased drug entrapment. However, Formulation 5, which exhibited hydration capacity exceeding that observed in Formulation 6, displayed substantially inferior drug entrapment results. Thus, it was concluded that the drug was unstable in the gelatinization and crosslinking media and this instability was the cause of the low drug entrapment of the SBP modified at the higher pH of the modification mediums.

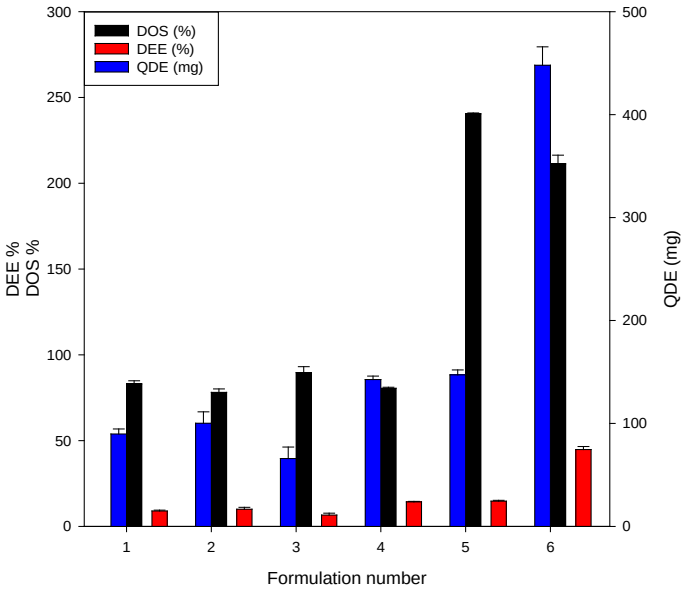


Figure 5.12: Correlation between hydration capacity and DPH entrapment of modified SBP (n=3 in all instances).

5.3.4.3.2. Drug release behavior of DPH from modified SBP

Figure 5.13 the drug release behavior of DPH from the modified and unmodified SBP. In both SIF and SGF, the control (Formulation 6) displayed a complete burst release within the first half hour within the dissolution media. The gelled SBP (Formulation 5) retarded drug release to a small extent by reducing the burst release but was not able to control the rate of drug release for a prolonged time as complete dissolution of the entrapped drug occurred within 1 hour in SGF and within 2 hours in SIF.

Crosslinking further reduced the burst effect and was able to control the release of drug for a longer time with all of the ECH-crosslinked SBP formulations displaying similar drug release profiles. However, Formulations 1 and 2 (crosslinked in hydration medium containing 40% ethanol:5mL NaOH) showed the greatest ability to control the release behavior with Formulation 1 retarding drug release for up to 4 hours in both dissolution media and Formulation 2 retarding drug release for up to 5 hours in SIF and for more than 6 hours in SGF. Upon comparison between the two dissolution media, more controlled drug release profiles were achieved in SGF and this could be due to the lower pH of this medium which penetrated more slowly into the SBP than SIF, which had a higher pH value. Thus, based on these drug release studies, crosslinking had a beneficial effect on the control of drug release and crosslinking in hydration medium containing 40% ethanol: 5mL NaOH provided the greatest control of drug release.

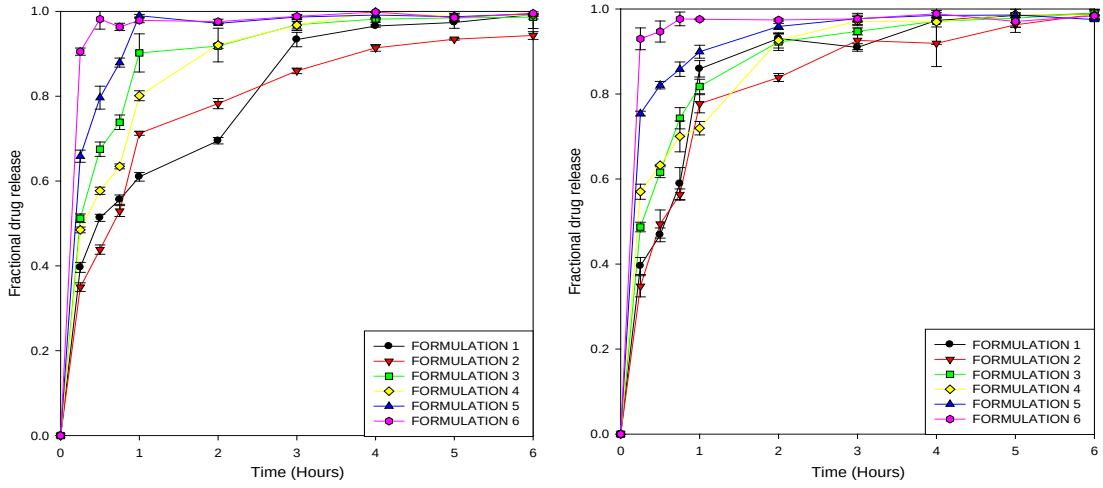


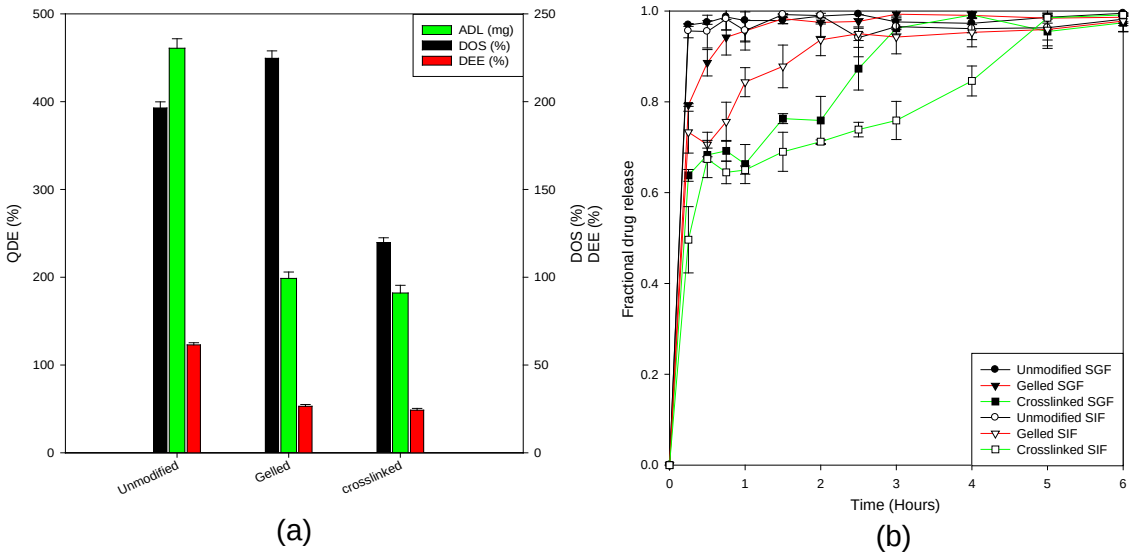
Figure 5.13: Comparative drug release of DPH from modified SBP in (a) SGF and (b) SIF (n=3 in all instances).

5.3.4.4. Effect of hydration time and crosslinking time on the functional characteristics of SBP employing captopril as the model drug

5.3.4.4.1. Effect of concurrent gelatinization and ECH-crosslinking on the functional characteristics of the SBP

Figure 5.14 illustrated that the drug entrapment of captopril within the SBP correlated with the DOS within the hydration medium. This observation was analogous to that of DPH where DOS affected the DEE of the SBP. Therefore the QDE was in the order of unmodified > gelled > Crosslinked. Furthermore, the large decrease in QDE and DEE of captopril, comparable to that observed with DPH, when exposed to the gelatinization medium further alluded to instability of captopril within the hydration medium.

The drug release profiles displayed similarities to those seen with DPH where control of drug release followed the order crosslinked > gelled > unmodified. However, in contrast to DPH, captopril release from the SBP was more controlled at the higher pH of SIF. Therefore, although modification reduced QDE within the SBP, the modifications resulted in more favorable SBPs to be employed as a MODDS. However, the issue with drug instability in the medium required for SBP modification need to be overcome.



(a) (b)

Figure 5.14: Effect of concurrent drug-loading and crosslinking of SBP on (a) the drug entrapment and (b) the *in vitro* drug release behavior of captopril (n=3 in all instances).

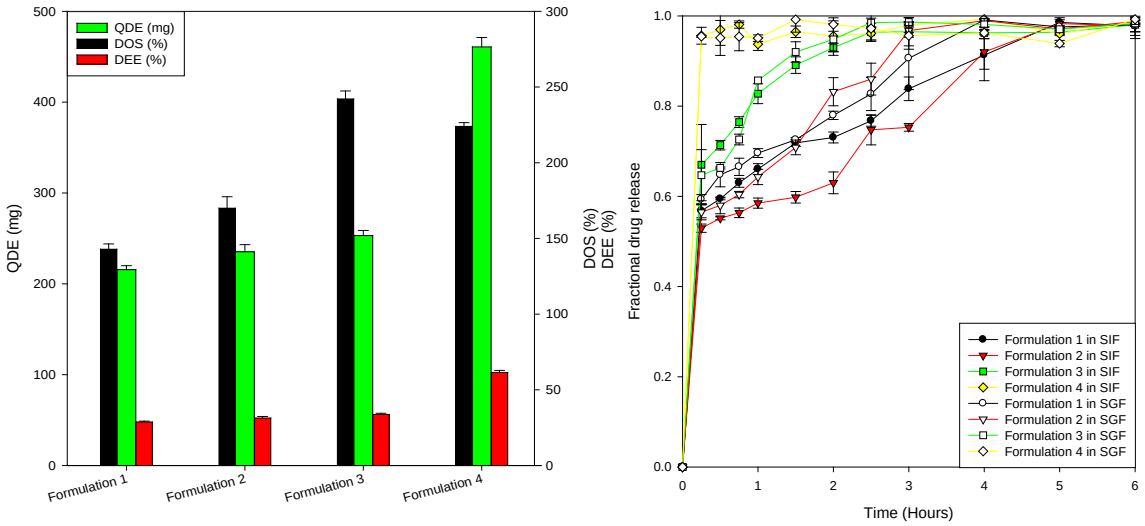
5.3.4.4.2. Effect of step-wise drug-loading, gelatinization and crosslinking on the functional characteristics of the SBP

Figure 5.15 illustrated that drug-loading of SBP prior to gelatinization and crosslinking increased the QDE by an average of 35mg, which translated into an average DEE increase of 20% when compared to concurrent drug-loading and crosslinking. However, there was no substantial improvement in the drug release profiles in both SGF and SIF when compared to the study described in Section 5.3.4.4.1.

When comparing the individual formulations in Figure 5.15, it was observed that crosslinking decreased the QDE within the SBP but retarded drug release to a greater extent than gelled SBP. The formulation which underwent separate hydration, gelatinization and crosslinking steps displayed intermediate drug entrapment but demonstrated the most promising drug release behavior. A possible explanation for this observation could be that during the initial gelatinization stage, captopril was incorporated within the SBP and became entrapped within the crosslinked network during the subsequent crosslinking stage. The SBP that were crosslinked from the beginning of the

study experienced a greatly reduced initial gelatinization phase and could account for both its lower drug entrapment as well as inferior drug release profile. In the case of basic gelatinized SBP, the trapping of drug within the SBP imparted by the crosslinker was absent and accounted for its inferior drug release behavior.

When compared to unmodified SBP, there was a substantial decrease (~50%) in the drug entrapment results. In all of the modified SBP formulations, although there was an improvement when compared to concurrent drug-loading and modification, the methods described in this section of the study does not adequately overcome the issue concerning drug instability.



(a) (b)

Figure 5.15: Effect of initial drug-loading followed by gelatinization and subsequent crosslinking of SBP on (a) the drug entrapment and (b) the drug release behavior of captopril (n=3 in all instances).

5.3.4.4.3. Effect of pre-modification on the functional characteristics of SBP

Figure 5.16 displayed that pre-modification of SBP prior to drug entrapment increased in their captopril entrapment potential. When placed into drug solution containing only deionized water, the QDE was greater than when placed in alkaline alcohol. This was in spite of the greater hydration experienced when placed in alkaline alcohol and was comparable to previous studies conducted with captopril and DPH in alkaline alcohol solution. The results obtained indicated that possible drug degradation in the alkaline alcohol medium was taking place during drug-loading. Crosslinking further decreased the QDE with crosslinking time displaying an inversely proportional relationship with DEE. This could be due to increased resistance to hydration and the reduction of pore volume and size within the SBP as a result of ECH-facilitated bond contraction, improvement in

SBP rigidity and thus provided an impediment to the entrance of drug solution into the SBP. Therefore, the highest drug entrapment was observed in gelatinized SBP without crosslinking followed by SBP crosslinked for 2 hours and lastly by SBP crosslinked for 4 hours.

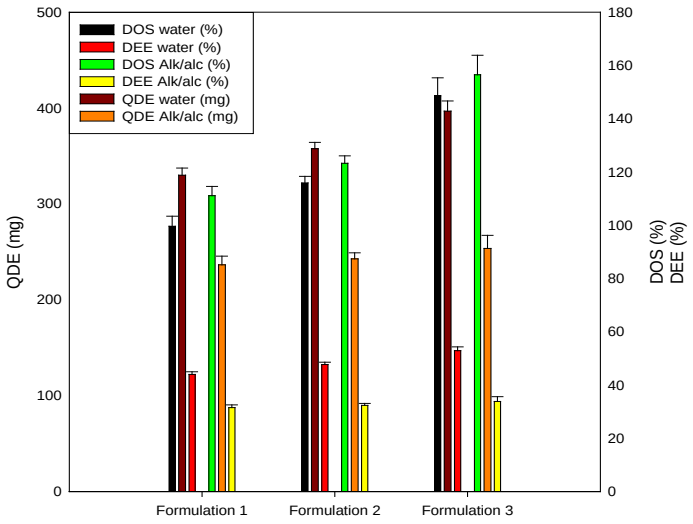


Figure 5.16: Effect of pre-modification of SBP on drug entrapment in different drug solution media (n=3 in all instances).

Drug release studies showed that the modified SBP samples which were drug-loaded in deionized water did not control the release of captopril to an acceptable extent but displayed superior drug release behavior than unmodified drug-loaded SBP (Figure 5.14b) and similar behavior to concurrently gelatinized and drug-loaded SBP (Figure 5.14b). However, concurrently crosslinked and drug loaded SBP (Figure 5.14b) as well as crosslinking of pre-drug-loaded SBP (Figure 5.15b) provided superior control of drug release.

On the other hand, comparison between Figure 5.17a and Figure 5.17b showed that SBP drug-loaded in alkaline alcohol offered better drug release characteristics than their water counterparts. This was true for all three of the modifications investigated. Furthermore, when compared to previous studies conducted, pre-modified SBP drug-loaded in alkaline alcohol demonstrated superior drug release profiles than concurrently modified and drug-loaded SBP (Figure 5.14b) and similar drug release profiles to pre-drug-loaded modified SBP (Figure 5.15b). However, pre-modified SBP drug-loaded in alkaline alcohol portrayed a slightly enhanced profile as it was able to control the release for a longer period of time.

Upon examining and comparing the individual profiles in Figure 5.17, it was found that the most excellent release behavior was obtained from SBP that were allowed to gelatinize before crosslinking followed by entirely crosslinked SBP and lastly by basic gelatinized SBP. This trend was observed in both SBP drug-loaded in alkaline alcohol as well as SBP drug-loaded in deionized water and in both simulated dissolution media.

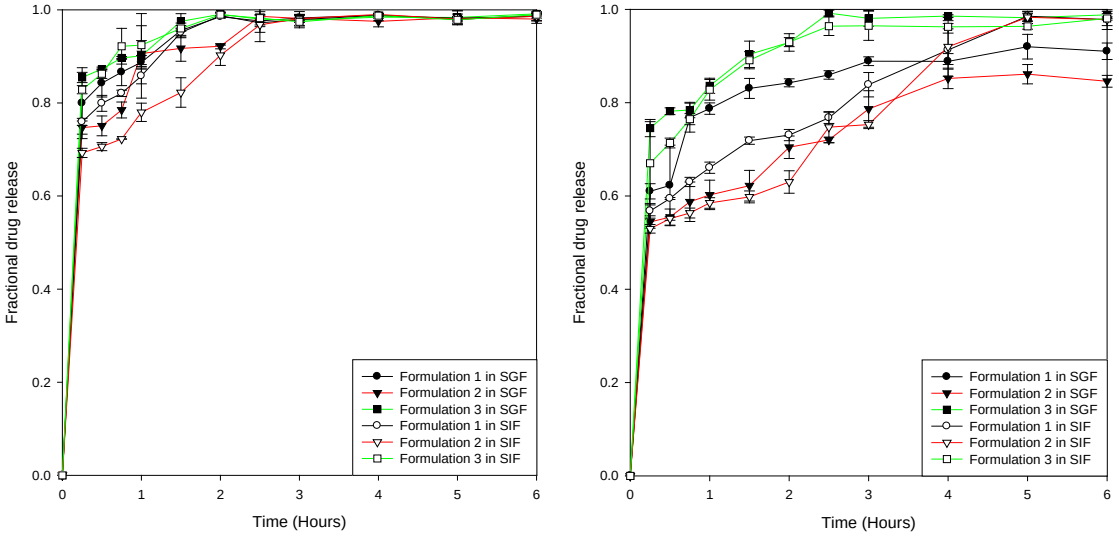


Figure 5.17: Effect of pre-modification on drug release behavior of SBP drug-loaded in (a) water-drug solution and (b) alkaline alcohol drug solution (n=3 in all instances).

5.3.5. Effect of periodate oxidation on the functional characteristics of SBP employing captopril as the model drug

During oxidation, the SBP showed no signs of modification when compared to simple hydration and their structure remained intact. However, immediately upon submerging the oxidized SBP into drug solution composed of captopril and water, the SBP began to develop a black color, which was observed in each of the four drug solutions. However, after some time, the color of the SBP placed within alkaline alcohol reverted to white while the formulation which was placed in water remained black, suggesting some sort of interaction with the alkaline alcohol drug medium.

In contrast, when the oxidized SBP were placed into the drug free alkaline alcohol media, the media displayed a color change from clear to orange and a gradual decrease in the size of the SBP were noted. With regard to the formulation placed in drug free water, no color change, either to black or orange, was observed and no major size reduction of the SBP was detected. The blackening of the SBP in drug solution and absence of this blackening in drug free solutions suggested that the residual oxidant within the SBP

caused oxidation of the captopril. The color reversal observed in alkaline alcohol could be attributed to a decrease in oxidation of the drug as the periodate exerted its action optimally at pH ranging between 3 and 5. Therefore, the SBP placed in water drug solution did not revert to white over time. The lack of color change of the SBP exposed to drug free water confirmed the deleterious effect of oxidation on the drug and thus the low DEE of these SBPs.

With regard to the loss of particle mass, oxidation resulted in ring opening of the composite glucose molecules and thus allowed an increase in NaOH facilitated gelatinization and solubilization of the SBP. This increased gelatinization allowed for a greater hydration potential as seen in Figure 5.18. Oxidation imparted a greater hygroscopic nature on the SBP as was observed from their increased DOS. When analyzing Figure 5.19, an interesting observation was noted where SBP samples that were placed within drug solution displayed positive DOS and a mass gain in contrast to the negative DOS and mass loss experienced by their respective placebos. This could be attributed to interactions between captopril and SBP, which fortified the SBP structure and increased their resistance to breakdown. The water placebo showed a positive DOS and this was due to the absence of NaOH induced gelatinization and solubilization. This mass gain was proportional to the drug entrapment capacity of the SBP.

Pre-oxidation of SBP was observed to produce a four-fold decrease in the drug entrapment capacity of the SBP when compared to unmodified SBP (Figure 5.14). When compared to crosslinked SBP, pre-oxidized SBP displayed an inferior entrapment potential than their regular counterparts with all formulations entrapping less than 200mg of captopril. Gelatinization of pre-oxidized SBP (Formulation 2) resulted in greater hydration than non-gelatinized SBP (Formulation 1) but did not provide any enhancement in drug entrapment. This could be due to solubilization of the SBP and decreased structural stability, which impeded drug entrapment. Pre-oxidized SBP that were exposed to crosslinking solution for the entire drug entrapment time (Formulation 3) displayed the highest entrapment efficiency. This could be due to fortification effect of the crosslinker from the onset of gelatinization and reduction of solubilization of oxidized bonds within the SBP. This, coupled with the SBP-drug-ECH interactions, allowed more captopril to be entrapped within the pre-oxidized SBP. Partially crosslinked (Formulation 4) displayed slightly lower drug entrapment capacity than entirely crosslinked SBP and this could be due to reduced stabilization of gelatinized SBP.

In addition, the fraction of drug that underwent oxidation during drug-loading could have absorbed at the same wavelength as the active drug leading to higher QDE and DEE values than were actually achieved. Thus, although crosslinking improved the stability of pre-oxidized SBP, oxidation itself was incompatible with the drug employed and decreased the entrapment efficiency of the SBP.

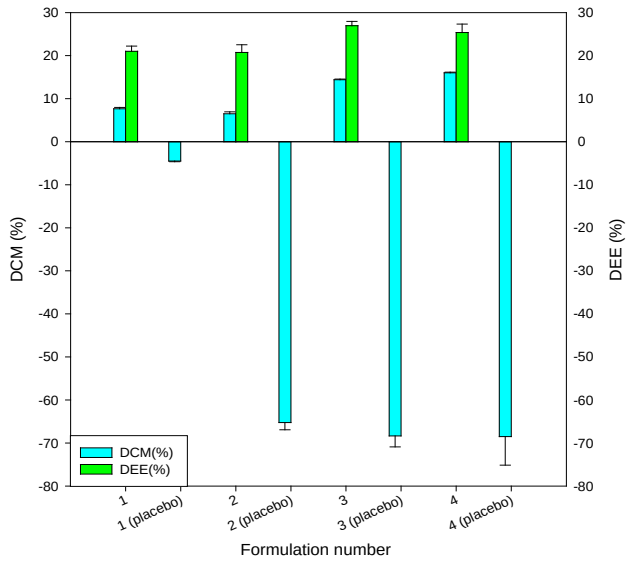


Figure 5.18: Effect of oxidation and subsequent cross inking on the structural integrity and drug entrapment efficiency of the SBP (n=3 in all instances).

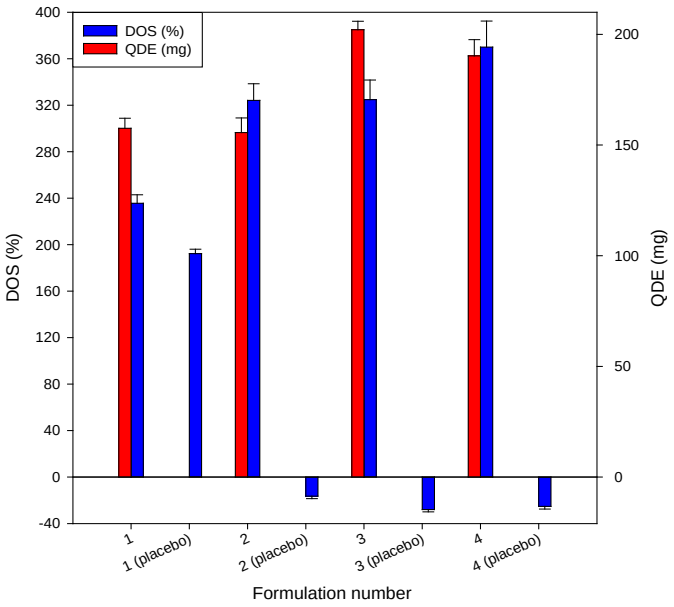


Figure 5.19: Effect of oxidation and subsequent crosslinking on the hydration capacity and drug-loading potential of the SBP (n=3 in all instances).

When analyzing the individual profiles in Figure 5.20, it was noted that further modification of pre-oxidized SBP enhanced the drug release behavior, with the purely oxidized SBP (Formulation 1) displaying the least control, followed by gelatinized SBP, then partially crosslinked SBP and lastly entirely crosslinked SBP. Thus, covalent crosslinking imparted favorable drug release characteristics on the SBP and the degree of crosslinking displayed a directly proportional relationship with the control of captopril release. This trend could be explained by the interactions between the drug, crosslinker and SBP during drug entrapment, which caused robust bonds between the molecules of the SBP and between drug and molecules of the SBP.

When comparing the effect of dissolution media, similar trends in drug release behavior from the pre-oxidized SBP were noticed (Figure 5.20a and Figure 5.20b). However, slightly superior control of captopril release was seen in SGF, where the burst effect was reduced and a more linear subsequent release profile was generated in comparison to drug release in SIF. This could be due to more inhibited entry of the lower pH SGF compared to the higher pH SIF. Nevertheless further modified pre-oxidized SBP, although providing more controlled drug release compared to unmodified SBP, provided inferior control of drug release than non-oxidized crosslinked SBP. These results, along with the residual oxidation of captopril during drug entrapment, proved to be a major preclusion from its use in developing the MODDS.

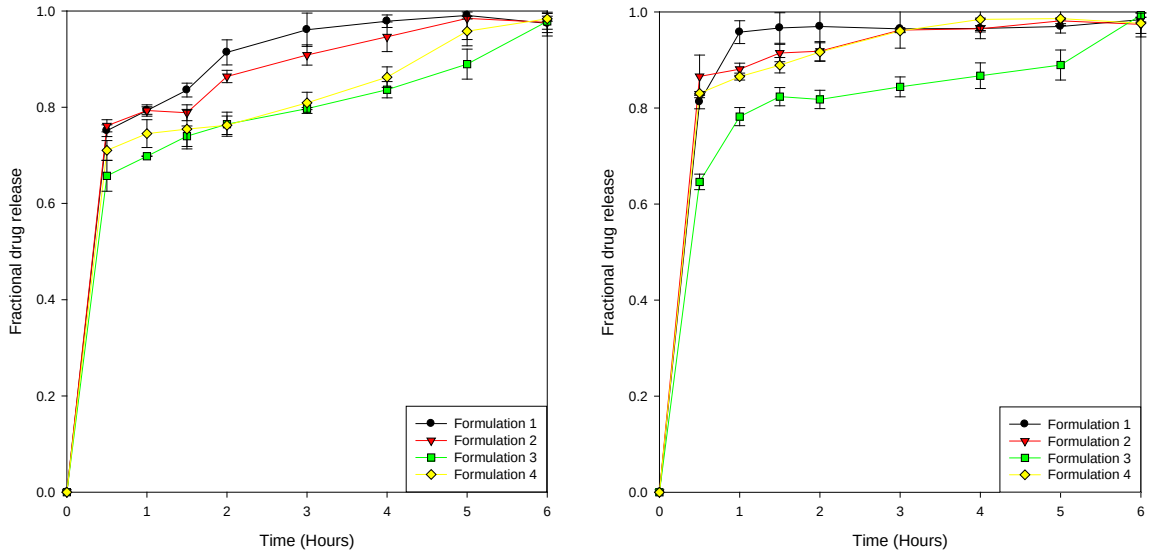


Figure 5.20: Effect of oxidation and subsequent crosslinking of the SBP on the drug release behavior of captopril in (a) SGF and (b) SIF (n=3 in all instances).

5.4. Concluding Remarks

Alcohol had protective and controlling effect on gelatinization of the SBP. NaOH induced gelatinization increased upon heating due to evaporation of ethanol as well as the combined effects of alkali and heat induced gelatinization. The most advantageous combination for controlled gelatinization was found to be using a ration of 40% ethanol: 5mL NaOH. Higher concentration of NaOH at low alcohol levels caused excess gelatinization and undesirable solubilization of the SBP. Use of cationic salts produced an encouraging impact on drug entrapment but conferred minimal effect in controlling the *in vitro* drug release behavior.

The crosslinking effects of Glut proved to be too strong and caused excess crosslinking, which resulted in decreased drug entrapment. Covalent crosslinking improved the drug release behavior of the SBP but neither Glut nor ECH showed superiority in this aspect as was observed by the similar drug release profiles which were obtained from these formulations. ECH offered milder formulation conditions as well as the novelty in utilizing alkaline alcohol as both a crosslinking medium and a controlled gelling medium and resulted in superior drug entrapment results.

The addition of ECH affected the hydration but the actual concentration of ECH within the hydration medium had minimal effect on the hydration capacity of the SBP. The DOS was directly proportional to the hydration time and inversely proportional to the crosslinking time with controlled gelatinization and ECH-crosslinking imparting greater structural stability on the SBP.

Crosslinking of SBP during entrapment of DPH resulted in a drastic reduction in QDE within the SBP as DPH was unstable in the alkali medium necessary for gelatinization and crosslinking. However, crosslinking had a beneficial effect on the control of DPH release and crosslinking in hydration medium containing 40% ethanol: 5mL NaOH provided the greatest control of drug release. Despite the favorable effects on drug release, the use of DPH was deemed unsuitable due to discouraging drug entrapment characteristics.

During concurrent modification and drug entrapment, a decrease in drug content within the SBP was observed. However, modification improved the drug release behavior and resulted in a more favorable SBP to be employed as a MODDS. However, the issue with captopril instability in the basic medium required for SBP modification need to be overcome.

Oxidation was incompatible with captopril and reduced the drug entrapment capacity of the SBP. Crosslinking of oxidized SBP resulted in increased stability of the SBP but did not enhance the drug entrapment when compared to crosslinking of non-oxidized SBP. Pre-oxidation provided an advantageous effect on the drug release behavior with further modification of pre-oxidized SBP further enhancing the drug release behavior in both SIF and SGF. However, pre-oxidized SBP was not able to improve on the release behavior of non-oxidized SBP that were crosslinked.

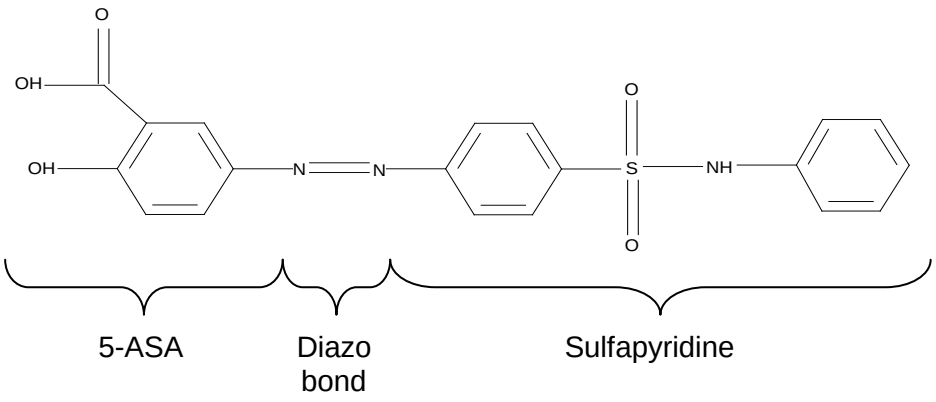
Thus, although decreasing the drug entrapment of the SBP, modifications of the SBP proved to improve the both the stability and drug release characteristics of the SBP successfully. However, the model drugs employed in the study were found to be incompatible with the formulation conditions required and thus modifications employing a more appropriate drug are necessary in order to employ the SBP within a MODDS.

CHAPTER 6
EMPLOYMENT OF AN ALKALI STABLE MODEL DRUG FOR THE DEVELOPMENT OF THE MULTIPARTICULATE ORAL DRUG DELIVERY SYSTEM

6.1. Introduction

Due to the instability of captopril and diphenhydramine in the media required for adequate functional modification of the sago Starch-Based Platform (SBP) as described in Chapter 5 and the unsatisfactory entrapment and *in vitro* drug release behaviour of furosemide and propranolol as described in Chapter 4, the use of an alternative, more suitable model drug was deemed necessary. Desirable properties of the proposed alternative drug included greater stability in alkaline medium, adequate solubility at high pH and thermo-stability at 100°C to avoid drug degradation during the determination of drug entrapment.

Sulfasalazine (SSZ) (Figure 6.1) is a prodrug, composed of 5-Aminosalacylic Acid (5-ASA) and Sulfapyridine (SP) bound together by a diazo bond. SSZ is used in the treatment of inflammatory bowel diseases (IBS) and in particular Crohn's Disease which is localized to the colon and lower jejunum (Chungi *et al.,* 1989; Milojevic *et al.,* 1996). Although thought to elicit antibacterial action in the colon, SP is principally inactive and regarded as a carrier molecule for 5-ASA, which is the active drug exerting anti-inflammatory effects. The diazo bond of SSZ is broken down by enzymes produced by colonic bacteria and releases 5-ASA that is required locally in the colon (Milojevic *et al.,* 1996). Physicochemically, SSZ is insoluble in water, slightly soluble in ethanol and soluble in solutions of alkali hydroxides. SSZ displays adequate heat stability with a melting point ~245°C and is stable at high pH (USP, 2000).



2-hydroxy-5-[(E)-2-{4-[(pyridin-2-yl)sulfamoyl]phenyl}diazen-1-yl]benzoic acid

Figure 6.1: Chemical structure of sulfasalazine.

These intrinsic characteristics portrayed by SSZ are compatible with the proposed modification and formulation processes and thus in this Chapter, SSZ was selected as the model drug. Furthermore, in this Chapter modifications attempted on captopril and diphenhydramine were attempted employing SSZ, and the modifications that imparted the best functional characteristics on the SBP were elucidated in order to develop the MODDS.

6.2. Materials and Methods

6.2.1. Materials

Sago Multiparticulates (SMP, food grade) were purchased from KOO South Africa (Tiger Brands Ltd., Bryanston, Johannesburg, South Africa) and were employed as the Starch-Based Platform (SBP). Sulfasalazine (SSZ, Mw=398.394g.mol^{-1}, ≥96.0%$^{w}/_{w}$, solubility=50mg.mL^{-1} in 1M NaOH solution) was purchased from Fluka, Biochemika, (Sigma-Aldrich Chemie GmbH, Steinheim, Switzerland). Sodium hydroxide (NaOH, Mw=40.00g.Mol^{-1}) was purchased from Saarchem-Holpro Analytic (Pty) Ltd., (Krugersdorp, Johannesburg, South Africa) and were of analytical grade. Ethanol (99%$^{v}/_{v}$, analytical grade) was purchased from Merck (Pty) Ltd. (Modderfontein, Johannesburg, South Africa). Sodium Trimetaphosphate (STMP, Mw=305.89g.Mol^{-1}, ≥96.0%$^{w}/_{w}$) and Epichlorohydrin (ECH, Mw=92.52g.Mol^{-1}, 99%$^{v}/_{v}$) were purchased from Sigma-Aldrich (Sigma-Aldrich Inc., St. Louis, USA). All other materials used were as describe in Chapter 2 and Chapter 5.

6.2.2. Construction of calibration curves

Stock solutions of SSZ were prepared by accurately weighing 10mg and 5mg SSZ and dissolving in 100mL Simulated Intestinal Fluid (SIF) and Simulated Gastric Fluid (SGF), respectively (SGF and SIF prepared as described in Chapter 2, Section 2.2.5.1.2 and Section 2.2.5.1.3, respectively). 5-fold serial dilutions were then performed on each stock solution (SIF concentrations: 0-0.0087mg.mL^{-1} and SGF concentrations: 0-0.0390mg.mL^{-1}) and each absorbance was determined with a UV spectrophotometer (diode array UV spectrophotometer, Specord 40, Analytik Jena AG, Jena) at the maximum absorbance wavelength of SSZ (λmax=359nm). Calibration curves were then constructed by plotting the observed absorbance on the y-axis against its corresponding concentration (mg.mL^{-1}) on the x-axis. All intercepts were set at 0 and the R^2 values were determined to be 0.9998 and 0.9983 in SIF and SGF, respectively.

6.2.3. Determination of the effects of concurrent modification and drug entrapment on the functional characteristics of the SBP

6.2.3.1. Preparation of modification solutions

6.2.3.1.1. Preparation of alkaline alcohol solution

NaOH solution (1M) was prepared by accurately weighing and dissolving 12g NaOH in 100mL deionized water. This solution was then made up to 300mL with deionized water and stored at 25°C. Alkaline alcohol solution (40% EtOH: 5mL NaOH) was then prepared by triturating 320mL ethanol (99%$^{v}/_{v}$), 100mL deionized water and 200mL NaOH solution and thereafter making up the solution to 1000mL with deionized water.

6.2.3.1.2. Preparation of oxidizing solution

Oxidizing solution (1.11M) was prepared by accurately weighing and dissolving 30.94g sodium (meta)periodate in 70mL phthalate buffer pH 4.6 (prepared as described in the USP 33) and then made up to 130mL with phthalate buffer pH 4.6.

6.2.3.1.3. Preparation of covalent crosslinking solution

Covalent crosslinking solution (5%$^{v}/_{v}$) was prepared by accurately measuring and dissolving 5mL of ECH (99%$^{v}/_{v}$) in 20mL alkaline alcohol and thereafter making up this solution to 100mL using alkaline alcohol (alkaline alcohol was prepared in Chapter 6, Section 6.2.3.1.1).

6.2.3.1.4. Preparation of ionic crosslinking solution

STMP solution (99%$^{w}/_{v}$) was prepared by accurately weighing and dissolving 9.90g STMP in 5mL deionized water and making this solution up to 10ML using deionized water. Ionic crosslinking solution (5%$^{v}/_{v}$) was then prepared by triturating 5mL of this STMP solution in 20mL of alkaline alcohol and thereafter making up this solution to 100mL using alkaline alcohol (alkaline alcohol was prepared in Chapter 6, Section 6.2.3.1.1).

6.2.3.2. Preparation of drug solutions

Drug solutions (75mg.mL^{-1}) were prepared by accurately weighing and dissolving 2250mg SSZ in 20mL of each of the modification solutions that were prepared in Chapter 6, Section 6.2.3.1 and thereafter made up to 30mL with its respective solution. A control drug solution was then prepared by accurately weighing and dissolving 2250mg SSZ in 20mL deionized water and thereafter making this solution up to 30mL with deionized water. Each of the drug solutions were maintained at 25°C under constant stirring on a magnetic stirrer until used.

6.2.3.3. Preparation of oxidized SBP

Aliquots (10mL) of oxidizing solution, prepared as described in Chapter 5, Section 5.2.5.5.1, were accurately measured and placed into experimental apparatuses. SBP samples (2g) were accurately weighed, submerged into the oxidizing solution and allowed to oxidize for 1.5 hours with the oxidizing solution maintained at 25±1°C and stirred at 50rpm in the experimental apparatuses. Thereafter the oxidized SBP samples were removed from the oxidation medium, washed with 1000mL deionized water to remove residual oxidizing agent, lightly blotted with tissue paper to remove excess moisture and immediately subjected to drug entrapment.

6.2.3.4. Concurrent modification and drug entrapment of the SBP

Oxidized SBP samples that were prepared in Section 6.2.3.3 were immediately placed into separate experimental apparatuses that contained a drug solution (5mL) prepared in Section 6.2.3.2. The SBP samples were allowed to entrap drug for 4 hours while maintained at 25±1°C and stirred at 50rpm. The drug-loaded oxidized SBP samples were then removed, lightly blotted with tissue paper to remove excess moisture and weighed in order to determine the hydration potential of these SBP. The SBP samples were then convection dried in a laboratory oven at 50°C and thereafter weighed. The Quantity of Drug Entrapped (QDE) of drug-loaded oxidized SBP samples were determined as described in Chapter 2, Section 2.2.8.2.2 with UV analysis being conducted at the maximum excitation wavelength of SSZ (λmax=359nm).

Separate unmodified SBP samples (2g) were accurately weighed and subjected to the same drug-loading process as pre-oxidized SBP samples. Furthermore, placebo SBP samples (both unmodified and pre-oxidized) were formulated in the same manner where the only difference was the absence of drug within the experimental apparatuses. Figure 6.2 portrays a schematic of the formulation process and the resultant SBPs of the study. The study was conducted in triplicate (n=3).

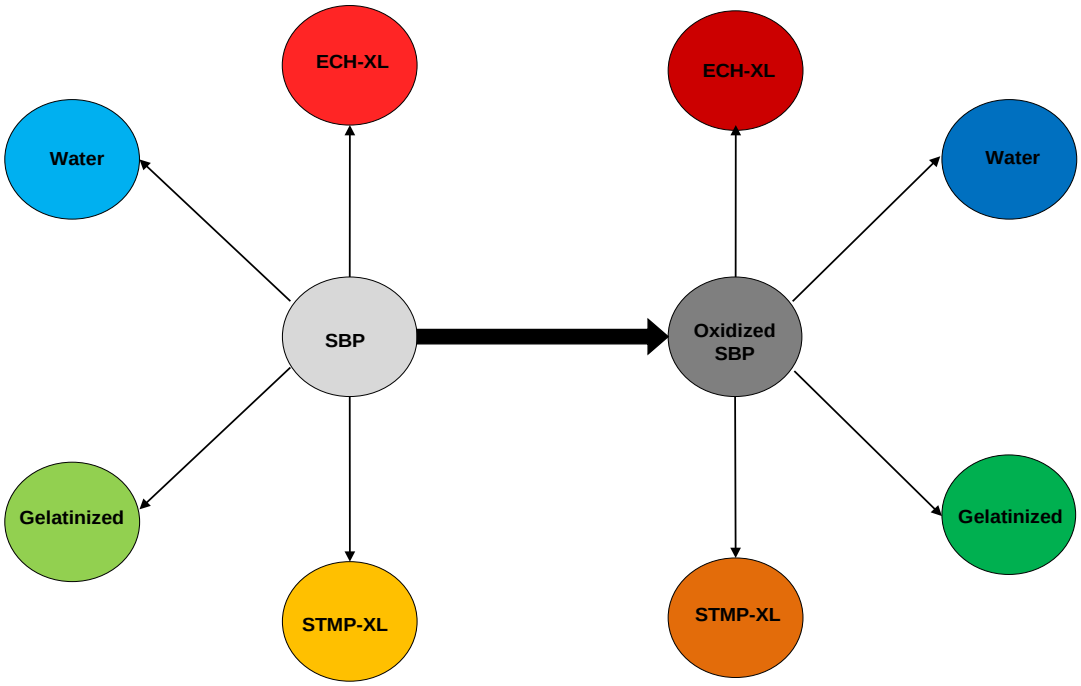


Figure 6.2: Schematic representation of resultant concurrently modified and SSZ-loaded SBPs.

6.2.3.5. Determination of the in vitro drug release behavior of SSZ-loaded SBP

The *in vitro* drug release behavior of each of the SSZ-loaded SBP formulations prepared in Section 6.2.3.4 was determined as described in Chapter 2, Section 2.2.8.3 with sampling occurring at time points which included 0.25 hours, 0.5 hours, then every half hour until 3 hours and thereafter every hour until 6 hours. Each sample was then adequately diluted and UV analysis was conducted at the λmax=359nm.

6.2.4. Determination of the effects of consolidated pre-modifications on the functional characteristics of the SBP

6.2.4.1. Preparation of modification solutions

6.2.4.1.1. Preparation of alkaline alcohol solution

Alkaline alcohol (40% EtOH: 5mL NaOH) solution was prepared as described in Section 6.2.3.1.1.

6.2.4.1.2. Preparation of oxidizing solution

Oxidizing solution (1.11M) was prepared by accurately weighing and dissolving 23.8g sodium (meta)periodate in 100mL phthalate buffer pH 4.6 and then made up to 150mL with phthalate buffer pH 4.6.

6.2.4.1.3. Preparation of covalent crosslinking solution

Covalent crosslinking solution ($5\%^{v}/_{v}$) was prepared by accurately measuring and dissolving 10mL of ECH ($99\%^{v}/_{v}$) in 50mL alkaline alcohol and thereafter making up this solution to 200mL using alkaline alcohol (alkaline alcohol was prepared in Section 6.2.4.1.1).

6.2.4.1.4. Preparation of ionic crosslinking solution

STMP solution ($99\%^{w}/_{v}$) was prepared by accurately weighing and dissolving 14.85g STMP in 5mL deionized water and making this solution up to 15ML using deionized water. Ionic crosslinking solution ($5\%^{v}/_{v}$) was then prepared by triturating 10mL of this STMP solution in 20mL of the alkaline alcohol and thereafter making up this solution to 200mL using alkaline alcohol (alkaline alcohol was prepared in Section 6.2.4.1.1).

6.2.4.2. Preparation of drug solution

Drug solution ($75mg.mL^{-1}$) was prepared by accurately weighing and dissolving 9000mg SSZ in 100mL of alkaline alcohol (prepared in Section 6.2.4.1.1) and thereafter making this solution up to 120mL with alkaline alcohol. The SSZ solution was maintained at 25±1°C under constant stirring on a magnetic stirrer until required.

6.2.4.3. Preparation of various modified SBPs

6.2.4.3.1. Preparation of pre-oxidized SBP

Equal volumes of oxidizing solution (50mL), prepared in Section 6.2.4.1.2, were accurately measured and placed into 3 experimental apparatuses. SBP samples (10g) were accurately weighed and submerged in an oxidizing solution. The SBP samples were then allowed to oxidize for 1.5 hours with the oxidizing solution maintained at 25±1°C and stirred at 50rpm in the experimental apparatuses. Thereafter the oxidized SBP samples were removed from the oxidation medium and washed with 1000mL deionized water to remove residual oxidizing agent. The hydrated oxidized SBP samples were then lightly blotted with tissue paper to remove excess moisture and allowed to convection dry in a laboratory oven maintained at 50°C until constant mass was attained. Once dry, the separate oxidized SBP samples were mixed and samples from the combined mass were employed in further studies.

6.2.4.3.2. Preparation of alkali pre-gelatinized SBP

SBP samples (60g) were accurately weighed, divided into 10g subsets and added to experimental apparatuses along with 50mL alkaline alcohol solution (prepared in Section 6.2.4.1.1). The SBP subsets were then allowed to gelatinize for 2 hours while maintained

at 25±1°C and stirred at 50rpm. Thereafter the gelatinized SBP subsets were removed from the gelatinization medium, lightly blotted with tissue paper to remove excess moisture and allowed to convection dry in a laboratory oven maintained at 50°C for 2 hours. Once dry, the separate gelatinized SBP subsets were mixed and samples from the combined mass were employed in further studies.

6.2.4.3.3. Preparation of ECH-crosslinked pre-gelatinized SBP

Pre-gelatinized SBP samples (20g), prepared in Section 6.2.4.3.2, were accurately weighed, divided into 10g subsets and each subset placed into experimental apparatuses. Covalent crosslinking solution (50mL), prepared in Section 6.2.4.1.3 was then introduced into the experimental apparatuses and the SBP subsets were allowed to crosslink for 2 hours while maintained at 25±1°C and stirred at 50rpm. Thereafter the crosslinked SBP subsets were removed from the crosslinking medium, lightly blotted with tissue paper to remove excess moisture and allowed to convection dry in a laboratory oven maintained at 50°C until constant mass was achieved. Once dry, the pre-gelatinized covalent crosslinked SBP subsets were mixed and samples from this combined mass were employed in further studies.

6.2.4.3.4. Preparation of ionic crosslinked pre-gelatinized SBP

Pre-gelatinized SBP samples (20g) were accurately weighed and subjected to the same method described in Section 6.2.4.3.3 with covalent crosslinking solution replaced by ionic crosslinking solution, prepared in Section 6.2.4.1.4.

6.2.4.3.5. Preparation of covalent crosslinked pre-oxidized SBP

Pre-oxidized SBP samples (8g), prepared in Section 6.2.4.3.1 were equally divided and placed into two experimental apparatuses. Covalent crosslinking solution (20mL), prepared in Section 6.2.4.1.3, was then introduced into each experimental apparatus and the pre-oxidized SBP samples were then subjected to the same procedure as described in Section 6.2.4.3.3.

6.2.4.3.6. Preparation of ionic crosslinked pre-oxidized SBP

Pre-oxidized SBP samples (8g), prepared in Section 6.2.4.3.1, were equally divided and placed into two experimental apparatuses. Ionic crosslinking solution (20mL), prepared in Section 6.2.4.1.4 was then introduced into each experimental apparatus and the pre-oxidized SBP samples were then subjected to the same procedure as described in Section 6.2.4.3.3.

6.2.4.4. Drug entrapment into modified SBPs

Aliquots (5mL) of SSZ drug solution prepared in Section 6.2.4.2 were accurately measured and placed in separate experimental apparatuses. Modified SBP samples (2g), prepared in Section 6.2.4.3, were accurately weighed and submerged into an experimental apparatus containing drug solution and allowed to entrap drug for 4 hours while maintained at 25±1°C and stirred at 50rpm. Thereafter the modified drug-loaded SBP samples were removed from drug solution, lightly blotted with tissue paper to remove excess moisture and allowed to convection dry in a laboratory oven maintained at 50°C until constant mass was achieved.

6.2.4.5. Secondary crosslinking of drug-loaded SBPs

6.2.4.5.1. Preparation of double covalent crosslinked drug-loaded SBP

A second set of pre-gelatinized covalent crosslinked SBP samples (2g), prepared in Section 6.2.4.3.3 were accurately weighed and subjected to the same drug entrapment procedure as described in Section 6.2.4.4, but were not removed from the drug solution after 4 hours. ECH solution (99%$^{v}/_{v}$; 0.25mL) was then added to these crosslinked drug-loaded SBP samples and allowed to crosslink for 1 hour while maintained at 25±1°C and stirred at 50rpm. The double covalent crosslinked drug-loaded SBP samples were then removed from the experimental apparatus, lightly blotted with tissue paper to remove excess moisture and allowed to convection dry in a laboratory oven maintained at 50°C until constant mass was achieved.

6.2.4.5.2. Preparation of double ionic crosslinked SBP

A second set of pre-gelatinized ionic crosslinked SBPs samples (2g), prepared in Section 6.2.4.3.4 were accurately weighed and subjected to the same procedure as described for pre-gelatinized covalent crosslinked SBP samples in Section 6.2.4.5.1 with ECH solution replaced by STMP solution (99%$^{w}/_{v}$; 0.25mL).

Figure 6.3 depicted the schematic representation of the formulation process and resultant drug-loaded SBPs prepared in Section 6.2.4.4 and Section 6.2.4.5. The study was conducted in triplicate (n=3).

6.2.4.6. Determination of the extent of drug entrapment into consolidated pre-modified SBP

The QDE and Drug Entrapment Efficiency (DEE) of consolidated pre-modified drug-loaded SBP samples were determined as described in Chapter 2, Section 2.2.8.2.2 with UV analysis conducted at the maximum excitation wavelength of SSZ (λmax=359nm).

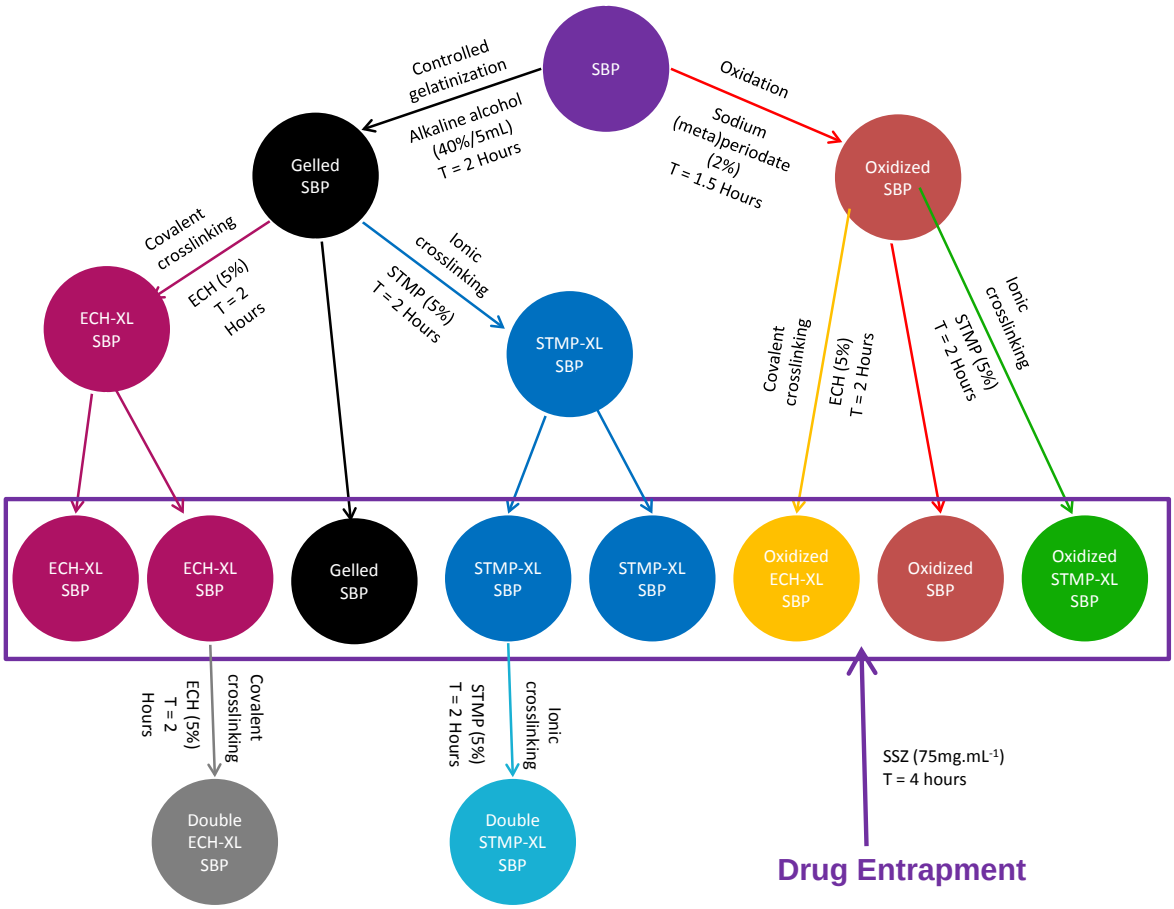


Figure 6.3: Schematic representation of the consolidated modification and drug-loading of the SBPs.

6.2.4.7. Determination of the in vitro drug release behavior of consolidated pre-modified SBPs

Due to the limited release of SSZ from the modified drug-loaded SBPs in SGF and the notably large burst release in SIF observed in the previous study, an *in vitro* drug release method, which provided a stepwise approach that more closely mimics the path of the MODDS in the GIT, was explored. The *in vitro* drug release studies on the modified drug-loaded SBPs were thus performed as described by Klein and co-workers (2008), with minor modifications utilizing a USP 33 dissolution apparatus III, reciprocating cylinder apparatus (Bio-Dis® CALEVA RRT8, Caleva Ltd., Sturminster Newton, Dorset, England). Separate drug-loaded modified SBP samples (containing 20mg SSZ, calculated using Equation 4.1 were accurately weighed and placed separately into glass cylinders enclosed with mesh at both the top and bottom ends (mesh sizes= 420µm). These cylinders were then lowered into 200mL SGF, maintained at 37±0.5°C, employing a dip rate of 10DPM. Samples (5mL) were manually withdrawn at 0.25, 0.5, 1, 1.5 and 2 hours and replenished with fresh SGF in order to maintain sink conditions. After 2 hours, the cylinders were raised above the dissolution medium and the SBP samples were drip-died

for 5 minutes. The cylinders were then lowered into 200mL SIF, maintained at 37±0.5°C, and a dip rate of 10DPM was employed for the remainder of the study. Samples (5mL) were manually withdrawn at 0.5-hour intervals for 2 hours, then hourly over the next 2 hours and thereafter 2-hourly until 12 hours. After each sampling, equivalent volumes of fresh SIF was entered into the dissolution medium in order to maintain sink conditions. The drug content of each sample was quantified using UV spectroscopy at a λmax=359nm and the corresponding predefined calibration curves (Section 6.2.2). The study was conducted in triplicate (n=3) and the results obtained were plotted as the average fractional drug release ± the standard deviation at each sampling time.

6.2.5. Determination of the effect of Drug-Loading Time and secondary Crosslinking Time on the performance of pre-gelatinized covalent crosslinked SBP

6.2.5.1. Preparation of pre-gelatinized crosslinked SBPs

Pre-gelatinized covalently crosslinked SBP were prepared as described in Section 6.2.4.3.3 and thereafter subjected to further modifications.

6.2.5.2. Drug-loading and secondary crosslinking of SBP

Drug-loading and secondary crosslinking of pregelatinized-covalent crosslinked SBPs were carried out as described in Section 6.2.4.4 and Section 6.2.4.5.1 respectively. However, Drug-Loading Time (DLT) was varied with secondary Crosslinking Time (CLT) kept constant at 2 hours as illustrated in Formulations 1-6 in Table 6.1. Thereafter, CLT was varied while maintaining the DLT at 4 hours as illustrated in Formulations 7-12 in Table 6.1. During the study, the experimental apparatus was maintained at 25±1°C and stirred at 50rpm. The study was conducted in triplicate (n=3).

Table 6.1: Variation of Drug-Loading Time and secondary Crosslinking Time

Formulation	DLT (Hours)	CLT (Hours)
1	1	2
2	2	2
3	4	2
4	8	2
5	12	2
6	24	2
7	4	1
8	4	2
9	4	4
10	4	8
11	4	12
12	4	24

Where DLT denoted Drug-Loading Time and CLT denoted secondary Crosslinking Time

6.2.5.3. Determination of the extent of drug entrapment into consolidated double covalent crosslinked SBP

The QDE and DEE of consolidated pre-modified drug-loaded SBP samples were determined as described in Section 6.2.4.6.

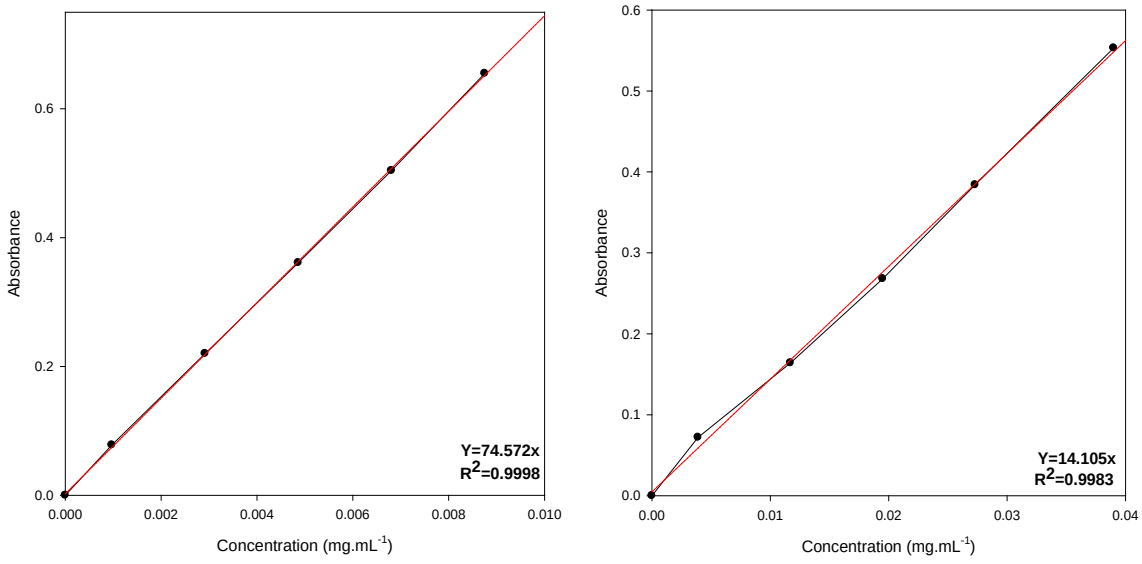
6.2.5.4. Determination of the effect of DLT and secondary CLT on the in vitro drug release behavior of double covalent crosslinked SBPs

In vitro drug release studies on double crosslinked SBPs were conducted as described in Section 6.2.4.7.

6.3. Results and Discussion

6.3.1. Calibration curves of SSZ in simulated physiological fluids

The calibration curves prepared for SSZ and depicted in Figure 6.4 displayed good linearity in both SIF and SGF with R^2 values of 0.9994 and 0.9983, respectively and was thus deemed appropriate to be utilized in determining functional characteristics of drug entrapment and *in vitro* drug release behavior in these media.



(a) (b)

Figure 6.4: Calibration curves of SSZ in (a) SIF and (b) in SGF.

6.3.2. Effect of concurrent modification and drug entrapment on the functional characteristics of the SBP

6.3.2.1. Effect of concurrent modification on the drug entrapment potential of the SBP

When analyzing the hydration of the various modified SBP formulations, it was observed that pre-oxidized SBP portrayed a diminished hydration capacity compared to previously unmodified SBP in all of the formulations prepared. This could be due to the reduced structural integrity, imparted by ring cleavage reactions during the oxidation process, which allowed the hydration media to erode away at the oxidized-SBP formulations to a greater extent. This ultimately resulted in a decrease in physical SBP available to imbibe the hydration medium and accounted for the lower DCM values expressed in Figure 6.5b compared to Figure 6.5a. The increased erosion was more evident when placed in drug free alkaline medium, as compared to water medium, and even crosslinking proved ineffective in impeding the disintegration. Thus pre-oxidized SBP formulations displayed negative DOS and DCM values, which translated into disintegration and net erosion of the SBP in alkaline medium.

When analyzing Figure 6.5a and Figure 6.5b, it was detected that SBP formulations (both previously unmodified and pre-oxidized) displayed greater hydration capacity and positive resultant DCM when submerged in drug solution as compared to their respective placebo formulations. This could be attributed to the hydration process, which caused relaxation of attractive forces between molecules of the SBP and allowed entry of hydration media within the SBP. This created new structural voids in addition to expansion of pre-existing voids within the SBP due to hydration facilitated erosion, gelatinization and solubilization of SBP interfaces. However, the hydration media containing SSZ facilitated the drug to interact with the SBP on a molecular level and thereby enhanced the structural integrity of the SBP. This effect, in turn, led to improved hydration as the SBP could undergo additional expansion with improved resistance to the erosive effect of the alkaline hydration medium. Furthermore, the incorporation of drug was determined to be a contributing factor observed in the mass gain of drug-loaded modified SBP as the drug now occupied the voids in comparison to the vacant voids that remained in the placebo formulations.

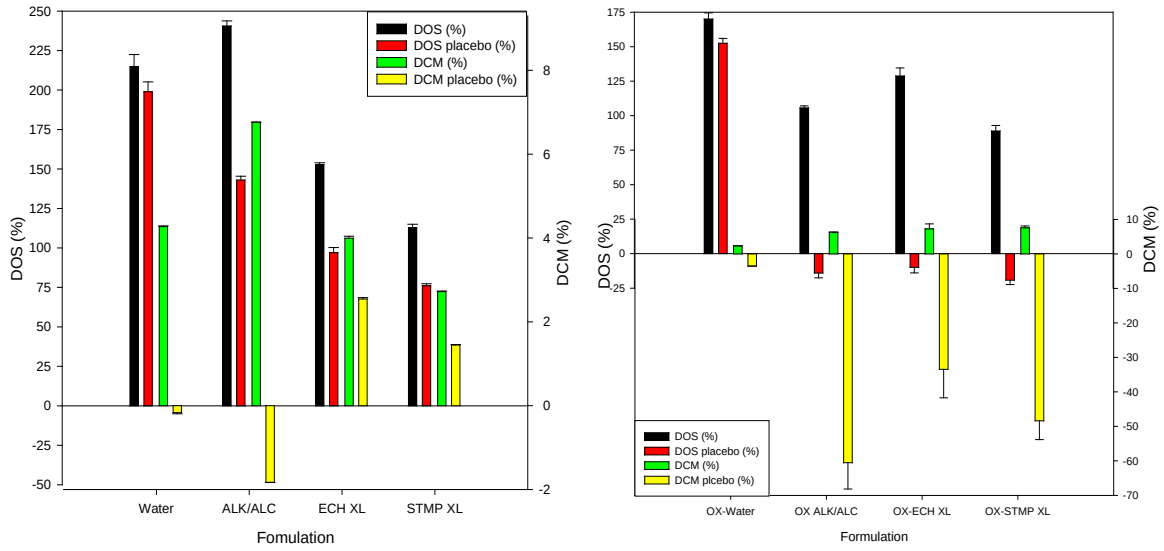


Figure 6.5: Comparative effect of modification on the hydration and erosion of (a) previously unmodified and (b) pre-oxidized SBP during drug entrapment (n=3 in all instances).

When the drug entrapment of each formulation in Figure 6.6 was compared, an interesting observation was made. Although undergoing inferior hydration and considerable erosion within the drug solution, pre-oxidized SBP formulations displayed superior drug entrapment capacity compared to previously unmodified SBP formulations. This was true for all further modifications performed on the SBP and provided further support for the drug-SBP interaction hypothesis explained above.

Comparison between the individual further modifications revealed that alkali gelatinization imparted the greatest drug entrapment capacity on both pre-oxidized and previously unmodified SBP. The QDE correlated with the high hydration observed in unmodified SBP and this was in accordance with observations made in previous studies employing other drugs. However, hydration of the pre-oxidized and subsequently gelatinized SBP was lower than its covalently crosslinked SBP counterpart, but exhibited greater drug entrapment potential. This could be due to the increased structural integrity conferred by ECH, which resulted in resistance to erosion and decreased the size and extent of internal void formation. In addition, the covalent crosslinking of pre-oxidized SBP resulted in greater structural stability than ionic crosslinking of pre-oxidized SBP. This allowed the covalent SBP to hydrate to a greater extent and furthermore offered more resistance to the erosive effect of the hydration medium. Ultimately, this translated into a higher drug entrapment for the covalently crosslinked SBPs.

When compared to the further modified SBP formulations, SBP (unmodified and pre-oxidized) drug-loaded in water displayed substantial hydration with minimal erosion. However, this did not translate into adequate QDE within these SBPs and demonstrated the lowest drug entrapment of all the formulations evaluated. This could be due to the insolubility of SSZ in water, which impeded the medium facilitated carriage of drug into the SBP. The low DQE of these SBPs rendered them unfeasible and was thus excluded from the *in vitro* drug release studies.

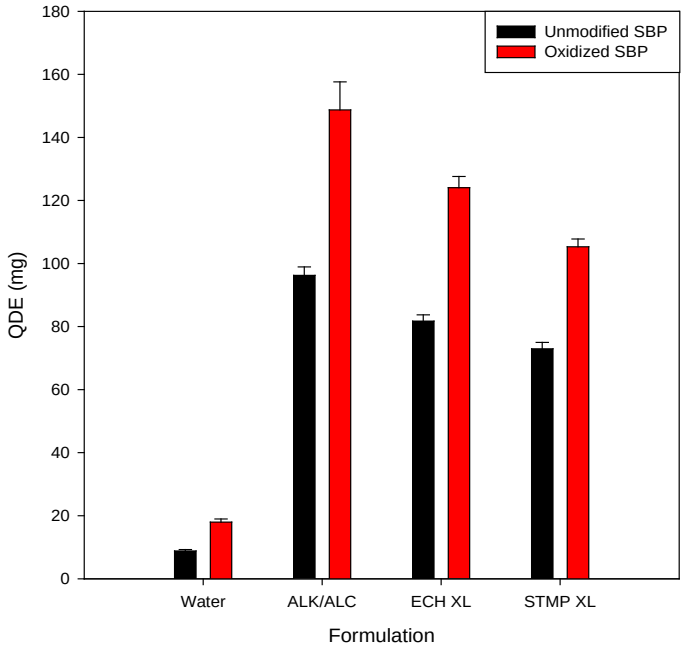


Figure 6.6: Comparison of modifications on the drug entrapment of previously unmodified and pre-oxidized SBP (n=3 in all instances).

6.3.2.2. In vitro SSZ release from concurrently modified and drug-loaded SBPs

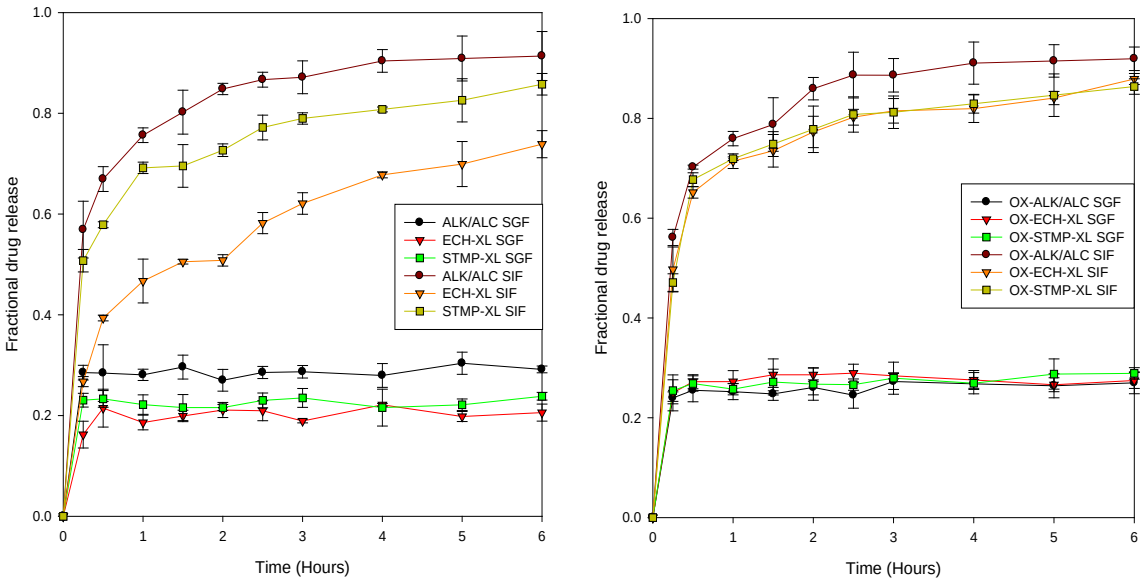
When analyzing the drug release behavior of the modified SBP formulations in SGF (Figure 6.7), it was found that the *in vitro* SSZ release from both previously unmodified and pre-oxidized SBP formulations displayed very similar profiles. The profiles demonstrated an initial burst release of between 15 and 30% of entrapped drug within the first 15 minutes and thereafter no notable drug release was observed over the 6 hours of the study. Further modifications had no effect on the release behavior of pre-oxidized SBP, as all of the formulations displayed almost identical drug release profiles. With regard to previously unmodified SBP formulations, minor differences in the SSZ release behavior were detected. The initial burst release decreased in the order alkali gelatinized (~29%) > ionic crosslinked (~23%) > covalent crosslinked (~16%). Thereafter minimal further SSZ was released from each of the formulations. The observed drug release

profiles could be attributed to the low drug solubility within the low pH of SGF. Therefore, the drug released could be drug that was adsorbed onto the surface of the SBP when being exposed to the dissolution medium and accounted for the burst release phase. Thereafter, the dissolution medium became saturated with drug and no further SSZ could be release into the medium and explained the plateau phase of the drug release profiles.

In SIF (Figure 6.7), the SBP formulations portrayed very dissimilar *in vitro* drug release behavior. The burst release of between 44% and 58% was much greater than that seen in SGF. This could again be attributed to drug solubility with SSZ known to be much more soluble in alkaline pH and thus facilitated the increased release of both surface adsorbed and core integrated SSZ. However, an anomaly in the form of previously unmodified covalently crosslinked SBP formulation was found, which released only ~27% of drug in the initial burst phase. Further drug release occurred in SIF and produced similar *in vitro* drug release profiles with maximum drug release of between 73% and 92% for all the formulations evaluated.

Comparison between Figure 6.7a and Figure 6.7b demonstrated no considerable effect of pre-oxidation on the *in vitro* drug release behavior from gelatinized or STMP-crosslinked SBP formulations. However, pre-oxidation resulted in inferior control of drug release in ECH-crosslinked SBP compared to previously unmodified SBP. When comparing individual pre-oxidized formulations, it was observed that crosslinking resulted in slightly superior control over alkali gelatinized SBP but neither method of crosslinking was superior to the other. On the other hand, with previously unmodified SBP formulations, STMP-crosslinking proved slightly superior to alkali gelatinization but ECH-crosslinked SBP displayed the most superior control of SSZ release.

The pre-hydrated state of the oxidized SBP samples employed in this study could have had a negative effect on the hydration potential of the SBP, and could thus have affected their drug entrapment capacity and subsequent control of SSZ release. Consolidated modification of the SBP by means of drying of gelatinized, crosslinked, oxidized or a combination of modifications prior to drug entrapment may enhance the performance of the SBP with regard to both drug entrapment and drug release.



(a) (b)

Figure 6.7: Effect of modifications on the comparative SSZ release behavior of (a) previously unmodified and (b) pre-oxidized SBP in SGF and SIF (n=3 in all instances).

6.3.3. Effect of consolidated modification on the functional characteristics of the SBP

6.3.3.1. Effect of consolidated modification on the drug-loading potential of SBP

Analysis of individual formulations in Figure 6.8 revealed that pre-oxidized SBP without additional modifications displayed the highest SSZ entrapment QDE~218mg which translated into a DEE of ~58%. Subsequent modifications in the form of simple crosslinking decreased the drug entrapment with average resultant QDE~144mg (DEE~38%) and ~170mg (DEE~45%) in pre-gelatinized and pre-oxidized SBP formulations, respectively. Double crosslinking further reduced the average QDE and DEE of the SBP to ~125mg and ~33%, respectively, conferring the lowest SSZ entrapment efficiency of all the formulations.

Scrutiny of the effect of different crosslinking methods employed revealed that covalent crosslinking imparted SSZ entrapment that was ~9% superior compared to ionic crosslinking. This was consistent with the trend observed during the study involving concurrently modified and drug-loaded SBP Figure 6.6 where covalent crosslinking resulted in SSZ entrapment that was ~13% superior compared to ionic crosslinking. Thus, it was proposed that more favorable interactions between SBP, SSZ and crosslinker resulted during covalent crosslinking compared to ionic crosslinking of the SBP.

Upon further analysis of Figure 6.8 and compared to Figure 6.6, it was observed that pre-oxidation increased the entrapment capacity of the SBP by ~13.5% compared to previously unmodified SBP. This was congruent to the increased entrapment observed when SBP formulations were concurrently modified and drug-loaded. However, compared to concurrently modified and drug-loaded SBP formulations, greater SSZ entrapment was displayed by consolidated pre-modified SBP formulations with regard to all subsequent modifications. Although no like for like comparisons for double crosslinked SBP formulations were available in the concurrent modification and drug-loading study, double crosslinked SBP formulations demonstrated superior SSZ entrapment values than all previously unmodified formulations in Figure 6.6. Additionally, the QDE values of 132mg and 117mg for ECH and STMP double crosslinked SBP formulations, respectively, were comparable to the pre-oxidized ECH-crosslinked SBP formulation and superior to the pre-oxidized STMP-crosslinked SBP formulation. Thus, consolidated pre-modifcation of the SBP prior to drug entrapment was determined to produce SBP with greater drug entrapment capacity.

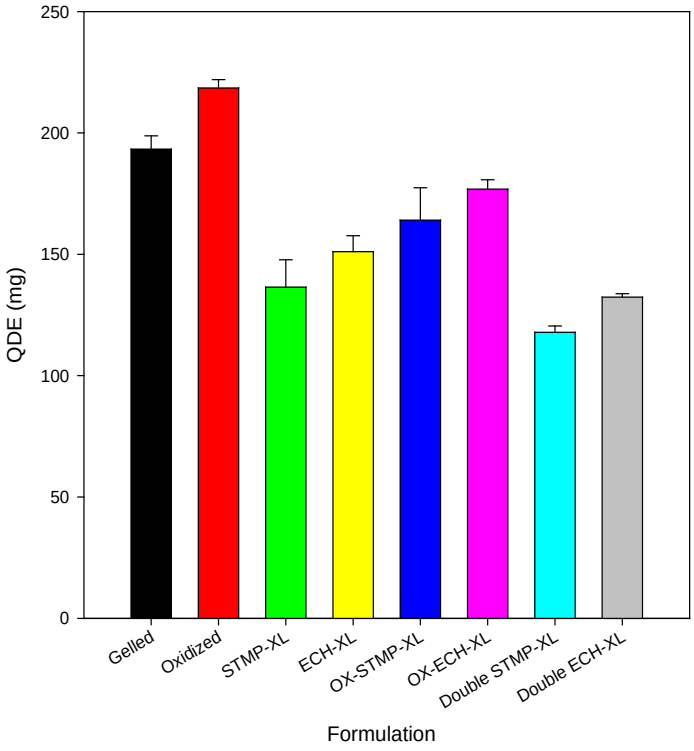


Figure 6.8: Comparative effect of consolidated modification on the drug-loading potential of SBP (n=3 in all instances).

6.3.3.2. Effect of consolidated pre-modification on the in vitro drug release behavior of SBP

In vitro drug release studies conducted in the Biodis® displayed a stepwise SSZ release profile resulting from the change of dissolution media (Figure 6.9). During the first 15 minutes, all of the modified SBP formulations displayed a burst release of SSZ ranging between 15% and 35% of total drug entrapped. Thereafter minimal increase in drug release was observed over the next 2 hours in SGF. This was comparable to the trend observed with concurrently modified and drug-loaded SBPs (Figure 6.7) and could be attributed to the low solubility of SSZ in SGF. On closer inspection and comparison of each formulation, it was noted that the double ECH-crosslinked SBP formulation demonstrated the smallest burst release while the alkali gelatinized SBP formulation displayed the least control over the burst release. In addition, no specific trend with regard to the effect of modifications or type of crosslinking in controlling of the burst release was discerned.

In contrast, upon shifting the SBP formulations into SIF, a clear distinction between the effects of each modification was apparent. Gelatinization and oxidation produced similar *in vitro* drug release profiles with the oxidized formulation displaying slightly superior control by releasing approximately ~96% of SSZ in 12 hours compared to the total SSZ released from the gelatinized SBP formulation in 10 hours. The *in vitro* drug release profiles of STMP-crosslinked SBP formulations followed the same trend as their non-crosslinked counterparts. However, STMP-crosslinking of pre-oxidized SBP proved to be a superior modification in controlling the *in vitro* drug release behavior with total drug release of 90% and 83% for gelatinized STMP-crosslinked SBP formulation and oxidized STMP-crosslinked SBP formulation, respectively, after 12 hours. These drug release profiles were almost identical to the profiles produced by concurrently modified and drug-loaded SBP formulations and thus consolidated pre-modification offered no enhancement in respect of controlling drug release in these instances.

Covalent crosslinking showed further enhancement in controlling the SSZ release from the SBP. Conversely, to STMP-crosslinked formulations, covalent crosslinking of gelatinized SBP formulations produced finer *in vitro* drug release profiles than pre-oxidized SBP formulations. When compared to concurrently modified and drug-loaded SBP formulations (Figure 6.7), the same trend was noted. However, consolidated pre-modification improved the retardation of SSZ release with total drug release of 75% and 69% for the gelatinized ECH-crosslinked SBP formulation and the oxidized ECH-crosslinked SBP formulation, respectively, after 12 hours.

Double crosslinking resulted in the best retardation of SSZ release from the SBP when compared to all other formulations in this study as well as in studies conducted previously. This was true for both ionic and covalent double crosslinked SBP formulations. In addition, an improvement in the linearity of the *in vitro* drug release profile in SIF was observed when double crosslinking was employed. Figure 6.9 showed that after 12 hours, total drug release was 65% from the double STMP-crosslinked SBP formulation and 58% from the double ECH-crosslinked SBP formulation. This, coupled with the superiority in drug entrapment over ionic crosslinking, proved that covalent crosslinking of the SBP resulted in the most favorable functional characteristics and was therefore selected for development of the MODDS.

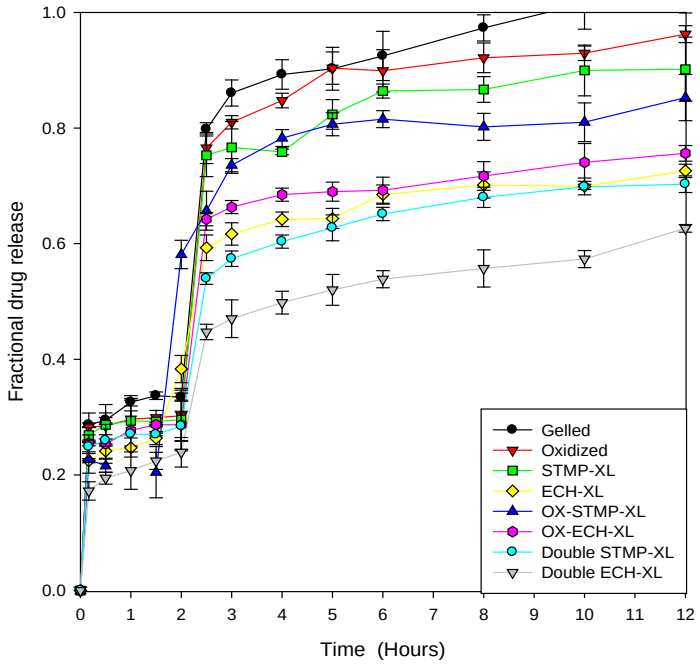


Figure 6.9: Comparative *in vitro* drug release behavior of consolidated pre-modified SBPs (n=3 in all instances).

6.3.4. Effect of DLT and secondary CLT on the functional characteristics of the pre-gelatinized ECH-crosslinked SBP

6.3.4.1. Effect of DLT and secondary CLT on the drug entrapment of double crosslinked SBP

Figure 6.10a illustrated that the amount of time spent by the pre-covalent crosslinked SBP samples within drug solution was directly proportional to the drug entrapped by the SBP. This was true until 8 hours at which point the maximum QDE of ~158mg (DEE~ 41%) was achieved. Thereafter the drug entrapment of the SBP tended to plateau with a slight decrease until 24 hours. The hydration potential of the SBP samples displayed a direct

correlation to the drug entrapment and maximum hydration corresponded to the maximum drug entrapment with further hydration inhibited due to saturation of the SBP at approximately 115%. The decrease in hydration after 8 hours of DLT could be attributed to increased erosion of the SBP by the alkaline medium of the drug solution with minimal further entrapment occurring.

Conversely, Figure 6.10b illustrated that the amount of time to which the pre-covalent crosslinked SBP samples were exposed to ECH during the secondary crosslinking phase displayed an inversely proportional relationship to the entrapment potential of the SBP. Thus, maximum drug entrapment of ~154mg (DEE~41%) was observed in Formulation 7, which underwent secondary crosslinking for the shortest period, i.e. 1 hour, and further crosslinking further reduced the drug entrapment. Once again, as seen in previously studies, the hydration potential showed close correlation to the SSZ entrapment of the SBP and decreased as the CLT increased. This phenomenon could be explained by the increase in degree of crosslinking and structural rigidity as the crosslinking time increased, resulting in reduced hydration of the SBP. This contraction in structure could cause both expulsion and restricted inflow of drug solution into the SBP which ultimately resulted in reduced drug entrapment.

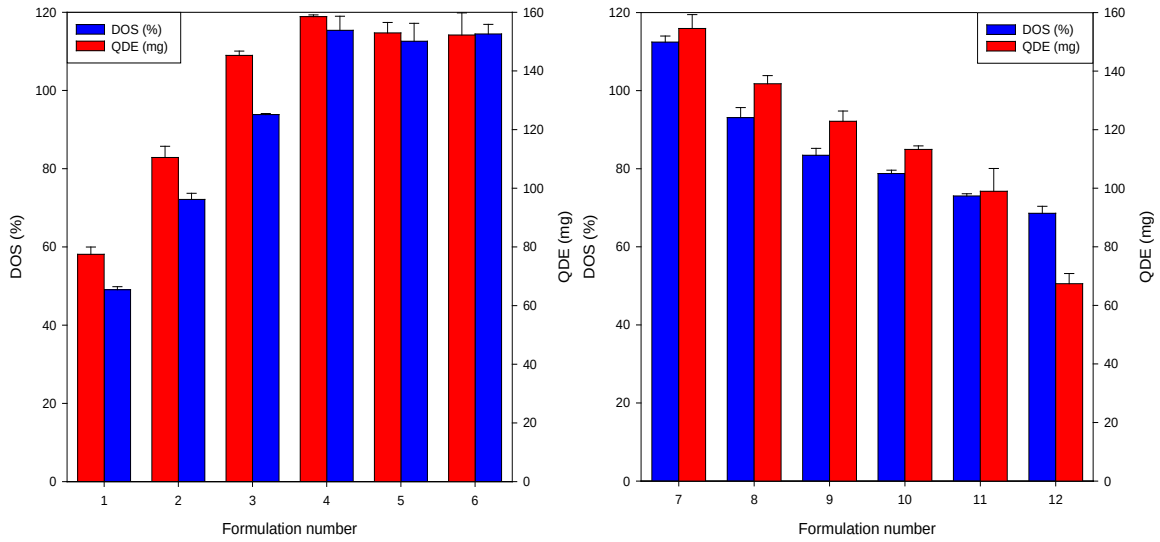


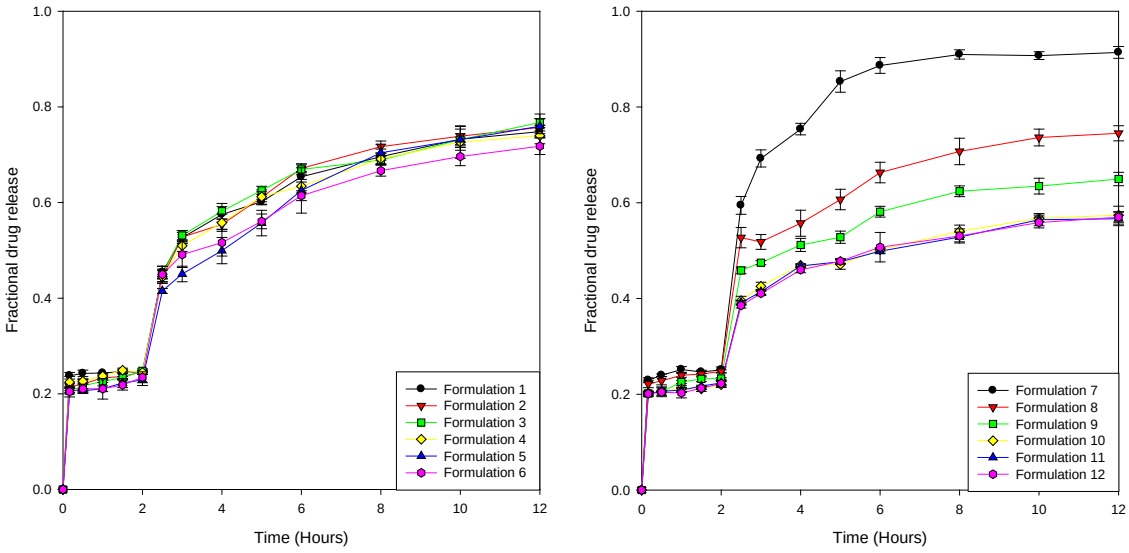
Figure 6.10: Effect of (a) drug-loading time and (b) secondary crosslinking time on the drug entrapment of double covalent crosslinked SBPs (n=3 in all instances).

6.3.4.2. Effect of DLT and secondary CLT on the in vitro drug release behavior of double ECH-crosslinked SBP

It was observed in Figure 6.11a that the *in vitro* drug release profiles produced by all of the formulations were almost identical with the burst release ranging between ~20% and 24% and minimal additional drug released in SGF. Upon shifting into SIF a second burst release of approximately ~20% of entrapped SSZ was observed after which relative control of drug release was displayed until 12 hours, at which point, all of the formulations had released between ~71% and 77% of entrapped drug. Thus, it was concluded that variation of DLT demonstrated no significant effect on the control of SSZ release from the double ECH-crosslinked SBP.

When analyzing Figure 6.11b, it was observed that all of the formulations prepared displayed indistinguishable *in vitro* SSZ release behavior to each other as well as to the formulations depicted in Figure 6.11a during the first 2 hours in SGF. However, upon submerging in SIF, the effect of secondary crosslinking was clearly visible with formulations that underwent lesser crosslinking imparting reduced control over SSZ release than their more crosslinked counterparts. Formulation 7, with crosslinking time of 1 hour, showed the highest burst release in SIF (~40%) with ~91% of entrapped SSZ released after 12 hours. Formulation 8 (crosslinking time= 2 hours) displayed a much lower SIF burst release (~25%), followed by controlled release and 12-hour release of 75% which was comparable to the SSZ release profiles produced by the formulations in Figure 6.11a. As the formulations in Figure 6.11a were exposed to 2 hours of secondary crosslinking, the control of SSZ could be attributed to the secondary crosslinking and this further confirmed the minor effect of DLT on SSZ release behavior.

Formulation 9 displayed superior control of SSZ release (12-hour release ~65%), when compared to Formulation 8. Upon increasing the CLT to 8 hours (Formulation 10), a further enhancement in SSZ release control was observed resulting in ~40% of drug released after 12 hours. Additional crosslinking up to 24 hours offered no improvement as the release profiles produced by Formulation 11 and Formulation 12 were identical to that observed when CLT of 8 hours was employed. Thus although the extent of crosslinking affected the drug release behavior of the SBP, minimal enhancement can be achieved beyond 8 hours of secondary crosslinking.



(a) (b)

Figure 6.11: Effect of (a) drug-loading time and (b) secondary crosslinking time on the *in vitro* drug release behavior of double covalent crosslinked SBPs (n=3 in all instances).

6.4. Concluding Remarks

It was found that SSZ was both soluble and stable in the hydration and modification mediums employed in the study. Furthermore, SSZ was compatible with the SBP and SSZ incorporation enhanced the structural stability on the SBP formulations and inhibited their disintegration within the drug-loading medium. Thus, SSZ was determined to be a suitable model drug for the development of the MODDS.

With regard to the effects of modifications performed onto the SBP, it was observed that even though periodate oxidation displayed a positive effect on drug entrapment, oxidation conferred minimal enhancement on the *in vitro* drug release behavior and diminished the stability of the SBP in the modification media. Crosslinking of the SBP reduced the drug entrapment but improved *in vitro* drug release behavior with covalent crosslinking proving to be superior to ionic crosslinking in this regard. In addition, in was elucidated that consolidation of the modifications performed offered improved functional characteristics of the SBP compared to concurrently drug-loaded and modified SBP formulations. However, subjecting pre-gelatinized, crosslinked and SSZ-loaded SBP to a second crosslinking step fortified the structure of the SBP and imparted the greatest control of drug release from the SBP with the use of ECH proving superior compared to STMP.

Furthermore, it was determined that the extent of hydration had a positive effect on drug entrapment with minimal effect on *in vitro* drug release behavior while the extent of secondary crosslinking displayed a negative effect on the drug entrapment potential of the pre-gelatinized, crosslinked and SSZ-loaded SBP with positive effect on *in vitro* drug release behavior. Due to the effects these parameters on the functional characteristics of the SBP, it was thus determined that DLT and CLT would be employed as the independent formulation variables in the statistical optimization of the SBP in order to develop the MODDS.

CHAPTER 7
OPTIMIZATION OF DOUBLE CROSSLINKED, SULFASALAZINE-LOADED STARCH-BASED PLATFORM

7.1. Introduction

Statistical design of experiments is a mathematical tool that allows for the selection of the most appropriate levels of process variables in order to reach end points with the highest desirability (Singh *et al.,* 2004; Mohajeri *et al.,* 2010). Response surface methodology is a factorial base design introduced by G.E.P. Box in the 1950s with the Face Centered Central Composite Design (FCCCD) being a widely used form of this approach (Hosseini and Khosravi-Darani, 2011). It provides a cost effective and time saving way by which multiple inputs can be simultaneously optimized and follows a generalized pattern as depicted in Figure 7.1 (Singh *et al.,* 2004; Nasrollahzadeh *et al.,* 2007; Petkovska *et al.,* 2008; Ray *et al.,* 2009; Ray *et al.,* 2010).

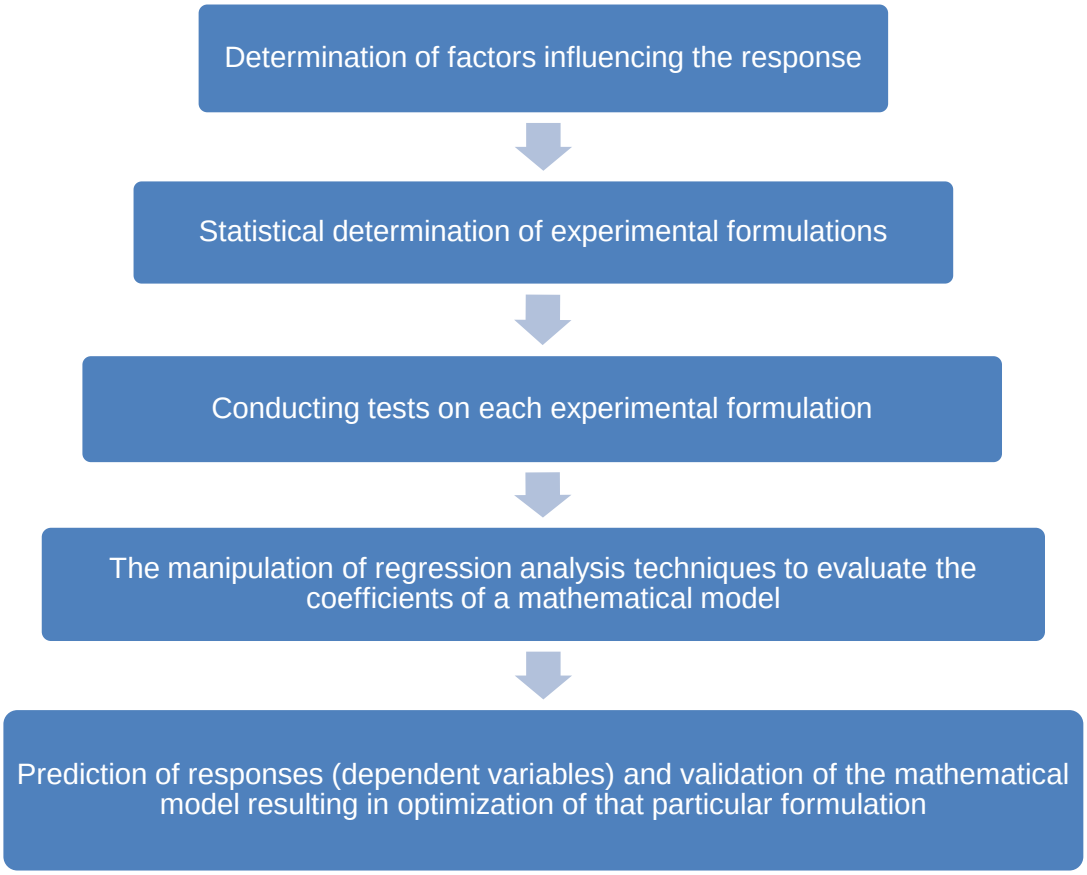


Figure 7.1: General process involved in statistical optimization.

For the purpose of this study, utilizing statistical design software MINITAB®, (V15, Minitab Inc, Pennsylvania, USA), a 2-factor-3-level (3^2) full factorial surface response FCCCD was applied to construct second-order polynomial models describing the effect of formulation factors on the Drug Entrapment Efficiency (DEE) and drug release behavior which was quantified as Mean Dissolution Time (MDT). The FCCCD was employed as it allowed for optimization utilizing only two formulation factors whereas the Box-Behnken design required a minimum of three formulation factors. In addition, The FCCCD method is efficient and flexible, providing sufficient information on the effects of variables and overall experimental error with a minimum number of experiments (Nasrollahzadeh *et al.,* 2007). Formulation factors were chosen as Drug Loading Time (DLT) and Secondary Crosslinking time (CLT) and the high and low levels of each factor was determined experimentally with the mid-ranged levels design generated. DEE and MDT at physiological pH were elucidate as the most crucial functional characteristics of the Starch-Based Platforms (SBP) and were thus selected as the measured responses for the design.

The initial aim of this Chapter was thus to statistically determine the optimum DLT and CLT necessary for maximum sulfasalazine (SSZ) entrapment while simultaneously retarding the release of SSZ to the greatest extent. Furthermore, in the subsequent segment of this Chapter, the optimized SSZ-loaded SBP was formulated and evaluated by various techniques in order to understand its functional and structural characteristics.

7.2. Optimization of functional characteristics of the SBP utilizing a Face Centred Central Composite Design

7.2.1. Materials

Materials used in this Chapter were as described in Chapter 5 and Chapter 6.

7.2.2. Preparation of covalent crosslinked SBP

SBP (80g) was accurately weighed, divided into 10g subsets and added to the experimental apparatus together with 50mL alkaline alcohol solution (40% EtOH: 5mL NaOH). The SBP subsets were then allowed to gel for 2 hours at a constant temperature of 25±1°C under constant stirring at 50rpm. Thereafter the gelled SBP subsets were removed from the gelatinization medium, lightly blotted with tissue paper to remove excess moisture and convection dried in a laboratory oven maintained at 50°C for 2 hours. Once dry, the separate gelatinized SBP subsets were mixed and samples (20g) were accurately weighed and divided into 10g samples, which were placed into the

experimental apparatus. Covalent crosslinking solution (5%, 50mL), prepared as described in Chapter 6, Section 6.2.4.1.3, was then introduced into the experimental apparatus and the SBP samples were allowed to crosslink under constant stirring at 50rpm for 2 hours at a constant temperature of 25±1°C. Thereafter the crosslinked SBP samples were removed from the crosslinking medium, lightly blotted with tissue paper to remove excess moisture and convection dried in a laboratory oven maintained at 50°C until constant mass was achieved. Once dry, the covalent crosslinked SBP subsets were mixed and samples (2g) were accurately weighed and subjected to drug entrapment.

7.2.3. Implementation and analysis of FCCCD

7.2.3.1. Generation of a FCCCD and subsequent analysis

Based on the time study conducted in Chapter 6, Section 6.2.5, it was determined that an increase in CLT resulted in a lower DEE but had favorable effects on the drug release behavior of the SBP. However, no enhancement of this effect was observed beyond 8 hours. With regard to the effect of increasing DLT, no notable difference was seen on the drug release behavior but an enhancement in DEE was observed until 8 hours after which the drug entrapment displayed a plateau. The upper and lower limits for the independent variables, DLT and CLT, were thus determined as depicted in Table 7.1.

Table 7.1: Independent variable limits and desired responses of (3^2) FCCCD

Independent variables	**Lower limit**	**Upper limit**	**-**
DLT (Hours)	1	8	-
CLT (Hours)	1	8	-
Response	**Lower limit**	**Upper limit**	**Objective**
DEE (%)	38	40	Maximize
MDT (Minutes)	160	170	Maximize

Where DLT denoted Drug loading Time, CLT denoted Secondary Crosslinking Time, DEE denoted Drug Entrapment Efficiency and MDT denoted Mean Dissolution Time

These limits were then employed as the basis of a 2-factor-3-level (3^2) full factorial FCCCD with an alpha value of 1 consisting of 13 formulations (4 cube points; 5 centre points; and 4 axial points) as depicted in Figure 7.2 and Table 7.2.

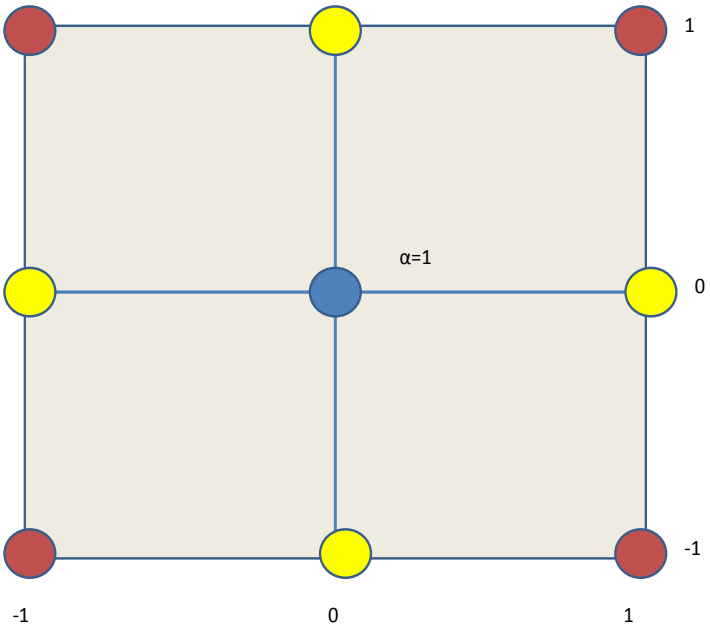


Figure 7.2: Schematic representation of design points for the 3^2 factor FCCCD.

Table 7.2: Design matrix for independent variables generated by the 3^2 factor FCCCD for double crosslinked SSZ-loaded SBP

Formulation	DLT (Hours)	CLT (Hours)
1	4.5	8.0
2	4.5	4.5
3	4.5	4.5
4	8.0	8.0
5	4.5	4.5
6	8.0	4.5
7	4.5	4.5
8	8.0	1.0
9	4.5	4.5
10	4.5	1.0
11	1.0	4.5
12	1.0	1.0
13	1.0	8.0

Where DLT denoted Drug loading Time and CLT denoted Secondary Crosslinking Time

These formulations were assessed to elucidate the effect of the experimental factors on the functional responses of the SBP. DEE and MDT at physiological pH were perceived as the most crucial functional characteristics of the SBP and were thus selected as the measured responses for the design. The objectives and corresponding limits of each response are depicted in Table 7.1. In addition to the above-mentioned responses, Quantity of Dug Entrapped (QDE) within the SBP was determined and the time required for 50% of drug to be released (T_{50}) was calculated according to the linearized Korsmeyer-Peppas model as described by Equation 7.1.

$$\log 50 = \log K + n \log t$$ ***Equation 7.1***

Where:
t = Time at which 50% of drug is released
K_P = Experimentally determined Korsmeyer-Peppas release constant
n = Experimentally determined Korsmeyer-Peppas diffusion constant

7.2.3.2. Drug entrapment into experimental design formulations

Aliquots of SSZ solution (75mg.mL^{-1}; 5mL) were prepared as described in Chapter 6, Section 6.2.4.2 and accurately measured into separate experimental apparatuses. Pre-gelatinized covalent crosslinked SBP samples (2g) were accurately weighed, submerged into the experimental apparatus containing drug solution, and allowed to entrap drug under constant stirring at 50rpm at 25±1°C. At the specified time, Epichlorohydrin (ECH) solution (99%$^{v}/_{v}$; 0.25mL) was added to the drug-loaded SBP and allowed to crosslink under constant stirring at 50rpm at 25±1°C. DLT and CLT for each formulation were specified in the design matrix (Table 7.2). The double crosslinked drug-loaded SBP were then subjected to the procedure as described in Chapter 6, Section 6.2.3.4. The extent of drug entrapment was determined as described in Chapter 2, Section 2.2.8.2.2 with UV analysis conducted at the maximum excitation wavelength of SSZ (λmax=359nm).

7.2.3.3. In vitro drug release behavior from experimental design formulations

Determination of the *in vitro* drug release behavior was conducted as described in Chapter 6, Section 6.2.4.7. In order to analyze the dissolution data of the various experimental formulations quantitatively, the model independent approach, Mean Dissolution Time (MDT), was calculated for each formulation. MDT was defined as the sum of different release fraction periods obtained for dissolution studies endured in simulated physiological fluids, divided by the initial loading dose and represented by Equation 7. 2.

$$MDT = \sum_{t=1}^{n} ti \frac{M_t}{M_\infty}$$ ***Equation 7.2***

Where:
MDT = Mean dissolution time (min)
$\frac{M_t}{M_\infty}$= Fractional drug release at time t_i
$t_i = (t_i - t_{i-1}) / 2$
M_∞ = Loading dose

A maximum MDT refers to the fastest drug release achievable

Measurements of the responses from the experimental formulations displayed similar drug-loading potential (ADL~140-157mg per 2g SBP and DEE ~37-42%) throughout the design (Table 7.3). However, Formulation 8, which was formulated with the highest DLT and lowest CLT, was identified as an outlier displaying ADL~175mg per 2g SBP and DEE ~47%. Formulations 4 and 8, which underwent longer drug-loading and shorter crosslinking, displayed higher DEE values compared to the other formulations. The drug release profiles of all the experimental formulations (Figure 7.3) were also observed to be similar and MDT values ranged between ~136-188 minutes. Formulations 1 and 13, which underwent longer crosslinking, displayed higher MDT values and were thus able to control drug release to the greatest extent. T_{50} values from each of the formulations varied considerably and ranged between ~145-823 minutes with no trend observed. The shape of the dug release profile was due to the varying solubility of SSZ in acidic and alkaline pH. Within the acidic pH of Simulated Gastric Fluid (SGF) (t=0-2 hours), only surface bound drug was released with very little core drug entering the dissolution medium. As soon as the drug-loaded SBP entered the more alkaline pH of Simulated Intestinal Fluid (SIF) (t>2 hours) an immediate increase in drug release was observed with the different formulations exhibiting varying levels of control. This level of initial control was closely related to the final fraction of drug released, as subsequent release patterns from all the experimental formulations were similar.

Table 7.3: Measured responses for experimental SBP formulations

Experimental formulation	DEE (%)	MDT (min)	QDE (mg)	T_{50} (min)
1	38.799	173.669	145.497	317.0033
2	40.545	156.040	152.045	405.7233
3	40.555	159.434	152.080	326.2843
4	41.819	170.614	156.823	548.2959
5	40.367	155.287	151.376	409.0642
6	39.736	168.749	149.011	145.5177
7	40.623	156.404	152.336	822.4685
8	46.750	148.797	175.311	194.5157
9	40.948	154.981	153.553	239.6216
10	41.634	145.219	156.126	338.1862
11	37.592	167.329	140.970	242.9171
12	39.484	136.915	148.066	204.6391
13	37.430	187.978	140.362	265.6204

Where DEE denoted Drug Entrapment Efficiency and MDT denoted Mean Dissolution Time, QDE denoted the Quantity of Drug Entrapped and T_{50} required for 50% of drug to be released. (n=3 in all instances, standard deviations were within: DEE±0.596, MDT±2.476, QDE±4.112, T_{50}±12.487)

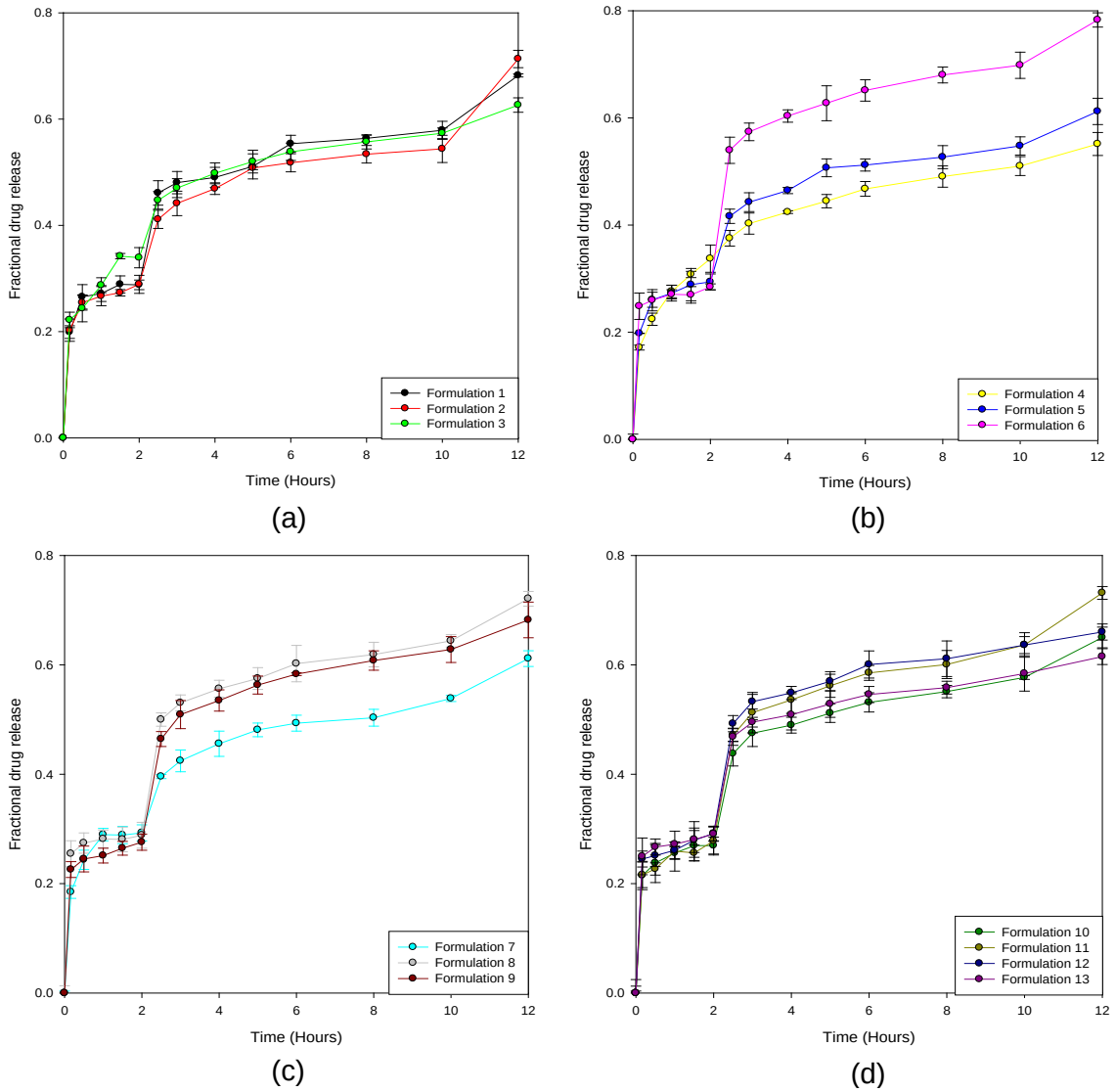


Figure 7.3: Composite drug release profiles (a-d) of design generated double crosslinked SBP formulations in SGF and SIF (n=3 in all instances).

7.2.3.4. Elucidation of mechanism of drug release of the design formulations

In order to elucidate the release kinetics and further understand the mechanism that facilitated drug release from the SBP, the results from the drug release study were fitted into various mathematical models described in Sections 7.2.3.4.1 - 7.2.3.4.5. Upon analysis, the model that displayed the best fit to the dissolution data (correlation coefficient, R^2 most closely = 1) was selected as the model describing the drug release from the SBP. Since drug release was performed in a sequential manner, the drug release kinetics of the SBP was determined in SGF, SIF and complete sequential dissolution.

7.2.3.4.1. Zero-order release model

This model describes the ideal drug release model where drug is released at a constant rate from the delivery device and is independent of drug concentration. Equation 7.3 describes the zero order model.

$$\frac{M_t}{M_\infty} = Q_{0_z} + K_z t \qquad \textbf{Equation 7.3}$$

Where:
$\frac{M_t}{M_\infty}$ *= Fraction of drug released at time t*
Q_{0_z} *= Initial drug in solution*
K_z *= Zero order release constant*

Linearization can be graphically portrayed by plotting fractional release against time with the K_z = slope of the graph and the burst release (if present) represented by the y-intercept (Q_{0_z}).

7.2.3.4.2. First order release model

The first order drug release model describes drug release that is dependent on the amount of drug remaining within the drug delivery system and is often fitted to highly water soluble drug incorporated into porous matrices. Equation 7.4 describes the First order model.

$$\frac{M_t}{M_\infty} = Q_{0_1} e^{-K_1 t} \qquad \textbf{Equation 7.4}$$

Where:
$\frac{M_t}{M_\infty}$ *= Fraction of drug remaining at time t*
Q_{0_1} *= Initial drug in solution*
K_1 *= First order release constant*

Linearization can be graphically portrayed by plotting logarithm of fraction of drug release against time (Equation 7.5) with the K_1 = slope of the graph and the burst release (if present,(Q_o)) calculated by subtracting the antilogarithm of the y-intercept from total drug in drug delivery device.

$$\log \frac{M_t}{M_\infty} = \log Q_{0_1} + \frac{Kt}{2.303} \qquad \textbf{Equation 7.5}$$

7.2.3.4.3. Higuchi model

The Higuchi model is one of the most often used in determining drug release kinetics and if obeyed, describes drug release that is controlled by diffusion. Equation 7.6 describes the Higuchi model**.**

$$\frac{M_t}{M_\infty} = K_H t^{\frac{1}{2}}$$ ***Equation 7.6***

Where:
$\frac{M_t}{M_\infty}$ *= Fraction of drug released at time t*
K_H *= Higuchi release constant*

If the drug release obeys the Higuchi model, a linear plot of fractional drug release and the square root of time will be achieved with K_H = slope of the graph.

7.2.3.4.4. Korsmeyer-Peppas model

The Korsmeyer-Peppas model is used to determine and explain drug release from polymers and is commonly known as the "power law" as it relates the release of drug exponentially to time. However, this model has a limitation in that it can only analyze the release data up to ~60-70% of total drug release. Equation 7.7 describes the Korsmeyer-Peppas model.

$$\frac{M_t}{M_\infty} = Q_{0_p} + K_P t^n$$ ***Equation 7.7***

Where:
$\frac{M_t}{M_\infty}$ *= Fraction of drug released at time t*
Q_{0_p} *= Initial drug in solution*
K_P *= Peppas release constant*
n *= Diffusion constant*

In Equation 7.7 K_P is an experimental constant that is characteristic of the structure and geometry of the drug delivery system and n is the diffusion constant that characterizes the drug release mechanism of the drug delivery system. The value of n describes whether drug is released primarily by diffusion, polymer relaxation (characteristic of swelling drug delivery systems) or a combination of both processes (anomalous drug release) as described in Table 7.4.

Table 7.4: Interpretation of $\boldsymbol{n}$ value with regard to the mechanism of drug release from delivery systems with differing geometries

n value				Rate as function of time	Drug release mechanism
Slab	**Thin film**	**Cylinder**	**Sphere**		
$0 < n < 0.5$	$0 < n < 0.5$	$0 < n < 0.45$	$0 < n < 0.43$	-	Quasi-Fickian Diffusion
0.5	0.5	0.45	0.43	$t^{0.5}$	Fickian diffusion
$0.5 < n < 1$	$0.5 < n < 1$	$0.45 < n < 0.89$	$0.5 < n < 0.85$	t^{n-1}	Anomalous drug release
1	1	0.89	0.85	t^{1}	Zero order Case II transport
> 1	> 1	> 0.89	> 0.85	t^{n-1}	Super Case II transport

Where n denoted the diffusion constant

K_P and n can be determined through linearization of Equation 7.7, achieved by plotting logarithm of fraction of drug released against the logarithm of time, with the n = slope of the graph and K_P = antilogarithm of the y-intercept (Equation 7.8).

$$\log\left(\frac{M_t}{M_\infty} - Q_{0_p}\right) = \log K_p + n \log t \qquad \textbf{\textit{Equation 7.8}}$$

7.2.3.4.5. Hixson-Crowell model

The Hixson-Crowell model describes drug release that is dependent on the drug solubility rather than its diffusion and is related to the surface area and volume of the drug delivery system. An important pre-requisite of the Hixson-Crowell model is the maintenance of device geometry and is described by Equation 7.9.

$$W_{0_{HC}}^{\frac{1}{3}} - W_t^{\frac{1}{3}} = K_{HC} t \qquad \textbf{Equation 7.9}$$

Where:
W_t= Amount of drug released at time t
$W_{0_{HC}}$ = Initial drug in drug delivery system
K_{HC} = Hixson-Crowell release constant defining surface to volume relationship

Linearization can be graphically portrayed by plotting the cube root of drug released against time with the K_{HC} = slope of the graph and the burst release (if present,(W_o)) calculated by subtracting the cube of the y-intercept from total drug in drug delivery device.

Analysis of fits of the dissolution data in SGF, SIF and sequentially in SGF and SIF to each of the kinetic models described above is depicted in Table 7.5, Table 7.6 and Table 7.7 with the R^2 values used to determine the model displaying the best fit. The R^2 values of the zero order model of 0.75-0.89, 0.90-0.96 and 0.81-0.93 in SGF, SIF and sequentially, respectively, showed that drug release does not follow a zero order profile, which was expected and in line with the observations made in the drug release profiles depicted in Figure 7.3. The R^2 values of the first order model showed values of 0.77-0.89, 0.91-0.96 and 0.87-0.94, in SGF, SIF and sequentially, respectively which were slightly higher than zero order but lower than the R^2 values of 0.84-0.95, 0.92-0.97 and 0.89-0.95 in SGF, SIF and sequentially, respectively, demonstrated by the Korsmeyer-Peppas model. This theorised the drug release to be diffusion controlled and the notion was strengthened by the exclusion of drug solubility dependent release supported by the drug Hixson-Crowell model, which displayed R^2 values of 0.73-0.89, 0.92-0.96 and 0.84-0.94 in SGF, SIF and sequentially, respectively. However, with R^2 values of 0.91-0.99, 0.94-0.99 and 0.91-0.98 in SGF, SIF and sequentially, respectively, the dissolution data was found to best fit the Higuchi model and thus SSZ release was deemed to be diffusion controlled.

The value of n from the Korsmeyer-Peppas model was consistently found to be less than 0.5 in SGF (Table 7.5), and particularly below 0.43 as the SBP portrayed a generally spherical geometry, which implied that quasi-diffusion was the sole mechanism of drug release in the initial stages. In SIF (Table 7.6), the n values of the design formulations were consistently between 0.43 and 0.85 and implied that anomalous drug transport was the mechanism of drug release. Anomalous drug transport involves both diffusion of drug through the matrix of the SBP as well as relaxation of intrinsic bonds of the SBP as a result of hydration and swelling. This was not surprising as previous studies on the SBP showed that hydration was an important parameter in the formulation of the SBP and that the alkaline natured SIF possessed the ability to penetrate the SBP and facilitate drug release. The n values of between 0.43 and 0.85 in Table 7.7 showed that drug release in the latter stages i.e. in SIF imparted a much more pronounced effect on the drug release as further evidenced by the drug release profiles in Figure 7.3.

Table 7.5: *In vitro* SSZ release kinetics of experimental formulations in SGF

Formulation	Zero order model			First order model			Higuchi model		Korsmeyer-Peppas model			Hixson-Crowell model		
	K_z	Q_{0_z}	R^2	K_1	Q_{0_1}	R^2	K_H	R^2	K_p	n	R^2	K_{HC}	$Q_{0_{HC}}$	R^2
1	0.077	21.702	0.764	-0.0005	21.837	0.779	1.175	**0.913**	2.244	0.306	0.864	-0.0015	21.707	0.774
2	0.065	21.641	0.789	-0.0004	21.657	0.801	0.995	**0.955**	1.574	0.344	0.885	-0.0012	21.652	0.797
3	0.069	21.393	0.824	-0.0004	21.476	0.837	1.044	**0.976**	1.271	0.398	0.915	-0.0013	21.377	0.832
4	0.105	16.854	0.821	-0.0006	16.824	0.839	3.057	**0.993**	1.892	0.404	0.872	-0.0019	16.833	0.833
5	0.075	21.598	0.756	-0.0004	21.657	0.770	1.156	**0.981**	2.075	0.321	0.867	-0.0014	21.542	0.736
6	0.073	21.626	0.793	-0.0004	21.657	0.807	1.116	**0.971**	1.742	0.347	0.890	-0.0014	21.652	0.802
7	0.088	19.668	0.817	-0.0005	19.832	0.832	1.346	**0.994**	1.603	0.403	0.913	-0.0017	19.658	0.827
8	0.054	22.993	0.786	-0.0003	23.087	0.797	1.579	**0.969**	1.321	0.342	0.842	-0.0001	23.017	0.793
9	0.077	21.486	0.829	-0.0005	21.476	0.842	1.169	**0.979**	1.340	0.410	0.919	-0.0015	21.487	0.838
10	0.051	22.389	0.819	-0.0003	22.375	0.828	0.761	**0.993**	1.153	0.414	0.917	-0.0009	22.419	0.825
11	0.063	21.321	0.811	-0.0003	21.476	0.822	0.911	**0.993**	1.153	0.392	0.909	-0.0011	21.322	0.818
12	0.067	21.642	0.885	-0.0004	21.657	0.895	0.997	**0.959**	1.312	0.407	0.951	-0.0013	21.652	0.891
13	0.061	23.645	0.843	-0.0004	23.616	0.853	0.925	**0.995**	1.186	0.387	0.934	-0.0012	23.667	0.855

Table 7.6: *In vitro* SSZ release kinetics of experimental formulations in SIF

Formulation	Zero order model			First order model			Higuchi model		Korsmeyer-Peppas model			Hixson-Crowell model		
	K_z	Q_{0_z}	R^2	K_1	Q_{0_1}	R^2	K_H	R^2	K_p	n	R^2	K_{HC}	$Q_{0_{HC}}$	R^2
1	0.039	38.817	0.918	-0.0004	36.027	0.925	1.491	**0.951**	0.619	0.615	0.936	-0.0001	37.145	0.922
2	0.034	37.265	0.912	-0.0002	38.482	0.921	1.368	**0.955**	0.410	0.670	0.937	-0.0008	36.335	0.929
3	0.036	38.294	0.941	-0.0003	36.173	0.956	1.456	**0.964**	0.604	0.622	0.957	-0.0001	37.003	0.953
4	0.055	34.618	0.956	-0.0005	30.498	0.963	1.988	**0.985**	0.220	0.803	0.976	-0.0005	32.183	0.971
5	0.031	38.253	0.919	-0.0003	28.386	0.939	1.233	**0.942**	0.627	0.593	0.941	-0.0008	37.382	0.927
6	0.049	43.221	0.926	-0.0006	37.913	0.944	1.958	**0.968**	0.863	0.615	0.956	-0.0015	40.178	0.949
7	0.031	36.703	0.930	-0.0003	35.137	0.935	1.247	**0.961**	0.530	0.612	0.949	-0.0008	35.663	0.939
8	0.044	41.048	0.923	-0.0005	34.385	0.925	1.769	**0.949**	0.843	0.602	0.939	-0.0013	38.604	0.928
9	0.038	41.684	0.902	-0.0004	39.466	0.923	1.531	**0.945**	0.767	0.674	0.931	-0.0001	40.361	0.929
10	0.039	37.934	0.956	-0.0004	35.286	0.959	1.563	**0.990**	1.279	0.516	0.975	-0.0001	36.335	0.966
11	0.046	37.345	0.902	-0.0005	33.930	0.911	1.867	**0.949**	0.378	0.724	0.933	-0.0013	35.326	0.923
12	0.051	38.202	0.924	-0.0006	33.626	0.932	2.047	**0.965**	0.315	0.762	0.957	-0.0014	35.374	0.946
13	0.034	42.793	0.944	-0.0004	40.707	0.921	1.348	**0.954**	1.268	0.514	0.941	-0.0009	41.499	0.926

Table 7.7: *In vitro* SSZ release kinetics of experimental formulations sequentially in SGF and SIF

Formulation	Zero order model			First order model			Higuchi model		Korsmeyer-Peppas model			Hixson-Crowell model		
	K_z	Q_{0_z}	R^2	K_1	Q_{0_1}	R^2	K_H	R^2	K_p	n	R^2	K_{HC}	$Q_{0_{HC}}$	R^2
1	0.062	27.023	0.863	-0.0005	25.527	0.881	2.006	**0.941**	0.497	0.706	0.901	-0.0015	26.123	0.890
2	0.056	26.303	0.857	-0.0004	25.527	0.896	1.833	**0.943**	0.338	0.753	0.908	-0.0013	25.806	0.905
3	0.061	26.355	0.861	-0.0005	25.183	0.906	1.976	**0.943**	0.307	0.789	0.916	-0.0014	25.647	0.899
4	0.073	23.044	0.933	-0.0006	20.750	0.943	2.373	**0.973**	0.635	0.692	0.948	-0.0017	21.707	0.942
5	0.053	27.057	0.841	-0.0004	26.379	0.892	1.763	**0.937**	0.564	0.669	0.907	-0.0012	26.598	0.876
6	0.081	27.183	0.858	-0.0008	23.967	0.882	2.639	**0.935**	0.267	0.746	0.915	-0.0021	25.435	0.904
7	0.054	25.775	0.851	-0.0004	25.011	0.901	1.769	**0.943**	0.664	0.646	0.924	-0.0012	25.275	0.885
8	0.072	27.133	0.862	-0.0006	24.664	0.892	2.341	**0.939**	0.154	0.713	0.907	-0.0018	25.753	0.873
9	0.067	27.442	0.838	-0.0006	26.039	0.902	2.192	**0.931**	0.338	0.784	0.912	-0.0016	26.650	0.845
10	0.060	26.597	0.817	-0.0005	25.698	0.877	1.963	**0.902**	0.134	0.734	0.890	-0.0014	26.018	0.858
11	0.071	25.238	0.879	-0.0006	23.264	0.935	2.282	**0.945**	0.179	0.683	0.938	-0.0017	24.044	0.918
12	0.076	25.783	0.891	-0.0007	23.087	0.923	2.444	**0.967**	0.153	0.727	0.939	-0.0019	24.206	0.934
13	0.062	28.827	0.831	-0.0005	27.723	0.896	2.036	**0.918**	0.202	0.755	0.908	-0.0015	28.112	0.875

Where K_z denoted the zero order model constant, Q_{0_z} denoted the initial drug in solution according to the zero order model, K_1 denoted the First order model constant, Q_{0_z} denoted the initial drug in solution according to the First order model, K_H denoted the Higuchi constant, K_p denoted the Korsmeyer-Peppas constant, n denoted the diffusion constant, K_{HC} denoted the Hixson-Crowell constant, $Q_{0_{HC}}$ denoted the initial drug in solution according to the Hixson-Crowell model and R^2 denoted the correlation coefficients of each of the models in Table 7.5, Table 7.6 and Table 7.7

7.2.3.5. Evaluation of the similarity of the drug release profiles

Similarity of the drug release profiles was tested using a pair wise method which involved determining the similarity factor and difference factor for each of the drug release profiles (Costa and Lobo, 2001). The difference factor (*F1)*, which was used to measure percent difference between the profiles at all time points, is described by Equation 7.10 with values between 0-15 implying similarity between the profiles.

$$F1 = \frac{\sum_{j=1}^{n}|R_j - T_j|}{\sum_{j=1}^{n}|R_j|} \qquad \textbf{Equation 7.10}$$

Where:
n *= The sampling number*
R_j*= Percent of drug released from the reference*
T_j *= Percent of drug released from the test*
j *= Time point*

The similarity factor (*F2*) as defined by Food and Drug Administration of the United States (FDA) and European Medicines Agency (EMEA) is a logarithmic reciprocal square root transformation of one plus the mean squared (the average sum of squares) differences of drug percent dissolved between the test and the reference product at all time points and is described by Equation 7.11. An F2 value between greater than 50 is implies similarity between the profiles with values close to 100 referring to increased similarity.

$$F2 = 50\ X \log\left\{\left[1 + \left({}^{1}/_{n}\right)\sum_{j=1}^{n}\left|R_j - T_j\right|^2\right]^{-0.5} X\ 100\right\} \qquad \textbf{Equation 7.11}$$

Where:
n *= The sampling number*
R_j*= Percent of drug released from the reference*
T_j *= Percent of drug released from the test*
j *= Time point*

Comparisons between the drug release profiles were performed utilizing the similarity factor as well as the difference factor. Formulation 1 was employed as the reference and Table 7.8 depicts the *F1* and *F2* values for Formulations 2-13 which were tested against Formulation 1. For each of the formulations, *F1* and *F2* were found to be between 0-15 and 50-100 respectively, and thus the formulations were concluded to be similar. In addition, the model constants and burst release depicted in Table 7.8 showed similar values for all of the formulations and further supported the similarity of the formulations.

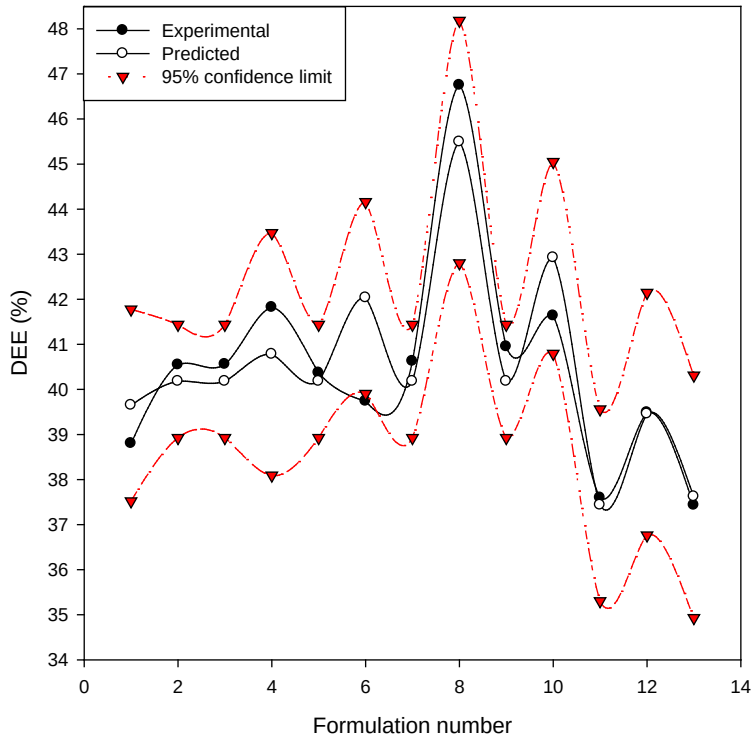
Table 7.8: Difference and similarity factors of the SSZ release profiles of the experimental formulations

Formulation	*F1*	*F2*
1	-	-
2	5.019	75.963
3	2.148	89.105
4	2.268	73.397
5	4.745	76.600
6	12.110	58.020
7	7.571	70.985
8	6.694	69.913
9	4.044	77.503
10	1.266	85.635
11	1.267	76.771
12	5.677	68.060
13	4.279	77.790

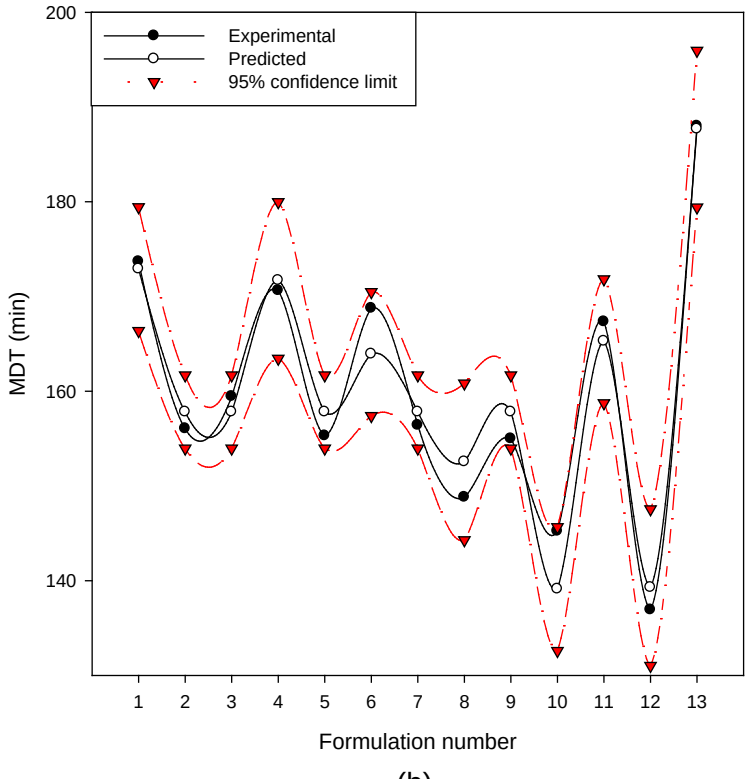
Where F1 denoted the difference factor and F2 denoted the similarity factor

7.2.3.6. Comparative analysis between experimental and predicted values for the design generated SBP formulations

Experimental results of each of the design formulations were plotted against the design predicted value for both responses, DEE and MDT, with resultant R^2 values of 0.823 and 0.950, respectively obtained. These R^2 values showed that a good correlation between the experimental and predicted values was achieved and thus authenticated the FCCCD used. In addition, the lower and upper 95% confidence limits were plotted in Figure 7.4. When compared to the experimental values attained, it was observed that all experimental values fell within the 95% confidence limits with regard to both DEE and MDT, further validating the FCCCD used.



(a)



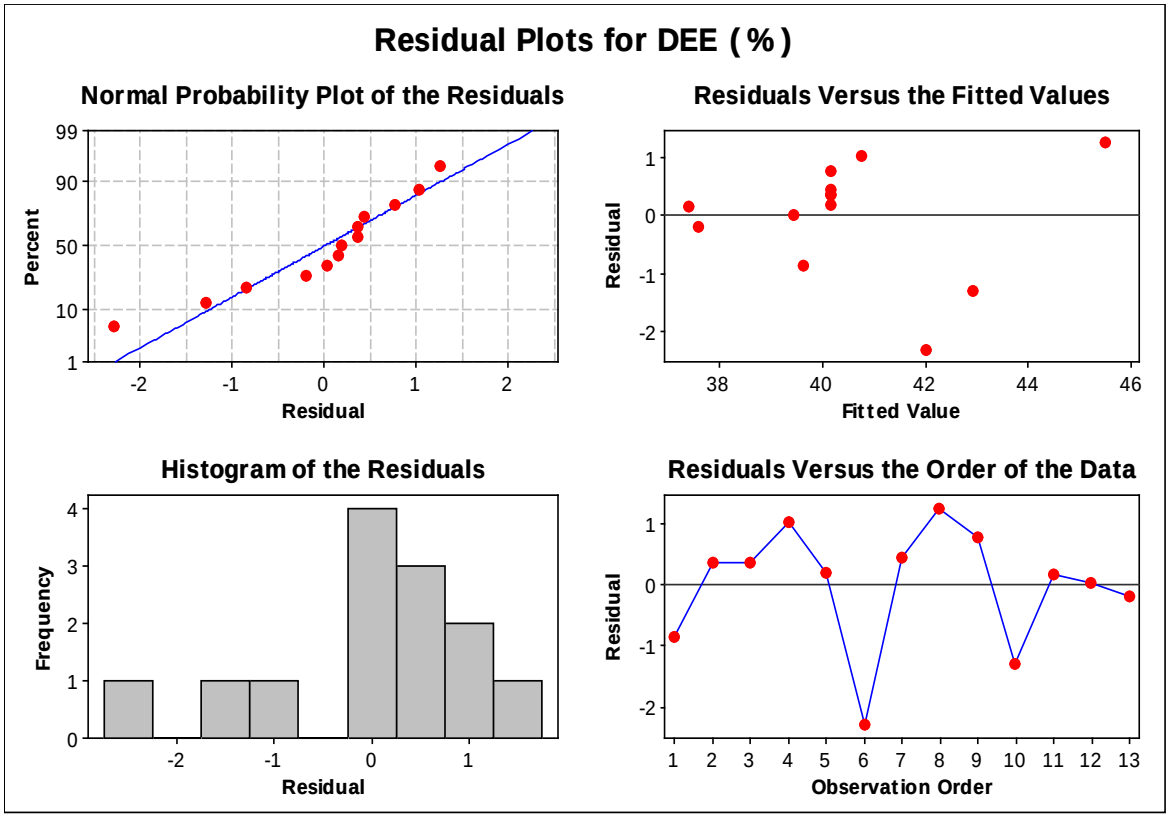
(b)

Figure 7.4: Regression plots comparing experimental and fitted values ±95% confidence interval for a) DEE and b) MDT.

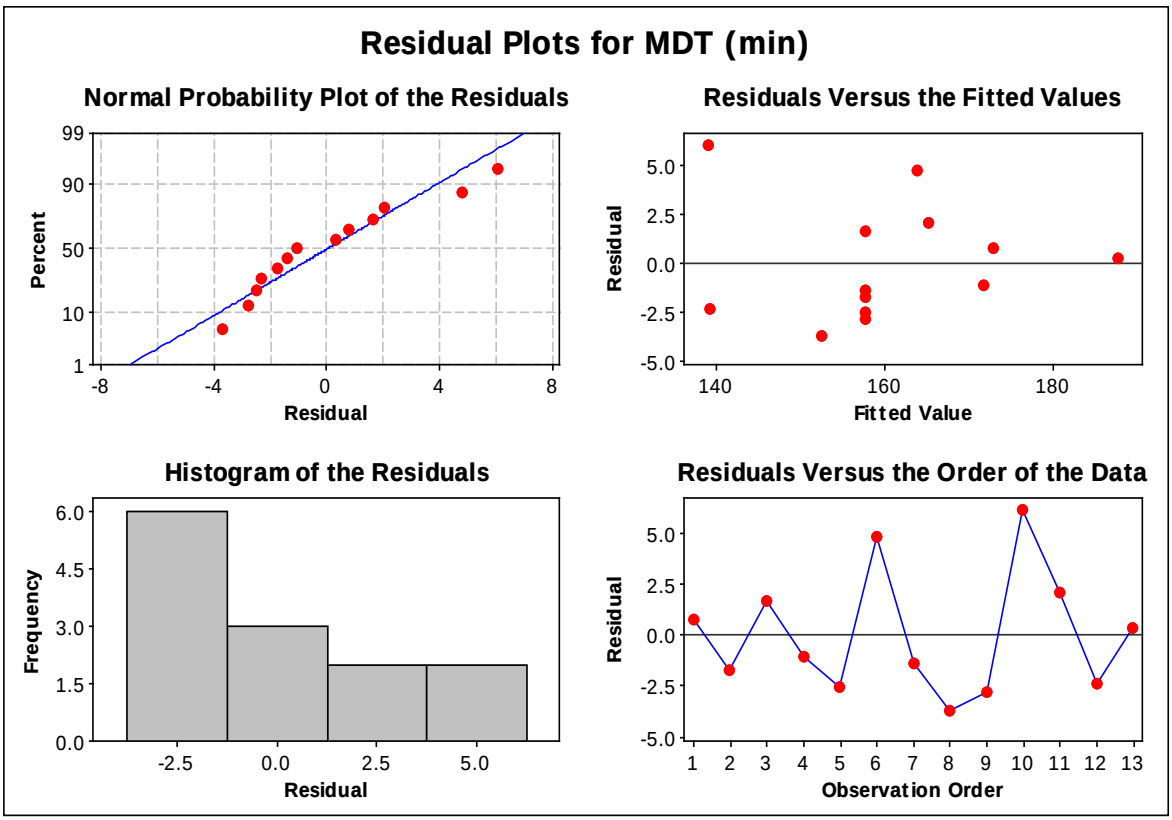
7.2.3.7. Analysis of Face Centred Central Composite Design

7.2.3.7.1. Residual analysis

Diagnostic residual analysis of the FCCCD was conducted in order to evaluate the suitability and robustness of the design and is depicted in Figure 7.5. Residuals with smaller values were desirable as they indicated less variance and higher design accuracy. Analysis of the normal probability plot of the residuals showed that the residuals fell on a straight line, thus confirming the normal distribution of data for both DEE and MDT. The histogram of the residuals for DEE confirmed the normal distribution with the mean at zero and constant variance. The histogram of the residuals for MDT also showed normal distribution with a mean of -2.5 and displayed positive skewness indicating a degree of non-constant variance. The residuals and standardized residuals indicated that the majority of cases were adequately fitted by the response surface model and only two outliers each, for DEE and MDT, in the form of Formulations 6 and 8 and Formulations 8 and 10 were found, respectively. The residuals versus fitted plot for both DEE and MDT showed randomly scattered residual data points around the horizontal line (residual = 0), with some fanning indicative of a degree of non-constant variance. Analysis of the residuals versus the order of the data was used to identify non-random error for DEE and MDT. The DEE plot showed both positive (clustering of Formulations 2-5) and negative correlation indicated by rapid changes in the signs (-/+) of the consecutive residuals. Similarly, the MDT plot displayed both positive (slight clustering of Formulations 7-9) and negative correlation for the remainder of the residuals.



(a)



(b)

Figure 7.5: Residual plots for (a) DEE and (b) MDT.

Table 7.9 illustrated the factor coefficient and significance of each term on the measured response. The positive coefficients of DLT and CLT x CLT implied direct correlation to the DEE (i.e. increasing the value of these terms would result in an increase in the response) while the negative coefficients of CLT, DLT x DLT and DLT x CLT implied inverse correlation to the DEE response (i.e. increasing the value of these terms would result in a decrease in the response). However, only the linear terms DLT and CLT had significant effect ($p<0.05$) on the DEE of the SBP with the quadratic and interaction terms having a much less significant effect on the DEE as their respective p-values are greater than 0.05.

With regard to the MDT regression terms, the positive coefficients of CLT, DLT x DLT and DLT x CLT implied direct correlation to the MDT while the negative coefficients of DLT and CLT x CLT implied inverse correlation to the MDT response. Furthermore, only the linear term CLT, the quadratic term DLT x DLT and the interaction term DLT x CLT displayed significance on MDT ($p<0.05$), whereas the effect DLT and CLT x CLT on the MDT response was deemed insignificant ($p>0.05$).

Overall, the DLT term was only significant in increasing DEE and had minimal significance in affecting the MDT as drug was merely incorporated into the SBP with minimal fortification of the bonds between the polymer chains and SSZ at this stage in the formulation process. In contrast, the term CLT was significant in decreasing DEE and increasing MDT, which could be due to the contraction and stabilization of bonds between the polymer chains and SSZ during crosslinking and thus reduced hydration capacity and drug-loading but afforded the SBP increased control over the release of SSZ incorporated into the SBP. Additionally, the regression models illustrated in Equation 7.12 and Equation 7.13 for DEE and MDT showed p-values of 0.015 and 0.000 respectively, indicating significant collective effect on the responses and combined with the R^2 values of 0.823 and 0.950 respectively, further affirmed the robustness of the design.

Table 7.9: ANOVA analysis indicated estimated regression coefficients and P-values for DEE and MDT

Term	DEE		MDT	
	Factor coefficient	**P-values**	**Factor coefficient**	**P-values**
Constant	40.180	0.000	157.805	0.000
DLT	2.299	0.003	-0.677	0.686
CLT	-1.636	0.017	16.888	0.000
DLT x DLT	-0.448	0.579	6.793	0.024
CLT x CLT	1.104	0.195	-1.802	0.471
DLT x CLT	-0.719	0.298	-7.312	0.007

Where DEE denoted Drug Entrapment Efficiency, MDT denoted Mean Dissolution Time, DLT denoted Drug-Loading Time and CLT denoted Secondary Crosslinking Time

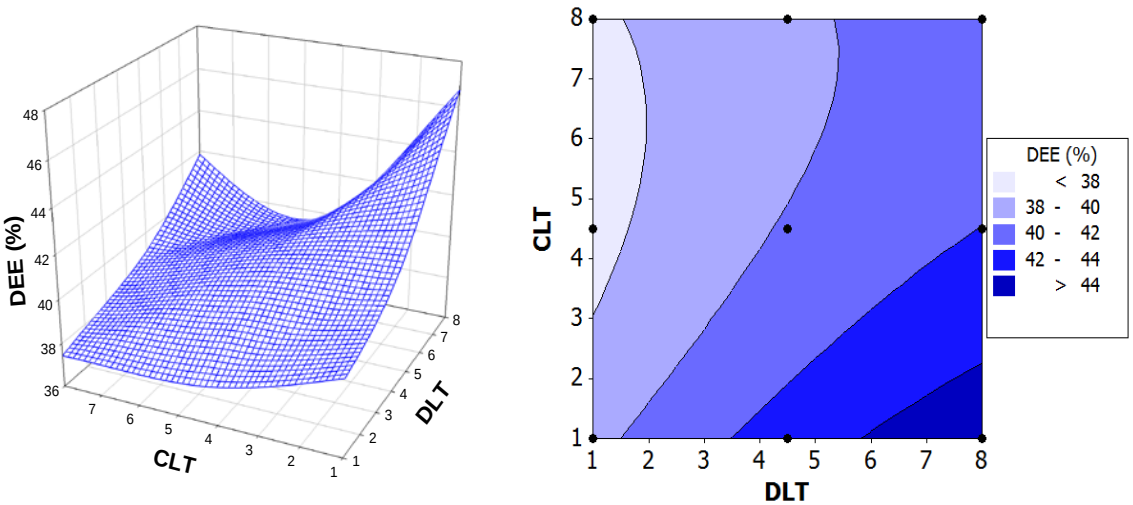
The complete regression equations representing the relationship between the independent variables and the responses of DEE and MDT are described by:

$$DEE = 40.180 + 2.299\,(DLT) - 1.636\,(CLT) - 0.448\,(DLT)\,(DLT) + 1.104\,(CLT)\,(CLT) - 0.719\,(DLT)\,(CLT) \quad \textbf{Equation 7.12}$$

$$MDT = 157.805 - 0.677\,(DLT) + 16.888\,(CLT) + 6.793\,(DLT)\,(DLT) - 1.802\,(CLT)\,(CLT) - 7.312\,(DLT)\,(CLT) \quad \textbf{Equation 7.13}$$

7.2.3.7.2. Response analysis of DEE for SSZ-entrapped SBP

The DEE response of the double crosslinked SBP was dependent on the amount of time exposed to drug solution as well as the amount of time exposed to secondary crosslinking solution. Figure 7.6a and Figure 7.6b showed that DEE portrayed a positive correlation with DLT depicted by the increased DEE as the DLT was increased. Conversely, CLT portrayed a negative correlation with DEE depicted by the decreased DEE as the CLT was increased. Thus, DEE > 44% was obtained by subjecting the SBP to DLT greater than 6 hours and CLT less than 2 hours with maximum DEE of 47% achieved at 8 hours and 1 hour for DLT and CLT, respectively. There was an interesting observation in Figure 7.6a where at CLT=8 hours DLT=8 hours resulted in a local DEE maxima of 42%. This could be attributed to fortification of the interactions between the SBP and SSZ.

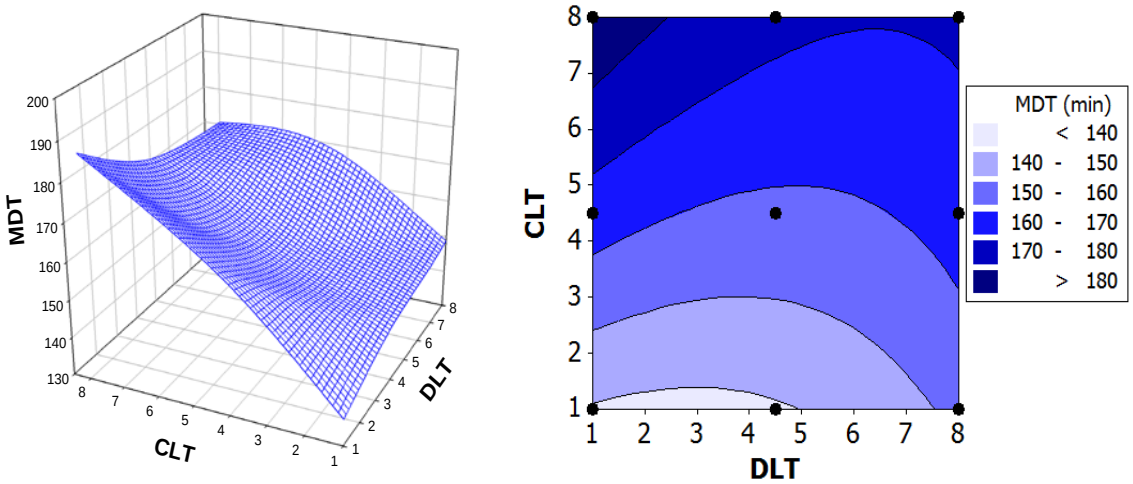


(a) (b)

Figure 7.6: Correlation of DEE with DLT and CLT utilizing (a) Response surface plot and (b) contour plot.

7.2.3.7.3. Response analysis of MDT for SSZ-entrapped SBP

Contrary to the effects of DLT and CLT on the DEE response, DLT was shown to render a negative correlation on MDT while CLT rendered a very positive correlation on the MDT of the double crosslinked SBP. This was depicted in Figure 7.7a and Figure 7.7b by the increased MDT as the CLT was increased and the decreased MDT as the DLT was increased. Thus MDT>180 minutes was obtained by subjecting the SBP to CLT greater than 7 hours and DLT less than 2 hours with maximum MDT of 186 minutes achieved 8 hours and 1 hour for CLT and DLT, respectively. Interestingly, it was observed in Figure 7.7b that relatively high MDT values of between 170-180min were achieved at simultaneously high DLT (> 6 hours) and CLT (> 7 hours) values.



(a) (b)

Figure 7.7: Correlation of DEE with DLT and CLT utilizing (a) Response surface plot and (b) contour plot.

7.2.4. Response optimization of the double crosslinked SSZ loaded SBP

Response optimization was conducted on MINITAB®, (V15, Minitab Inc, Pennsylvania, USA) in order to elucidate the optimal independent parameters for the formulation of SBP displaying maximal drug entrapment capacity while offering maximal retardation of SSZ release. Figure 7.8 showed the optimal levels of the independent variables and predicted values for each measured response with its accompanying statistical desirability. The composite statistical desirability of the formulation was 1 and thus authenticated the congruency of the factor levels of each response.

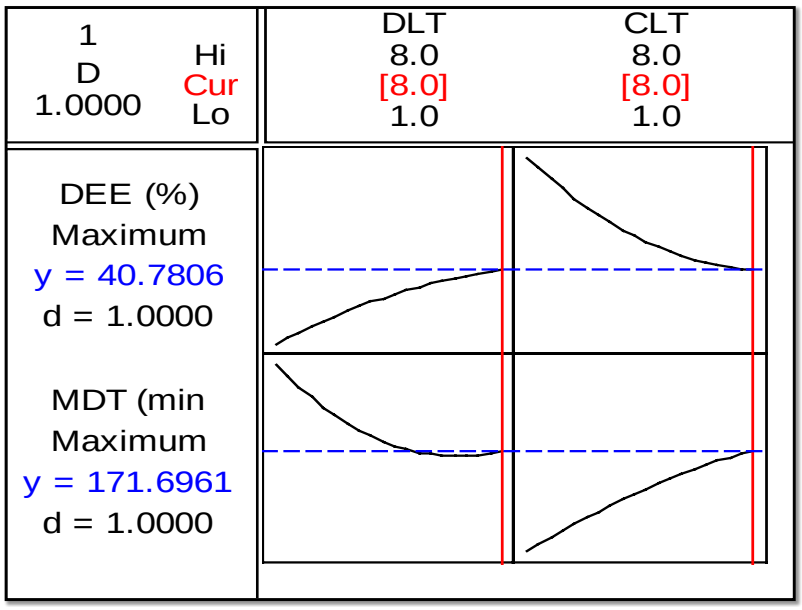


Figure 7.8: Optimization plots of the SBP indicating optimal factors, factor levels and desirability.

7.3. Evaluation of the Characteristics of the Optimized Double ECH-Crosslinked SBP

7.3.1. Materials and Methods

7.3.1.1. Materials

Materials used in this section of the Chapter were as described previously in Section 7.2.1.

7.3.1.2. Determination of the SSZ entrapment potential of the optimized double crosslinked SBP

Formulation of pre-gelatinized-covalently crosslinked SBP, drug entrapment and secondary crosslinking was preformed as described for the design formulations with optimized time constraints of 8 hours each for both formulation parameters (Figure 7.8). Furthermore, up-scaling of the formulation process was conducted by drug-loading pre-gelatinized-covalently crosslinked SBP samples (10g) (as prepared in Section 7.2.2) in SSZ solution (75mg.mL^{-1}; 25mL) and increasing the quantity of ECH used for secondary crosslinking to 1.25mL in order to maintain the ratios of the optimized formulation. DLT and CLT remained at 8 hours and 8 hours respectively, and procedure for determining the extent of drug entrapment remained unchanged. The study was conducted in triplicate (n=3).

7.3.1.3. Microscopic analysis of the surface and core of the optimized SBP

Due to the color of the SSZ, coloration of the areas of the SBP where drug was incorporated was expected. Microscopic analysis was conducted using an Olympus® Stereo Microscope (Model SZX-D2-200) fitted with an Olympus® SZX-TR30camera (Tokyo, Japan) fixed at 10X magnification in order to assess the impact of optimization on the surface structure of the SBP and elucidate the extent of penetration of SSZ into the SBP. Imaging of the surface of the optimized SBP was used to visually analyze the shape and contours of the SBP while transverse sections through the core were used to determine depth of SSZ penetration. Imaging of the unmodified surface and transverse sections through the core was conducted to provide a reference source.

7.3.1.4. Scanning Electron Microscopy analysis of the surface and core of the optimized SBP

In order to obtain a more descriptive view of the effect of optimization on structure and morphology of the optimized SBP, Scanning Electron Microscopy (SEM) was performed on the surface and transverse sections of optimized SBP samples. Samples were firmly mounted on aluminium stubs with carbon tape and gold sputter coated with argon gas whilst under a vacuum of 0.1Torr using a SPI-MODULETM Sputter Coater and SPI-MODULETM Control (SPI Supplies, Division of Structure Probe Inc., West Chester, PA, USA). Each sample required 4.5 minutes of coating at 90-second intervals to ensure complete coverage of the sample, which minimized sample activation during viewing. Subsequent viewing was performed at various magnifications (500X, 1000X, 3000X and 5000X magnifications) under the PhenomTM desktop scanning electron microscope (FEI CompanyTM, Hillsboro, OR, USA). Unmodified SBP samples were analyzed in the same manner to elicit a comparison to the optimized SBP.

7.3.1.5. Analysis of the surface area and porosity of the optimized SBP

Surface area and porosity analysis was conducted using a Porositometer (Micromeritics ASAP 2020, Norcross, GA, USA). Optimized and unmodified SBP samples (200mg) were accurately weighed, placed into a glass sample tube and degassed for a total of 6 hours. The degassing procedure, which consisted of an evacuation phase and heating phase under the parameters described in Table 7.10, was used to remove surface moisture and impurities from the samples after which analysis was conducted at the adsorptive properties depicted in Table 7.10.

Table 7.10: Parameters employed for degassing and analysis of SBP samples

Evacuation phase parameters	
Temperature Ramp Rate	10°C.min^{-1}
Target Temperature	50°C
Evacuation Rate	50.0 mmHg.s^{-1}
Unrestricted evacuation	30.0 mmHg
Vacuum Set Point	500 mug
Evacuation Time	60 min
Heating phase parameters	
Temperature Ramp Rate	10°C.min^{-1}
Hold Temperature	120°C
Hold Time	900 min
Adsorptive properties during the analysis process	
Adsorptive gas	Nitrogen
Maximum manifold pressure	925.00 mmHg
Non-ideality factor	0.0000620
Density conversion factor	0.0015468
Hard sphere diameter	3.860Å
Molecular cross-sectional area	0.162nm^2
Inside diameter of sample tube	9.53mm

Adsorption isotherms were generated by allowing the adsorbate (Nitrogen) to undergo physiosorption through Van der Waals forces on the adsorbent (SBP) with the quantity of adsorbate adsorbed (n) poltted against the relative pressure $\left(\frac{p}{p_o}\right)$ (EP, 2005). Progression of pore filling proceeded in the order of pore size with micropores (d< 2nm) being filled first, followed by monolayer adsorption, then capillary condensation within mesopores (2 <d> 50) and lastly filling and condensation of macropores (d>50nm) (Siminiceanu *et al.,* 2008)**.** The process was then reversed and the desorption isotherm was generated which gave further information on the geometry and shape of the pores as well as presence of mesopores (Condon, 2006).

Surface area of the SBP was calculated using the computations proposed by Brunauer-Emmett-Teller (BET), which is among the most commonly used. The BET method involved monolayer adsorbate layer formation and was measured at the partial pressure range of $0.05<\left(\frac{p}{p_o}\right)>0.35$ (EP, 2005; Walton and Snurr, 2007; Siminiceanu *et al.,* 2008; Bawa *et al.,* 2011)**.** The BET total surface area (A_{ts}) computation was related the monolayer capacity of the adsorbate (n_m), the molecular cross-sectional area of the adsorbate (a_m) and Avogadro's number (L) as described by Equation 7.14.

$$A_{ts} = n_m \text{ x } a_m \text{ x } L \qquad \textbf{\textit{Equation 7.14}}$$

In the above equation, a_m was a known constant for nitrogen, the value of L was well known and n_m was derived using Equation 7.15.

$$\frac{p}{n\left(\frac{p_o}{p}-1\right)} = \frac{1}{n_m C} + \frac{(C-1)}{n_m C}\left(\frac{p}{p_o}\right) \qquad \textbf{Equation 7.15}$$

Where, n and $\left(\frac{p}{p_o}\right)$ were as described above and *C* was exponentially related to the enthalpy of adsorption in the first adsorbed layer.

Equation 7.15 was then linearized by plotting $\frac{p}{n\left(\frac{p_o}{p}-1\right)}$ against $\left(\frac{p}{p_o}\right)$ with the y intercept (*i*) defined by $\frac{1}{n_m C}$ and the slope (*s*) defined by $\frac{(C-1)}{n_m C}$.

The value of C was obtained using Equation 7.16

$$C = \left(\frac{s}{i}\right) + 1 \qquad \textbf{Equation 7.16}$$

And the value of n_m was obtained using Equation 7.17

$$n_m = \frac{1}{i+s} \qquad \textbf{Equation 7.17}$$

Finally, the specific surface area (A_{ss}) relating to the quantity of SBP tested was determined using Equation 7.18 where m was the mass of the sample of SBP.

$$A_{ss} = \frac{A_{ts}}{m} \qquad \textbf{Equation 7.18}$$

Pore size, pore volume and pore area were determined using the method described by Barrett, Joyner and Halenda (BJH) and involved capillary filling and condensation once the monolayer had been formed (Siminiceanu *et al.,* 2008; Bawa *et al.,* 2011). In addition, the presence of micropores within the SBP was determined using the t-plot, described by Lippens and De Boer, which plotted the quantity of adsorbate adsorbed (V_a) at different P/P0 values against the thickness (t). The linear range of this plot was found between monolayer formation and capillary condensation as no further filling of micropores was possible (Siminiceanu *et al.,* 2008). The slope of the t-plot was used to determine the external surface area, which encompassed the exterior surface, mesopores and macropores of the SBP. When compared to the experimental isotherm, the presence of micropores was determined by a positive result (surface area > 0) after subtracting the external surface area from the BET surface area (Condon, 2006; Siminiceanu *et al.,* 2008).

7.3.1.6. In vitro drug release behavior from the optimized SBP

Determination of the *in vitro* drug release behavior and quantitative analysis by means of determination of MDT was conducted as described for the design formulations. With regard to the up-scaled formulations prepared, the quantity of SBP containing 500mg SSZ was determined using Equation 4.1 and subjected to drug release studies as described for the optimized SBP. The study was conducted in triplicate (n=3).

7.3.1.7. Determination of extent of hydration and erosion of SBP matrix during drug release from the optimized SBP

Separate drug-loaded SBP samples containing 10mg SSZ was determined and accurately weighed using an analytical mass balance. These SBP samples were then subjected to the same conditions employed for *in vitro* drug release studies (Section 7.3.1.6) with the SBP being completely removed from the dissolution apparatus at each drug release sampling time. These SBP were then lightly blotted with tissue paper to remove excess surface moisture and weighed to determine their hydrated mass. The hydration of the SBP was then calculated according to Equation 2.1. The SBP were then allowed to air dry until constant mass was achieved after which the dry mass was determined. The extent of erosion during drug release was then determined according to Equation 2.2. The study was conducted in triplicate (n=3).

7.3.1.8. Determination of the drug release kinetics and similarity of the optimized SBP

The drug release kinetics and mechanism of drug release from the SBP was determined by fitting the dissolution results into the zero order, first order, Higuchi, Korsmeyer-Peppas and Hixson Crowell models with the model of best fit determined by evaluating the R^2 values (Section 7.2.3.4). The diffusion coefficient (n) from the Korsmeyer-Peppas model was used to determine the mechanism of drug release. Similarity between the drug release profiles of the optimized and scaled-up optimized formulations were elucidated by determining the difference factor (*F1*) and the similarity factor (*F2*) (Section 7.2.3.5).

7.3.2. Results and discussion describing the characteristics of optimized double ECH-crosslinked SBP

7.3.2.1. Drug entrapment efficiency of optimized SBP

Experimental DEE values for the optimized formulation showed close correlation (R^2 = 0.981) to the design predicted value and thus validated the design and response optimization procedure. In addition, the experimental drug entrapment values for the scaled-up optimized formulation showed good correlation to both the predicted (R^2 =

0.989) as well as the optimized formulation (R^2 = 0.971). This further authenticated the method utilized and implied that scaling up can be performed confidently with very little variance expected. The actual DEE values obtained were depicted in Table 7.11.

Table 7.11: Comparative DEE of predicted, experimental and scale up optimized formulations

	Predicted	Optimized SBP	Scaled-up optimized SBP
DEE (%)	40.780	40.022 ± 2.244	41.220 ± 1.271
MDT (min)	171.696	163.972 ± 1.910	166.011 ± 2.738

Where DEE denoted Drug Entrapment Efficiency and MDT denoted Mean Dissolution Time (n=3 in all instances)

7.3.2.2. SEM imaging demonstrating the effect of optimization on the structure of the SBP

SEM imaging of the surface morphology of the double crosslinked optimized SBP was depicted in Figure 7.9a and was observed to be almost continuous displaying roughness and containing random fissures and pores. This was in stark contrast to the surface of the unmodified SBP (Figure 7.9c) which comprised principally of individual starch granules with a low degree of merging of adjacent granules. The continuous nature of the surface was further emphasized at higher magnifications and this confirmed the elevated levels of gelatinization and crosslinking of the starch granules, which was desired during the formulation process. The modifications imparted on the optimized SBP caused drug to be incorporated into the gelatinized crosslinked network and decreased the porosity of the SBP, as discussed in the porosity study, thus minimizing the burst drug release and controlling further drug release. However, due to the uneven surface gelatinization observed and presence of surface pores, variations in drug release was expected.

Analysis of Figure 7.9b revealed that the core of the SBP had been modified during optimization as gelatinization and crosslinking of the core granules could be seen with decreased inter-granular spaces compared to the unmodified SBP core (Figure 7.9d). However, the extent to which the modifications had taken place at the core was less than at the surface of the optimized SBP. At higher magnifications, the granules were confirmed to undergo complete gelatinization and with reference to the color change observed at the core of the SBP during light microscopy, incorporation of drug into the core was thus verified. Furthermore, due to the double crosslinking and reduction in SBP pores at both the surface and interior, drug release was expected to be more controlled over a longer period.

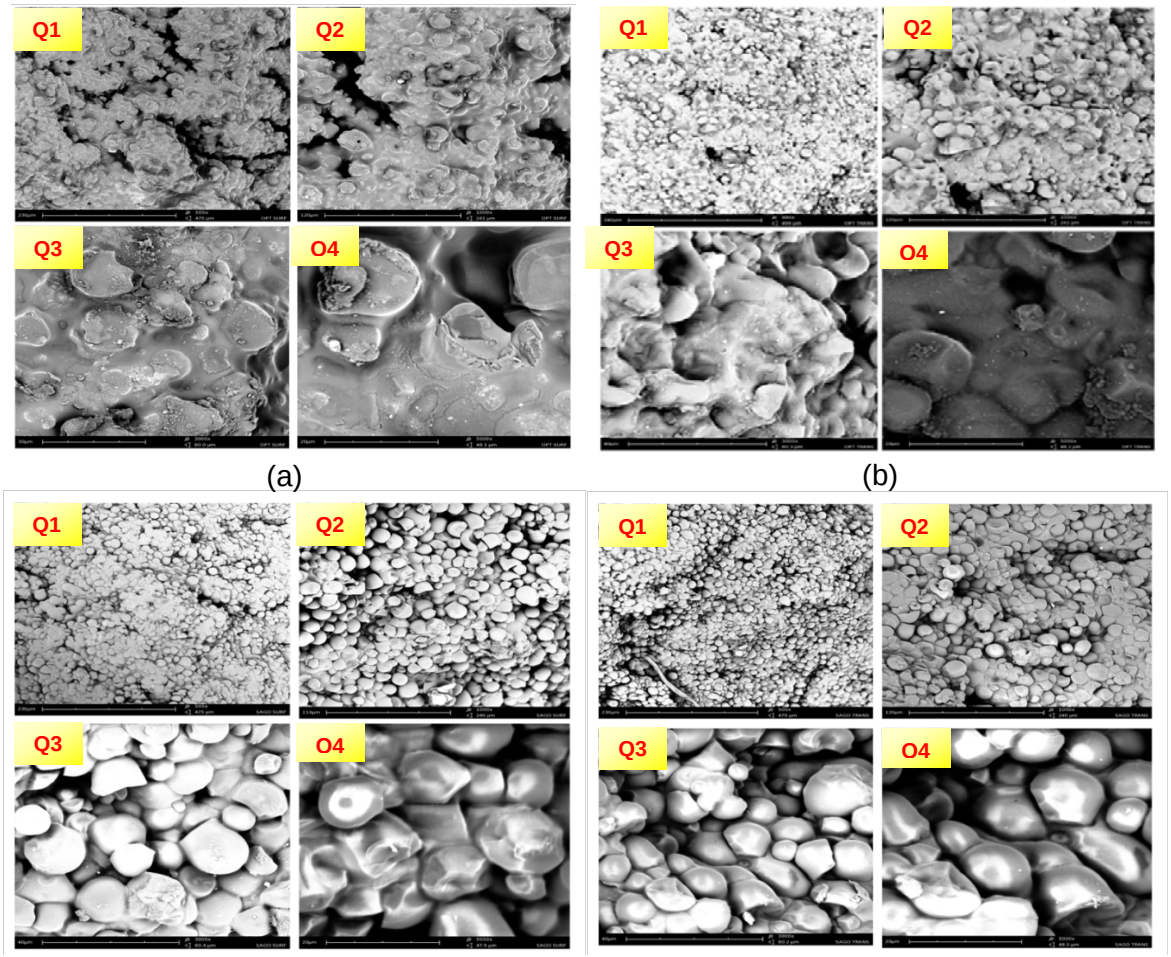


Figure 7.9: SEM imaging of optimized SBP (a) surface and (b) core and unmodified SBP (c) surface and (d) core (magnifications in figures a1-b2 were: Q1=500X; Q2=1000X; Q3=3000X; Q4=5000X).

7.3.2.3. Effects of optimization on the surface area and porosity of the SBP

Figure 7.10 showed the various types of gas adsorption isotherms as classified by the IUPAC (Siminiceanu *et al.,* 2008; Bawa *et al.,* 2011). Type I isotherms, also called pseudo-Langmuir isotherms, are indicative of microporous materials. The steep rise was due to strong interactions and filling of micropores followed by a plateau as no further filling of micropores took place. Type I isotherms may also represent chemisorption which describes chemical bonding instead of Van der Waals interactions as was observed in physiosorption (Siminiceanu *et al.,* 2008). Type II isotherms are characteristic of non-porous or very macorporous materials with a strong interaction with the adsorbate (Siminiceanu *et al.,* 2008). This was suggested by the pronounced “knee” at the point labeled B, which represented the beginning of monolayer formation followed by the linear portion of the isotherm, which was used to calculate BET surface area and the lack of hysteresis suggested an absence of mesopores. Type III isotherms are similar to type II and imply a non-porous or very macorporous material but the absence of the knee

signifies weak adsorbent-adsorbate interaction. Type IV and type V isotherms can be described as porous forms of type II and type III isotherms respectively with the hysteresis loops indicating the presence of mesopores within the material surface structure. Type VI isotherms may be described as step-wise adsorption due to different pore sizes and different enthalpy interactions as seen by multiple “knees” in the isotherm. Additionally, chemisorption may be present in conjunction with physiosorption (Donohue and Aronovich,1998; Condon, 2006; Siminiceanu *et al.,* 2008).

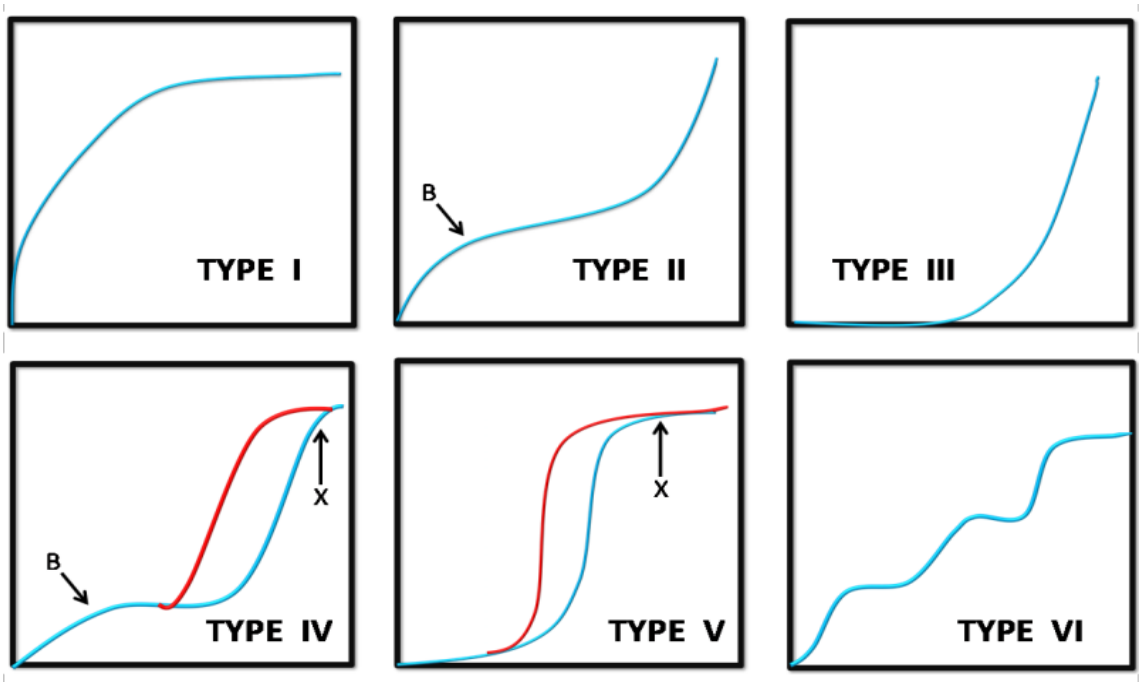


Figure 7.10: IUPAC classification of adsorption isotherms (adapted from Siminiceanu *et al.,* 2008; Bawa *et al.,* 2011).

Type IV and type V isotherms showed the presence of hysteresis loops and these hysteresis loops are characterized by the IUPAC as depicted in Figure 7.11. Type 1 hysteresis (H1) is depicted as nearly vertical and parallel adsorption and desorption branches and describe a material that is regularly porous with no interconnecting pores and channels into underlying areas. Type 2 hysteresis is reminiscent of pores that are not regularly shaped or sized and may contained channels and interconnections and is represented by a sloping adsorption branch and nearly vertical desorption branch. Type 3 hysteresis (H3) shows almost parallel sloping branches over a wide $\frac{p}{p_o}$ range and is indicative of slit-like pores with few channels. Type 4 hysteresis (H4) are analogous to the type 1 isotherm containing a large pore size range and may consist of micropores and very small mesopores (Burgess *et al.,* 1989; Condon, 2006; Grosman and Ortega 2008; Siminiceanu *et al.,* 2008).

In addition to the classifying the hysteresis, Figure 7.11 also depicted the process and important events occurring during adsorption and desorption as portrayed by the isotherms. At low partial pressures, micropore filling occurs after which monolayer adsorption begins (point B). The shape of point B (knee of isotherm) is dependent on the enthalpy of adsorption (C value in Equation 7.15) with high enthalpy denoting strong interactions between adsorbent and adsorbate (Kowalczyk *et al.,* 2005). Once the monolayer had formed, multilayer pore filling with capillary condensation, defined as the process of condensation of absorptive gas molecules in small capillaries and pores at vapor pressures below the saturated vapor pressure occurs, and is seen as the start point of the hysteresis loop (point F). Mesopore followed by macropore filling proceeds with closure of the hysteresis loop at higher $\frac{p}{p_o}$ seen when all pores are filled (point X). Desorption then takes place until a sudden drop in quantity adsorbed at a material determined partial pressure causes the closure of the hysteresis (point T). This sudden closure of the hysteresis is related to the gas-liquid enthalpy of the adsorptive and referred to as the tensile strength failure (TSF). The dashed line beyond the closure of the hysteresis loop indicates projected desorption branch TSF was absent (Burgess *et al.,* 1989; Kowalczyk *et al.,* 2005; Condon, 2006; Siminiceanu *et al.,* 2008).

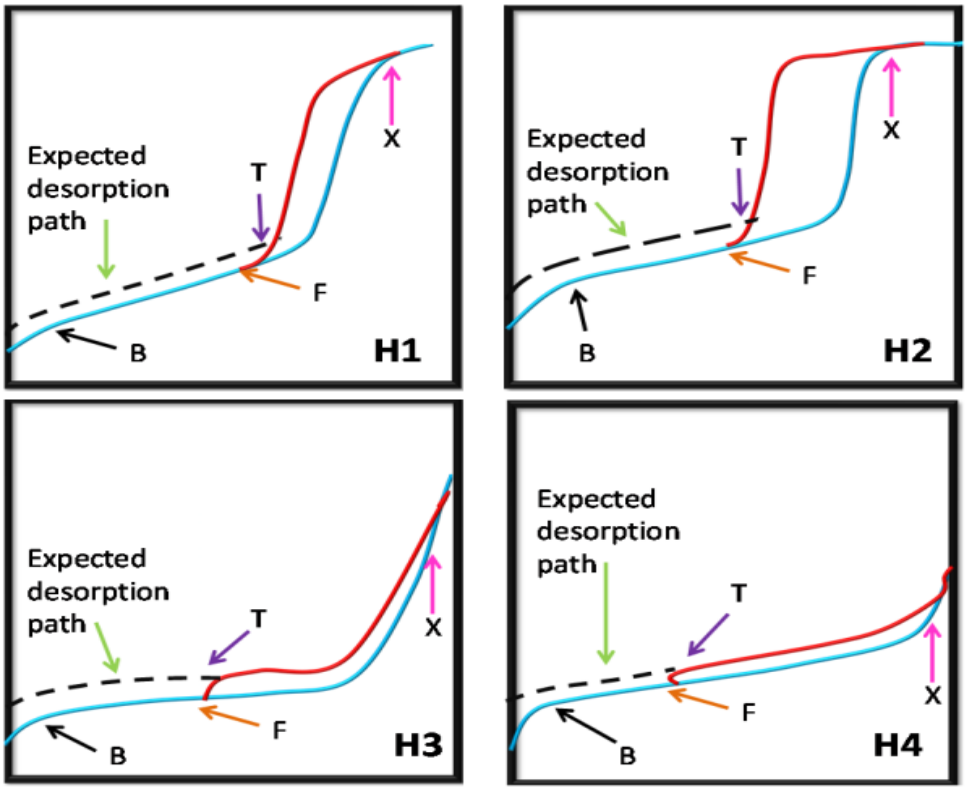


Figure 7.11: IUPAC classification of hysteresis (adapted from Siminiceanu *et al.,* 2008; Bawa *et al.,* 2011).

The isotherms generated for optimized SBP during nitrogen adsorption and desorption at various partial pressures are represented in Figure 7.12a, and when compared to the IUPAC classification (Figure 7.10 and Figure 7.11) displayed characteristics which most closely resembled that of a type IV isotherm displaying characteristics of both H3 and H4 hysteresis. The H4 characteristics pointed towards the presence of small mesopores and micropores while the H3 characteristics indicated the presence of slit-like mesopores and channels accompanied with capillary condensation of the pores within the SBP. The deduction for H4 was supported by the pore size distributions (Figure 7.12c and Figure 7.12d) which show that pore sizes were between 1.6nm and 31nm with majority of the pores <10nm and the average pore diameter of 2.6020nm and 4.0835nm for adsorption and desorption branches respectively (Table 7.13).

Furthermore, upon analysis of the t-Plot (Figure 7.12b), the slope of greatest linearity was found at the partial pressure range ($0.0801 < \left(\frac{p}{p_o}\right) < 0.2504$) and utilizing the slope of this t-Plot, a positive micropore surface area (Table 7.12) was obtained, signifying the presence of micropores within the SBP. Evidence supporting the H3 deduction was also obtained from the pore distribution plots of the optimized SBP which showed lager mesopore presence especially in the desorption branch (Figure 7.12c2 and Figure 7.12d2). Additionally, SEM imaging (Figure 7.9a and Figure 7.9b) illustrated that the pores penetrated deeper into the SBP between the coalesced granules.

Closer inspection of the isotherm demonstrated a steep portion at high $\frac{p}{p_o}$ and further suggested the possible presence of macropores (d>50nm). The pore distribution plots further show the presence of pores <2nm confirming the observations from the t-Plot of the presence of micropores. However, pore sizes >50nm were not observed and thus the steeper rise at the high relative pressures were concluded to be a result of filling of larger mesopores and not due to the presumed presence of macropores. Thus, the optimized SBP were determined to be composed of pores within the mesopore range with a degree of microporosity.

Pore volume distribution plots (Figure 7.12c) demonstrated that pores ~2-4nm contributed most appreciably to the cumulative pore volume in the adsorption branch (Figure 7.12c1) while in the desorption branch (Figure 7.12c2), pores ~7nm provided the greatest contribution with larger mesopores ~20nm contributing extensively to the cumulative pore volume. Pore area plots (Figure 7.12d) showed similar pore sizes to the pore volume distribution plots with pores 2-4nm contributing the bulk of the cumulative surface area of

the adsorption branch (Figure 7.12d1). With regard to the desorption branch (Figure 7.12d2), the major contributors to the cumulative pore surface area were pores sized ~2nm, 4nm and 8nm with a less pronounced input from larger mesopores. Overall, higher cumulative pore volume and higher cumulative pore surface area was observed in the adsorption branch as illustrated in Table 7.13.

Scrutiny of the surface area and porosity of the unmodified SBP (Figure 7.13) revealed that nitrogen adsorption and desorption produced a type IV isotherm with an H3 hysteresis and a steep area at high $\frac{p}{p_o}$ (Figure 7.10 and Figure 7.11). This, as was the case with optimized SBP, may have been the result of the presence of mesopores with capillary condensation and the presence of macropores. However, contrary to the optimized SBP, the presence of macropores was confirmed with pore sizes in range of 2.2nm <d> 58nm with average pore sizes of 6.5464nm and 5.9983nm for adsorption and desorption branches respectively (Table 7.13). Furthermore, upon analysis of the t-Plot (Figure 7.13b), the slope of greatest linearity was found at partial pressures range (0.15 $<\left(\frac{p}{p_o}\right)<$ 0.35). However, the t-plot yielded a negative micropore surface area (Table 7.13) indicating the absence of micropores within the SBP.

With regard to the unmodified SBP, the pore volume distribution plot for the adsorption branch (Figure 7.13c1) showed that pores ~4nm and ~8nm accounted most notably for the cumulative pore volume. However, large mesopores into the macropore range displaying relatively large pore volumes were present and contributed substantially to the cumulative pore volume. The desorption branch (Figure 7.13c2), although exhibiting no macropores, showed that the greatest contributor to pore volume was pores ~24nm and smaller pores having less impact on the pore volume. Pore area plots depicted in Figure 7.13d demonstrated similar pore sizes to the pore volume distribution plots with the bulk of the cumulative pore surface area provided by small mesopores and much smaller contributions offered by the larger pores. This was true for both the adsorption branch (Figure 7.13d1) and the desorption branch (Figure 7.13d2).

Overall, a higher cumulative pore volume and a higher cumulative pore surface area were observed in the adsorption branch as illustrated in (Table 7.12). Additionally, larger pore sizes were observed in the adsorption branch compared to the desorption branch. The differences observed between the adsorption and desorption branches could be attributed to adsorbate-adsorbent interactions as well as pore filling and emptying mechanisms. Additionally, these larger surface areas and pore volumes at larger pore sizes suggested

that there was a greater abundance of larger mesopores and macropores in the unmodified SBP with no micropores present. Thus when compared to optimized SBP, which displayed smaller pore sizes with micropores and no macropores, it can be deduced that the optimization processes decrease the porosity of the SBP.

Table 7.12: Effect of optimization on the surface area SBP

SBP formulation	BET surface area ($m^2.g^{-1}$)	t-Plot micropore area ($m^2.g^{-1}$)
Unmodified	2.5342	-1.0385
Optimized	0.8262	0.2540

Where SBP denoted Starch-Based platforms and BET denoted the Brunauer-Emmett-Teller method of calculating surface area

Table 7.13: Effect of optimization on the porosity of the SBP

	BJH Adsorption			BJH Desorption		
SBP formulation	**Cumulative surface area of pores ($m^2.g^{-1}$)**	**Cumulative volume of pores ($cm^3.g^{-1}$)**	**Average pore diameter (nm)**	**Cumulative surface area of pores ($m^2.g^{-1}$)**	**Cumulative volume of pores ($cm^3.g^{-1}$)**	**Average pore diameter (nm)**
Unmodified	1.7670	0.001796	6.5464	1.3805	0.001515	5.9983
Optimized	0.2630	0.000171	2.6020	0.1182	0.000150	4.0835

Where SBP denoted Starch-Based platforms and BJH denoted the Barrett, Joyner and Halenda method of calculating surface are, pore size and pore volume

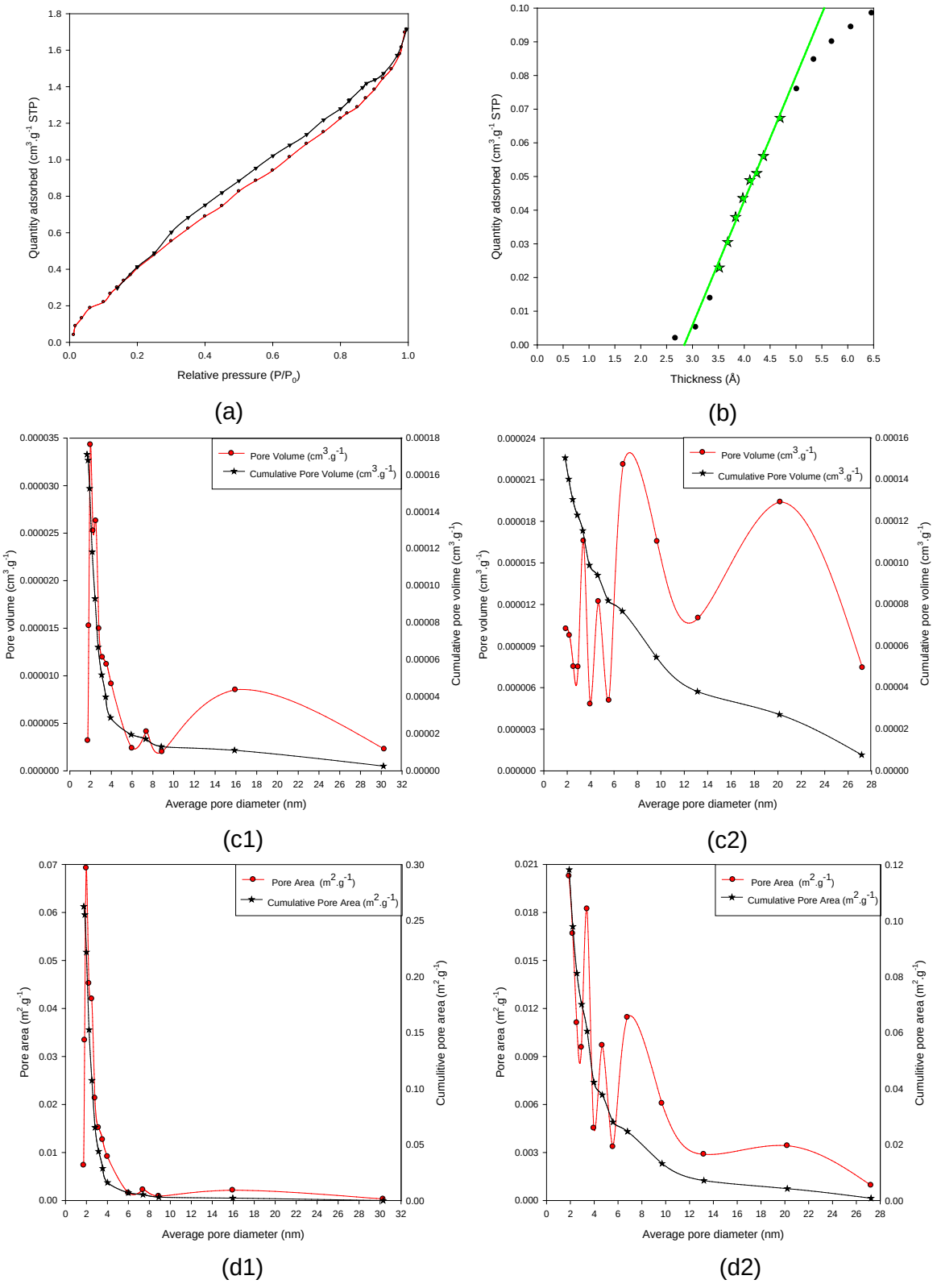


Figure 7.12: Depiction of surface area and porosity of optimized SBP with (a) Linear isotherm, (b) t-Plot, (c) pore volume distribution according to pore size with respect to (c1) adsorption branch and (c2) desorption branch and (d) pore area distribution according to pore size with respect to (d1) adsorption branch and (d2) desorption branch.

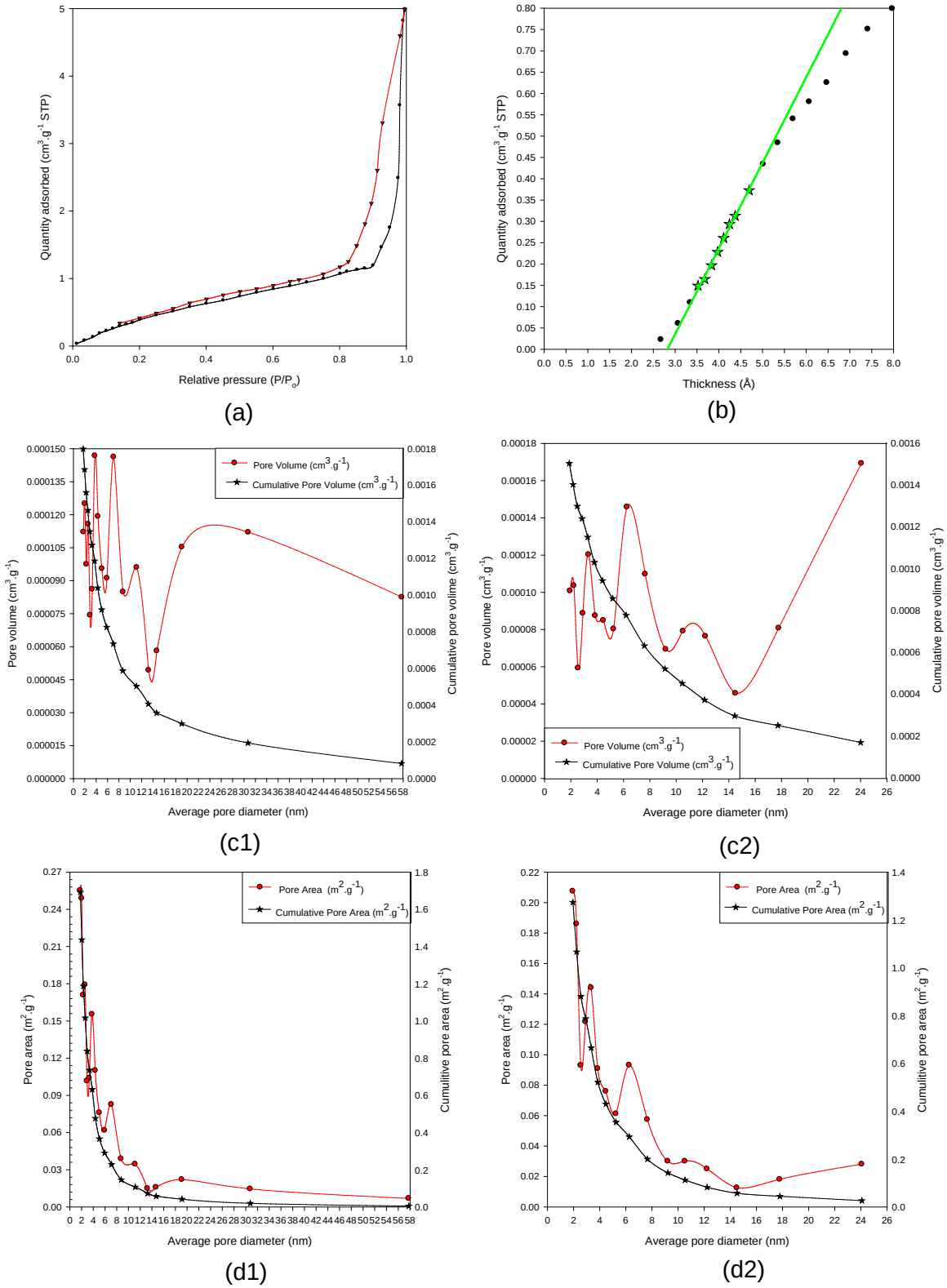


Figure 7.13: Depiction of surface area and porosity of unmodified SBP with (a) Linear isotherm, (b) t-Plot, (c) pore volume distribution according to pore size with respect to (c1) adsorption branch and (c2) desorption branch and (d) pore area distribution according to pore size with respect to (d1) adsorption branch and (d2) desorption branch.

The results obtained from the porosity study were not peculiar with respect to the shape, size and modifications to the SBP. The presence of the "knee" in the isotherm of both unmodified and optimized SBP and the values of "C" ($C_{Unmodified}$=20.5883 and $C_{Optimized}$=7.2684) symbolized that sufficient interaction enthalpy between adsorbent and adsorbate existed and applicability of BET to calculate the surface area. The calculated BET surface area was found to be low (Table 7.12) in unmodified SBP due to its size and structure and was further reduced during the optimization process. The isotherms and pore distributions were additionally representative of the observations made during SEM imaging which showed the surface to be composed of singular granules with slight merging of few surface granules and porous channels. Furthermore, porous channels into the SBP with interconnected pores were observed in Figure 7.9a and Figure 7.9b. Upon optimization, the surface granules underwent increased merging through gelatinization resulting in decreased inter-granular pores and subsequent crosslinking causing contraction of the gelled surface, further reducing the surface area and porosity of the SBP. This amalgamation of surface granules and the reduced surface area of the SBP were influential in regulating drug release from the SBP (Andersson *et al.,* 2000).

7.3.2.4. Effect of optimization on the in vitro drug release behavior of the SBP

Experimental MDT values obtained in Table 7.11 were in accordance with those observed for DEE and thus further validated the design and optimization method employed as well as the reliability of up-scaling of the optimization process. Good correlation was produced between the optimized formulation and the design predicted value, between the scaled-up optimized formulation and predicted values, and between the scaled-up optimized formulation and the optimized formulation with R^2 values of 95.501, 96.689 and 98.772, respectively. Furthermore, the *F1* and *F2* values between the scaled-up optimized formulation and the exact optimized formulation was determined to be 0.570 and 94.352, respectively, thus validating the similarity between the optimized and scaled-up optimized formulations. Further verification of the similarity was obtained by the relatively close model coefficients and *n* values portrayed in Table 7.5, Table 7.6 and Table 7.7 for both experimental formulations.

The complete *in vitro* drug release profiles exhibited by the optimized and scaled-up formulations were compared in Figure 7.14a. The shape of the release profiles, initial release (~18%), as well as final fraction released after 12 hours (~70%) were almost identical for both optimized formulations. Magnified representation of the SGF and SIF portions of the SSZ release profiles were depicted in Figure 7.14b and Figure 7.14c respectively. Additionally, microscopic images (magnification=10X) of the surface and

transverse section through the core of the optimized SBP accompanied Figure 7.14b and Figure 7.14c, respectively. Furthermore, the representative placement of these images depicts the location from where majority of drug release during each phase was postulated to occur. Analyses of these images demonstrate that, in addition to being adsorbed onto the surface of the SBP, SSZ penetrates deep and is incorporated into the core of the SBP. However, higher drug content is observed closer to the surface with lower quantities seen at the centre depicted by the color intensities induced by SSZ incorporation at the various regions. This uneven distribution can be associated with the burst effects seen in the drug release profiles. With regard to the shape of the SBP, optimization methods have minimal effect on the surface Figure 7.15a as the SBP still portrayed a highly spherical morphology consistent to that observed with unmodified SBP but the core appeared to be more eroded than the core of the unmodified SBP (Figure 7.15b).

Thus, during the first 2 hours, interaction of the surface of the SBP, and to a much smaller extent the underlying layers, accounted for SSZ released. This could be explained by the substantially low solubility of SSZ at the low pH of SGF, which results in saturation of dissolution medium at low concentrations of SSZ and thus prevented further release. Additionally, SGF due to its low pH had a diminished ability to weaken the bonds between SSZ and the SBP and to penetrate deep into the core resulting in reduction of SSZ released into this dissolution medium.

In contrast to SGF, SIF had a much higher pH and thus facilitated a greater degree of solubilization of SSZ as well as increased interaction between deeper layers of the SBP and dissolution medium. Thus, increased dissolution of SSZ was observed after 2 hours. However, the favorable modifications imparted to the SBP during formulation processes inhibited rapid penetration of the dissolution medium and subsequent dissolution of drug from the core of the SBP. This controlled retardation was desired and resulted in ~70% drug release in the 12 hours of the study.

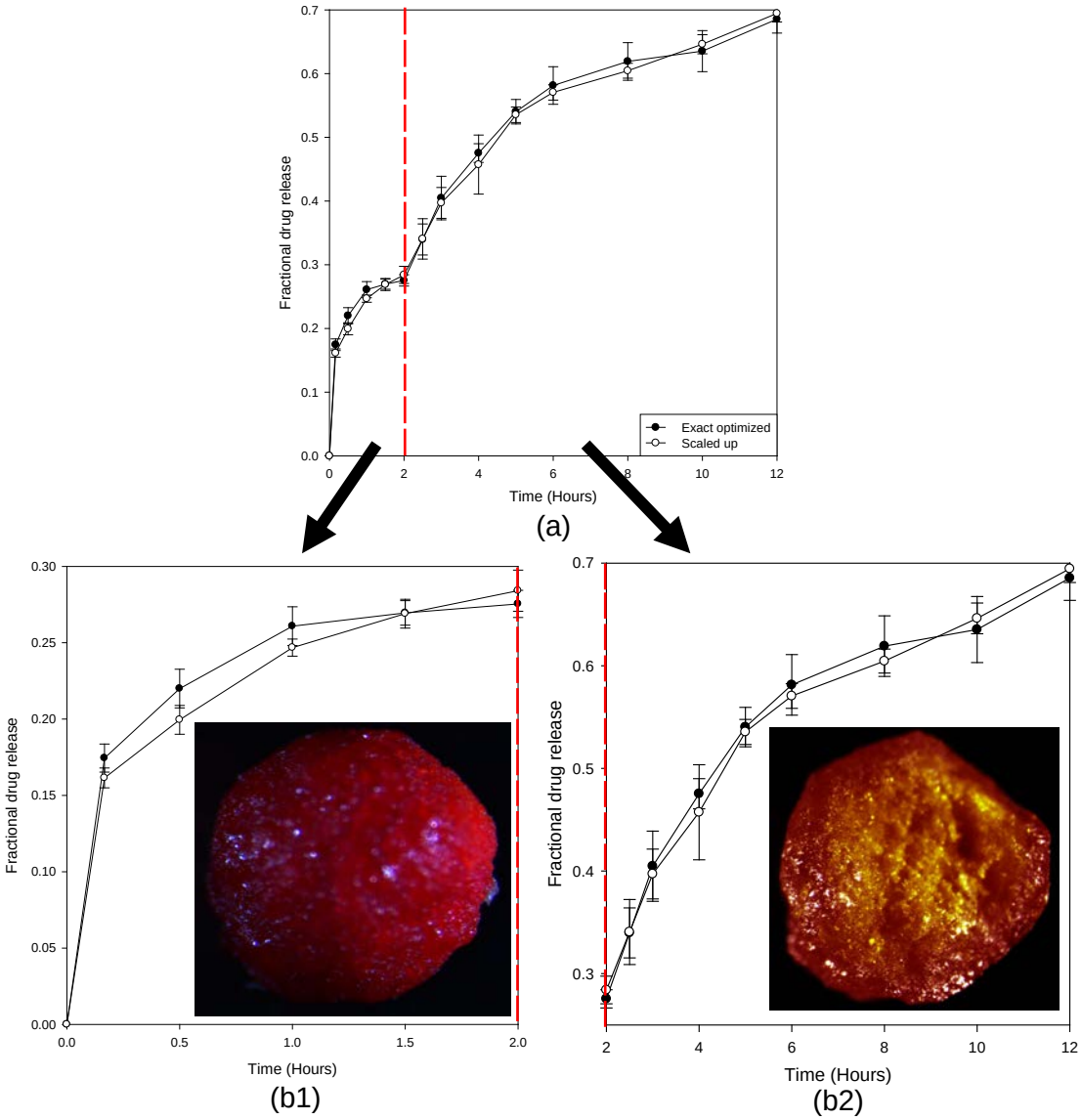


Figure 7.14: *In vitro* drug release profiles of optimized SBP (a) sequentially and (b) separately magnified (b1) SGF phase with microscopic image of surface of SBP and (b2) SIF phase with microscopic image of core of SBP (n=3 in all instances).



(a) (b)

Figure 7.15: Microscopic images (10X magnification) of (a) the surface and (b) the core of unmodified SBP.

7.3.2.5. Drug release kinetics of optimized SBP

Upon analysis of Table 7.14, Table 7.15 and Table 7.16, the R^2 values of 0.983 and 0.996 in SGF for the optimized and scaled-up optimized formulations, respectively, were found to be the highest for Higuchi model compared to the other drug release models, and thus indicated that the dissolution data in SGF best fitted the Higuchi model. This finding implied that the drug release was diffusion controlled and the value of the Korsmeyer-Peppas diffusion coefficient of <0.43 (n = 0.377 optimized and n = 0.416 scaled-up optimized) indicated the mechanism of drug release was Quasi-fickian diffusion. The burst effect accounted for surface drug released and further release was facilitated through drug diffusion as the dissolution medium entered the upper layers of the SBP. Polymer relaxation was almost nonexistent as very limited hydration occurred in SGF (DOS<20% in first 2 hours) (Figure 7.16). This phenomenon, combined with the low erosion values (DCM < 2% in first 2 hours), taking in to account that majority of the mass loss observed in Figure 7.16 was due to the drug exiting the SBP, further enhanced the finding that drug release was diffusion controlled.

In SIF, although the *in vitro* dissolution data best fitted the Higuchi model with R^2 values of 0.995 and 0.997 for the optimized and scaled-up optimized formulations, respectively, indicating diffusion to be implicated in controlling drug release, the Korsmeyer-Peppas diffusion coefficient was found to be between 0.43 and 0.85 (n = 0.719 for optimized and n = 0.757 for scaled-up optimized). These n values indicated that the mechanism of drug release was anomalous drug transport and involved both diffusion as well as polymer relaxation. Figure 7.16 supported this conclusion as it exhibited much greater hydration and swelling of the SBP in SIF which facilitated intrinsic bond relaxation and further drug release.

The R^2 value of the sequential drug release portrayed a combination of the effects of each dissolution mediums and was thus best fitted to the Higuchi model. Mechanistically the n value indicated that drug release was achieved through diffusion and through polymer relaxation. Figure 7.16 further extinguished the theory of erosion based drug release occurring by showing low values of erosion (DCM <8%) for the entire duration of the study.

Table 7.14: *In vitro* SSZ release kinetics of optimized SBP in SGF

Formulation	zero order model			First order model			Higuchi model		Korsmeyer-Peppas model			Hixson-Crowell model		
	K_z	Q_{0_z}	R^2	K_1	Q_{0_1}	R^2	K_H	R^2	K_p	n	R^2	K_{HC}	$Q_{0_{HC}}$	R^2
Optimized	0.111	16.534	0.829	-0.0006	16.478	0.847	1.668	**0.996**	1.872	0.416	0.922	-0.0020	16.501	0.841
Scaled-up	0.103	17.000	0.809	-0.0006	16.958	0.827	1.554	**0.983**	2.111	0.377	0.905	-0.0019	16.981	0.821

Table 7.15: *In vitro* SSZ release kinetics of optimized SBP in SIF

Formulation	zero order model			First order model			Higuchi model		Korsmeyer-Peppas model			Hixson-Crowell model		
	K_z	Q_{0_z}	R^2	K_1	Q_{0_1}	R^2	K_H	R^2	K_p	n	R^2	K_{HC}	$Q_{0_{HC}}$	R^2
Optimized	0.054	32.622	0.976	-0.0005	27.356	0.954	2.139	**0.997**	0.131	0.757	0.966	-0.0014	29.555	0.981
Scaled-up	0.046	35.591	0.981	-0.0005	31.719	0.947	1.827	**0.995**	0.362	0.719	0.963	-0.0012	33.299	0.921

Table 7.16: *In vitro* SSZ release kinetics of optimized SBP sequentially in SGF and SIF

Formulation	Zero order model			First order model			Higuchi model		Korsmeyer-Peppas model			Hixson-Crowell model		
	K_z	Q_{0_z}	R^2	K_1	Q_{0_1}	R^2	K_H	R^2	K_p	n	R^2	K_{HC}	$Q_{0_{HC}}$	R^2
Optimized	0.075	22.441	0.922	-0.0006	19.573	0.963	2.398	**0.984**	0.677	0.681	0.977	-0.0018	20.809	0.981
Scaled-up	0.071	23.415	0.890	-0.0006	21.259	0.937	2.299	**0.968**	0.637	0.679	0.954	-0.0017	22.178	0.921

Where K_z denoted the zero order model constant, Q_{0_z} denoted the initial drug in solution according to the zero order model, K_1 denoted the First order model constant, Q_{0_1} denoted the initial drug in solution according to the First order model, K_H denoted the Higuchi constant, K_p denoted the Korsmeyer-Peppas constant, n denoted the diffusion constant, K_{HC} denoted the Hixson-Crowell constant, $Q_{0_{HC}}$ denoted the initial drug in solution according to the Hixson-Crowell model and R^2 denoted the correlation coefficients of each of the models in Table 7.14, Table 7.15 *and* Table 7.16

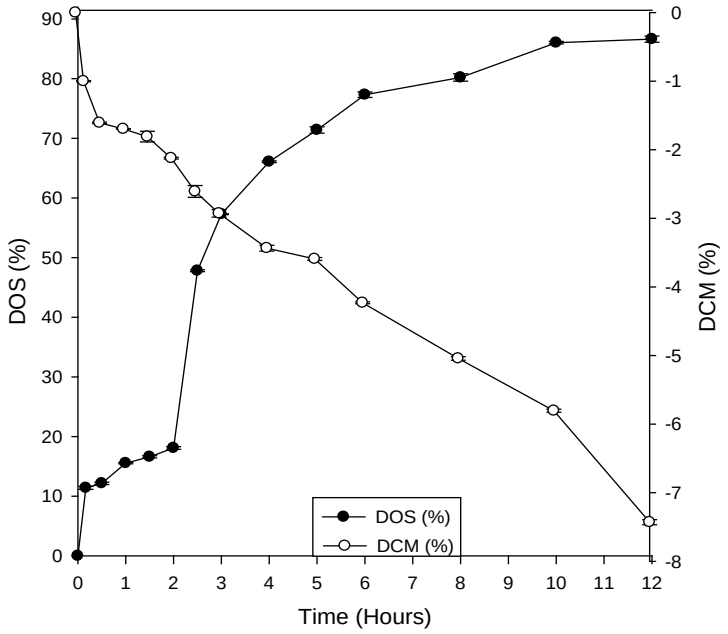


Figure 7.16: Degree of hydration and erosion of optimized SBP during drug release(n=3 in all instances).

7.4. Concluding Remarks

The FCCCD, which statistically varied the DLT and CLT, was employed to optimize the SBP with respect to both drug entrapment and control of drug release. The design used proved successful in yielding regression models that adequately described the effects and interactions of the process variables and demonstrated close correlations between experimental and predicted responses. Furthermore, residual analysis and fitting of drug release data showed that validation of the FCCCD was achieved.

These modifications were desirable as it enhanced both drug entrapment and aided in the control of drug release. Microscopic imaging of the surface and the core of the optimized SBP showed that SSZ had been incorporated throughout the SBP structure with drug incorporation imparting favorable stability characteristics on the SBP. SSZ concentrations varied at different depths within the SBP with highest concentrations at the surface. This, coupled with the drug solubility in the different physiological fluids, characterized the drug release profiles. The kinetic modelling of the *in vitro* drug release data showed that drug release best fitted the Higuchi model and the overall n value showed fickian diffusion as well as polymer relaxation during SBP hydration was the main mechanisms controlling drug release. Thus, the choice of SSZ as the model drug as well as the processes employed in the formulation of the optimized SBP were found to be beneficial with regard to SBP stability, drug entrapment and *in vitro* drug release.

CHAPTER 8
IN VIVO ASSESSMENT OF OPTIMIZED SULFASALAZINE-LOADED STARCH-BASED PLATFORM IN THE LARGE WHITE PIG MODEL

8.1. Introduction

Ideally, the evaluation of factors influencing the delivery of drugs should be conducted in healthy or diseased humans (Cryan *et al.,* 2007). However, in most circumstances, this is initially impossible due to ethical and legal reasons. Thus, assessing the performance of drugs and drug delivery systems through a process of *in vivo* animal studies has an important role in correlating *in vitro* performance to *in vivo* performance. Furthermore, *in vivo* animal studies form a vital aspect in understanding the actual physiological and toxicological effects of the drugs or drug delivery within the body and these results can be extrapolated to humans. Selecting a suitable candidate animal model is crucial to the design and success of the *in vivo* study as it affects the route of administration, size of dosage that can be used, blood sampling in terms of both quantity and frequency, as well as accuracy with regard extrapolation of results to humans (DeSesso and Jacobson, 2001; Hunter *et al.,* 2012). In addition, legal, ethical, cost and availability issues affect the choice of the animal model that can be used in these studies (Vargas *et al.,* 2007).

In terms of drug delivery via the oral route, the animal model must provide a gastrointestinal tract (GIT) environment that most closely resembles the environment of the GIT of humans in terms of both structure and function (Yang *et al.,* 2002). Although studies have been conducted on rodents and other small animals, these animals show vast deviations in size, diet, luminal fluid properties, locations of absorption epithelia and quantity of mucosal barrier compared to humans (DeSesso and Jacobson, 2001; Sutton *et al.,* 2006; Hunter *et al.,* 2012). Thus larger animal models such as dogs, sheep, pigs, monkeys and other non-human primates are used to assess oral drug delivery (Tuleu *et al.,* 1999; Yang *et al.,* 2002; Cryan *et al.,* 2007).

The pig model represents the most appropriate animal model to be used in oral drug delivery as it displays similarities in size, diet (omnivorous as in humans), GIT anatomy, digestive physiology, coronary artery distribution, colonic bacterial population and metabolic pathways (Kidder *et al.*, 1961; Ochia, 1973; Pond and Houpt, 1978; Yamada *et al.*, 1995; Brown and Terris, 1996; Gardner *et al.*, 1996; Reeds and Odle, 1996; Yang *et al.*, 2002; Brunet *et al.*, 2006). Furthermore, sourcing of pigs is less complicated in terms

of ethical issues, cost and availability compared to dogs and primates and has thus been used extensively as the animal model for *in vivo* assessment of drugs and drug delivery systems (Kidder *et al.*, 1961; Ochia, 1973; Pond and Houpt, 1978; Kumar *et al*., 1992; Dorkoosh *et al.,* 2002).

The pharmacokinetics of sulfasalazine (SSZ) is interesting in that it is a prodrug, which is broken down into two separate drug molecules in colon. Following oral administration, SSZ is only partly absorbed in the upper gastrointestinal tract and it is estimated that less than 30% is taken up by the small intestine (Wolf *et al.,* 2002). Thus, SSZ is classified by the Biopharmaceutics Classification System (BCS) as a type 2 drug with low solubility and high permeability (Lindenberg *et al.*, 2004; Dahan and Amidon, 2009). However, a large portion of this absorbed portion is returned intact to the gut via the bile and efflux transporters within the intestinal wall thus reducing the permeability of SSZ. This enterohepatic recirculation of SSZ results in a bioavailability of approximately 10-15% and relegating SSZ to the status of a type IV drug (Lindenberg *et al.*, 2004, Theobald Jr., 2007; Dahan and Amidon, 2010). The portion of SSZ that reaches the systemic circulation is highly bound to albumin (>99.3%), displays a half-life of between 5 and 10 hours and is excreted unchanged in the urine (Rains *et al.*, 1992; Corea, 2007; Kenakin, 2009).

Upon reaching the colon, SSZ is reduced by the bacterial azo-reductase enzymes which reduce sulfasalazine to its two main components sulfapyridine (SP) and 5-aminosalicylic acid (5-ASA) (Chungi, 1989; Wolf *et al.*, 2002, Rubinstein, 2005). Although showing good absorption with an estimated bioavailability of 60%, SP is implicated in most of side effects of SSZ and its antibacterial efficacy in treating inflammatory bowel diseases has been regarded to be trivial (Theobald Jr., 2007; Alonso *et al.*, 2009). SP is thus used merely as a carrier molecule for the active therapeutic moiety of SSZ, 5-ASA and was not relevant to this study (Alonso *et al.*, 2009).

Although displaying pharmacological activity, 5-ASA is less well absorbed from the gastrointestinal tract with an estimated bioavailability of between 10-30%. (Theobald Jr., 2007). This may not be a disadvantage as 5-ASA is required for its local anti-inflammatory effect in the colon. However, in cases where it is intended for treatment of systemic inflammation, increased absorption is required (Mor *et al.*, 2008). The elimination half-life of 5-ASA is reported to be about 1 hour and the drug ~40–50% bound to plasma proteins (Nobilis *et al.*, 2006). 5-ASA is metabolized by both the liver and by the intestinal wall with the main metabolite identified as N-acetyl-5-ASA, which has a half-life of up to 10 hours and is ~80% bound to plasma proteins. The acetylated metabolites are excreted mainly in

the urine by tubular secretion together with 5-ASA (Rains *et al.*, 1992; Nobilis *et al.*, 2006; Corea, 2007). The portion of SSZ, 5-ASA, N-acetyl-5-ASA and SP that is not absorbed remains in the colon and is subsequently excreted in the faeces (Rains *et al.*, 1992; Nobilis *et al.*, 2006; Corea, 2007). Figure 8.1 depicts the pharmacokinetic pathways of SSZ, 5-ASA, N-acetyl-5-ASA and SP.

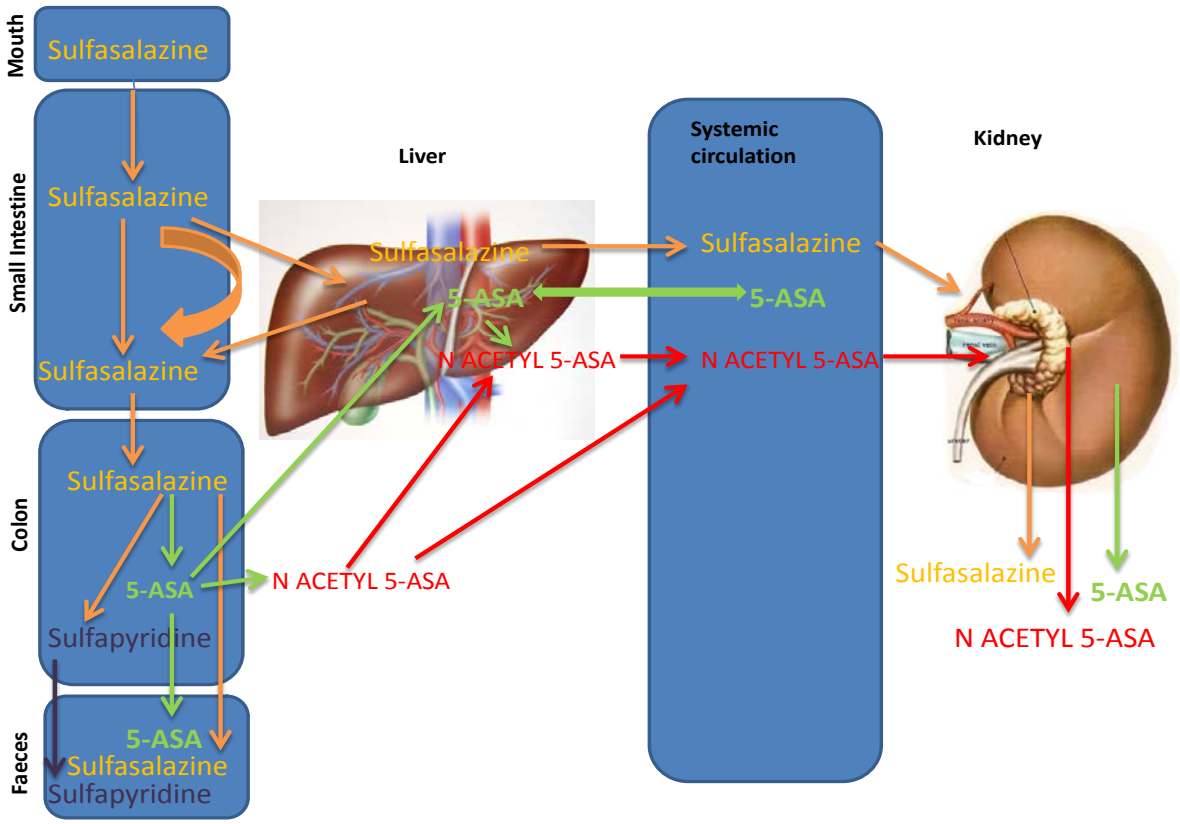


Figure 8.1: Schematic depiction of the pharmacokinetics of SSZ.

The aim of this phase of the study was thus to determine the performance of the optimized Starch-Based Platform (SBP) as an MODDS *in vivo* in the pig model by adequate measuring of the SSZ plasma concentrations and correlating this to the *in vitro* behavior observed. Furthermore, the performance was compared quantitatively to the performance of the conventional commercially available SSZ formulation, Salazopyrin® tablets. In order to achieve this, a direct measurement (SSZ concentration in plasma) and an indirect measurement (5-ASA and N-Acetyl-5-ASA concentrations in plasma) was performed. However, an important requirement to the achievement of these aims was the establishment of a suitable and effective chromatographic method for the simultaneous direct and indirect analysis of SSZ. Figure 8.2 depicts the schematic overview of the *in vivo* study performed in this Chapter.

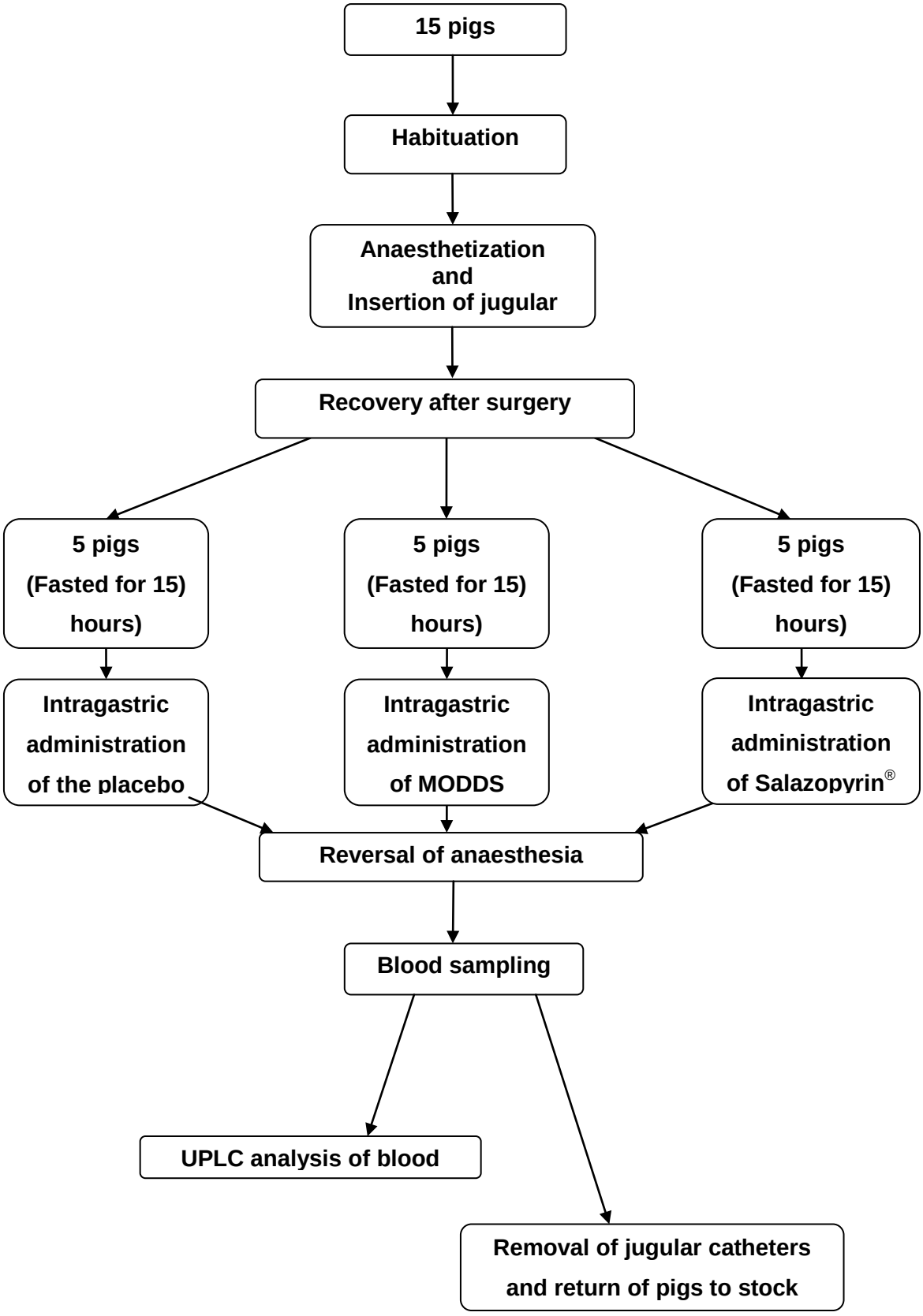


Figure 8.2: Schematic overview of *in vivo* animal study.

8.2. Materials and Methods

8.2.1. Materials

Sulfasalazine (SSZ, Mw=398.394g.Mol^{-1}, solubility=50mg.mL^{-1} in 1M NaOH solution) was purchased from Fluka, Biochemika, (Sigma-Aldrich Chemie GmbH, Steinheim, Switzerland). 5-Aminosalicyclic acid (5-ASA, Mw=153.14g.Mol^{-1}, solubility= 1.7mg.mL^{-1} at 25°C in water) was obtained from Sigma-Aldrich (St.Louis, MO, USA). Isoniazid (INH, Mw=137.14g.Mol^{-1}, solubility= 125mg.mL^{-1} in water at 25°C) was obtained from (Sigma Aldrich.Inc St. Louis, Missouri, USA) and used as the internal standard for UPLC analysis. Salazopyrin® tablets manufactured by Pfiza (Pty) Ltd. was purchased from Eastern Medicine Depot (Benoni, Johannesburg, South Africa) and used as the conventional dosage form. Drugs employed during the surgical procedure included ketamine (purchased from Bayer (Pty) Ltd. (Isando, South Africa)), midazolam (procured from Roche Products (Pty) Ltd. (Isando, South Africa)), Buprenorphine (purchased from Schering-Plough (Pty) Ltd (Rio de Janeiro, Brazil)), Carprofen (purchased from Pfizer Ltd, (Kent, UK)) and isoflurane (purchased from Safeline Pharmaceuticals (Pty) Ltd. (Johannesburg, South Africa). Solvents used for UPLC measurements were of UPLC grade, and all other reagents were of analytical grade. Acetonitrile 200 (ACN, ROMIL-SpSTM Super Purity Solvent, Assay>99.9%) and methanol (ROMIL-SpSTM Super Purity Solvent, Assay>99.9%) was purchased from Romil Pure Chemistry (Waterbeach, Cambridge, England) and double de-ionized water was obtained from a Milli-Q water purification system (Milli-Q, Millipore, Billerica, MA, USA). Acetic anhydride (Mw= 102.09g.mol^{-1}, >99% purity) was obtained from Sigma-Aldrich (St. Louis, MO, USA), Fresh blank plasma was routinely drawn from the catheterized pigs. 7-French gauge double lumen 35cm catheters (CS-28702) were purchased from Arrow Deutschland GmbH (Erding, Germany). Heparin vials (5000i.u./5mL) and isotonic saline (1L) bags were purchased from Eastern Medicine Depot (Benoni, Johannesburg, South Africa). Filters employed in the study were 0.22µm pore size Cameo Acetate membrane filter (Millipore Co., Bedford, Massachusetts). A BEH Shield RP18 (2.1×100mm, 1.7µm) column was obtained from Waters Corporation (Milford, MA, USA).

8.2.2. Preparation of optimized SBP for application as the MODDS

Due to the comparable functional results displayed by the optimized and scaled-up optimized formulations in Chapter 7, Section 7.3.2.1, SBP were prepared, at adequate quantities for all further studies on the MODDS, according to the scaled-up conditions as described in Chapter 7, Section 7.2.4. Drug Entrapment Efficiency (DEE) of the prepared SBP was elucidated as described in Chapter 2, Section 2.2.8.2.2 with UV analysis

conducted at the maximum excitation wavelength of SSZ (λmax=359nm) to ensure drug content was accurate for further studies to be conducted on the MODDS. In addition, placebo MODDS was prepared to elucidate the incidence of adverse effects due to the components of the MODDS.

8.2.3. Comparison of *in vitro* SSZ release from the MODDS and Salazopyrin® tablets

The quantity of MODDS containing 500mg SSZ was determined according to Equation 4.1 and accurately weighed in order to compare the performance of the MODDS to the conventional commercially available SSZ formulation. Salazopyrin® tablets and MODDS comprising 500mg SSZ were subjected to *in vitro* drug release studies as described in Chapter 6, Section 6.2.4.7. The drug content of each sample was quantified using UV spectroscopy at a λmax=359nm and the corresponding predefined calibration curves (Chapter 6, Section 6.2.2). In order to compare the drug release performance of the conventional dosage form and the MODDS in simulated Gastro-intestinal (GI) fluids, results from both formulations were plotted as the average fractional drug release ± the standard deviation at each sampling time. The study was conducted in triplicate.

8.2.4. Experimental subjects, habituation and living conditions

In order to conduct *in vivo* analysis, healthy female white pigs with mass 35±3kg were used in the study. Upon arrival, the pigs were placed into a large concrete-floored pen within the farm area of the Central Animal Services (CAS) at the University of Witwatersrand with adequate straw for comfort. The pigs then underwent a habituation process wherein they became accustomed to the researchers and their new surroundings. The habituation process included spending time with, feeding and caring for the pigs in the confines of the pen. Feeding of the pigs began with buckets being placed into the pen and gradually progressed to hand feeding (Figure 8.3a) as they became more comfortable with the researchers, allowing the researchers to touch them at which point habituation was deemed complete. The entire habituation process took approximately 2 weeks to accomplish.

Following surgery, the subjects were placed into individual smaller pens so as not to damage the jugular catheters. The individual pens were however large enough to allow adequate movement and activity (Figure 8.3b). The caring of the pigs was undertaken by the staff of the CAS and included cleaning of the pens twice a day, health checks, feeding with commercially available fodder twice a day and the turning off of lights at night to promote normal circadian rhythms for the farm animals. Water was provided through taps, which the pigs had learned to self-operate, and was available *ad libitum*.

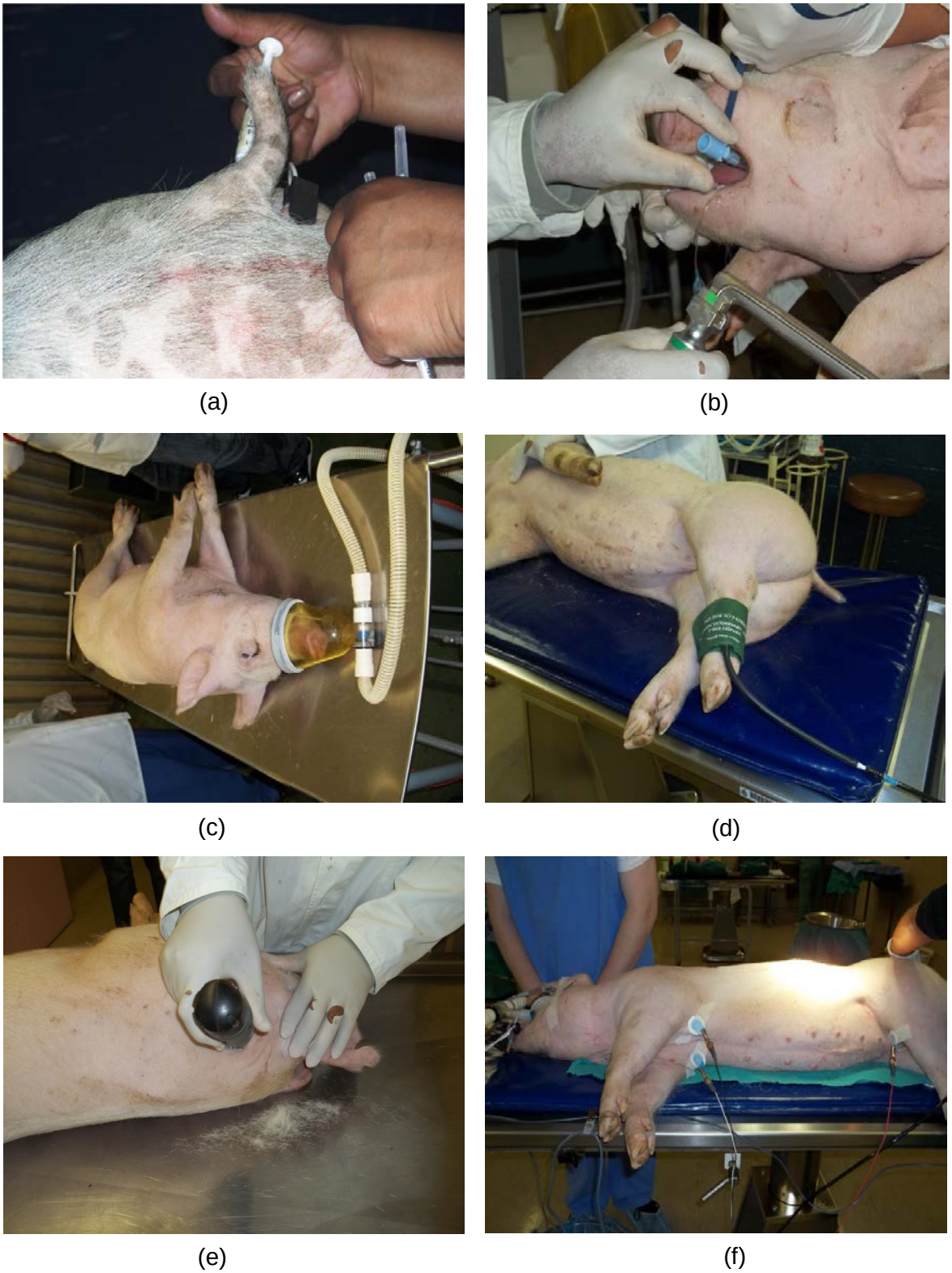


(a) (b)

Figure 8.3: Digital images depicting (a) habituation and hand feeding process and (b) individual pens.

8.2.5. Surgical insertion of a chronic jugular catheter

In order to insert the jugular catheter, the pigs were anaesthetized with Ketamine (11mg.kg^{-1}, I.M.) and Midazolam, (0.3mg.kg^{-1}, I.M.). With the purpose of providing analgesia and treat inflammation, Buprenorphine (0.05mg.kg^{-1}, I.M.) and Carpofen (4mg.kg^{-1}, I.M.) were administered (Figure 8.4a). Pigs were then intubated (Figure 8.4b) and anesthesia was maintained with 2% Isoflurane in 100% oxygen (Figure 8.4c) with constant monitoring of temperature, blood pressure and pulse (Figure 8.4d). The hair around the neck area was then shaved off (Figure 8.4e) and the skin disinfected and prepped prior to surgery (Figure 8.4f).



(a) (b)

(c) (d)

(e) (f)

Figure 8.4: Digital images depicting (a) intramuscular administration of Buprenorphine and Carpofen, (b) intubation of the pig (c) maintenance of anesthesia, (d) monitoring of temperature, blood pressure and pulse, (e) shaving of the hair around the neck area and (f) the disinfection of the skin in preparation for surgical insertion of chronic jugular catheter.

Under aseptic conditions, an incision was made dorsal to the jugular groove on the left lateral aspect of the neck to expose the jugular vein which was isolated via blunt dissection (Figure 8.5a). Thereafter, a 7-French gauge double lumen 35cm catheter (CS-28702) (Arrow Deutschland GmdH, Erding, Germany) (Figure 8.5b) was surgically inserted 10cm into the lumen into the left jugular vein (Figure 8.5c). The catheter was then fastened to the wall of the vein using a purse suture technique with the remaining length of the catheter (25cm) tunneled subcutaneously to an exit point cranial to the dorsal aspect of the scapula using a trocar (Figure 8.5d). The externalized injection ports of the catheter were sutured to the skin of the pig in order to limit excessive movement and bending (Figure 8.5e). The incision wound was then stitched (Figure 8.5f). Blood was removed via the catheter and the catheter was flushed with heparinized saline (5000i.u. of heparin in 1L of 0.9% saline). Thereafter the animal was allowed 10 days to recover from the surgical procedure. During this time, the incision wounds were disinfected using Betadine® ointment and pigs were habituated to the process of blood sampling. Routine flushing consisted of flushing the catheter with heparinized saline 3 times a day to prevent blocking of the catheter lumen due to clotting of blood.



Figure 8.5: Digital images depicting the surgical insertion of chronic jugular catheter procedure which included (a) isolation of jugular vein via blunt dissection, (b) the 7-French gauge double lumen 35cm catheter, (c) the surgical insertion of the catheter into the jugular vein, (d) subcutaneous tunneling of the catheter an exit point cranial to the dorsal aspect of the scapula using a trocar, (e) suturing of the externalized injection ports of the catheter and (f) suturing of the incision wound.

8.2.6. Intragastric dose administration

In order to insert the intragastric tube (Figure 8.6a), the pigs (fasted for 12 hours) were anaesthetized using a cocktail composed of midazolam (0.3mg.kg^{-1},) and buprenorphine (0.05mg.kg^{-1}) injected directly into the jugular vein catheter (Figure 8.6b). Anesthesia was then maintained using 2% isoflurane and 100% oxygen with constant monitoring of temperature, blood pressure and pulse, as was the case during preparation for surgery in Section 8.2.5. Thereafter the pig was positioned vertically with the esophagus and stomach kept in line and the intragastric tube was inserted directed into the stomach (Figure 8.6c). The Multiparticulate Oral Drug Delivery System (MODDS, placebo or Salazopyrin® tablets) was then inserted into the oral end of the intragastric tube and flushed into the stomach with an adequate quantity of water. Following dose administration, the pigs were returned to their respective pens and allowed to recover under continuous observation.



(a)



(b)



(c)

Figure 8.6: Digital images depicting (a) the intragastric tube, (b) administration of anesthetics and (c) dosing during the intragastric dose administration process.

8.2.7. Blood sampling and plasma storage procedure

Blood sampling was conducted prior to dose administration in order to obtain drug free blood samples and thereafter at predetermined times (2, 4, 6, 8, 10, 12, 16, 20 and 24 hours) after dose administration. Prior to blood sampling, the catheter ports were disinfected (Figure 8.7a) and the catheter flushed using (5mL) heparinized saline in order to remove any blockages due to clotting (Figure 8.7b). In order to prevent dilution of the blood sample by heparinized saline that remained in the catheter, a small blood sample was then drawn into the syringe and discarded immediately. Thereafter, blood samples (5mL) were drawn, placed into heparinized Monovette® vials (Sarstedt, Germany) and centrifuged immediately at 5000rpm for 10 minutes. The separated plasma was then placed into eppendorf tubes (1mL), appropriately labeled and stored at -70°C.



(a) (b)

Figure 8.7: Digital images depicting (a) the disinfection and (b) the flushing of catheter ports during blood sampling.

It is important to note that habituation, surgical catheter insertion, intragastric dose administration and blood sampling was conducted as per methods and protocols of the CAS at the University of Witwatersrand and as approved in the ethics application.

8.2.8. Determination of the *in vivo* drug release behavior of SSZ from Salazopyrin® tablets and MODDS

8.2.8.1. Development of a method for sample analysis employing Ultra Performance liquid chromatography

High Pressure Liquid Chromatography (HPLC) has long been used for the determination of drug concentrations in the blood (Homma *et al.*, 1999; Madej *et al.*, 2003; Juřica *et al.*, 2010; Nageswari *et al.*, 2012). However, HPLC has its drawbacks in terms of long run times, large volumes of biological samples, complicated sample processing procedures

and inadequate sensitivity (Tettey-Amlalo and Kanfer, 2009; Ye *et al.*, 2011; Nageswari *et al.*, 2012). Ultra Pressure Liquid Chromatography (UPLC) is an advancement on HPLC in that it employs chromatographic separations based on a sub 2µm stationary phase operated at high pressures to give high flow rates and low instrument dead volume (Pedraglio *et al.*, 2007; Athersuch *et al.*, 2008; Tettey-Amlalo and Kanfer, 2009; Nageswari *et al.*, 2012). These features of UPLC result in drastic improvement in sensitivity, peak separation and resolution, speed of analysis and requires smaller sample injection volumes giving a considerable saving in both instrument and analyst time (Pedraglio *et al.*, 2007; Athersuch *et al.*, 2008; Tettey-Amlalo and Kanfer, 2009; Nageswari *et al.*, 2012).

8.2.8.1.1. Equipment employed for Ultra Performance liquid chromatography analysis

The Waters Acquity Ultra Performance Liquid Chromatography (UPLC) system (Waters, Milford, MA, USA) with a PDA detector was utilized in the study. The machine was equipped with a binary solvent manager that contained four lines (A1, A2, B1 and B2) for the flow of mobile phase solvents. The A-lines were used for inorganic liquids with line A1 exclusively used for water while line A2 was for the exclusive use of inorganic mobile phases. On the other hand, the B-lines were used for inorganic solvents with lines B1 and B2 reserved for methanol and ACN respectively.

8.2.8.1.2. Priming of pumps for Ultra Performance liquid chromatography analysis

The stationary phase of column used in the study was stored in ACN. Prior to analysis, priming of the pumps was necessary and was achieved in a step-wise manner, the first step being the running of pure ACN through the column for 5 minutes. A strong wash, comprising 90% ACN and 10% water, and thereafter a weak wash, comprising 10% ACN and 90% water was pumped through the column for 5 minutes each in order to wash the column. Finally, the binary mixture of organic and inorganic mobile phases that was relevant to the study was pumped through the column in order to complete the priming process. Upon completion of analysis, washing of the column was crucial. This was achieved by slowly increasing the ACN concentration in the binary mixture with each step-up allowed to be pumped through the column for 5 minutes and finally 100% ACN was pumped through the column for 10 minutes to ensure that the stationary phase of column used in the study was stored in ACN.

It is important to note that only double de-ionized water (Milli-Q, Millipore, Johannesburg) with a resistivity of 18.2MΩcm^{-1} was used for all UPLC solvents employed for sample analysis. In addition, the mobile phases, weak and strong washes and all solvents used for sample preparation were filtered using a 0.22µm pore size Cameo Acetate membrane filter (Millipore Co., Bedford, Massachusetts) prior to being pumped through the UPLC column.

8.2.8.1.3. Derivatization of 5-ASA to N-acetyl-5-ASA

SSZ is absorbed to a small extent in the small intestine and upon reaching the colon releases the active drug moiety 5-ASA as depicted in Figure 8.1. 5-ASA is absorbed in the colon but undergoes extensive metabolism in the liver and gut wall to many degradation products, the principle moiety being N-acetyl-5-ASA (Tjornelund and Hansen, 1991). Thus in order to assess the *in vivo* drug release of SSZ, measurement of actual SSZ as well as the measurement of 5-ASA in the blood was necessary as one molecule of SSZ releases one molecule of 5-ASA (Figure 6.1). Since 5-ASA is converted to N-acetyl-5-ASA to a large extent *in vivo*, determining the blood levels of N-acetyl-5-ASA represent the levels of 5-ASA and thus corresponds to the *in vivo* release of SSZ. Therefore, in addition to elucidating the levels of SSZ and 5-ASA, it was important to determine the levels of N-acetyl-5-ASA in the blood.

N-acetyl-5-ASA was synthesized *in vitro* according to the method proposed by Nobilis and co-workers (2006). Synthesis involved dissolving 5-ASA (1g, 0.0065mol) in acetic anhydride solution and stirring the reaction mixture for 3 hours at 25°C. The reaction mixture was allowed to stand for 24 hours after which the crude crystalline product was filtered off and washed with double de-ionized water and subsequently dried over P_2O_5. Figure 8.8 depicts the chemical reaction for the synthesis of N-acetyl 5-ASA.

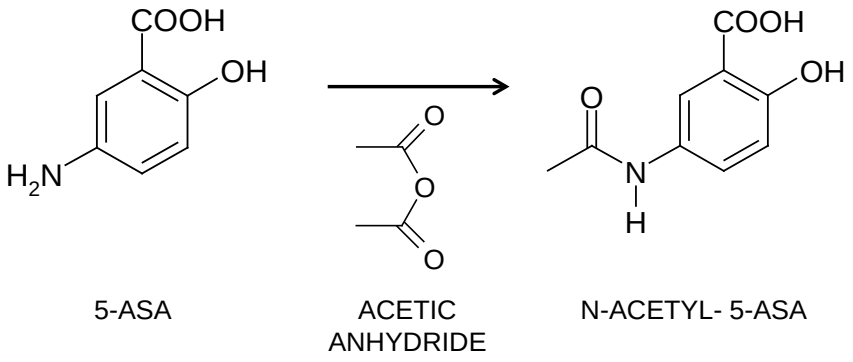


Figure 8.8: Chemical reaction for the synthesis of N-acetyl 5-ASA.

8.2.8.1.4. Determination of UPLC parameters for adequate separation of SSZ, 5-ASA and N-Acetyl-5-ASA

Important parameters that influence the separation of compounds and their subsequent detection during UPLC analysis include the UPLC column, column temperature, binary mobile phases, the flow rate of the mobile phases through the column, sample injection volume and maximum excitation wavelength (λmax). In addition, the employment of an isocratic or gradient elution method affects the peak resolution and has a direct impact on the run time of the analysis. Thus, all of the above-mentioned parameters were methodically manipulated in order to obtain adequate separation of SSZ, 5-ASA and N-Acetyl-5-ASA. The optimum separation of the analytes was achieved on the Acquity UPLC® BEH Shield RP18 column (2.1mm x100mm, 1.7µm particle size) maintained at 25°C. A gradient elution method was chosen employing ACN as the organic component and formic water (FW, 1%$^{v}/_{v}$) as the inorganic component of the binary mobile phase at a flow rate of 0.4mL.min^{-1} as shown in Table 8.1. Injection volume was standardized at 3µL and UV detection was performed at λmax=313nm. Upon optimizing the UPLC method, INH was selected as the internal standard.

Table 8.1: Parameters employed in the gradient elution UPLC method for the separation of SSZ, 5-ASA and N-Acetyl-5-ASA

Time (min)	Flow rate (mL.min^{-1})	Organic Phase ACN (%)	Inorganic Phase 1%$^{v}/_{v}$ FW (%)
0	0.4	95	5
1	0.4	65	35
2	0.4	30	70
3	0.4	5	95
3.5	0.4	95	5

Where ACN denoted Acetonitrile and FW denoted Formic Water

8.2.8.2. Selection of a suitable method of deproteinization and drug extraction from plasma for UPLC analysis

Due to the high protein binding of the analytes (SSZ >99%, 5-ASA ~40-50% and *N*-acetyl-5-ASA ~80%), plasma samples required deproteinization prior to analysis (Klotz, 1985; Rains, 1992; Parfitt, 1999; Corea, 2007; Kenakin, 2009). Separate solutions (2µg/mL) were prepared by dissolving 10mg of SSZ, 5-ASA and N-Acetyl-5-ASA in 5mL ACN. Thereafter defrosted blank plasma 350µL was transferred into a 2mL eppendorf tube, spiked with 50µL of each drug solution and vortex mixed (Vortex-Genie 2, Scientific Industries Inc., Bohemia, NY, USA) for 1 minute to allow for protein binding of analytes. The plasma was then subjected to deproteinization and drug extraction. Furthermore, a 0.43µg.mL^{-1} solution of INH was prepared and used as the internal standard.

8.2.8.2.1. Solid phase extraction

Solid Phase Extraction (SPE) is a common and one of the most popular methods of sample preparation and essentially involves partitioning of analytes between a liquid, which could be the sample matrix or solvent with analytes, and a solid, which is the sorbent in the SPE cartridge. The liquid is regarded as the mobile phase while the solid is considered the stationary phase (He *et al.*, 2007; Golmohammed, 2012). There are several types of SPE techniques including normal-phase, reversed-phase, ionic, and use of other special sorbents (He *et al.*, 2007), all of which comprise steps which include extraction of analytes from the mobile phase into the stationary phase and subsequently, elution of the extracted analytes from the stationary phase using a liquid which in which the analytes are more soluble or which disrupt the interactions between analytes and stationary phase (He *et al.*, 2007; Sadeghi and Sheikhzadeh, 2008; Golmohammed 2012). This allows extraction, purification and concentration of analytes using minimal time and organic solvents. Furthermore, SPE offers the ability to handle a wide range of sample volumes, ease of use and potentially excellent selectivity due to a wide range of available sorbents *(*Corta *et al.,* 1999; He *et al.*, 2007; Xue *et al.*, 2007; Sadeghi and Sheikzadeh, 2008, Golmohammed, 2012). Due to these advantages, analyte-spiked plasma was subjected to SPE in an attempt to extract SSZ, 5-ASA and N-Acetyl-5-ASA from plasma.

A 2%$^{v}/_{v}$ Phosphoric acid solution was prepared and 500µL of this solution was added to the spiked plasma samples. The mixture was vortex mixed for 1 minute to adequately interact with the plasma proteins and facilitate deproteinization of the drugs. Thereafter this mixture was centrifuged (Optima® LE-80K, Beckman, USA) for 10 minutes at 3000rpm and the supernatant added drop-wise into the preconditioned SPE cartridge (conditioning of the SPE cartridges involved eluting methanol (1mL) followed by water (1mL) through the sorbent). The cartridge was then washed with HCl (0.1M, 1mL) followed by methanol (1mL) and allowed to dry for approximately 1 minute. Elution of the entrapped drug was then performed by adding ammonia in methanol solution ($5^{v}/_{v}$%, 1mL) to the SPE cartridge and collected in a clean test tube. Finally the eluted drug solution was spiked with 20µL of INH, filtered through a 0.22µm pore size Cameo Acetate membrane filter (Millipore Co., Bedford, Massachusetts) into the UPLC vials (Waters® LCMS certified vials with a pre-slit screw top, Waters, Milford, MA, USA) and subjected to UPLC analysis. Figure 8.9 represents a schematic overview of the SPE procedure employed.

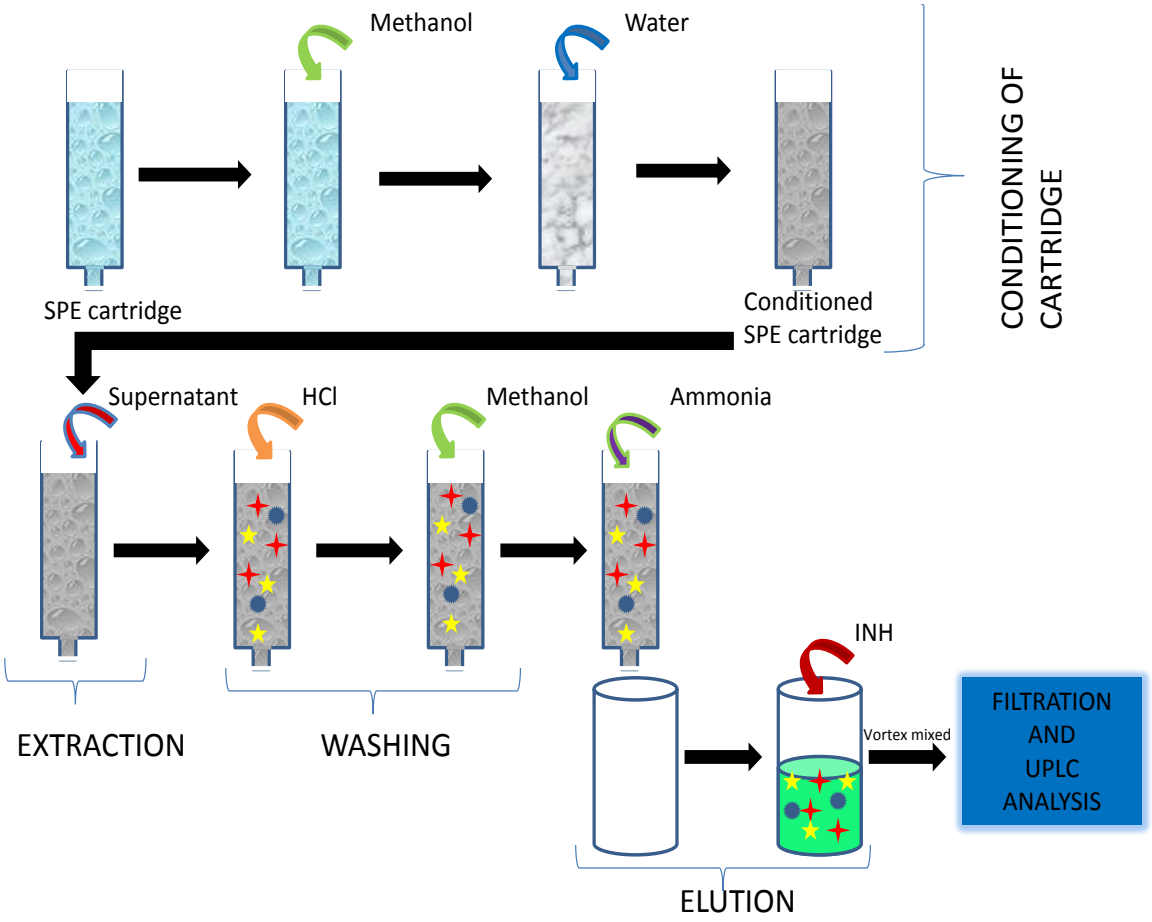


Figure 8.9: Schematic overview of the SPE procedure.

In order to elicit the effectiveness of SPE in analyte recovery from plasma, the same SPE process was followed with plasma being substituted with water and the recovery calculated by comparing the peak analyte: INH ratio obtained from extracted analytes to those obtained from standard solutions at the same concentrations according to Equation 8.1, Equation 8.2 and Equation 8.3.

$$Water\ ratio = \frac{AUC_{drug}}{AUC_{INH}} \qquad \textit{Equation 8.1}$$

$$Plasma\ ratio = \frac{AUC_{drug}}{AUC_{INH}} \qquad \textit{Equation 8.2}$$

$$Recovery = \frac{Water\ ratio}{Plasma\ ratio} X\ 100 \qquad \textit{Equation 8.3}$$

8.2.8.2.2. Liquid-liquid extraction

Due to the inability of Solid Phase Extraction (SPE) to provide adequate extraction of SSZ, 5-ASA and N-Acetyl-5-ASA from plasma, Liquid-Liquid Extraction (LLE) was employed. LLE has always been used as an alternative to SPE because it is cost effective, easy to develop, and capable of providing very clean sample extracts (Xue *et al.*, 2007*).* Like SPE, LLE involves partitioning of analytes between 2 phases. However, in contrast to SPE, the 2 phases are both liquid with one being organic and the other inorganic with extraction occurring due to the affinity of the analytes for a particular phase (Muller *et al.*, 2008; Golmohammed 2012).

LLE employing different organic solvents was attempted in order to achieve the highest recovery of all analytes from plasma (inorganic phase). Perchloric acid, methanol and ACN were added to spiked plasma samples in the ratio of 0.1:1, 3:1 and 2:1 respectively, and vortex mixed for 1 minute to adequately interact with the plasma proteins and facilitate deproteinization of the drugs. Thereafter this mixture was centrifuged (Optima® LE-80K, Beckman, USA) for 10 minutes at 3000rpm and the supernatant removed and placed into clean test tubes. The supernatant was then spiked with 20µL of INH, filtered through a 0.22µm pore size Cameo Acetate membrane filter (Millipore Co., Bedford, Massachusetts) into the UPLC vials (Waters® LCMS certified vials with a pre-slit screw top, Waters, Milford, MA, USA) and subjected to UPLC analysis. In order to elicit the effectiveness of SPE in analyte recovery from plasma, the same LLE process was followed with plasma being substituted with water and the recovery calculated by comparing the peak analyte: INH ratio obtained from extracted analytes to those obtained from standard solutions at the same concentrations according to Equation 8.1, Equation 8.2 and Equation 8.3. Figure 8.10 represents a schematic overview of the LLE procedure employed.

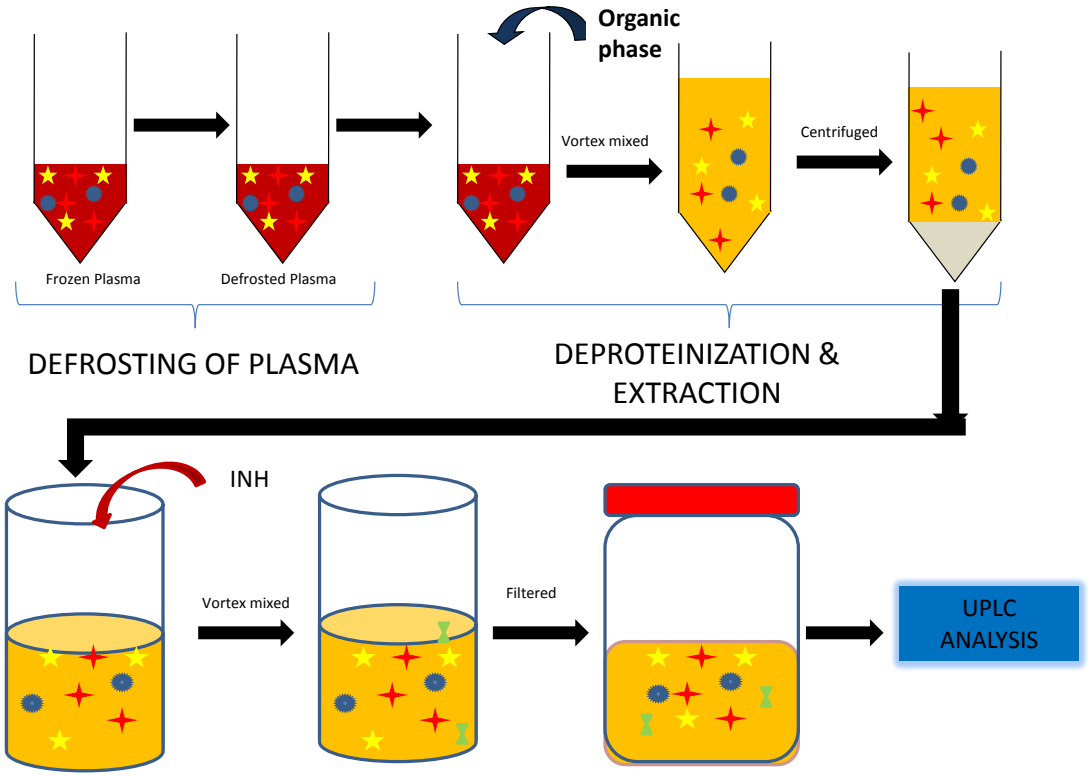


Figure 8.10: Schematic overview of the LLE procedure.

8.2.8.3. Preparation of analytical standards for the calibration series

Stock solutions of SSZ, 5-ASA and N-Acetyl-5-ASA were prepared by accurately weighing and dissolving 5mg of each drug in 50mL ACN. Aliquots (10mL) of each stock solution were then accurately measured and combined to form a new stock solution on which 6-fold serial dilutions were performed in order to construct the calibration curves. Drug free plasma (350µL) was then spiked with these stock solutions (150µL) and subjected to the same LLE procedure described in Section 8.2.8.2.2 utilizing ACN (1mL) as the deproteinization and extraction agent. Following the addition of INH (20µL), the serially diluted solution concentrations ranged from 0.0005625mg.mL^{-1} to 0.036mg.mL^{-1}, 0.000583mg.mL^{-1} to 0.0373mg.mL^{-1} and 0.00059375mg.mL^{-1} to 0.038mg.mL^{-1} for SSZ, 5-ASA and N-Acetyl-5-ASA respectively. Each solution was then filtered through a 0.22µm pore size Cameo Acetate membrane filter (Millipore Co., Bedford, Massachusetts) into the UPLC vials (Waters® LCMS certified vials with a pre-slit screw top, Waters, Milford, MA, USA) and subjected to UPLC analysis. The calibration curve was constructed by plotting the peak area ratios of the analyte and INH on the y-axis against the corresponding analyte concentrations (expressed as µg/mL) on the x-axis. Intercepts were set at 0 and linearity equations and correlation coefficients (R^2) were obtained by means of the least square method.

8.2.8.4. UPLC analysis of drug release after the in vivo administration of Salazopyrin® and the MODDS

Upon determining adequate plasma extraction and UPLC separation procedures and construction of appropriate calibration curves for SSZ, 5-ASA and N-Acetyl-5-ASA, the plasma samples drawn during the *in vivo* animal studies could be analyzed. The plasma samples (500µL) were allowed to defrost and subjected to the same LLE procedure described in Section 8.2.8.2.2, devoid of spiking with solution, utilizing ACN (1mL) as the deproteinization and extraction agent. INH (20µL) was then added to the sample solutions which were filtered through a 0.22µm pore size Cameo Acetate membrane filter (Millipore Co., Bedford, Massachusetts) into the UPLC vials (Waters® LCMS certified vials with a pre-slit screw top, Waters, Milford, MA, USA) and subjected to UPLC analysis. UPLC analysis was carried out under the parameters as described in Section 8.2.8.1.4.

8.3. Results and Discussion

8.3.1. Comparative *in vitro* drug release behavior of Salazopyrin® tablets and the MODDS

Drug entrapment showed DEE values that were very similar to that observed when preparing the optimized SBP and scaling up the optimization process in Chapter 7, Section 7.3.2.1. Similarly, the drug release profile generated by the MODDS (Figure 8.11) was fitted into Equation 7.10 and Equation 7.11 and was found to be almost identical to that depicted in Chapter 7, Section 7.3.2.4 with regard to the shape and displayed *F1* and *F2* values of 0.538 and 95.278 respectively. These results show the robustness and reproducibility of the optimized formulation and scaling up process employed in developing the MODDS.

In vitro drug release profiles of SSZ from Salazopyrin® and the MODDS were depicted in Figure 8.11. The profile of the conventional Salazopyrin® tablets show that drug release started immediately upon submerging the tablet into the dissolution medium and was complete within one hour. The behavior shown by the release profile can be explained by the visual scrutiny of Salazopyrin® within the dissolution medium. It was noted that upon interaction with the dissolution medium, air-bubbles were seen emerging from the Salazopyrin® tablet with accompanying erosion of the surface. The dissolution medium became increasing orange as a result of further drug release until a maximum intensity at approximately 45 minutes was reached. At this stage, it was observed that the Salazopyrin® tablet had undergone complete disintegration and thus all SSZ was released.

Conversely, the profile of the MODDS showed much more control of drug release as was discussed in Chapter 7, Section 7.3.2.4. Visually, there was a gradual increase in color intensity of the dissolution media, which correlated to the fractional SSZ release observed in Figure 8.11. Upon conclusion of the 12-hour study, the SBP from the MODDS remained intact with a fair quantity of SSZ remaining within the SBP. Thus, the MODDS had shown a substantial improvement in controlling drug release when compared to the conventional Salazopyrin® tablets *in vitro*.

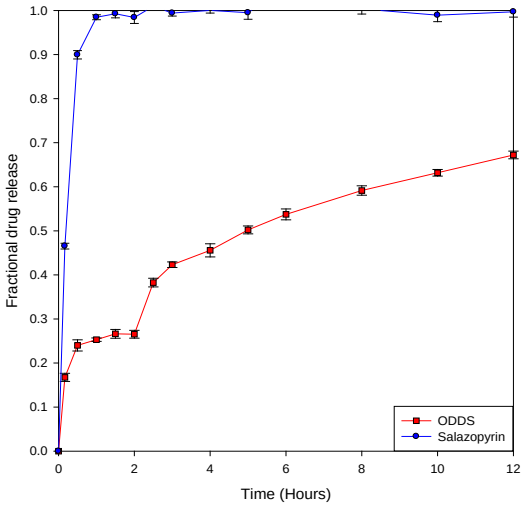


Figure 8.11: Comparative *in vitro* drug release behavior of SSZ from Salazopyrin® EN and the MODDS (n=3 in all instances).

8.3.2. Effect of habituation, catheterization, dosing and blood sampling

Upon arrival of the pigs, interaction with humans was found to be very difficult as the pigs were in unfamiliar surroundings and fearful of human contact. Therefore, it was very important to acclimatize the pigs to their new surroundings and allow them time to adjust to the presence of, and further along the study, direct contact with humans. During this habituation process, we as researchers also gained knowledge of the behavior of the pigs and through continuous exposure, we were able to interact with the pigs to the extent of hand feeding and petting.

Following catheterization, the pigs showed excellent recovery with no adverse effects on the behavior of the pigs towards the researchers. This was crucial as it allowed the researchers to touch the pigs and apply disinfectant ointment onto the wounds to prevent infection. Furthermore, disinfecting of the catheters prior to flushing and drawing of blood and regular flushing of the catheters with heparinized saline was important to prevent clotting of blood within the catheter and at the opening in the jugular vein and thus ensure the viability of blood sampling from the catheters for a prolonged period.

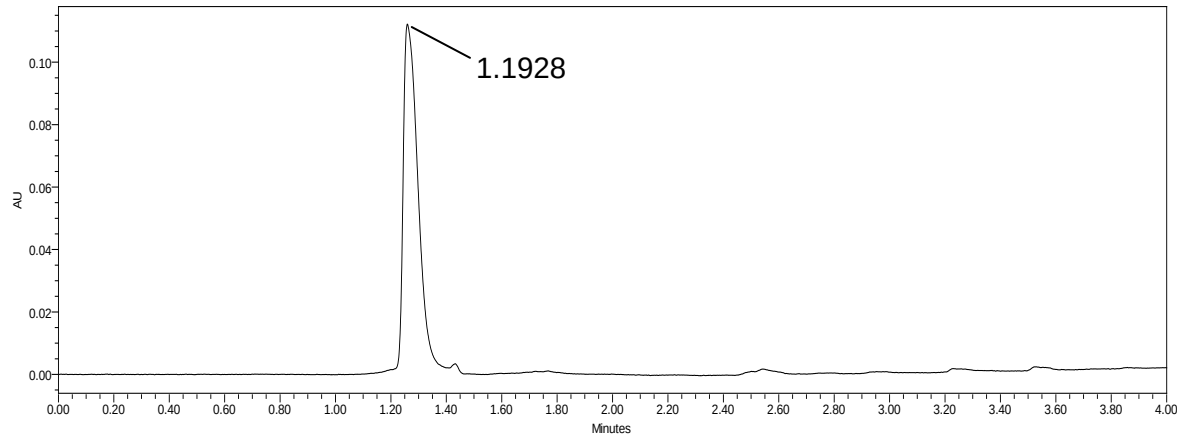
Following dosing of the pigs, no adverse effects either due to SSZ (in Salazopyrin® and the MODDS) or the components of the MODDS (placebo MODDS) were observed and the pigs displayed the usual levels of activity and appetite as previously observed. Sampling of blood at each time point was relatively simple and did not consume much time as the pigs were comfortable with the presence of the researchers and the catheters were adequately maintained. Thus, the process of habituation was adjudged to be successful as direct human-pig interactions was possible which in turn allowed for efficient sampling for the duration of the *in vivo* study.

8.3.3. *In vivo* analysis of plasma samples subsequent to administration of Salazopyrin® tablets and the MODDS

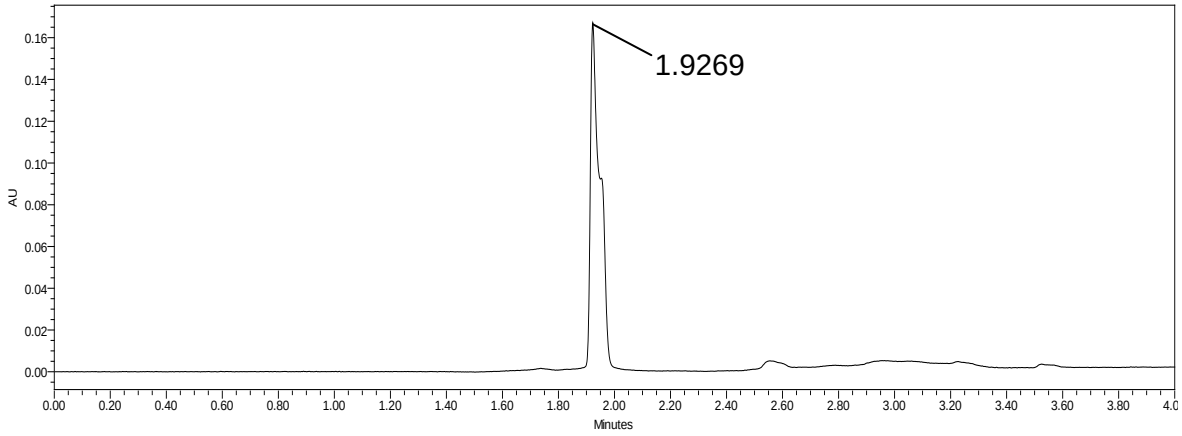
8.3.3.1. Derivatization of 5-ASA to N-acetyl 5-ASA

Due to the large extent of 5-ASA to N-Acetyl-5-ASA metabolism *in vivo*, it was important to determine the plasma drug levels of N-Acetyl-5-ASA. However, N-Acetyl-5-ASA was not commercially available and *in vitro* synthesis was required through a process of acetylation of the amino group on the 5-ASA molecule. Derivatization of pure 5-ASA was necessary prior to UPLC analysis as acetylating of the entire plasma sample could result in superfluous derivatization of SSZ within the plasma and complicate the UPLC analysis of SSZ. Furthermore, there would be an underestimation of the quantity of 5-ASA in the event of incomplete derivatization of 5-ASA within plasma which would result in inaccurate interpretation of the *in vivo* drug release of SSZ from the formulations.

Subsequent to synthesis of N-Acetyl-5-ASA, solutions of 5-ASA and N-Acetyl-5-ASA in ACN were prepared and subjected to UPLC analysis according to the method developed. The resultant chromatograms show 5-ASA (Figure 8.12a) displayed a peak at a retention time (RT) of 1.1928 minutes and N-Acetyl-5-ASA (Figure 8.12b) displayed a peak at a RT of 1.9269 minutes. The different RTs displayed by 5-ASA and N-Acetyl-5-ASA solutions at identical UPLC conditions prove that the molecules were different and that the derivatization procedure was successful.



(a)



(b)

Figure 8.12: Chromatograms illustrating the retention time peaks of a) 5-ASA (RT=1.1928) and b) N-Acetyl-5-ASA (RT=1.9269).

8.3.3.2. Validation of developed method for UPLC analysis of plasma samples

A solution of SSZ in ACN was prepared and subjected to the UPLC method employed in determining the derivatization of 5-ASA to N-Acetyl-5-ASA. The chromatogram produced showed a peak at RT of 2.4951 as depicted in Figure 8.13.

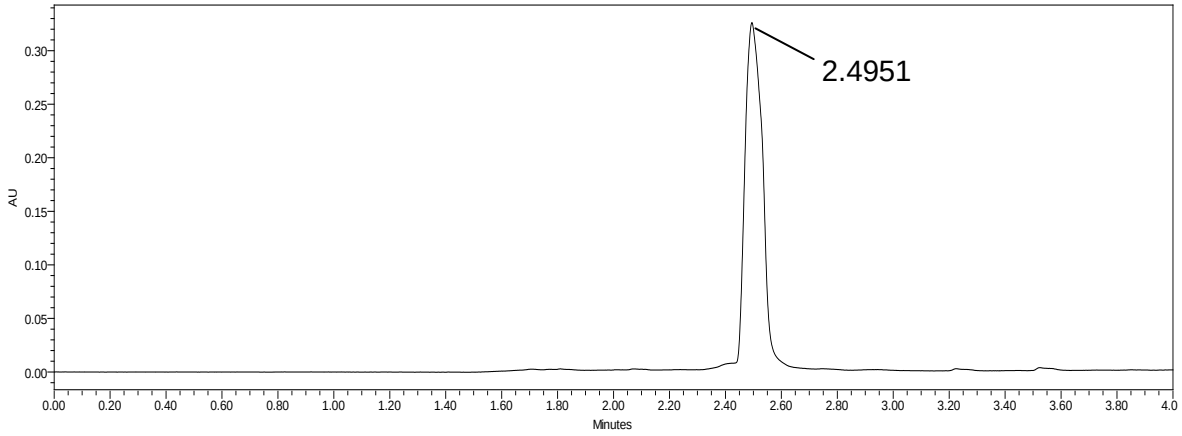


Figure 8.13: Chromatogram illustrating the retention time peak of SSZ (RT=2.4951 minutes).

A stock solution of 5-ASA and N-Acetyl-5-ASA and SSZ was then prepared and subjected to the UPLC method developed to ensure that adequate separation of all the analytes expected to be found during UPLC analysis of plasma was achieved. Figure 8.14 illustrated that excellent separation and resolution of all the analytes was achieved and the RTs of all the analytes were identical to that observed when each analyte was analyzed individually.

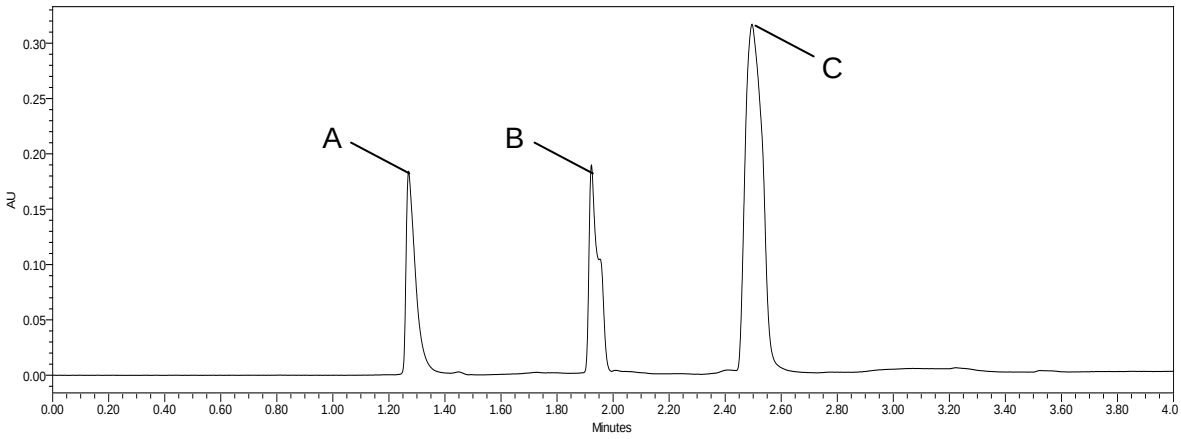


Figure 8.14: Chromatogram illustrating the separation of the retention time peaks of (A) 5-ASA (RT=1.1928 minutes), (B) N-Acetyl-5-ASA (RT=1.9269 minutes) and (C) SSZ (RT=2.4951 minutes).

The use of an internal standard is important in UPLC analysis as it allows for normalization of the analytes being determined and accounts for routine variation in the response of the chromatographic system. In this study, a UPLC method that ensured separation of all analytes was developed with only a suitable internal standard required. Many candidate molecules were tested but only INH displayed suitability to the pre-developed UPLC method with good resolution and a RT of 1.0151 minutes (Figure 8.15) and thus INH was selected as the internal standard for the study.

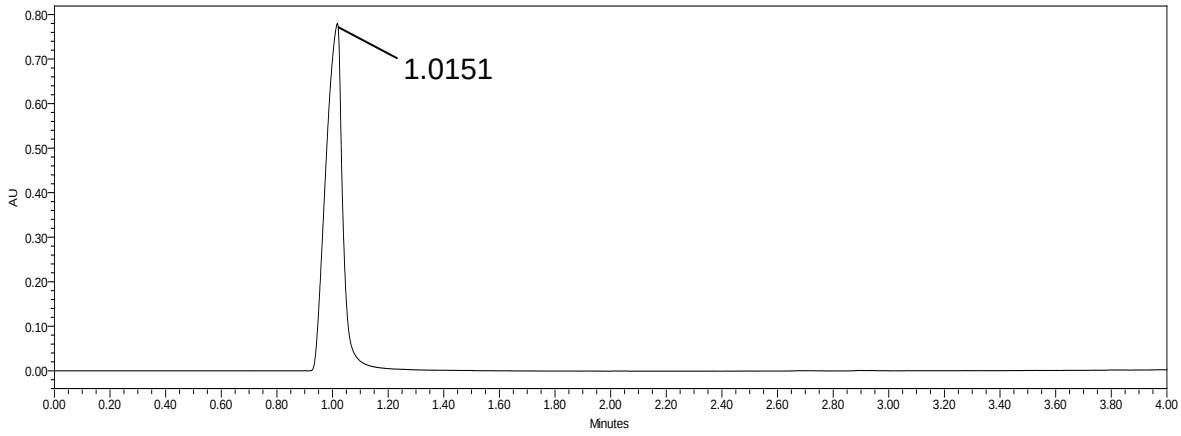


Figure 8.15: Chromatogram illustrating the retention time peak INH (RT=1.0151 minutes).

The stock solution containing the three analytes was then spiked with INH and subjected to UPLC analysis with the resultant chromatogram depicted in Figure 8.16. Scrutiny of the chromatogram shows that with the addition of internal standard, shifting of retention times occurred (5-ASA RT=1.1928 to RT=1.2623, N-Acetyl-5-ASA RT=1.9269 to RT=2.0235, SSZ RT=2.4951 to RT=2.6266 and INH RT=1.0151 to RT=0.9961). However, there was still excellent separation and resolution of all the peaks in the chromatogram.

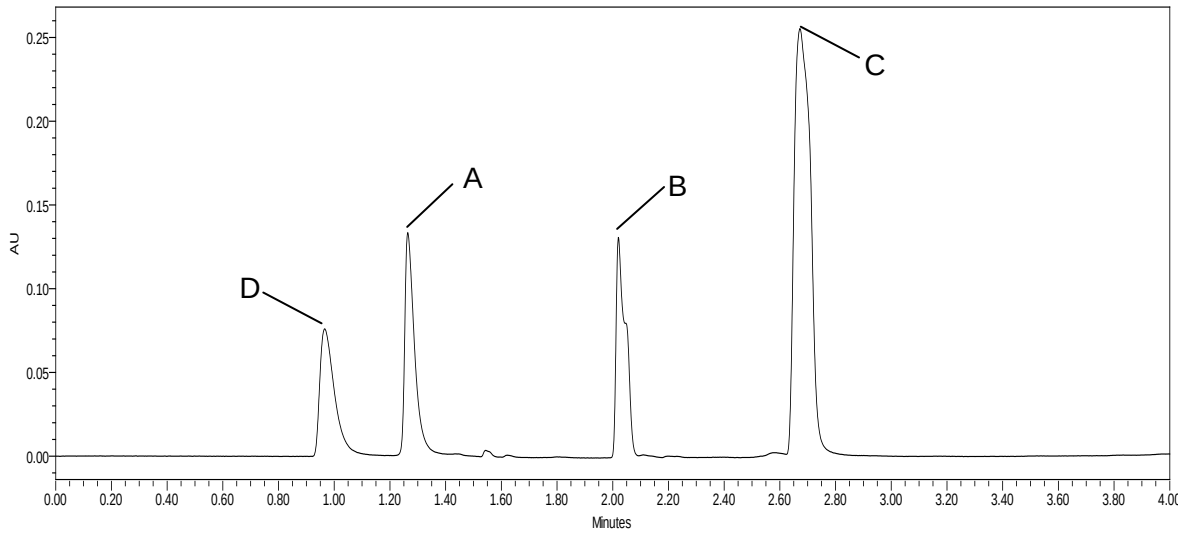


Figure 8.16: Chromatogram illustrating the separation of the retention time peaks of (A) 5-ASA (RT=1.2623 minutes), (B) N-Acetyl-5-ASA (RT=2.0235 minutes) and (C) SSZ (RT=2.6266 minutes) in the presence of (D) INH (RT=0.9961 minutes).

8.3.3.3. Deproteinization and drug extraction

Table 8.2 illustrated the extent of analyte recovery employing different solvents SPE and LLE. Blank plasma, and separately water to determine the water ratio, was spiked with a known concentration of a single analyte and subjected to the analyte extraction process. The sample was then spiked with a known concentration of INH, filtered and subjected to the UPLC analysis employing the method developed. The peak analyte: INH ratio was used to determine the extent of recovery of the analytes from plasma using the different methods stated. SPE was initially employed, due to its advantages as mentioned previously, but showed unsatisfactory analyte recovery and was not pursued further.

LLE was then introduced with perchloric acid initially used as the organic solvent. However, the analyte recovery showed only a slight improvement to that seen with SPE and it was postulated that the acidic environment of perchloric acid was not conducive to satisfactory extraction of the analytes. Methanol and ACN, which exert good deproteinization properties, were then employed as the organic phase in LLE and both showed a marked improvement in the extent of analyte extraction with the effect of ACN

being superior to that of methanol. The solubility of the analytes in ACN was important as it allowed deproteinization and extraction in a single step and thus ACN was selected as the deproteinization and extraction agent for the study.

Table 8.2: Recovery of analytes subsequent to various deproteinization and extraction methods

Analyte	Extraction method			
	SPE	LLE		
		Perchloric acid	Methanol	ACN
5-ASA	38.72%	44.89%	33.72%	95.71%
N-Acetyl-5-ASA	28.47%	40.58%	64.30%	95.76%
SSZ	33.98%	39.89%	71.25%	97.71%

Where SPE denoted solid-phase extraction, LLE denoted liquid-liquid extraction, 5-ASA denoted 5-aminosalacylic acid, N-Acetyl-5-ASA denoted N-Acetyl derivative of 5-aminosalacylic acid, and SSZ denoted Sulfasalazine

Once an appropriate extraction method was determined, blank plasma was spiked with a combination of 5-ASA and N-Acetyl-5-ASA and SSZ and subjected to the developed analyte extraction method, followed by INH spiking and UPLC analysis. The chromatogram produced (Figure 8.17) showed slight shifting of retention times for INH (RT=0.9961 to RT=0.9648) and 5-ASA (RT=1.2623 to RT=1.1856) and negligible shifts in the RT of N-Acetyl-5-ASA and SSZ. However, there was still excellent separation and resolution of all the peaks in the chromatogram and the extraction and UPLC methods developed were confirmed to be suitable for plasma analyte quantification.

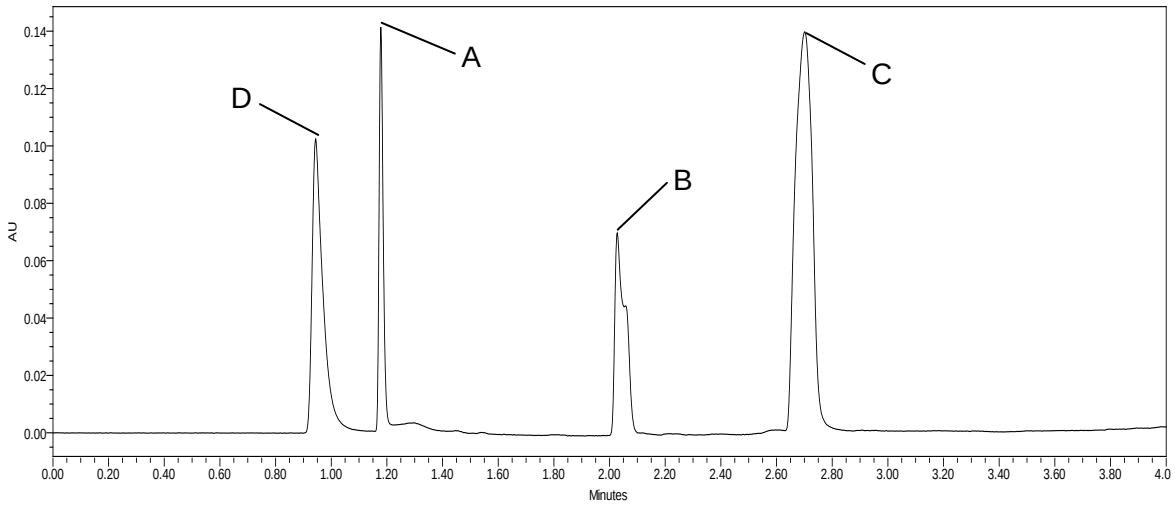


Figure 8.17: Chromatogram illustrating the separation of the retention time peaks of (A) 5-ASA (RT=1.1866 minutes), (B) N-Acetyl-5-ASA (RT=2.0228 minutes) and (C) SSZ (RT=2.6310 minutes) and (D) INH (RT=0.9961 minutes) subsequent to plasma extraction.

8.3.4. Calibration curves constructed for the quantitative analysis of SSZ, 5-ASA and N-Acetyl-5-ASA in plasma

The calibration curves constructed for each of the analytes in depicted in Figure 8.18. Samples of the calibration series were analyzed at a λmax=313nm for all analytes and INH. Sample analyte concentrations ranged from 0-36.548µg.mL^{-1}; 0-37.394µg.mL^{-1} and 0-38.243µg.mL^{-1} for SSZ; 5-ASA and N-Acetyl-5-ASA respectively. Each of the calibration curves showed good linearity (R^2 of SSZ=0.9975, R^2 of 5-ASA=0.9978 and R^2 of N-Acetyl-5-ASA=0.9928) and all sample points were within the 95% prediction band.

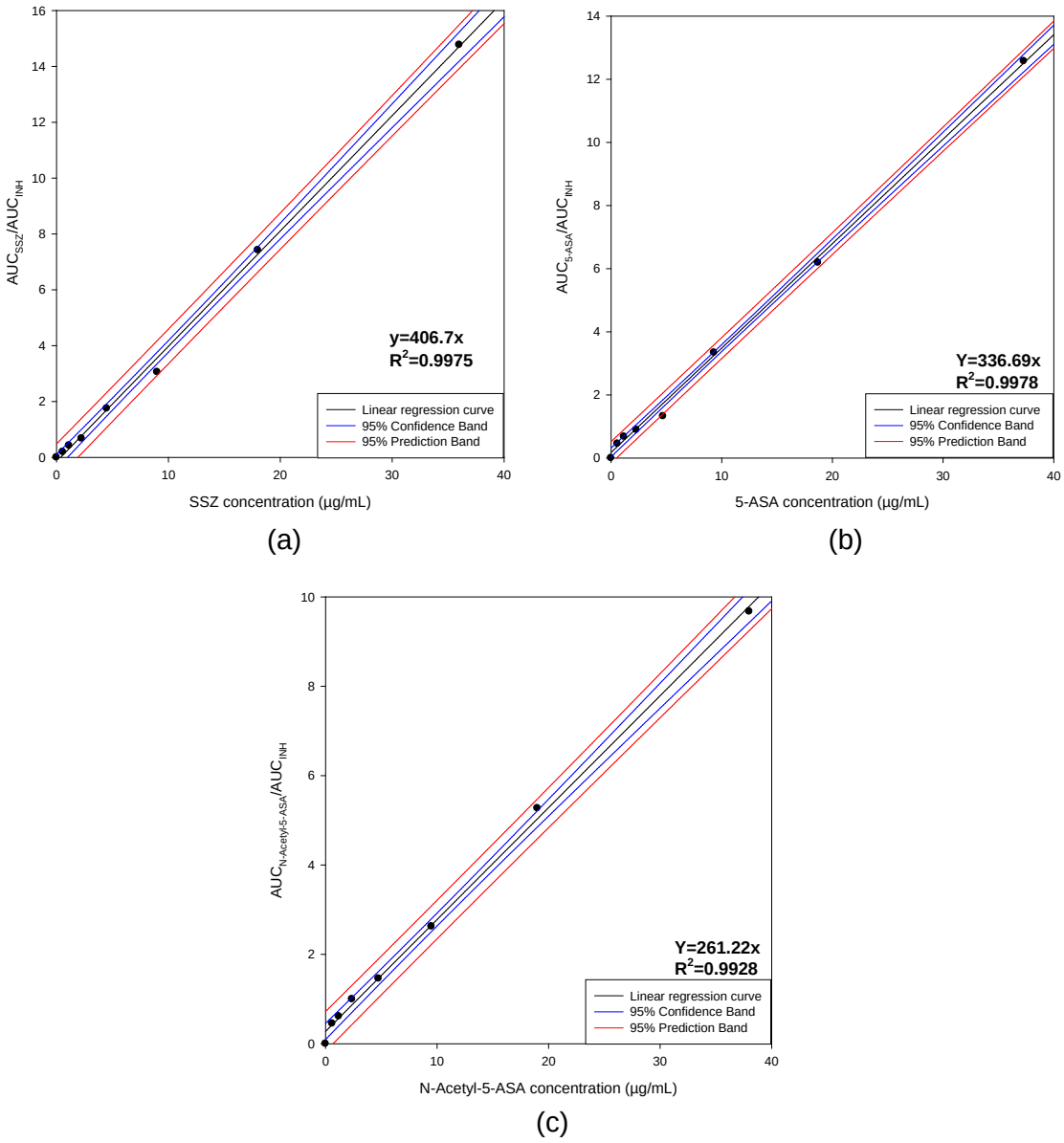


Figure 8.18: Plasma calibration curves of a) SSZ, b) 5-ASA and c) N-Acetyl-5-ASA.

8.3.5. *In vivo* drug release behavior of SSZ from Salazopyrin® tablets and MODDS

The ultimate aim of the study was to compare the *in vivo* drug release behavior of SSZ from Salazopyrin® tablets to the MODDS and relate this to the *in vitro* behavior determined in Section 8.3.1. In order to achieve this aim it was important to analyze the SSZ, 5-ASA and N-Acetyl-5-ASA plasma levels, as explained in Section 8.2.8.1.3. Utilizing the calibration curves constructed in Section 8.3.4, plasma profiles for SSZ, 5-ASA and N-Acetyl-5-ASA were generated as depicted in Figure 8.19, Figure 8.20a, and Figure 8.20b respectively.

The SSZ profile for Salazopyrin® showed a steep rise plasma concentration with peak plasma concentration (C_{max}= 2.874µg.mL^{-1}) occurring two hours post dosing. Thereafter the SSZ levels decreased steadily up to 8 hours after which the plasma concentration remained at constantly low levels. The SSZ profile generated by Salazopyrin® is consistent with its *in vitro* behavior which showed total disintegration with complete drug release within the first hour, which accounts for the spike in plasma concentration followed by gradual decline due to excretion.

Comparison of the SSZ profile of the MODDS to that produced by Salazopyrin® showed that in addition to an increase in time taken to reach plasma concentration, the MODDS achieved a higher peak plasma concentration (C_{max}= 5.5572µg.mL^{-1}) compared to Salazopyrin® and showed a second absorption cycle after approximately 10 hours. In the first two hours, the plasma profiles correlate to the *in vitro* drug release as the initial rise in SSZ plasma concentration could be attributed to release of surface bound SSZ. Additionally the higher concentration in the first two hours may be due to the multiparticulate nature of the MODDS. The MODDS is composed of starch-Based platform (SBP) and due to the GIT physiology of the pig, some of the SBP progressed into the small intestine where SSZ is more soluble facilitating absorption. The movement of the SBP into the small intestine and subsequent further release of SSZ there accounts for the increase to peak plasma concentration seen at four hours. Thereafter, majority of the SBP is moved beyond the absorption site and the effect SSZ excretion is observed in the decrease of plasma SSZ concentrations.

The second rise in plasma concentration was attributed to the multiparticulate nature of the MODDS and the GIT physiology of the pig, which is known to undergo incomplete gastric emptying. Thus, the portion of SBP that remained in the stomach of the pigs was emptied into the duodenum and resulted in release and subsequent absorption of SSZ. Thereafter, no further absorption occurred and SSZ excretion was the primary

pharmacokinetic event portrayed for the remainder of the 24 hours. SSZ is known to have a low bioavailability as seen with Salazopyrin® but the MODDS was shown to improve the bioavailability with higher SSZ plasma concentrations over the 24 hours of the study and doubling of the peak plasma concentration of SSZ.

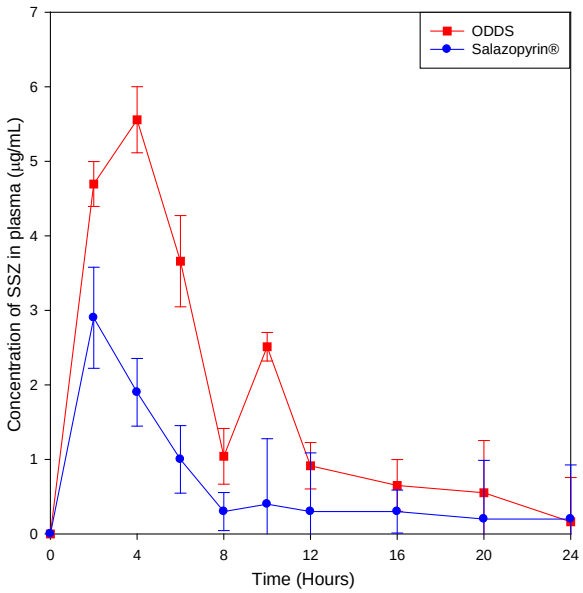
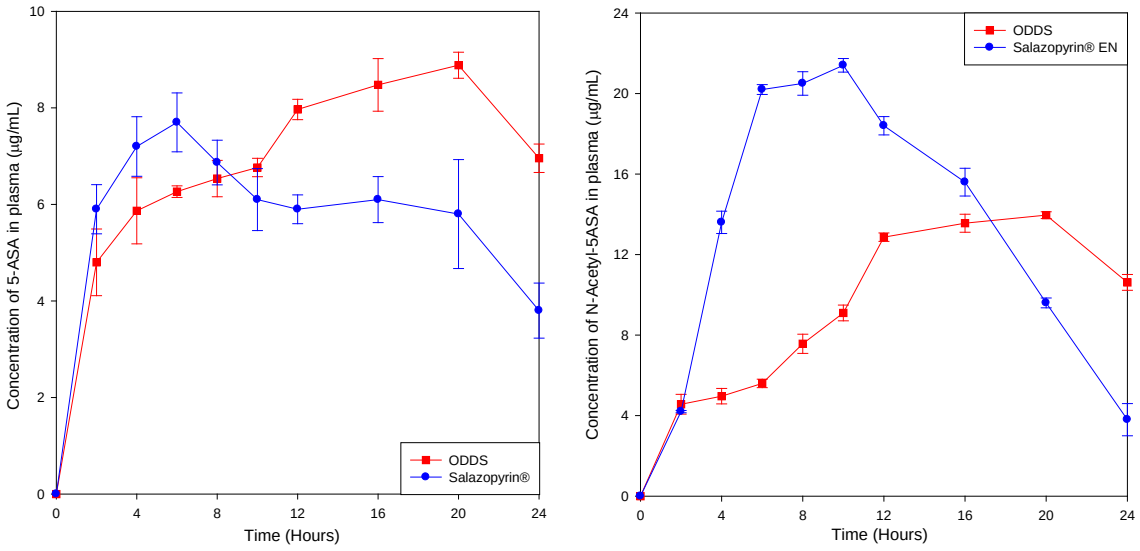


Figure 8.19: Comparative plasma SSZ concentration profiles of the MODDS and Salazopyrin (n=5 in all instances).

Due to the pig GIT physiology and motility, SSZ reached the colon in the initial stages of the study as can be seen by the presence of 5-ASA and N-Acetyl-5-ASA in the pig plasma. The 5-ASA profile for Salazopyrin® showed a rise in plasma concentration as SSZ released in the stomach reached the colon with peak plasma concentration (C_{max}=7.664µg.mL^{-1}) occurring 6 hours post dosing. Thereafter, metabolism and excretion dominated the profile for the remainder of the study. The N-Acetyl 5-ASA plasma concentration profile for Salazopyrin® was similar to that observed for 5-ASA as its appearance in plasma was dependent on the presence of 5-ASA in the colon and blood, which as mentioned, was dependent on the SSZ released in the stomach. However, the peak plasma concentration (C_{max}=22.170µg.mL^{-1}) was higher than 5-ASA and occurred 10 hours post dosing. This phenomenon could be attributed to the short plasma half-life and the high degree of metabolism of 5-ASA *in vivo*.

As was observed for Salazopyrin®, surface bound SSZ released from the MODDS in the stomach reached the colon in the early stages of the study resulting in steep rises in both 5-ASA and N-Acetyl-5-ASA plasma concentrations. Upon reaching the colon, the portion

of SBP which was initially emptied from the stomach released SSZ in a manner which mimicked the *in vitro* SSZ release behavior as both 5-ASA and N-Acetyl-5-ASA plasma concentrations steadily escalated up to preliminary peak plasma concentrations (C_{max1}=6.7649µg.mL^{-1} and C_{max1}=9.125µg.mL^{-1} for 5-ASA and N-Acetyl-5-ASA, respectively). The preliminary peak plasma concentrations occurred at 10 hours post dosing after which the second portion of SBP reached the colon. This resulted in a sudden rise in plasma concentrations and then controlled release from the "new" SBP until 20 hours. In the last 4 hours of the study, it was observed that plasma concentration of both analytes decreased and this was attributed to a decrease in drug release and increased excretion.



(a) (b)

Figure 8.20: Comparative plasma drug concentration profiles of a) 5-ASA and b) N-Acetyl-5-ASA (n=5 in all instances).

The *In vitro* SSZ release profile from the MODDS showed that SSZ was released steadily over a minimum of 12 hours. However, *in vivo* SSZ plasma concentration profiles are only representative of approximately the first 4 hours of drug release. Thus in order to correlate the *in vivo* drug release to that observed *in vitro*, release of SSZ further along the GIT (measured by 5-ASA and N-Acetyl-5-ASA plasma concentrations) was combined with the actual SSZ plasma concentration profile as depicted in Figure 8.21. With regard to Salazopyrin® tablets, only the SSZ plasma concentration profile is representative of the *in vivo* drug release behavior, as the 5-ASA and N-Acetyl-5-ASA plasma concentration profiles were produced from the already released SSZ in the stomach, and was thus used as the composite SSZ plasma concentration profile of Salazopyrin® depicted in Figure 8.21.

Comparison of the composite SSZ plasma concentration profile of Salazopyrin® and the MODDS show that the MODDS demonstrated a substantial increase in the SSZ plasma concentration, which was due to the prolonged release of SSZ throughout the GIT. The composite SSZ plasma concentration profile of the MODDS was generally representative of the *in vitro* SSZ release but displayed deviations which could be attributed to portions of SBP and SSZ reaching the colon sooner than anticipated and the presence of the second portion of SBP being emptied from the stomach later in the study.

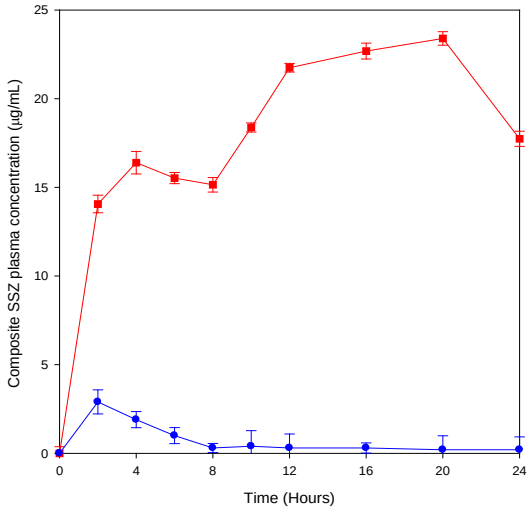


Figure 8.21: Comparison of the composite SSZ plasma concentrations due to release from the MODDS and Salazopyrin® (n=5 in all instances).

8.4. Concluding Remarks

This Chapter ultimately aimed to assess the *in vivo* SSZ release behavior of the MODDS and correlate the behavior to that observed *in vitro*. Furthermore, this phase of the study aimed to compare the *in vivo* SSZ release behavior of the MODDS to the conventional commercially available oral SSZ formulation, Salazopyrin® tablets. To achieve this aim, an efficient blood sampling procedure employing a jugular catheter was used. Additionally, a plasma extraction method for the three analytes and UPLC method was developed which produced chromatograms with good separation of 5-ASA and N-Acetyl-5-ASA and SSZ, which in turn allowed for successful determination of their plasma concentrations. Following UPLC analysis, it was concluded that the SSZ release from the MODDS *in vivo* correlated to the *in vitro* behavior particularly in the first 4 hours of the SSZ plasma concentration profile and between 4-10 hours in the 5-ASA and N-Acetyl-5-ASA plasma concentration profiles. Lastly, the MODDS showed superiority when compared to Salazopyrin® tablets with a substantial increase in SSZ plasma concentration, which was due to the prolonged release of SSZ throughout the GIT.

CHAPTER 9
CONCLUSIONS AND RECOMMENDATIONS

9.1. Conclusions

The oral route presents the most convenient, least invasive and therefore the most widely used route for the administration of drugs (Sugawara *et al.*, 2005; Scholz *et al.,* 2008). However, there are shortcomings associated with the oral route which include stability of drugs in the GIT, site specific absorption and specific GIT conditions and pathologies. These limitations result in complicated dosage regimens, peak-trough cycles in plasma, which consequently affects patient compliance and clinical efficacy of drugs.

Developemet of new drug molecules is difficult, expensive, time consuming and their approval and success is not guaranteed (Camejo *et al.,* 2011; Morgan *et al.,* 2011). Due to the known efficacy of existing drug molecules, methods to improve the use of existing molecules is being increasingly explored. To this end, controlled drug delivery systems employing existing drugs are being developed and include multiparticulate drug delivery systems that comprise of many discrete units, each loaded with a fraction of the total dose (Borgquist *et al.,* 2004) and each possessing the ability to release entrapped drug independently. However, novel drug delivery systems posess disadvantages in that they may be expensive and difficult to reproduce on a large scale (Streubel *et al.,* 2006). Additionally, employment of synthetic polymers within controlled release drug delivery systems is common and may not be broken down nor excreted to a sufficient extent *in vivo* (Jain *et al.,* 2005).

In order to improve and expand the use of novel oral drug delivery systems, use of biocompatible and biodegradable polymers is advocated. Starch is a natural polymer composed mainly of highly branched amylopectin and linear chains of amylose and is one of the most abundant food sources in the world. Starch is widely available, inexpensive and can be modified in various ways and is thus available in numerous forms and compositions allowing them to be utilized for various applications within the pharmaceutical industry (Tuovinen *et al.,* 2004).

The essential aim and novelty of the study was to develop a Multiparticulate Oral Drug Delivery System (MODDS) through functionalization of inert, inexpensive, commercially available, food-grade Starch-Based Multiparticulates (SBM). This was achieved by exploiting the intrinsic physicochemical and physicomechanical properties of the SBM to facilitate drug incorporation and subsequently, control the drug release behavior of the MODDS.

Comprehensive preliminary studies were undertaken to characterize and determine the most appropriate SBM and candidate drug molecule to be employed within the MODDS. Furthermore, various modifications were imparted onto the SBP in order to improve the functionality of the SBP. The prepared formulations were subjected to extensive *in vitro* studies to assess the capability of modified SBP to entrap drug, improve its stability and enhance the control of drug release.

Upon establishing the limits of the formulation factors, a 2-factor-3-level (3^2) full factorial surface response face centered central composite design (FCCCD) was applied to construct second-order polynomial models describing the effect of formulation factors on the Drug Entrapment Efficiency (DEE) and drug release behavior (MDT). A total of 13 formulations were prepared and tested and upon statistical analysis, a single optimized formulation was elucidated. The optimized formulation was then subjected to various analytical techniques such as DEE, drug release, hydration ad erosion, scanning electron microscopy (SEM) and surface area and porosity analysis in order to understand the functional characteristics and elucidate the mechanism that facilitated drug release.

The process of optimization of the SBP as the MODDS was successfully scaled-up and was evaluated *in vivo* in the pig model. *In vivo* sulfasalazine (SSZ) release throughout the GIT was determined directly by measuring plasma SSZ concentrations and indirectly by measuring the plasma 5-ASA and N-Acetyl-5-ASA concentrations and showed general correlation to the *in vitro* SSZ behavior determined previously. Furthermore, the *in vivo* SSZ release was compared to a conventional commercially available SSZ formulation, Salazopyrin® and displayed superior SSZ release characteristics and a vast improvement in the bioavailability of SSZ compared to Salazopyrin®. Thus, an MODDS incorporating inexpensive food grade material was successfully developed and was shown to outperform the commercially available product.

9.2. Recommendations

Despite the promise shown in the development of the MODDS, there exist many facets of the MODDS where improvements can be made. It is thus recommended that further studies be conducted on SBP in which alternate modifications are applied in order to achieve improved drug entrapment and in so doing, decrease the quantity of SBP required within the MODDS. Furthermore, the alternate modifications may impart differing functional characteristics as required in specific circumstances.

It is further recommended that methods to incorporate other drugs into the SBP be determined. This will allow SBPs comprising different drugs to be incorporated into the MODDS, and thus be used to treat multiple symptoms/conditions or as multiple therapy in a single dosage to treat a specific condition, consequently reducing the pill burden and improving patient compliance with multi-drug regimens.

Furthermore, the drug-loaded SBP can be combined with new-age smart polymers, which are biocompatible and biodegradable to form tablets or capsules, and formulated as pH and/or enzyme responsive and can thus be functionalized to deliver drugs throughout the GIT or at particular sites in the GIT as required for the treatment of specific conditions. The smart polymers can control the initial burst of surface bound drug and may be separately drug-loaded to deliver additional drugs.

Lastly, it is recommended that the SBP be manipulated to perform as a gastro-retentive formulation, which is a definite possibility as the phenomenon was observed in the *in vivo* study. By deliberately formulating the SBP within the MODDS to be gastro-retentive, enhancement in bioavailability and clinical efficacy of drugs absorbed in the stomach as well as drugs displaying narrow absorption windows in the intestine can be achieved.

REFERENCES

Abbas, K.A., Khalil, S.K. and Hussin, A.S.M., (2010). Modified starches and their usages in selected food products: A review study. *Journal of Agricultural Science*, ***2,*** 90-100.

Adebowale, A., Sanni, L.O. and Kuye, A., (2006). Effect of roasting methods on sorption isotherms of tapioca grafts*. Electronic Journal of Environmental, Agricultural Food Chemistry,* **5,** 1649-1653.

Ahmad, F.B., Williams, P.A., Doublier, J.L., Durand, S. and Buleon, A., (1999). Physico-chemical characterisation of sago starch. *Carbohydrate Polymers, **38,*** 361-370.

Ai, H., Jones, S.A., de Villiers, M.M. and Lvov, Y.M., (2003). Nano-encapsulation of furosemide microcrystals for controlled drug release. *Journal of Controlled Release*, ***86,*** 59-68.

Al-Baggou', B.K. and Mohammad, F.K., (1999). Antagonism of methomyl-induced toxicosis by diphenhydramine in rats. *Environmental Toxicology and Pharmacology*, ***7,*** 119–125.

Almeida, M.R., Alves, R.S., Nascimbem, L.B.L.R., Stephani, R., Poppi, R.J. and de Oliveira, L.F.C., (2010). Determination of amylose content in starch using Raman spectroscopy and multivariate calibration analysis. *Analytical Bioanalytical Chemistry*, ***397,*** 2693–2701.

Alonso V., Linares, V., Bellés, M.L., Sirvent, J.J., Domingo, J.L., and Sánchez, D.J., (2009). Sulfasalazine induced oxidative stress: A possible mechanism of male infertility. *Reproductive Toxicology*, ***27,*** 35-40.

Ameye, D., Voorspoels, J., Foreman, P., Tsai, J., Richardson, P., Geresh, S. and Remon, J.P., (2001). Trypsin inhibition, calcium and zinc ion binding of starch–gpoly (acrylic acid) copolymers and starch / poly (acrylic acid) mixtures for peroral peptide drug delivery. *Journal of Controlled Release*, ***75,*** 357–364.

Amini, M., Zarghi, A. and Vatanpour, H., (1999). Sensitive high-performance liquid chromatographic method for determination of captopril in plasma. *Pharmaceutica Acta Helvetiae,* ***73***, 303–306.

Andersson, M., Quist, B., Linquist, J., Nilsson, O. and Wahlund, K.G., (2000). Analysis of film coating thickness and surface area of pharmaceutical pellets using fluorescence microscopy and image analysis. *Journal of Pharmaceutical and Biomedical Analysis,* ***22***, 325-339.

Andrews, C.N., Bharucha, A.E., Camilleri, M., Low, P.A., Seide, B., Burton, D., Baxter, K. and Zinsmeister, A.R., (2007). Nitrergic contribution to gastric relaxation induced by glucagon-like peptide-1(GLP-1) in healthy adults. *American Journal of Physiology-Gastrointestinal and Liver Physiology,* ***292***, 1359–1365.

Apopei, D.F., Dinu, M.V. and Dragan, E.S., (2012). Graft polymerization of acrylonitrile onto potatoes starch by ceric ion. *Digest Journal of Nanomaterials and Biostructures,* ***7***, 707- 716.

AppaRao, B., Shivalingam, M.R., Reddy Y.V.K., Sunitha, N., Jyothibasu, T. and Shyam, T., (2010). Design and evaluation of sustained release microcapsules containing diclofenac sodium. *International Journal of Pharmaceutical and Biomedical Research*, ***1***, 90-93.

Aronow, W.S., Fleg, J.L., Pepine, C.J., Artinian, N.T., Bakris,G., Brown,A.S., Ferdinand, K.C., Forciea,M.A., Frishman, W.H., Jaigobin, C., Kostis, J.B., Mancia, G., Oparil, S., Ortiz, E., Reisin, E., Rich, M.W., Schocken, D.D., Weber, M.A., Wesley, D.J. and Harrington, R.A., (2011). ACCF/AHA 2011 expert consensus document on hypertension in the elderly: A report of the american college of cardiology foundation task force on clinical expert consensus documents developed in collaboration with the American Academy of Neurology, American Geriatrics Society, American Society for Preventive Cardiology, American Society of Hypertension, American Society of Nephrology, Association of Black Cardiologists, and European Society of Hypertension. *Journal of the American Society of Hypertension*, ***5***, 259-352.

Asghar, L.F.A. and Chandran, S., (2006). Multiparticulate formulation approach to colon specific drug delivery: Current perspectives. *Journal of Pharmaceutical Sciences,* **9**, 327-338.

Atichokudomchaia, N. and Varavinita, S., (2002). Characterization and utilization of acid-modified cross-linked tapioca starch in pharmaceutical tablets. *Carbohydrate Polymers*, **53**, 263-270.

Atichokudomchaia, N., Varavinita, S. and Chinachoti, P., (2004). A study of ordered structure in acid-modified tapioca starch by 13C CP/MAS solid-state NMR. *Carbohydrate Polymers*, ***58***, 383–389.

Athersuch, T.J., Sison, R.L., Kenyon, A.S.J., Clarkson-Jones, J.A. and Wilson, I.D., (2008). Evaluation of the use of UPLC-TOFMS with simultaneous [14C]-radioflow detection for drug metabolite profiling: Application to propranolol metabolites in rat urine. *Journal of Pharmaceutical and Biomedical Analysis, **48**,* 151-157.

Badkar, D.S., Pandey, K.S. and Buvanashekaran, G., (2010). Effects of laser phase transformation-hardening parameters on heat input and hardened-bead profile quality of unalloyed titanium. *Transactions of Nonferrous Metals Society of China*, ***20**, 1*078-1091.

Bakris, G., (2010). Are there effects of renin–angiotensin system antagonists beyond blood pressure control? *The American Journal of Cardiology*, ***105**,* 21A-29A.

Balimane, P.V., Chong, S. and Morrison, R.A., (2000). Current methodologies used for evaluation of intestinal permeability and absorption. *Journal of Pharmacological and Toxicological Methods, **44***, 301-312.

Balmayor, E.R., Tuzlakoglu, K., Marques, A.P., Azevedo, H.S. and Reis, R.L., (2008). A novel enzymatically-mediated drug delivery carrier for bone tissue engineering applications: Combining biodegradable starch-based microparticles and differentiation agents. *Journal of Materials Science: Materials in Medicine, **19***, 1617-1623.

Bardonnet, P.L., Faivre, V., Pugh, W.J., Piffaretti, J.C. and Falson, F., (2006). Gastro-retentive dosage forms: Overview and special case of Helicobacter pylori. *Journal of Controlled Release*, ***111***, 1-18.

Bashir, K.A. and Nanjundaswamy, N.G., (2009). Formulation and evaluation of sustained release matrix tablets of propranolol hydrochloride using sodium carboxymethyl guar as rate sustaining polymer. *Archives of Pharmaceutical Sciences and Research, **1**,* 203 – 206.

Basak, S.C., Kumar, K.S. and Ramalingam, M., (2008). Design and release characteristics of sustained release tablet containing metformin HCL. *Brazilian Journal of Pharmaceutical Sciences,* **44**, 135-139.

Batterham, R.L., Le Roux, C.W., Cohen, M.A., Park, A.J., Ellis, S.M., Patterson, M., Frost, G.S., Ghatei, M.A. and Bloom, S.R., (2003). Pancreatic polypeptide reduces appetite and food intake in humans. *Journal of Clinical Endocrinology and Metabolism*, ***88***, 3989 - 92.

Bawa, P., Pillay, V., Choonara, Y.E., du Toit, L.C., Ndesendo, V.M.K. and Kumar, P., (2011). A composite polyelectrolytic matrix for controlled oral drug delivery. *AAPS Pharmceutical Science Technology,* **12,** 227-238.

Beevers, G., Lip, G.Y.H. and O'Brien, E., (2001). The pathophysiology of hypertension. *British Medical Journal, **322**,* 912-916.

Bernazzani, P., Peyyavula, V.K., Agarwal, S. and Tatikonda, R.K., (2008). Evaluation of the phase composition of amylose by FTIR and isothermalimmersion heats. *Polymer*, **49**, 4150–4158.

Bhattachar, S.N., Deschenes, L.A. and Wesley, J.A., (2006). Solubility: it's not just for physical chemist. *Drug Delivery Today,* **11**, 1012-1018.

Bialleck, S. and Rein, H., (2011). Preparation of starch-based pellets by hot-melt extrusion. *European Journal of Pharmaceutics and Biopharmaceutics*, ***79***, 440-448.

Blom, W.A., Lluch, A., Stafleu, A., Vinoy, S., Holst, J.J., Schaafsma, G. and Hendriks, H.F., (2006). Effect of a high-protein breakfast on the postprandial ghrelin response. *American Journal of Clinical Nutrition, **84***, 664-666.

Boriwanwattanarak, P., Ingkaninan, K., Khorana, N. and Viyoch, J., (2008). Development of curcuminoids hydrogel patches using chitosan from various sources as controlled-release matrix. *International Journal of Cosmetic Science*, ***30***, 205-218.

Borgquist, P., Nevsten, P., Nilsson, B., Wallenberg, L. R. and Axelsson, A., (2004). Simulation of the release from a multiparticulate system validated by single pellet and dose release experiments. *Journal of Controlled Release, **97***, 453-465.

Bourn, E.J. and Peat, S., (1949). The amylose component of waxy maize starch. *Journal of Chemistry Society,* 5-9.

Brittain, H.G, and Kadin, H., (1990). Ultraviolet (UV) absorption and circular dichroism (DC) spectra of captopril. *Pharmaceutical Research, **7***, 1082-1085.

Brown, D.R. and Terris J.M., (1996). Swine in physiological and pathophysiological research. *Advances in Swine in Biomedical Research,* **1**, 5-6.

Brouillet, F., Bataille, B. and Cartilier, L., (2008). High-amylose sodium carboxymethyl starch matrices for oral, sustained drug-release: Formulation aspects and *in vitro* drug-release evaluation. *International Journal of Pharmaceutics, **356***, 52-60.

Brunet, B., Douceta, C., Venisseb, N., Haueta, T., Hébrardc, W., Papetb, Y., Maucoa, G. and Mura, P., (2009). Validation of Large White Pig as an animal model for the study of cannabinoids metabolism: Application to the study of THC distribution in tissues. *Forensic Science International, **161***, 169-174.

Burgess, C.G.V., Everett, H.D. and Nuttall, S., (1989). Adsorption hysteresis in porous materials. *Pure and Applied Chemistry, **61***, 1845-1852.

Bysell, H., Månsson, R., Hansson, P. and Malmsten, M., (2011). Microgels and microcapsules in peptide and protein drug delivery. *Advanced Drug Delivery Reviews*, ***63,*** 1172-1185.

Camejo, R.R., McGrath, C. and Herings, R., (2011). A dynamic perspective on pharmaceutical competition, drug development and cost effectiveness. *Health Policy*, ***100,*** 18-24.

Carell, i V., Di Colo, G., Gesi, M., Martini, F.and Nannipieri, E., (1997). Mechanism of drug release from silicone microspheres containing polycarbophil. *International Journal of Pharmaceutics, **153***, 105-114.

Carlson, B.B., Trevitt, J.T. and Salamone, J.D., (2000). Effects of H1 antagonists on cholinomimetic-induced tremulous jaw movements: Studies of Diphenhydramine, Doxepin, and Mepyramine, *Pharmacology Biochemistry and Behavior*, ***65,*** 683-689.

Casas, M., Ferrero, C. and Jiménez-Castellanos, M.R., (2009). Graft tapioca starch copolymers as novel excipients for controlled-release matrix tablets. *Carbohydrate Polymers*, ***80***, 71–77.

Charman, W.N., Porter, C.J.H., Mithani, S. and Dressman, JB., (1997). Physicochemical and physiological mechanisms for the effects of food on drug absorption: The role of lipids and pH. *Journal of Pharmaceutical Sciences*, ***86***, 269-282.

Charoenkul, N., Uttapap, D., Pathipanawat, W. and Takeda, Y., (2006). Simultaneous determination of amylose content and unit chain distribution of amylopectins of cassava starches by fluorescent labeling/HPSEC. *Carbohydrate Polymers,* ***65***, 102–108.

Chavanpatil, M.D., Jain, P., Chaudhari, S., Shear, R. and Vavia, P.R., (2006). Novel sustained release, swellable and bioadhesive gastro-retentive drug delivery system for ofloxacin. *International Journal of Pharmaceutics,* ***316***, 86-92.

Chen, L., Li, X., Li L. and Guo S., (2007) Acetylated starch-based biodegradable materials with potential biomedical applications as drug delivery systems. *Current Applied Physics,* **7***,* 90-93.

Chen, M.L., (2008). Lipid excipients and delivery systems for pharmaceutical development: A regulatory perspective. *Advanced Drug Delivery Reviews*, ***60***, 768–777.

Chen, A.H., Yang, C.Y., Chen, C.Y., Chen, C.Y. and Chen, C.W., (2009). The chemically crosslinked metal-complexed chitosans for comparative adsorptions of Cu(II), Zn(II), Ni(II) and Pb(II) ions in aqueous medium. *Journal of Hazardous Materials*, ***163***, 1068–1075.

Chin, S.F., Pang, S.C. and Tay, S.H., (2011). Size controlled synthesis of starch nanoparticles by a simple nanoprecipitation method. *Carbohydrate Polymers*, ***86***, 1817–1819.

Cho, C.W., Choi, J.S. and Shin, S.C., (2005). Controlled release of furosemide from the ethylene-vinyl acetate matrix. *International Journal of Pharmaceutics*, ***299***,127–133.

Christensen, B.E., Aasprong, E. and Stokke, B.T., (2001). Gelation of periodate oxidized scleroglucan (scleraldehyde). *Carbohydrate Polymers,* ***46***, 241-248.

Chungi, V.S., Rekhi G.S. and Shargel, L., (1989). A simple and rapid liquid chromatographic method for the determination of major metabolites of sulfasalazine in biological fluids. *Journal of Pharmaceutical Sciences,* ***78***, 235.

Chungi, V.S., Dittert, L.W. and Shargel, L., (1989). Pharmakokinetics of sulfasalazine metabolites in rats following concomitant oral administration of riboflavin. *Pharmaceutical Research ,* ***6***, 1067-1072.

Clegg, M.E., Pratt, M., Markey, O., Shafat, A. and Henry, J.K., (2012). Addition of different fats to a carbohydrate food: Impact on gastric emptying, glycaemic and satiety responses and comparison with *in vitro* digestion. *Food Research International,* ***48***, 91–97.

Cloetens, L., Swennen, K., De Preter, V., Broekaert, W.F., Courtin, C.M., Delcour, J.A., Rutgeerts, P. and Verbeke, K., (2008). Effect of arabinoxylo-oligosaccharides on proximal gastrointestinal motility and digestion in healthy volunteers. *E-SPEN, the European e-Journal of Clinical Nutrition and Metabolism,* ***3,*** 220-225.

Collado, L.S., and Corke, H., (1998). Pasting properties of commercial and experimental starch pearls. *Carbohydrate Polymers,* ***35***, 89-96.

Condon, J.B., (2006). Surface area and porosity determinations by physisorption: Measurements and Theory. First Edition. Elsevier Science and Technology.

Corea, N., (2007). Sulfasalazine. *xPharm: The Comprehensive Pharmacology Reference*, ***5***, 1-5.

Corta, E., Bakkali, A., Berrueta, L.A., Gallo, B., Vicente, F., Gonzalo, A., Lucero, M.L., Orjales, A., (1999). Semi-automated solid-phase extraction procedure for the high-performance liquid chromatographic determination of alinastine in biological fluids. *Journal of Chromatography B: Biomedical Sciences and Applications*, ***727****, 131-138.*

Costa, P. and Lobo, J.M.S., (2001). Modeling and comparison of dissolution profiles. *European Journal of Pharmaceutical Sciences,* ***13***, 123-133.

Crcarevska, M., Dodov, M.G. and Goracinova, K., (2008). Chitosan coated Ca–alginate microparticles loaded with budesonide for delivery to the inflamed colonic mucosa. *European Journal of Pharmaceutics and Biopharmaceutics,* ***68***, 565-578.

Crowley, P.J. and Martin, L.G., (2004). Formulation design: new drugs from old. *Drug discovery today: therapeutic strategies,* ***1***, 4.

Cruz, J.E., Maness, D.D. and Yakatan, G.J., (1979). Kinetics and mechanism of hydrolysis of furosemide. *International Journal of Pharmaceutics,* ***2***, 275-281.

Cryan, S.A., Sivadas, N. and Garcia-Contreras, L., (2007). In vivo animal models for drug delivery across the lung mucosal barrier. *Advanced Drug Delivery Reviews*, ***59****,* 1133-1151.

Custodio, J.M., Wu, C.Y. and Benet, L.Z., (2008). Predicting drug disposition, absorption/ elimination/ transporter interplay and the role of food on drug absorption. *Advance Drug Delivery Reviews,* ***60***, 717-733.

Dahan, A. and Amidon G.L., (2010). MRP2 mediated drug–drug interaction: Indomethacin increases sulfasalazine absorption in the small intestine, potentially decreasing its colonic targeting. *International Journal of Pharmaceutics*, ***386****,* 216-220.

Danjaji, I.D., Nawang, R., Ishiaku, U.S., Ismail, H. and IshakZ, A.M., (2002). Degradation studies and moisture uptake of sago-starch-filled linear low-density polyethylene composites. *Polymer Testing,* ***21***, 75-81.

Dash, S., Murthy, N.P., Nath, L. and Chowdhury, P., (2010). Kinetic modelling on drug release from controlled drug delievery system. *Polish Pharmaceutical Society, Drug Research,* ***6***, 217-223.

Davis, S.S., (2005). Formulation strategies for absorption windows. *Drug Discovery Today*, ***10***, 249-257.

Davis, S., (2007). Captopril. *xPharm: The Comprehensive Pharmacology Reference*, 1-7.

Dey, N.S., Majumdar, S. and Rao, M.E.B., (2008). Multiparticulate drug delivery systems for controlled release. *Tropical Journal of Pharmaceutical Research,* ***7***, 1067-1075.

DeSesso, J.M. and Jacobson, C.F., (2001). Anatomical and physiological parameters affecting gastrointestinal absorption in humans and rats. *Food and Chemical toxicology*, ***39***, 209-228.

Digenis, G.A., Beihn, R.M., Theodorakis, M.C. and Shambhu, M.S. (1977). Use of Tc-99m-Iabeled triethylenetetramine-polystyrene resin for measuring gastric emptying rate in humans. *Journal of Pharmaceutical Sciences*, ***66***, 442-443.

Digenis, G.A., Sandefer, E.P., Parr, A.F., Beihn, R., McClain, C., Scheinthal, B.M., Ghebre-Sellassie, I., Iyer, U., Nesbitt, R.U. and Randinitis, E., (1990). Gastrointestinal behavior of orally administered radiolabeled erythromycin pellets in man as determined by gamma scintigraphy. *Journal of Clinical Pharmacology, **30***, 621.

Dobson, C.L., Davis, S.S., Chauhan, S., Sparrow, R.A. and Wilding, I.R., (2000). Does the site of intestinal delivery of oleic acid alter the ileal brake response? *International Journal of Pharmaceutics, **195,*** 63–70.

Donohue, M.D. and Aranovich, G.L,. (1998). Adsorption hysteresis in porous solids. *Journal of Colloid and Interface Science, **205***, 121-130.

Dorkoosh, F.A., Verhoef, J.C., Borchard, G., Rafiee-Tehrani, M., Verheijden, J.H.M. and Junginger, H.E., (2002). Intestinal absorption of human insulin in pigs using delivery systems based on superporous hydrogel polymers. *International Journal of Pharmaceutics, **247***, 47-55.

Drugbank, 2012, (http://www.drugbank.ca/drugs/DB01425#captopril,
http://www.drugbank.ca/drugs/DB014587#furosemide,
http://www.drugbank.ca/drugs/DB02547#hypertension,
http://www.drugbank.ca/drugs/DB02654#propranolol,
http://www.drugbank.ca/drugs/DB02369#pharmacology,
http://www.drugbank.ca/drugs/DB01197#pharmacology) access date 15 December 2012.

Dung, T.H., Lee, S.R., Han, S.D., Kim, S.J., Ju, Y.M., Kim, M.S. and Yoo, H., (2007). Chitosan-TPP nanoparticle as a release system of antisense oligonucleotide in the oral environment. *Journal of Nanoscience and Nanotechnology*, ***7***, 3695-3699.

Dziczkowski, J. and Soucek, M.D., (2012). Factors influencing the stability and film properties of acrylic/alkyd water-reducible hybrid systems using a response surface technique. *Progress in Organic Coatings*, ***73,*** 330-343.

El-Kamel, A.H., l-Fagih, I.M. and Alsarra, I.A., (2007). Testosterone solid lipid microparticles for transdermal drug delivery. Formulation and physicochemical characterization. *Journal of Microencapsulation, **24***, 457-75.

El-Tahlawy, K., Venditti, R.A.and Pawlak, J.J., (2007). Aspects of the preparation of starch microcellular foam particles crosslinked with glutaraldehyde using a solvent exchange technique. *Carbohydrate Polymers*, ***67***, 319–331.

Elliott, H., (2006). Epidemiology, aetiology and prognosis of hypertension. *Medicine*, ***34***, 286-289.

Englyst, H.N. and Hudson, G.J., (1996). The classification and measurement of dietary carbohydrates. *Food Chemistry*, ***7***, 15-21.

Ensafi, A.A., Karimi-Maleh, H., Mallakpour, S. and Rezaei, B., (2011). Highly sensitive voltammetric sensor based on catechol-derivative-multiwall carbon nanotubes for the catalytic determination of captopril in patient human urine samples, *Colloids and Surfaces B: Biointerfaces*, ***87***, 480-488.

EP, (2005). *European Pharmacopoeia.* Fifth Edition. Council of Europe, Strasbourg.

Escuder-Gilabert, L., Mart´ınez-Pla, J.J., Sagrado, S., Villanueva-Camañas, R.M. and Medina-Hernández, M.J., (2003). Biopartitioning micellar separation methods: Modelling drug absorption B. *Journal of Chromatography B, **797***, 21-35.

Ezra, A., and Golomb, G,. (2000). Administration routes and delivery systems of bisphosphonates for the treatment of bone resorption. *Advanced Drug Delivery Reviews, **42***, 175-195.

Fama, L., Goyanes, S. and Gerschenson, L., (2007). Influence of storage time at room temperature on the physicochemical properties of cassava starch films. *Carbohydrate Polymers, **70**,* 265–273.

Fitzgerald, M., Bergman, C.J., Resurreccion, A.P., Möller, J., Jimenez, R., Reinke, R.F., Martin, M., Blanco, P., Molina, F., Chen, M.H., Kuri, V.K., Romero, M.V., Habibi, F., Umemoto, T., Jongdee, S., Graterol, E., Reddy, R., Bassinello, P.Z., Sivakami, R., Rani, N.S., Das, S., Wang, Y.J., Indrasari, S.D., Ramli, A., Ahmad, R., Dipti, S.S., Xie, L., Lang,

N.T., Singh, P., Toro, D.C., Tavasoli, F., Mestres,C., (2009). Addressing the dilemmas of measuring amylose in rice. *Cereal Chemistry*. ***86***, 492–498.

Flores, S., Conte, A., Campos, C., Gerschenson, L. and Nobile, M.D., (2007). Mass transport properties of tapioca-based active edible films. *Journal of Food Engineering*, ***81***, 580–586.

French, S.J. and Cecil, J.E., (2001). Oral, gastric and intestinal influences on human feeding. *Physiology and Behavior, **74***, 729– 734.

Frenning, G., Fichtner, F. and Alderborn G., (2005). A new method for characterizing the release of drugs from single agglomerates. *Chemical Engineering Science, **60***, 3909-3918.

Fukuda, M., Peppas, N.A. and McGinity, J.W., (2006). Floating hot-melt extruded tablets for gastro-retentive controlled drug release system. *Journal of Controlled Release, **115***, 121-129.

Galat, A., (1980). Study of the raman scattering and infrared absorption spectra of branched polysaccharides. *Acta Biochimica Polonica, **27***, 2.

Galeotti, N., Bartolini, A. and Ghelardini, C., (2003). Diphenhydramine-induced amnesia is mediated by Gi-protein activation. *Neuroscience*, ***122,*** 471-478.

Galland, S., Ruiz, T. and Delalonde, M., (2007). Twin product/process approach for pellet preparation by extrusion/spheronisation, Part I: Hydro-textural aspects. *International Journal of Pharmaceutics, **337***, 239-245.

Gan, L.S., Thakker, L. and Dhiren, R., (1997). Applications of the Caco-2 model in the design and development of orally active drugs: Elucidation of biochemical and physical barriers posed by the intestinal epithelium. *Advanced Drug Delivery Reviews, **23***, 77-98.

Gardner, N., Haresign, W., Spiller, R., Farraj, N., Wiseman, J., Norbury, H. and Illum, L., (1996). Development and validation of a pig model for colon-specific drug delivery, *Journal of Pharmaceautics and Pharmacology*, ***7***, 689-693.

Gentilcore, D., Chaikomin, R., Jones, K.L., Russo, A., Feinle-Bisset, C., Wishart, J.M., Rayner, C.K. and Horowitz, M., (2006). Effects of fat on gastric emptying and the glycemic, insulin, and incretin responses to a carbohydrate meal in Type 2 Diabetes. *The Journal of Clinical Endocrinology and Metabolism,* ***91***, 2062–2067.

Ge´rard, C., Barron, C., Colonna, P. and Planchot, V., (2001). Amylose determination in genetically modified starches. *Carbohydrate Polymers*, ***44***, 19–27.

Geresh, S., Gdalevskyn, G.Y., Gilboa, I., Voorspoels, J., Remon, J.P. and Kost, J., (2004). Bioadhesive grafted starch copolymers as platforms for peroral drug delivery: A study of theophylline release. *Journal of Controlled Release*, ***94***, 391– 399.

Gershkovich, P. and Hoffman, A., (2005). Uptake of lipophilic drugs by plasma derived isolated chylomicrons: Linear correlation with intestinal lymphatic bioavailability. *European Journal of Pharmaceutical Sciences,* ***26***, 394–404.

Golmohammad, F., Eikani, M.H. and Maymandi, H.M., (2012). Cinnamon bark volatile oils separation and determination using solid-phase extraction and gas chromatography. *Procedia Engineering,* ***42***, 276-289.

Goto, D.M., Torres, G.M., Seguro, A.C., Saldiva, P.H.N., Lorenzi-Filho, G. and Nakagawa, N.K., (2010). Furosemide impairs nasal mucociliary clearance in humans. *Respiratory Physiology and Neurobiology*, ***170,*** 246-252.

Grigoriev, D.O. and Miller, R., (2008). Mono- and multilayer covered drops as carriers. *Current Opinions in Colloid Interface Science,* ***11,*** 904-909.

Grosman, A. and Ortega, C., (2008). Capillary condensation in porous materials. Hysteresis and interaction. Mechanism without pore blocking/percolation process. *Langmuir,* ***24***, 3977-3986.

Gui-Jie, M., Peng, W., Xiang-Sheng, M., Xing, Z. and Tong, Z., (2006). Crosslinking of corn starch with sodium trimetaphosphate in solid state by microwave irradiation. *Journal of Applied Polymer Science,* ***102***, 5854-5860.

Guo, Y. and Shen, H., (2004). pKa, Solubility, and lipophilicity: Assessing physicochemical properties of lead compounds, optimization in drug discovery: *In vitro Methods, Methods in Pharmacology and Toxicology,* 1-17.

Guo, W.Q., Ren, N.Q., Wang, X.J., Xiang, W.S., Ding, J., You, Y. and Liu, B.F., (2009). Optimization of culture conditions for hydrogen production by Ethanoligenens harbinense B49 using response surface methodology. *Bioresource Technology*, ***100,*** 1192-1196.

Hamdi, G., Ponchel, G. and Duchêne, D., (2001). Formulation of epichlorohydrin cross-linked starch microspheres. *Journal of Microencapsulation*, ***18***, 373-383.

Hamerstrand, G.E., Hofreiter, B.T. and Mehltretter, C.L., (1960). Determination of the extent of reaction between epichlorohydrin and starch. *Cereal Chemistry,* **37**, 519-524.

He, C., Long, Y., Pan, J., Li, K. and Liu, F., (2007). Application of molecularly imprinted polymers to solid-phase extraction of analytes from real samples. *Journal of Biochemical and Biophysical Methods, **70**,* 133-150.

Heeres, A., van Doren, H.A., Gotlieb, K.F., Bleeker, I.P., and Kellogg, R.M., (1998), Cross-linking of starch with bifunctional precursors of nitroalkenes. *Carbohydrate Research*, ***310***, 191-201.

Helliwell, M., (1993). The use of bioadhesives in targeted delivery within the gastrointestinal tract. *Advanced Drug Delivery Reviews*, ***11***, 221-251.

Hillaert, S. and Van den Bossche, W., (1999). Determination of captopril and its degradation products by capillary electrophoresis*. Journal of Pharmaceutical and Biomedical Analysis, **21**,* 65-73.

Hoffman, A. and Qadri, B.A., (2006). Gastro-retentive systems. Encyclopedia of Pharmaceutical Technology, Third Edition. CRC Press.

Holzer, P., Reichmann, F. and Farzi, A., (2012). Neuropeptide Y, peptide YY and pancreatic polypeptide in the gut–brain axis. *Neuropeptides*, ***46,*** 261-274*.*

Homma, M., Jayewardene, A.L., Gambertoglio, J. and Aweeka, F., (1999). High-performance liquid chromatographic determination of ribavirin in whole blood to assess disposition in erythrocytes. *Antimicrobial Agents Chemotherapy,* ***43***, 2716–2719.

Hoover, R. and Ratnayake, W.S., (2001). Determination of total amylose content of starch. *Current Protocols in Food Analytical Chemistry*.

Hosseini, S.M. and Khosravi-Darani, K., (2011). Response surface methodology for mycoprotein production by Fusarium Venenatum ATCC 20334. *Journal of Bioprocessing and Biotechniques,* ***1***, 1-5.

Hung, C.H., Chu, C.C., Chen, Y.C., Chen, Y.W., Li, Z.Y. and Wang, J.Y., (2011). Spinal anesthesia with diphenhydramine and pheniramine in rats. *European Journal of Pharmacology*, ***673****,* 20-24.

Hunter, A.C., Elsom, J., Wibroe, P.P. and Moghimi, S.M., (2012). Polymeric particulate technologies for oral drug delivery and targeting: a pathophysiological perspective. Nanomedicine: *Nanotechnology, Biology, and Medicine,* ***8***, S5–S20.

Iannuccelli, V., Coppi, G., Leo, E., Fontana, F. and Bernabei, M.T., (2000). PVP solid dispersions for the controlled release of furosemide from a floating multiple-unit system. *Drug Development and Industrial Pharmacy*, ***26***, 595–603.

Iida, Y., Tuziuti, T., Yasui, K., Towata, A. and Kozuka T., (2008). Control of viscosity in starch and polysaccharide solutions with ultrasound after gelatinization. *Innovative Food Science and Emerging Technologies,* ***9***, 140-146.

Iizuka, K. and Aishima, T., (1999). Starch gelation process observed by FT-IR/ATR spectrometry with multivariate data analysis. *Journal of Food Science*, ***64***, 653-658.

Ivanovic, D., Medenica, M., Malenovic, A. and Jancic, B., (2004). Validation of the RP–HPLC method for analysis of hydrochlorothiazide and captopril in tablets. *Accreditation and Quality Assurance*, ***9***, 76–81.

Itthisoponkul, T., Mitchell, J.R., Taylor, A.J. and Farhat, I.A., (2007). Inclusion complexes of tapioca starch with xavour compounds. *Carbohydrate Polymers,* ***69***, 106–115.

Jain, J.P., Modi, S., Domb, A.J. and Kumar, N., (2005). Role of polyanhydrides as localized drug carriers. *Journal of Controlled Release*, ***103***, 541-563.

Jane, J., Xu, A., Radosavljevic, M. and Seib, P.A., (1992). Location of amylose in normal starch granules. I. Susceptibility of amylose and amylopectin to crosslinking reagents. *Cereal Chemistry, **69***, 405-409.

Javeer, S.D., Pandit, R., Jain, S.P. and Amin, P., (2010). Formulation and evaluation of trimetazidine dihydrochloride extended release tablets by melt congealing method. *Indian Journal of Pharmaceutical Sciences, **72***, 704-709.

Jeffery, A.D. and Lytle-Saddler, T., (2008). Diphenhydramine overdose in a 26-year-old woman. *Journal of Emergency Nursing*, ***34,*** 543-544.

Jin, K.M. and Kim, Y.H., (2008). Injectable, thermo-reversible and complex coacervate combination gels for protein drug delivery. *Journal of Controlled Release*, ***127**, 249-256.*

Jouyban-Gharamaleki, A., Dastmalchi, S., Chan, H.K., Hanaee, J., Javanmard, A. and Barzegar-Jalali, M., (2001). Solubility prediction for furosemide in water-cosolvent mixtures using the minimum number of experiments. *Drug Development and Industrial Pharmacy*, ***27***, 577-583.

Juřica, J., Konečný, J., Zahradníková, L.Z. and Tomand. J., (2010). Simultaneous HPLC determination of tolbutamide, phenacetin and their metabolites as markers of cytochromes 1A2 and 2C6/11 in rat liver perfusate. *Journal of Pharmaceutical and Biomedical Analysis*, ***52,*** 557-564.

Julius, S., Kaciroti, N., Egan, B.M., Nesbitt, S. and Michelson, E.L., (2008). TROPHY study: Outcomes based on the seventh report of the Joint National Committee on Hypertension definition of hypertension. *Journal of the American Society of Hypertension*, ***2***, 39-43.

Karhunen, L.J., Juvonen, K.R., Huotari, A., Purhonen, A.K. and Herzig, K.H., (2008). Effect of protein, fat, carbohydrate and fibre on gastrointestinal peptide release in humans. *Regulatory Peptides*, ***149***, 70–78.

Karim, A.A., Nadiha, M.Z., Chen, F.K., Phuah, Y.P., Chui, Y.M. and Fazilah, A., (2008). Pasting and retrogradation properties of alkali-treated sago (Metroxylon sagu) starch. *Food Hydrocolloids,* ***22***, 1044-1053.

Katopo, H., Song, Y. and Jane, J., (2002). Effect and mechanism of ultrahigh hydrostatic pressure on the structure and properties of starches. *Carbohydrate Polymers,* ***47***, 233-244.

Kavitha, K., Puneeth, K.P. and Mani, T., (2010). Development and evaluation of Rosiglitazone maleate floating tablets. *International Journal of Applied Pharmaceutics*, **2**, 6-10.

Keita, K. and Imai, M., (2012). Chapter 1: Advanced membrane material from marine biological polymer and sensitive molecular-size recognition for promising separation technology, *Advancing Desalination.*

Kenakin, T.P., (2009). Chapter 9: Pharmacokinetics. A Pharmacology Primer. Third Edition. Academic Press.179-214.

Kenyon, C.J., Hooper, G., Tierney, D., Butler, J., Devane, J. and Wilding, I.R., (1995). The effect of food on the gastrointestinal transit and systemic absorption of naproxen from a novel sustained release formulation. *Journal of Controlled Release,* ***34***, 31-36.

Kidder, D. E., Manners, M. J. and McCrea, M. R., (1961). The passage of food through the alimentary tract of the piglet. *Research of Vetrinary Science*, ***2***, 227-231.

Kimura, T. and Higaki, K., (2002). Gastrointestinal transit and drug absorption. *Biological and Pharmacological Bulletin*, **25**, 149–164.

Kiriyama, A., Honbo, A. and Iga, k., (2008). Analysis of hepatic metabolism affecting pharmacokinetics of propranolol in humans. *International Journal of Pharmaceutics*, ***349,*** *53-60.*

Klein, S., Rudolph, M.W., Skalsky, B., Petereit, H.U. and Dressman, J.B., (2008). Use of the BioDis to generate a physiologically relevant IVIVC. *Journal of Controlled Release,* ***130***, 216-219.

Klotz, U., (1985). Clinical pharmacokinetics of sulphasalazine, its metabolites and other prodrugs of 5-aminosalicylic acid. *Clinical Pharmacokinetics, **10**,* 285-302.

Knutson, C.A., (1986). Simplified colorimetric procedure for determination of amylose in maize starches. *Cereal Chemistry*, ***63***, 89-92.

Kopp, W., (2005). Pathogenesis and etiology of essential hypertension: role of dietary carbohydrate. *Medical Hypotheses*, ***64***, 782–787.

Kotwal, V., Bhise, K. and Thube, R., (2007). Enhancement of iontophoretic transport of diphenhydramine hydrochloride thermosensitive gel by optimization of pH, polymer concentration, electrode design, and pulse rate. *AAPS PharmSciTech, **8***, 4, Article 120.

Kowalczyk, P., Kaneko, K., Solarz, L., Terzyk, A.P., Tanaka, H. and Hołyst, R., (2005). Modeling of the hysteresis phenomena in finite-sized slitlike nanopores. Revision of the recent results by rigorous numerical analysis. *Langmuir, **21***, 6613-6627.

Kumar, M., Tripathi, B.P. and Shah, V.K., (2009). Crosslinked chitosan/polyvinyl alcohol blend beads for removal and recovery of Cd (II) from wastewater. *Journal of Hazardous Materials*, ***172**,* 1041-1048.

Kumar, S., Char, H., Patel, S., Piemontese, D., Malick, A.W., Iqbal, K., Neugroschel, E. and Behl, C.R., (1992). *In vivo* transdermal iontophoretic delivery of growth hormone releasing factor GRF (1–44) in hairless guinea pigs*. Journal of Controlled Release, **18***, 213-220.

Kumari, K. and Rani, U., (2011). Controlled Release of Metformin hydrochloride through crosslinked blends of chitosan-starch. *Advances in Applied Science Research*, ***2***, 48-54.

Lalouel, J.M., (1995). Genetics of the renin-angiotensin system in human hypertension. *American Journal of Hypertension, **8**, 3628.*

Lau, C.E. and Falk, J.L., (1991). Sustained synergism by chronic caffeine of the motor control deficit produced by midazolam. *Pharmacology, Biochemistry and Behavior*, ***40***, 723-731.

Laulicht, B., Tripathi, A. and Mathiowitz, E., (2011). Diuretic bioactivity optimization of furosemide in rats. *European Journal of Pharmaceutics and Biopharmaceutics*, ***79,*** 314-319.

Lawal, O.S. (2004). Composition, physicochemical properties and retrogradation characteristics of native, oxidised, acetylated and acid-thinned new cocoyam (Xanthosoma sagittifolium). *Food Chemistry,* ***87***, 205-218.

Lawrence, R.A. and Lawrence, R.M., (2005). Chapter 11: Drugs in breast milk. Breastfeeding. Sixth Edition. Mosby. 377-426.

Lee, H., Lee J.Y., Suh, M.H., Sim, S.S., Lee, M.W. and Kim, C.J., (2010). Hydrolysable tannins depress cardiac papillary muscle contraction and propranolol-induced negative inotropism. *Fitoterapia*, *The Journal for the Study of Medicinal Plants,* ***81,*** 820-825.

Lee, J.D., Wu, H. and Englezos, P., (2007). Cationic starches as gas hydrate kinetic inhibitors. *Chemical Engineering Science*, ***62***, 6548 – 6555.

Lennernäs, H., (2007). Animal data: The contributions of the Ussing Chamber and perfusion systems to predicting human oral drug delivery *in vivo*. *Advanced Drug Delivery Reviews,* ***59***, 1103-1120.

Leong, C.W., Newton, J.M., Basit, A.W., Podczeck, F., Cummings, J.H. and Ring, S.R., (2002). The formation of colonic digestible films of amylose and ethylcellulose from aqueous dispersions at temperatures below 37°C. *European Journal of Pharmaceutics and Biopharmaceutics*, ***54***, 291–297.

Leong, K.W. and Langer, R., (1987). Polymeric controlled drug delivery. *Advanced Drug Delivery* Reviews, ***1***, 199-233.

Lertworasirikul, S., (2008). Drying kinetics of semi-finished cassava crackers: A comparative study. *LWT - Food Science and Technology,* ***41*****,** 1360-1371.

Lesmes, U., Barchechath, J. and Shimoni, E., (2008). Continuous dual feed homogenization for the production of starch inclusion complexes for controlled release of nutrients. *Innovative Food Science and Emerging Technologies*, ***5***, 857-875.

Levy, I., Paldi, T. and Shoseyov, O., (2004). Engineering a bifunctional starch–cellulose cross-bridge protein. *Biomaterials, **25***, 1841–1849.

Li, B.Z., Wang, L., Li, D., Chiu, Y.L., Zhang, Z., Shi, J., Chen, X.D. and Mao, Z.H., (2009). Physical properties and loading capacity of starch-based microparticles crosslinked with trisodium trimetaphosphate. *Journal of Food Engineering*, ***92***, 255-260.

Li, G., Zeng, X., Xie, Y., Cai, Z., Moore, J.C., Yuan, X., Cheng, Z. and Ji, G., (2012). Pharmacokinetic properties of isorhamnetin, kaempferol and quercetin after oral gavage of total flavones of Hippophae rhamnoides L. in rats using a UPLC–MS method. *Fitoterapia, The Journal for the Study of Medicinal Plants, **83**,*182-191.

Lim, S. and Seib, P.A., (1993). Preparation and pasting properties of wheat and corn starch phosphates. *Cereal Chemistry, **70***, 137-144.

Lin, S.Y., Lin, K.H. and Li, M.J., (2002). Influence of excipients, drugs, and osmotic agent in the inner core on the time-controlled disintegration of compression-coated ethylcellulose tablets. *Journal of Controlled Release*, ***70***, 321-328.

Lin, J.H. and Lu. A.Y.H., (1997). Role of pharmacokinetics and metabolism in drug discovery and development. *Pharmacological Reviews, **49***, 403-449.

Lindenberg, M., Kopp, S. and Dressman, J.B., (2004). Classification of orally administered drugs on the World Health Organization Model list of essential medicines according to the biopharmaceutics classification system. *European Journal of Pharmaceutics and Biopharmaceutics*, ***58***, 265–278.

Liu, H., Yang, X.G., Nie, S.F., Wei, L.L., Zhoub, L.L., Liu, H., Tang, R. and Pan, W.S., (2007). Chitosan-based controlled porosity osmotic pump for colon-specific delivery system: Screening of formulation variables and *in vitro* investigation. *International Journal of Pharmaceutics, **220***, 115-124.

Lutfor, M.R., Sidik, S., Wan Yunus, W.M.Z., Rahman, A.M.Z., Mansoor, A. and Jelas, H., (2001). Preparation and swelling of polymeric absorbent containing hydroxamic acid group from polymer grafted sago starch. *Carbohydrate Polymers, **45***, 95-100.

Maaruf, A.G., Che Man, Y.B, Asbi, B.A., Junainah, A.H. and Kennedy, J.F., (2001). Effect of water content on the gelatinization temperature of sago starch. *Carbohydrate Polymers, **48***, 331-337.

MacDonald, T.T. and Monteleone, G., (2005). Immunity, inflammation, and allergy in the gut. *Science, **25**,* 1920–1925.

Madej, K., Parczewski, A, and Kała, M., (2003). HPLC/DAD screening method for selected psychotropic drugs in blood*. Toxicology Mechanisms and Methods, **13***, 121-127.

Maryland, B., (2004). The 7th report of the Joint National Committee on prevention, detection, evaluation, and treatment of high blood pressure (JNC VI). National Institutes of Health. National Heart, Lung, and Blood Institute. National High Blood Pressure Education Program NIH. Publication No. 04-5230.

Masaoka, Y., Tanaka, Y., Kataoka, M., Sakuma, S. and Yamashita, S., (2006). Site of drug absorption after oral administration: Assessment of membrane permeability and luminal concentration of drugs in each segment of gastrointestinal tract. *European Journal of Pharmaceutical Sciences, **29***, 240–250.

Matheson, N.K., (1971). Amylose changes in the starch of developing wheat grains. *Phytochemistry, **10***, 3213–3219.

Matzinger, D., Degen, L., Drewe, J., Meuli, J., Duebendorfer, R., Ruckstuhl, N., D'Amato, M., Rovati, L. and Beglinger, C., (2000). The role of long chain fatty acids in regulating food intake and cholecystokinin release in humans. *Gut*, ***46***, 688–693.

McConnell, E.L, (2008). Gut instincts: Explorations in intestinal physiology and drug delivery. *International Journal of Pharmaceutics, **364**,* 213-226.

McLaughlin, J., Grazia Lucà, M., Jones, M.N., D'Amato, M., Dockray, G.J. and Thompson, D.G., (1999). Fatty acid chain length determines cholecystokinin secretion and effect on human gastric motility. *Gastroenterology*, ***116***, 46-53.

Mehta, F., Kartikayen, C. and Trivedi, P., (2011). Formulation and characterization of medicated chewing gum delivery of Diphenhydramine Hydrochloride. *Der Pharmacia Sinica, An International Peer Reviewed Journal for Pharmaceautical Sciences, **2***, 182-193.

Mi, F.L., Tan, Y.C., Liang, H.F. and Sung, H.W., *In vivo* biocompatibility and degradability of a novel injectable-chitosan-based implant. *Biomaterials*, ***23***,181–191.

Milojevic, S., Newton, J.M., Cummings, J.H., Gibson, G.R., Botham, R.L., Ring, S.G., Stockham, M. and Allwood, M.C., (1996). Amylose as a coating for drug delivery to the colon: Preparation and *in vitro* evaluation using 5-aminosalicylic acid pellets. *Journal of Controlled Release, **38***, 75-84.

Mishima, K., (2008). Biodegradable particle formation for drug and gene delivery using supercritical fluid and dense gas. *Advanced Drug Delivery Reviews*, ***60***, 411–432.

Mishra, A.K., Kumar, A. and Mishra, A., (2010), Development and validation of UV spectrophotometric method for estimation of Diphenhydramine hydrochloride in soft gelatin capsule. *International Journal of Pharmaceutics, **1***, 144-148.

Mizuuchi, H., Katsura, T., Saito, H., Hashimoto, Y., and Inui, K.I., (1999). Transport characteristics of Diphenhydramine in human intestinal epithelial Caco-2 cells: Contribution of pH-dependent transport system. *The Journal of Pharmacology and Experimental Therapeautics, **290***, 388-392.

Mohajeri, L., Aziz, H.A., Isa, M.H. and Zahed, M.A., (2010). A statistical experiment design approach for optimizing biodegradation of weathered crude oil in coastal sediments. *Bioresource Technology*, ***101***, 893–900.

Mor, A., Pillinger, M.H., Wortmann, R.L. and Mitnick, H.J., (2008). Drug-induced arthritic and connective tissue disorders.*Seminars in Arthritis and Rheumatism*, ***38,*** 249-264.

Moraes, A.P., Schwarz, A., Spinosa, H.S., Florio, J.C. and Bernardi, M.M., (2004). Maternal exposure to diphenhydramine during the fetal period in rats: Effects on physical and neurobehavioral development and on neurochemical parameters. *Neurotoxicology and Teratology*, ***26,*** 681-692.

Morgan, S., Grootendorst, P., Lexchin, J., Cunningham, C. and Greyson, D., (2011). The cost of drug development: A systematic review. *Health Policy*, ***100,*** 4-17.

Muadklay, J. and Charoenrein, S., (2008). Effects of hydrocolloids and freezing rates on freeze–thaw stability of tapioca starch gels. *Food Hydrocolloids,* ***22***, 1268-1272.

Muhammad, K., Hussin, F., Man, Y. C., Ghazali, H. M. and Kennedy, J.F., (2000), Effect of pH on phosphorylation of sago starch. *Carbohydrate Polymers,* ***42***, 85-90.

Mukerjea, R., Slocum, G., and Robyt, J.F., (2007). Determination of the maximum water solubility of eight native starches and the solubility of their acidic-methanol and ethanol modified analogues. *Carbohydrate Research,* ***342***, 103-110.

Müller, E., Berger, R., Blass, E., Sluyts, D. and Pfennig, A., (2008). Liquid–liquid extraction. *Ullmann's Encyclopedia of Industrial Chemistry*.

Mussatto, S.I. and Mancilha, I.M., (2007). Non-digestible oligosaccharides: A review. *Carbohydrate Polymers*, ***68***, 587-597.

Nabais, T., Brouillet, F., Kyriacos, S., Mroueh, M., da Silva, A.P., Bataille, B., Chebli, C. and Cartilier, L., (2007). High-amylose carboxymethyl starch matrices for oral sustained drug-release: *In vitro* and *in vivo* evaluation. *European Journal of Pharmaceutics and Biopharmaceutics*, ***65***, 371–378.

Nandgude, T.D., Bhise, K.S. and Gupta, V.B., (2008). Characterization of hydrochloride and tannate salts of diphenhydramine. *Indian Journal of Pharmaceautical Sciences,* ***70,*** 482–486.

Nasrollahzadeh, H. S., Najafpour, G.D. and Aghamohammadi, N., (2007). Biodegradation of phenanthrene by mixed culture consortia in batch bioreactor using Central Composite Face-Centered Design. *International Journal of Environmental Research,* **1**, 80-87.

Natarajan, R., Kaveri, N. and Rajndran, N.N.R., (2011). Formulation and evaluation of aceclofenac gastro retentive drug delivery system. *Research Journal of Pharmaceutical Biological and Chemical Sciences,* ***2****, 765-771.*

Nageswari, A., Reddy K.V.S.R. and Mukkanti, K., (2012). Stability-indicating UPLC method for determination of Imatinib Mesylate and their degradation products in active pharmaceutical ingredient and pharmaceutical dosage forms. *Journal of Pharmaceutical and Biomedical Analysis*, ***66***, 109-115.

Neuhoff, S., Ungell, A.L., Zamora, I. and Artursson, P., (2005). pH-Dependent passive and active transport of acidic drugs across Caco-2 cell monolayers. *European Journal of Pharmaceutical Sciences, **25***, 211-220.

Neutel, C.I. and Appel, W.C., (2000). The effect of alcohol abuse on the risk of NSAID-related gastrointestinal events. *Annals of Epidemiology, The Official Journal of the American College of Epidemiology.**10***, 246-250.

Nevsten, P., Borgquist, P., Axelsson, A. and Wallenberg, L.R., (2005). XEDS-mapping for explaining release patterns from single pellets. *International Journal of Pharmaceutics, **290***, 109-120.

Nnamani, P.O., Ibezim, E.C., Attama, A.A. and Adikwu, M.U., (2010). Surface modified solid lipid microparticles based on homolipids and Softisan® 142: preliminary characterization. *Asian Pacific Journal of Tropical Medicine, **3,** 205-210.*

Nobilis, M., Vyb´ıralov´a, Z., Sl´adkov´a, K., L´ısa, M., Holˇcapek, M. and Kvˇetina, J., (2006). High-performance liquid-chromatographic determination of 5-aminosalicylic acid and its metabolites in blood plasma. *Journal of Chromatography A, **1119***, 299–308.

Noosuk, P., Hill, S.E., Pradipasena, P. and Mitchell, J.R., (2003). Structure-viscosity relationships for thai rice starches. *Starch, **55***, 337–344.

Nor Nadiha, M.Z., Fazilah, A., Bhat, R. and Karim, A.A., (2010). Comparative susceptibilities of sago, potato and corn starches to alkali treatment. *Food Chemistry, **121***, 1053-1059.

Ochia, B. A., (1973). Gastric emptying in young pigs, *Journal of Physiology*, ***233***, 467-480.

Oh, H.E., Pinder, D.N., Hemar, Y., Anema, S.G. and Wong, M., (2008). Effect of high-pressure treatment on various starch-in-water suspensions. *Food Hydrocolloids, **22***, 50-155.

Oluwolea, O.S.A., Onabolub, A.O., Mtundac, K. and Mlingi, N., (2007). Characterization of cassava (Manihot esculenta Crantz) varieties in Nigeria and Tanzania, and farmers' perception of toxicity of cassava. *Journal of Food Composition and Analysis*, ***20***, 559–567.

O'Reilly, S.E., Wilson, C.G. and Hardy, J.G., (1984). The influence of food on the gastric emptying of multiparticulate dosage forms. *International Journal of Pharmaceautics, **34***, 213-216.

Pal, K., Banthia,, A.K. and Majumdar, D.K., (2008). Effect of heat treatment of starch on the properties of the starch hydrogels. *Materials Letters*, ***62,*** 215-218.

Pan, C.M., Fan, Y.T., Xing, Y., Hou, H.W. and Zhang, M.L., (2008). Statistical optimization of process parameters on biohydrogen production from glucose by Clostridium sp. Fanp2. *Bioresource Technology*, ***99,*** 3146-3154.

Pandit, J.K., Singh, S. and Muthu, M.S., (2006). Controlled release formulations in neurology practice. *Annals of Indian Academy of Neurology*, ***9***, 207-216.

Parfitt, K., (1999). The Complete Drug Reference. Thirty second Edition. The Pharmaceautical Press.

Pasut, G. and Veronese, F.M., (2007). Polymer–drug conjugation, recent achievements and general strategies. *Progress in Polymer Science, **32***, 933–961.

Pedraglio, S., Rozio, M.G., Misiano, P., Reali, V., Dondio, G. and Bigogno, C., *(2007).* New perspectives in bio-analytical techniques for preclinical characterization of a drug candidate: UPLC-MS/MS in *in vitro* metabolism and pharmacokinetic studies. *Journal of Pharmaceutical and Biomedical Analysis, **44,*** 665-673.

Peppas, L. B., (1992). Design and mathematical analysis of controlled release from microsphere-containing polymeric implants. *Journal of Contolled Release, **20***, 201-208.

Pereswetoff-Morath, L., (1998). Microspheres as nasal drug delivery system. *Advanced Drug Delivery Review, **29***, 185-194.

Petkovska, R., Cornett, C. and Dimitrovska, A., (2008). Experimental design approach for the development and validation of enanttiospecific RP-HPLC method for simultaneous determination of clopidogrel and relate compounds. *Macedonian Journal of Chemistry and Chemical Engineering*, ***27***, 53-64.

Phale, M.D. and Gothoskar, A.V., (2011). Multiunit particulate systems: A current drug-delivery technology. *Pharmaceutical Technology*, ***35***, 60-66.

Pilichiewicz, A.N., Chaikomin, R., Brennan, I.M., Wishart, J.M., Rayner, C.K., Jones, K.L., Smout, A.J.P.M., Horowitz, M. and Feinle-Bisset, C., (2007). Load-dependent effects of duodenal glucose on glycemia, gastrointestinal hormones, antropyloroduodenal motility, and energy intake in healthy men*. American Journal of Physiology, Endocrinology, Metabolism, **293***, E743–E753.

Pond, W. G. and Houpt, K. A., (1978). *The Biology of the Pig,* Cornell University Press, Ithaca, N.Y.

Pongsawatmanit, P., Temsiripong, T., Ikeda, S. and Nishinari, K., (2006). Influence of tamarind seed xyloglucan on rheological properties and thermal stability of tapioca starch. *Journal of Food Engineering*, ***77***, 41–50.

Pongsawatmanit, P., Temsiripong, T. and Suwonsichon, T., (2007). Thermal and rheological properties of tapioca starch and xyloglucan mixtures in the presence of sucrose. *Food Research International, **40***, 239–248.

Ponto, L.L. and Schoenwald, R.D., (1990). Furosemide: A pharmacokinetic/ pharmacodynamic review (Part I). *Clinical Pharmacokinetics*, ***18***, 381-408.

Porter, C.J.H. and Charman, W.N., (2001). *In vitro* assessment of oral lipid based formulations. *Advanced Drug Delivery Reviews, **50***, S127 –S147.

Porth, C.M. and Matfin G., (2010). Gastrointestinal system. Concepts of Altered Health States, Eighth Edition. Lippincott Williams and Wilkins.

Ragheb, A.A., Abdel-Thalouth, I. and Tawfik, S., (1995). Gelatinization of starch in aqueous alkaline solutions. *Starch*, ***47***, 338-345.

Rahman, N., Singh, M. and Hoda, M.D.N., (2005). Validation of simultaneous volumetric and spectrophotometric methods for the determination of captopril in pharmaceutical formulations. *Il Farmaco*, ***60,*** 569-574.

Rains, C.P., Noble, S. and Faulds, D., (1995). Sulfasalazine. A review of its pharmacological properties and therapeutic efficacy in the treatment of rheumatoid arthritis*. Drugs*, ***50***, 137-56.

Rajan, A., Sudha, J.D. and Abraham, T.E., (2008). Enzymatic modification of cassava starch by fungal lipase. *Industrial Crops and Products*, ***2***, 50–59.

Rankin, J.C. and Mehltretterd, C.L., (1965). Determination of dialdehyde units in periodate-oxidized cornstarches. *Analytical Chemistry, **28***, 1012-1014.

Ranjbar, S., Ghobadi, S., Khodarahmi, R. and Nemati, H., (2012). Spectroscopic characterization of furosemide binding to human carbonic anhydrase II. *International Journal of Biological Macromolecules*, ***50,*** 910-917.

Rao, M.A. and Tattiyakul, J., (2007). Granule size and rheological behavior of heated tapioca starch dispersions. *Carbohydrate Polymers*, ***38***, 123-132.

Ratnayake, W.S. and Jackson, D.S., (2009). Starch gelatinization. *Advances in Food and Nutrition Research, **55***, 221-268.

Ray, S., Lalman, J.A. and Biswas, N., (2009). Using the Box-Benkhen technique to statistically model phenol photocatalytic degradation by titanium dioxide nanoparticles. *Chemical Engineering Journal*, ***150***, 15-24.

Ray, S., Reaume, S.J. and Lalman, J.A., (2010). Developing a statistical model to predict hydrogen production by a mixed anaerobic mesophilic culture. *International Journal of Hydrogen Energy, **35***, 5332-5342.

Raybould, H.E., (1999). Nutrient tasting and signaling mechanisms in the gut. Sensing of lipid by the intestinal mucosa. *American Journal of Physiology, **277**,* G751–G755.

Reeds, P. and Odle, J., (1996). Pigs as models for nutrient functional interaction. *Advances in Swine in Biomedical Research, **2**,* 709-711.

Reis, F., Tavares, P. and Teixeira, F., (2000). The distribution of catecholamines between plasma and platelets in cyclopsporin A-induced hypertensive rats. *Pharmacological Research, **41**,* 129-135.

Reyes, A.C., Triana, M.T., Jimenez-Kairuz, A.F., Manzo, R.H. and Martı´nez, F., (2008). Thermodynamics of partitioning of propranolol in some organic solvent/buffer systems. *Journal of Chemical and Engineering Data*, ***53***, 2810–2815.

Roberfroid, M. and Slavin, J., (2000). Nondigestible oligosaccharides. *Critical Reviews in Food Science and Nutrition, **40***, 461-480.

Robinson, J.R. and Gauger, L.J., (1986). Formulation of controlled-release products. *Journal of Allergy and Clinical Immunology, **78***, 676-81.

Rubinstein, A., (2005). Colonic drug delivery. *Drug Discovery Today: Technologies*, ***2**,* 33-37.

Sadeghi, S. and Sheikhzadeh, E., (2008). Solid phase extraction using silica gel functionalized with Sulfasalazine for preconcentration of uranium (VI) ions from water samples*. Microchimica Acta, An International Journal on Analytical, Micro and Nanochemistry, **163***, 313–320.

Sae-kang, V., and Suphantharika, V., (2006). Influence of pH and xanthan gum addition on freeze-thaw stability of tapioca starch pastes. *Carbohydrate Polymers, **65***, 371–380.

Sajomsang, W., Ruktanonchai, U.R., Gonil, P. and Nuchuchua, O., (2009). Mucoadhesive property and biocompatibility of methylated N-aryl chitosan derivatives. *Carbohydrate Polymers*, ***78***, 945-952.

Sakuma, S., Tanno, F.K., Masaoka, Y., Kataoka, M., Kozaki, T., Kamaguchi, R., Kokubo, H. and Yamashita, S., (2007). Effect of administration site in the gastrointestinal tract on bioavailability of poorly absorbed drugs taken after a meal. *Journal of Controlled Release, **118***, 59-64.

Salama, N.N., Fasano, A., Thakar, M. and Eddington, N.D., (2004). The effect of delta G on the transport and oral absorption of macromolecules. *Journal of Pharmaceutical Science, **93***, 1310–1319.

Salminen, S., Bouley, C., Boutron-Ruault, M.C., Cummings, J.H., Franck, A., Gibson, G.R., Isolauri, E., Mores, M.C., Roberfroid, M. and Rowland, I., (1998). Functional food science and gastrointestinal physiology and function. *British Journal of Nutrition,* ***80***, S147-Sl71.

Sangeker, S., Vadino, W.A., Chandry, I., Parr, A., Beihn, R.M. and Digenis, G.A., (1987). Evaluation of the effect of food and specific gravity of tablets on gastric retention time. *International Journal Pharm*aceautics, ***35***, 187-191.

Scholz, O.A., Wolff, A., Schumacer, A., Giannola, L.I., Campisi, G., Ciach, T. and Velten, T., (2008). Drug delivery from the oral cavity: focus on a novel mechatronic delivery device. *Drug Discovery Today,* ***13***, 247-253.

Schuster-Wolff-Bühring, R., Fischer, L. and Hinrichs, J., (2010). Production and physiological action of the disaccharide lactulose. *International Dairy Journal*, ***20***, 731–741.

Senel, S. and McClure, S.J., (2004). Potential applications of chitosan in veterinary medicine. *Advanced Drug Delivery Reviews,* ***56***, 1467– 1480.

Sharma, R., Walker, R.B. and Pathak, K., (2011). Evaluation of the kinetics and mechanism of drug release from Econazole nitrate nanosponge loaded Carbapol Hydrogel. *Indian Journal of Pharmaceutical Educational Research,* ***45,*** 25-31*.*

Sheriff, N.M., Gupta, N.K., Velmurugan, R. and Shanmugapriyan, N., (2008). Optimization of thin conical frusta for impact energy absorption. *Thin-Walled Structures*, ***46,*** 653-666.

Shey, J., Holtman, K.M., Wong, R.Y., Gregorski, K.S., Klamczynski, A.P., Orts, W.J., Glenn, G.M., Imam, S.H., (2006). The azidation of starch. *Carbohydrate Polymers*, ***65***, 529–534.

Shi, Y., Xiang, P., Shen, B. and Shen, M., (2012). A rapid and accurate UPLC/MS/MS method for the simultaneous determination of zolpidem and its main metabolites in biological fluids and its application in a forensic context*. Journal of Chromatography B: Analytical Technologies in the Biomedical and Life Sciences,* ***911***,140-146.

Sica, A.D. and Gehr, T.W, (2007). Chapter 31: Pharmacologic treatment of hypertension. Cardiovascular Therapeutics. Third Edition. Cardiotext Publishers, McGraw-Hill. 578-599.

Silva, G.A., Costa, F.J., Neves, N.M., Coutinho, O.P., Dias, A.C.P. and Reis, R.L., (2005). Entrapment ability and release profile of corticosteroids from starch-based microparticles. *Journal of Biomedical Material Research Part A,* ***73***, 234-43.

Siminiceanu, I., Lazau, I., Ecsedi, Z., Lupa, L. and Burciag, C., (2008). Textural characterization of a new iron-based ammonia synthesis catalyst. *Chemical Bulletin of "POLITEHNICA" University of Timisoara*, ***53***, 1-2.

Singh, B., Kumar, R. and Ahuja, N., (2004). Optimizing drug delivery systems using systematic "Design of Experiments."Part I: Fundamental aspects. *Critical Reviews in Therapeutic Drug Carrier Systems,* ***22***, 27-105.

Singh, B., Sharma, D.K., Kumar, R., Gupta, A., (2010). Development of a new controlled pesticide delivery system based on neem leaf powder. *Journal of Hazardous Materials*, ***177***, 290-299.

Singhal, R.S., Kennedy, J.F., Gopalakrishnan, S.M., Kaczmarek, A., Knill, C.J. and Akmar, P.F., (2008). Industrial production, processing, and utilization of sago palm-derived products. *Carbohydrate Polymers*, ***72***, 1-20.

.

Sommers, D.K., van Wyk, M., Moncrieff, J. and Schoeman, H.S., (1984). Influence of food and reduced gastric acidity on the bioavailability of bacampicillin and cefuroxime axetil. *British Journal of Clinical Pharmacology,* ***18***, 535–539.

Springate C.M., Jackson, J.K., Gleave, M.E. and Burt, H.M., (2008). Clusterin antisense complexed with chitosan for controlled intratumoral delivery. *International Journal of Pharmaceutics*, ***350***, 53-64.

Streubel, A., Siepmann, J. and Bodmeier, R., (2006). Drug delivery to the upper small intestine window using gastro-retentive technologies. *Current Opinion in Pharmacology,* ***6***, 501-508.

Stewart, S., Carrington, M.J., Swemmer, C., Kurstjens, N. and Jennings, G.L., (2011). Optimising management of hypertension in primary care: The Valsartan Intensified Primary Care Reduction of Blood Pressure (Viper-Bp) Study. *International Journal of Cardiology,* ***153****,* 317-322.

Sugawara, M., Takekuma, Y., Yamada, H., Kobayashi, M., Iseki, K. and Miyazaki, K., (1998). A General approach for the prediction of the intestinal absorption of drugs: regression analysis using the physicochemical properties and drug-membrane electrostatic interaction. *Journal of Pharmaceutical Scieces,* ***87***, 960-966.

Sugawara, M., Kadomura, S., Heb, X., Takekuma, Y., Kohri, N. and Miyazaki, K., (2005). The use of an *in vitro* dissolution and absorption system to evaluate oral absorption of two weak bases ih pH - independent controlled-release formulations. *European Journal of Pharmaceutical Sciences*, ***26***, 1-8.

Sungthongjeen, S., Sriamornsak, P. and Puttipipatkhachorn, S., (2007). Design and evaluation of floating multi-layer coated tablets based on gas formation. *European Journal of Pharmaceutics and Biopharmaceutics*, ***67***, 211-219.

Sutton, S.C., Evans, L.A., Fortner, J.H., McCarthy, J.M. and Sweeney, K., (2006). Dog colonoscopy model for predicting human colon absorption. *Pharmaceutical Research, Vitamins and Hormones,* ***80***, 217-244.

Swenson, E.S. and Curatolo, W.J., (1992). Means to Enhance Penetration (2) Intestinal permeability enhancement for proteins, peptides and other polar drugs: mechanisms and potential toxicity. *Advanced Drug Delivery Reviews*, ***8***, 39-92.

Syed, K.H., Al-Assaf, G.S. and O' Phillips, G., (2011). Chapter 5: Hydrogels: Methods of preparation, characterisation and applications. *Progress in Molecular and Environmental Bioengineering - From Analysis and Modeling to Technology Applications.*

Szepes, A.,Makai, Z., Blu¨mer, C., Ma¨der, K., Ka´sa Jr. P. and ´-Re´ve´sz, P.Z., (2008). Characterization and drug delivery behaviour of starch-based hydrogels prepared via isostatic ultrahigh pressure. *Carbohydrate Polymers,* ***72***, 571-578.

Tay, S.H., Pang, S.C. and Chin, S.F., (2012). Facile synthesis of starch-maleate monoesters from native sago starch. *Carbohydrate Polymers*, ***88****,* 1195-1200.

Te Wierik, G.H.P., Eissens, A.C., Bergsma, J., Arends-Scholte, A.W. and Bolhuis, G.K., (1997). A new generation starch product as excipient in pharmaceutical Tablets III. Parameters affecting controlled drug release from tablets based on high surface area retrograded pregelatinized potato starch. *International Journal of Pharmaceutics,* ***157***, 181–187.

Tettey-Amlalo, R.N.O. and Kanfer, I., (2009). Rapid UPLC–MS/MS method for the determination of ketoprofen in human dermal microdialysis samples. *Journal of Pharmaceutical and Biomedical Analysis*, ***50,*** 580-586.

Temsiriponga, T., Pongsawatmanit, R. and Katsuyoshi, I.S., (2005). Influence of xyloglucan on gelatinization and retrogradation of tapioca starch*. Food Hydrocolloids*, ***19***, 1054–1063.

Thakur, A.C., Aslam, A.K., Aslam, A.F., Vasavada, B.C., Sacchi, T.J. and Khan, I.A., (2005). QT interval prolongation in diphenhydramine toxicity. *International Journal of Cardiology*, ***98***, 341– 343

The Japanese pharmacopeia, Fourteenth Edition, English version, part 1: official monographs for part 1, 307

Theobald Jr R.J., (2007). Sulfapyridine. *xPharm: The Comprehensive Pharmacology Reference*, 1-4.

Thormann, M., Amthauer, H., Adolf, D., Wollrab, A., Ricke, J. and Speck, O., (2011). Efficacy of diphenhydramine in the prevention of vertigo and nausea at 7 T MRI. *European Journal of Radiology*, ***82***, 768-772.

Tikuisis, T., (1993). Nondestructive quantitative determination of starch content in polyethylene by solid state NMR and FTIR. *Polymer Engineering and Science*, ***33***, 135-138.

Tjornelund, J. and Hansen, S.H., (1991). High-performace liquid chromatography assay of 5-aminosalicylic acid (5-ASA) and its metabolites N-β-D-glucopyranosyl-5-ASA, N-acetyl-5-ASA, N-formyl-5-ASA and N-buturyl-5-ASA in biological fluids, *Journal of Chromatography,* ***570****,* 109-117.

Torres, N., Noriega, L. and Tovar, A.R., (2009). Nutrient modulation of insulin secretion. *Vitamins and Hormones*, ***80,*** 217-240.

Tuleu, C., Andrieux, C., Boy, P.and Chaumeil, J.C., (1999). Gastrointestinal transit of pellets in rats: effect of size and density. *International Journal of Pharmaceutics,* ***180***, 123–131.

Tuovinen, L., Peltonen, S., Liikola, M., Hotakainen, M., Lahtela-Kakkonen, M., Poso, A. and Jarvinen, K., (2004). Drug release from starch-acetate microparticles and films with and without incorporated α-amylase. *Biomaterials,* ***25***, 4355-4362.

Ugwoke, M.I., Kaufmann, G., Verbeke, N. and Kinget, R., (2000). Intranasal bioavailability of apomorphine from carboxymethylcellulose-based drug delivery systems*. International Journal of Pharmaceutics*, ***202***, 125–131.

USP 33. (2009). *The United States Pharmacopoeia,* ***33***, US Pharmacopoeial Convention, Rockville.

Uwai, K., Tani, M., Ohtake, Y., Abe, S., Maruko, A., Chiba, T., Hamaya, Y., Ohkubo, Y. and Takeshita, M., (2005). Photodegradation products of propranolol: The structures and pharmacological studies. *Life Sciences*, ***78,*** 357-365*.*

Valenta, C., (2005). The use of mucoadhesive polymers in vaginal delivery. *Advanced Drug Delivery Reviews*, ***57***, 1692– 1712.

Vancea, S., Imre, S., Donáth-Nagy, G., Béla, T., Nyulas, M., Muntean, T. and Borka-Balás, R., (2009). Determination of free captopril in human plasma by liquid chromatography with mass spectrometry detection. *Talanta: The International Journal of Pure and Applied Analytical Chemistry*, ***79,*** 436-441.

Vallejo-Cremades, M.T., Go´mez-Garcı´a, L., Chacatas-Cortesao, M., Moreno, C., Sa´nchez, M., De Miguel, E. and Go´mez de Segura, I.A., (2004). Enriched protein diet-modified ghrelin expression and secretion in rats. *Regulatory Peptides,* ***121***, 113– 119.

van Erk, M.J., Blom, W.A., van Ommen, B. and Hendriks, H.F., (2006). High-protein and high-carbohydrate breakfasts differentially change the transcriptome of human blood cells. *American Journal of Clinical Nutrition,* ***84***, 1233-41.

Vargas, A., Zeisser-Labouèbe, M., Lange, N., Gurny, R. and Delie, F., (2007). The chick embryo and its chorioallantoic membrane (CAM) for the *in vivo* evaluation of drug delivery systems. *Advanced Drug Delivery Reviews*, ***59,*** 1162-1176.

Veelaert, S., de Wit, D. and Tournois, H., (1994). An improved kinetic model for the periodate oxidation of starch. *Polymer, **35***, 5091-5097.

Vermeylen, R., Goderis, B., Reynaers, H. and Delcour, J.A., (2004). Amylopectin molecular structure reflected in macromolecular organization of granular starch. *Biomacromolecules, **5***, 1775-1786.

Vilivalam, V.D., Illum, L. and Iqbal, K., (2000). Starch capsules: an alternative system for oral drug delivery. *Pharmaceutical Science and Technology Today*, ***3***, 64-69.

Vijayaraghavan, K. and Deedwania, P., (2011). Renin-angiotensin-aldosterone blockade for cardiovascular disease prevention. *Cardiology Clinics*, **29**, 137-156.

Viyoch, J., Patcharaworakulchai, P., Songmek, R., Pimsan, V. and Wittaya-Areekul, S., (2003). Formulation and development of a patch containing tamarind fruit extract by using the blended chitosan-starch as a rate-controlling matrix. *International Journal of Cosmetic Science*, ***25***, 113-125.

Viyoch, J., Sudedmark, T., Srema, W. and Suwongkrua, W., (2005). Development of hydrogel patch for controlled release of alpha-hydroxy acid contained in tamarind fruit pulp extract. *International Journal of Cosmetic Science*, ***27***, 89-99.

Walton, K.S. and Snurr, R.Q., (2007). Applicability of the BET method for determining surface areas of microporous metal-organic frameworks. *Journal of the American Chemical Society, **129***, 8552-8556.

Wang, J., Zhang, Y., Yang, X., Wang, X., Zhang, J., Fang, J. and Jiang, X., (2012). hemodynamic effects of furosemide on renal perfusion as evaluated by ASL-MRI. *Academic Radiology*, ***19,*** 1194-1200.

Warren, F.J., Royall, P.G., Butterworth, P.J. and Ellis, P.R., (2012). Immersion mode material pocket dynamic mechanical analysis (IMP-DMA): A novel tool to study

gelatinisation of purified starches and starch-containing plant materials. *Carbohydrate Polymers*, ***90***, 628-636.

Weiner, A.L., (1989). Liposomes as carriers for polypeptides. *Advanced Drug Delivery Reviews, **3***, 307-341.

Wilson, P.J. and Basit, A.W., (2005). Exploiting gastrointestinal bacteria to target drugs to the colon: An *in vitro* study using amylose coated tablets. *International Journal of Pharmaceutics*, ***300***, 89-94.

Winstanley, P.A. and Orme, M.L., (1989). The effects of food on drug bioavailability. *British Journal of Clinical Pharmacology*, ***28***, 621–628.

Wolf, R., Matz, H., Orion, E., Tüzün, B. and Tüzün, Y., (2002). Miscellaneous treatments, I: sulfasalazine and pentoxifylline: unapproved uses, dosages, or indications . *Clinics in Dermatology*, ***20,*** 531-546.

Wongsagon, R., Shobsngob, S., and Varavinit, S., (2005). Preparation and physicochemical properties of dialdehyde tapioca starch. *Starch, **57***, 166-172.

Wootton, M. and Ho, P., (1989). Alkali gelatinisation of wheat starch. *Starch, **41***, 261-265.

Wu, X., Noda, A., Noda, H. and Imamura, A., (2001). Side-chain metabolism of propranolol: involvement of monoamine oxidase and aldehyde reductase in the metabolism of N-desisopropylpropranolol to propranolol glycol in rat liver. *Comparative Biochemistry and Physiology Part C: Toxicology and Pharmacology*, ***129***, 361-368.

Xiao, H., Lin, Q. and Liu, G.Q., (2012). Effect of cross-linking and enzymatic hydrolysis composite modification on the properties of rice starches. *Molecules, **17***, 8136-8146.

Xiao, H., Lin, Q., Liu, G.Q., Wu, Y., Wu, W. and Fu, X., (2011). Physicochemical properties of chemically modified starches from different botanical origin. *Scientific Research and Essays, **6***, 4517-4525.

Xue, Y., Hieda, Y., Fujihara, J., Takayama, K. and Takeshita, H., (2007). Specific determination of Linear Alkylbenzenesulfonates (LAS) in commercial detergents and whole blood by high-performance liquid chromatography with solid-phase extraction. *Journal of Analytical Toxicology*, ***31***, 7-43.

Yamada, A., Furuya, M., Akimoto, T., Maki, T., Suwa, H. and Ogata, H., (1995). Evaluation of gastrointestinal transit controlled-beagle dog as a suitable animal model for bioavailability testing of sustained-release acetaminophen dosage form. *International Journal of Pharmaceutics*, ***119,*** 1-10.

Yáñez, J.A., Wang, S.W.J., Knemeyer, I.W., Wirth, M.A. and Alton, K.B., (2011). Intestinal lymphatic transport for drug delivery. *Advanced Drug Delivery Reviews*, ***63***, 923–942.

Yang, L., Chu, J. and Fix J.A., (2002). Colon-specific drug delivery: new approaches and *in vitro*/*in vivo* evaluation. *International Journal of Pharmaceutics*, ***235,*** 1-15.

Yavagal, S.T., Patil, R., Halakatti, P.C., Patted, S.V., Ambar, S., Amarkhed, B. and Kotur, P.F., (2011). JNC-7 definition of hypertension needs alteration. *Journal of Indian College of Cardiology,* ***1,*** 5-9.

Ye, X., Tang, M., Liu, J., Wang, X., Ma, L., Zheng, H., Hu, J., Chen, X., Duan,X. and Chen, L., (2011). Development and validation of a UPLC–MS/MS method for quantification of SKLB010, an investigational anti-inflammatory compound, and its application to pharmacokinetic studies in beagle dogs. *Journal of Pharmaceutical and Biomedical Analysis*, ***56,*** 366-372.

Yu, C.Y., Zhang, X.C., Zhou, F.Z., Zhang, X.Z., Cheng, S.X. and Zhuo, R.X., (2008). Sustained release of antineoplastic drugs fromchitosan-reinforced alginate microparticle drug delivery systems. *International Journal of Pharmaceutics*, ***357***, 15-21.

Zarzycki, R., Modrzejewska, Z. and NawroteK, K., (2010). Drug release from hydrogel matrices. *Ecological Chemistry and Engineering,* ***17***, 117-136.

Zhao, L., Zhao, Y., Li, Q., Chen, X., Xiao, F., He, B., Wang, J. and Bi, K., (2012). A fast, sensitive, and high throughput method for the determination of cefuroxime lysine in dog plasma by UPLC–MS/MS. *Talanta: The International Journal of Pure and Applied Analytical Chemistry,* ***89,*** 84-90.

Zhu, Q. and Bertoft, E., (1997). Enzymic analysis of the structure of oxidized potato starches. *International Journal of Biological Macromolcules,* ***21***, 131-135.

Zhu, T., Jackson, D.S., Wehling, R.L. and Geera, B., (2008). Comparison of amylose determination methods and the development of a dual wavelength iodine binding technique. *Cereal Chemistry*, ***85***, 51-58.

Zvonar, A., Berginc, K., Kristl, A. and Gašperlin, M., (2010). Microencapsulation of self-microemulsifying system: Improving solubility and permeability of furosemide. *International Journal of Pharmaceutics*, ***388,*** 151-158.

APPENDICES

APPENDIX A

Abstracts of conference proceedings

APPENDIX A1

Influence of hydration on the drug loading capacity, mechanical strength and resilience of cellulosic multiparticulates

Yusuf Dawood, Asma Seedat, Viness Pillay*, Yahya E. Choonara and Lisa C. du Toit
University of the Witwatersrand, Department of Pharmacy and Pharmacology, 7 York Road, Parktown, 2193, Johannesburg, South Africa
*Correspondence: viness.pillay@wits.ac.za

Introduction

To determining the feasibility of particle hydration as a mechanism of drug entrapment and the influence of hydration on the mechanical strength and resilience of cellulose multiparticulates.

Methods

Multiparticulate bead-like samples (1g) were hydrated in a concentrated diphenhydramine (DPH) solution (100mg/mL) for 1, 2, 4, 8, 12, 18, and 24 hours. Upon removal and subsequent drying, the beaded structures were homogenised in PBS (pH 12.5; 37ºC) followed by UV spectroscopy analysis in order to determine DPH content entrapped. A second set underwent a similar experimental procedure with the exception of the drying process. Samples (0.130g) were immersed in 5mL deionized water and allowed to hydrate for 1, 2, 4, 8, 12, 18, and 24 hours. Textural profile analysis was then performed in order to establish the matrix resilience, hardness and deformation energy of the beads as a result of hydration.

Results

Maximum hydration of 193% was observed after 8 hours within the DPH solution. Thereafter hydration remained constant up to 24 hours. DPH entrapment closely correlated with the degree of swelling as the quantity of DPH loaded plateaus at the maximum hydration of the multiparticulates. Beads which did not undergo drying demonstrated a 5.5% superior DPH loading capacity. The matrix resilience initially decreased substantially upon hydration but maintained a consistency of approximately 11% as the degree of hydration varied. Hardness and deformation energy values displayed similar behaviour as matrix resilience with the initial drastic decline upon hydration followed by a constant level during further hydration.

Conclusions

Hydration of the cellulosic multiparticulates influenced the drug loading capacity and may be employed as a mechanism for manipulating drug entrapment. Although hydration decreased the mechanical strength and matrix resilience of the bead-like structures, the degree of hydration had no influence on these parameters. Further stability studies are underway.

APPENDIX A2

Determination of the entrapment efficiency, friability and release profile of Diphenhydramine from cellulosic multiparticulates

Yusuf Dawood, Viness Pillay*, Yahya E. Choonara and Lisa C. du Toit
University of the Witwatersrand, Department of Pharmacy and Pharmacology, 7 York Road, Parktown, 2193, Johannesburg, South Africa
*Correspondence: viness.pillay@wits.ac.za

Purpose:
To elucidate the feasibility of utilizing food grade cellulosic multiparticulates in the development of a novel drug delivery system.

Methods:
2g samples of sago beads were accurately weighed out, placed into 10ml of 150mg/ml concentration diphenhydramine (DPH) solution and allowed to hydrate for 4 hours. The beads were then removed, placed on petri dishes, weighed and allowed to dry at 50ºC until constant mass was achieved. During the drying process, the clusters of beads were manually separated on the petri dishes. Approximately 6.5g of drug-loaded multiparticulates were weighed out and dusted carefully before accurately weighing the beads. These beads were placed in the friability testing apparatus and allowed to rotate 100 cycles at 25rpm as prescribed in the USP. The beads were then carefully removed and weighed and the mass loss was calculated. The rate and extent of drug release from the multiparticulates was elucidated by placing 1g of drug-loaded beads into USP rotating paddle apparatus with 900ml of buffer (pH 1.2 and 37^{0}C). Samples were removed every hour after which UV spectrometry was used to determine drug concentrations at each time point.

Results:
The cellulosic multiparticulates swelled up to 187% of its initial mass during the entrapment process and entrapped ~445mg of DPH, which represents a drug entrapment efficiency (DEE) of ~30%. The results show that the beads pass the USP test for friability with a mass loss of 0.74 (±0.12%). The drug-loaded beads are thus stable and minimum drug loss will occur during further processing. The results also show that the beads are suitable for coating. These drug-loaded multiparticulates then displayed a complete burst effect by releasing majority of the drug in simulated gastric conditions within the 1st hour. This could be attributed to the partial disintegration of the multiparticulates or even suggest surface adsorption of drug onto the beads.

Conclusion:
The cellulosic multiparticulates display an adequate DEE to be utilized in formulating them as a dosage form. However, further test are required to elucidate the exact mechanism of drug loading. They further exhibit adequate friability and can thus be coated or combined with other natural grade polymers to improve the current unsatisfactory release rate.

APPENDIX A3

Elucidation of the potential of starch-based multiparticulates for use as a platform in novel drug delivery systems

Y. Dawood, V. Pillay*, Y.E. Choonara, L.C. du Toit
University of the Witwatersrand, Department of Pharmacy and Pharmacology, 7 York Road, Parktown, 2193, Johannesburg, South Africa
Correspondence: viness.pillay@wits.ac.za

INTRODUCTION

Starch is a widely available and inexpensive natural food source which is used within the pharmaceutical industry as simple excipients [1]. The study is therefore aimed at expanding the use of commercial starch products by employing them as the actual core of drug delivery systems thus eliminating the cost and process required to formulate a core.

MATERIALS AND METHODS

1) *Determination of drug entrapment efficiency*: 5g samples of starch-based multiparticulates (SBM) were accurately weighed out and placed into 15mL diphenhydramine (DPH) solution (100mg/mL). The SBM were allowed to hydrate at a temperature of 50ºC for 1 hour. The SBM were then removed, placed on petri dishes, weighed and allowed to dry at a temperature of 25ºC until constant mass was achieved. The SBM were weighed and 1g samples of the drug-loaded SBM were homogenized in 10mL deionized water for 120 seconds. The homogenized suspension was then made up to 500mL with water maintained at 100°C, stirred and allowed to cool. Three 10mL samples from the cooled suspension were then centrifuged for 90 minutes after which they were filtered through a 0.45µm filter. The filtered samples were then analyzed using UV spectroscopy at a wavelength (λ max) of 254nm to determine the drug content within the SBM.

2) *Preparation of tablets*: 12 tablet formulations each having a mass of 1000mg were prepared as depicted in table 1. In formulations 1-4 260mg of drug-loaded SBM represents the equivalent of 50mg DPH. In formulations 5-8 granules were formed from the tablet substituents prior to tableting and in formulations 9-12 direct compression of powder blends was performed.

	1	*2*	*3*	*4*	*5*	*6*	*7*	*8*	*9*	*10*	*11*	*12*
Drug loaded SBM	260	260	260	260								
DPH					50	50	50	50	50	50	50	50
Starch	740			370	950			475	950			475
Ethylcellulose		740		370		950		475		950		475
Chitosan			740				950				950	

Table 1. Preparation of tablets

3) Fourier transform infrared spectroscopy (FTIR) analysis: FTIR was carried out to elucidate the mechanism of drug entrapment within the SBM.

4) *In vitro* drug release studies: These were performed on the tablets using the USP dissolution apparatus II (paddle method) in 900mL pH 6.8 phosphate buffer solution (PBS), at 37 ± 0.1^0C and rotated at 50 rpm. Samples (5mL) were withdrawn every 30 minutes over a 12 hour period and replenished with fresh buffer to maintain sink conditions. The absorbance values were measured using UV spectroscopy at a wavelength of 254nm (λ max) and drug release was calculated using a predefined calibration curve.

RESULTS AND DISCUSSION

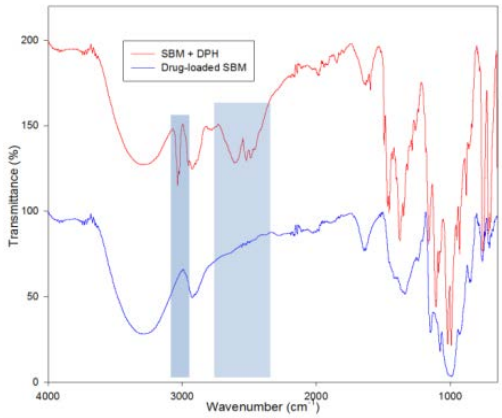


Figure 1. FTIR spectra depicting drug-loaded SBM and composite multiparticulates and DPH

The drug entrapment efficiency was calculated as 52±1.1 % with FTIR illustrating possible bond formation between the drug and the SBM at a wavenumber 3012 and in the region between wavenumber 2040 and 2070.

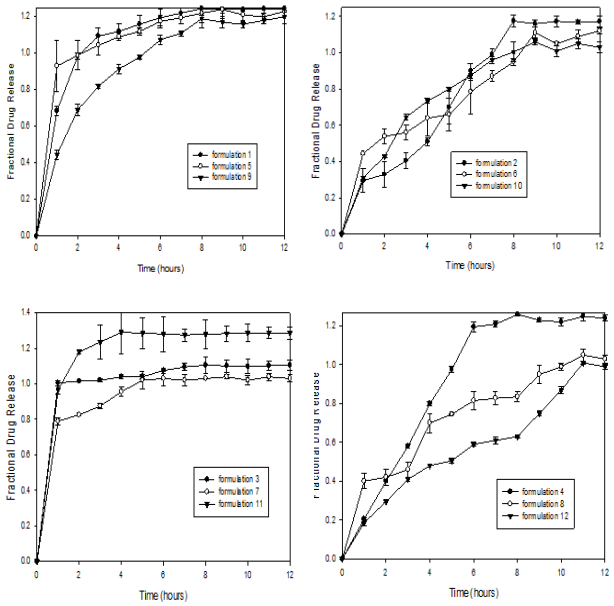


Figure 2. Drug release profiles of tablet formulations

Drug release profiles show that the SBM/polymer formulations (1-4) control release to the greatest extent over the first 8 hours compared to the granulated or powder blend formulations. The SBM/Ethylcellulose formulation (2) displayed the most favourable drug release kinetics.

CONCLUSIONS

Starch based multiparticulates demonstrate satisfactory entrapment efficiency and serves as a functional platform for controlled release drug delivery systems.

REFERENCES

[1] S. Galland, T. Ruiz and M. Delalonde, “Twin product/process approach for pellet preparation by extrusion/spheronisation Part I: Hydro-textural aspects”, *Int. J. Pharm*. 337 (2007) 239–245.

ABSTRACT/371

APPENDIX A4

Elucidation of the Effect of Oxidation and Crosslinking on the Drug Entrapment Efficiency and *In vitro* drug release behaviour of a Starch-Based Multiparticulate Drug Delivery System

Yusuf Dawood, Pradeep Kumar, Viness Pillay*, Yahya E. Choonara and Lisa C. du Toit.
Department of Pharmacy and Pharmacology, University of the Witwatersrand, 7 York Road, Parktown, 2193 Johannesburg, South Africa
*Corresponding author: viness.pillay@.wits.ac.za

Purpose:
The purpose of the study was to modify a starch-based multiparticulate drug delivery system by oxidizing using sodium (meta)periodate and crosslinking using epichlorohydrin and evaluate the effects that these modifications have on their drug entrapment efficiency and drug release behavior.

Methods: modification of starch multiparticulates
Oxidation: multiparticulate samples (5g) were immersed in 50mL sodium(meta)periodate solution (0.2M) and allowed to oxidize under constant stirring for 1.5 hours at a constant temperature of 25±1°C. Thereafter the oxidized beads were removed from the oxidation medium, washed with 1000mL deionized water and allowed to dry at 50°C for 4 hours.

Crosslinking: 2 sets of multiparticulate samples (4g) were each immersed into 28.5mL of a gelling solution composed of 20% sodium hydroxide, 32% ethanol (99%$^{v}/_{v}$) and 48% deionized water and allowed to gel for 4 hours. 1.5mL epichlorohydrin (99%$^{v}/_{v}$) and was then added to the 1st set and 1.5mL sodium trimetaphosphate (60%$^{w}/_{v}$) to the 2nd set. Both sets of mulitiparticulates were allowed to crosslink under constant stirring for a further 2 hours at 25°C before being removed and dried at 50°C for 4 hours. The same procedure as above was carried out on oxidized multiparticulates.

Drug entrapment: unmodified, oxidized, crosslinked and oxidized-crosslinked multiparticulate batch (1g) were each placed into 5mL drug solution (75mg/mL) and allowed to hydrate under constant stirring for 4 hours at 25°C before being removed lightly tapped dry with tissue and dried at 50°C for 4 hours. Samples from each batch (0.2g) were then homoginized in 10mL sodium hydroxide solution and UV spectroscopy was then carried out to determine the drug entrapment efficiency of each batch.

Scanning electron microscopy: These were carried out to determine surface morphology and core morphology

FTIR: these were carried out to observe the effect of modification on bead structure and mechanism of drug entrapment

In vitro drug release: These were performed using a USP dissolution apparatus II. Separate drug-loaded bead samples (0.2g) were accurately weighed out and placed into 900mL pH 6.8 phosphate buffer solution (PBS). The medium was maintained at 37 ± 0.5^{0}C and rotated at 50rpm. Samples (5mL) were withdrawn every 30 minutes over the first 2 hours and then every hour over a 12 hour period and replenished with fresh buffer in order to maintain sink conditions. The absorbance values were measured using UV spectroscopy at the wavelength of 214nm and fractional drug release was calculated using the predefined calibration curve.

Results: Drug entrapment results demonstrate that modification of multiparticulaes enhance their drug entrapment efficiency and that crosslinking of oxidized beads show the highest DEE 0f 39%. FTIR results show that the multiparticulates are modified during oxidation and crosslinking and show interactions with sulfasalazine uring dug entrapment not seen with unmodified beads. SEM results show drug adsorbed onto the surface of the multiparticulates which could explain the burst release observed during *in vitro* drug release as well as drug within the core of the SM which could explain the extended release observed. *In vitro* drug release studies show that oxidized-crosslinked beads have the lowest burst release (11%) after 10 minutes and released only 48% of drug within 12 hours.

APPENDIX B

Abstracts of Papers Published/Submitted

APPENDIX B1

Effects of modifications and subsequent optimization of a multiparticulate starch based oral drug delivery system employing sulfasalazine as the model drug

Y. Dawood, V. Pillay*, Y.E. Choonara, L.C. du Toit. P. Kumar

University of the Witwatersrand, Department of Pharmacy and Pharmacology, 7 York Road, Parktown, 2193, Johannesburg, South Africa
*Correspondence: viness.pillay@wits.ac.za

Abstract: Starch-based multiparticulates derived from the sago palm (*Metroxylon sagu*) were subjected to various modification techniques, including gelatinization, Epichlorohydrin (ECH) crosslinking, Sodium Trimetaphosphate (STMP) crosslinking, periodate oxidation and combinations of these techniques. The structural stability and functional characteristics of drug-loading and *in vitro* drug release were evaluated to elucidate the most beneficial modification in order to employ these multiparticulates as a Starch-Based Platform (SBP) in a multiparticulate oral drug delivery system (MODDS). ECH-facilitated crosslinking followed by drug loading with sulfasalazine (SSZ) and finally secondary ECH crosslinking conferred the best control of drug release with satisfactory drug entrapment and excellent structural stability while maintaining the multiparticulate nature of the SBP. The formulation procedure was optimized using a Face Centred Central Composite Design by evaluating the effects of varying the Drug Loading Time (DLT) and secondary Crosslinking tTme (CLT) on the responses of Drug Entrapment Efficiency (DEE) and Mean Dissolution Time (MDT). The optimum formulation conditions was found to be DLT = 8 hours and CLT = 8 hours with predicted DEE and MDT of 40.78% and 171.696 minutes, respectively. Formulation, up-scaling and analysis of the optimized SBPs revealed that gelatinization and crosslinking had occurred throughout the SBP resulting in SSZ being incorporated into the structure of the SBPs both at the surface and at core of the SBPs. Experimental DEE values for the optimized and scaled-up formulations showed close correlation to the predicted DEE with R^2 values of 98.13 and 98.93 respectively. The modifications imparted during optimization caused coalescence of the surface granules resulting in a decrease in surface area and porosity of the SBPs. This in turn affected the drug release resulting in MDT values of 163.972 and 166.011 minutes, which translated into R^2 values of 95.501 and 96.689 for the optimized and scaled up formulations respectively. Drug release from the SBPs was found to best follow the Higuchi model with quasi-fickian diffusion occurring in simulated gastric fluid (SGF) and anomalous drug transport in simulated intestinal fluid (SIF) resulting in an overall anomalous drug transport mechanism of drug release. Thus, the optimized modifications imparted adequate functionality on the SBPs for the SBPs to be used as a ODDS.

Keywords: Starch, Sago, Multiparticulate, Oral drug delivery, Gelatinization, Crosslinking, Epichlorohydrin, Sodium trimetaphosphate, Periodate oxidation, Sulfasalazine, Face Centred Central Composite Design

APPENDIX C

Animal Ethics Clearance

APPENDIX C1

Animal Ethics Clearance Certificate

UNIVERSITY OF THE WITWATERSRAND, JOHANNESBURG

STRICTLY CONFIDENTIAL

ANIMAL ETHICS SCREENING COMMITTEE (AESC)

CLEARANCE CERTIFICATE NO. 2009/01/05

APPLICANT:	Prof V Pillay
SCHOOL:	Pharmacy and Pharmacology
DEPARTMENT:	
LOCATION:	
PROJECT TITLE:	**In vivo assessment of novel biocompatible polymeric drug delivery systems in pigs**

Number and Species

40 pigs

Approval was given for the use of animals for the project described above at an AESC meeting held on 27.01.2009. This approval remains valid until 27.01.2011

The use of these animals is subject to AESC guidelines for the use and care of animals, is limited to the procedures described in the application form and to the following additional conditions:

a) **Clinical monitoring of the animals for the first 24 hours after drug dosing to ensure that no unwanted side-effects occur. This monitoring should be performed by the investigators as guided by the CAS veterinarian.**
b) **A written report should be submitted to the AESC on the clinical safety of the drug combinations observed in one animal per drug combination before proceeding to further animals in each drug combination group.**
c) **A letter addressed to the chairperson of AESC should be provided to indicate the exact pharmacological combinations being studied and the route of delivery of these combinations . Obviously this should be provided when the appropriate combinations are known.**
d) **The protocol should be revised with the inclusion of a detailed description of the procedure that will be employed for intraduodenal infusion and the person qualified to do this.**
e) **The protocol should be revised with a justification and rationale for the use of 2 calcium channel blockers employed together as implied by the present protocol.**
f) **Discussion should occur with the CAS veterinarian regarding the precise procedures required for the collection of blood and CSF samples.**

Signed: NORTON (Chairperson, AESC) Date: 06/02/2009

I am satisfied that the persons listed in this application are competent to perform the procedures therein, in terms of Section 23 (1) (c) of the Veterinary and Para-Veterinary Professions Act (19 of 1982)

Signed: _____ (Registered Veterinarian) Date: 09/02/09

cc: Supervisor:
Director: CAS
Works 2000/lain0015/AESCCert.wps

APPENDIX C2

Animal Ethics Research Outcome Report

Central Animal Service

Medical School, 7 York Road, Parktown 2193, South Africa • Tel: +27 11 717-1301 • Fax: +27 11 643-4318

RESEARCH OUTCOME REPORT

Clearance Certificate No: 2009/01/05

Applicant: Professor Viness Pillay

Department: Pharmacy and Pharmacology

Title: *In Vivo* assessment of novel biocompatible polymeric drug delivery systems in pigs

Dear Animal Users

It is with great satisfaction that we can relay the positive outcome of the research entitled "*In Vivo* assessment of novel biocompatible polymeric drug delivery systems in pigs" with clearance certificate number: 2009/01/05. Central Animal Service acquired a batch of 40 pigs for *in vivo* research with the department of Pharmacy and Pharmacology, for the determination of the biocompatibility of novel polymeric drug delivery systems.

The afore mentioned applicant, Professor Viness Pillay, and his research group, including Mr. Yusuf Dawood, ensured that an ongoing surveillance program continued on a daily basis to assess the health and well being of the pigs during and post study. Furthermore, the CAS team ensured that the animals were assessed for their health status both before and after the study to determine whether the researchers or research material caused any effects which detrimentally affected the pigs' health and well-being. We are confident to say that no unforeseen or fatal circumstance due to the researcher or research material were observed as the pigs maintained an acceptable health status both during the study, and after completion of the study.

Kind regards

Dr. Marcus Eide
Director of the Central Animal Services
University of the Witwatersrand

21.05.2013
Date